Synthesis And Reactivity Of Low Coordinate Nickel(I) Complexes Bearing Ring Expanded N-Heterocyclic Carbene Ligands

Poulten, Rebecca

Award date:
2015

Awarding institution:
University of Bath

SYNTHESIS AND REACTIVITY OF LOW COORDINATE NICKEL(I) COMPLEXES BEARING RING EXPANDED N-HETEROCYCLIC CARBENE LIGANDS

Rebecca Charlotte Poulten

A thesis submitted in partial fulfilment of the requirements for the degree of

Doctor of Philosophy

University of Bath

Department of Chemistry

March 2015

Acknowledgements

Inevitably, there are a large number of people I would like to thank now I am finally ending this PhD journey. Firstly, to Prof. Mike Whittlesey, who not only adopted me into his research group as an innocent MChem and subsequently as a PhD student, but also allowed my chemistry career to initially blossom by graciously accepting me as an undergraduate student after my 'OK' UCAS interview over seven years ago. You have answered more than your fair share of science questions, as well as broadened my knowledge in all things Planet Rock, golf and cricket. I hope I have reciprocated this by educating you on equally important things, such as Strictly, texting emoticons (☺, ☹) and The MailOnline. All your continued support, kindness and patience is very much appreciated. Long may your Zen continue.

I would also like to thank Dr. Mary Mahon for her endless assistance with X-ray crystallography, while patiently and speedily putting up with my constant queries and requests – thanks here must also go to Dr. Ian Riddlestone, who has helped no end in my quest to conquer disorder. Dr. John Lowe must not be forgotten for his continuous help with anything NMR related and his enthusiastic chats about the weekends and alike. Numerous collaborators have proved vital for this doctorate, including Dr. Anneke Lubben, Prof. Damien Murphy/Dr. Emma Carter, Jen Le Roy, Isidoro López/Prof. Antoni Llobet and Prof. Stuart Macgregor for instrumental assistance and much needed explanation in mass spectrometry, EPR, SQUID, electrochemistry and DFT wizardry respectively. Also, to Prof. Phil Power for what proved to be a hugely valuable 'quick' discussion.

I also acknowledge my lab mates, past and present, who have all provided me with a fantastic, unforgettable and thoroughly enjoyable experience. To Dr. Mike Page (who must be individually recognised for opening the nickel(I) door of unanswered questions), Minty Ledger, Charlie Ellul and Tom Martin for initiating me into the Whittlesey gang. I hope I flew the flag well. For 'Team Girly': Caroline 'CJED' Davies and my roomie Nicola Bramananthan, the laughs and support are cherished. Lastly, to 'The Whittlesey LaDDs': Dr. Ian Riddlestone (King of Drying Solvents), Mateusz 'Kanapka' Cybulski and Lee Collins, for not only creating an 'extremely friendly department to work in', but also for allowing me to be an honorary LaDD member (denoted by the subclause: 'and Da Bec'). I will miss the banter and the kanapkas….definitely the kanapkas. BOOM! A special mention must be made to Ian for his constant help, tips, patience and knowledge over the last year…even though none of his abstraction suggestions really worked!

Thanks must also go to all my friends and family who have endlessly supported me through my university days. To my fabulous little sister, Jen (Marshy), who despite having a geek for a big sister, never fails to make me laugh and smile. Your humour will always be needed. To my fantastic parents for their continuous love, support (financially as well as emotionally) and, most of all, encouragement. You are always there and I have tried my upmost to stick to the mantra you instilled into me growing up: "always do your best". Finally to Simon, for giving me more than he can ever imagine. Your constant faith, love, support, humour, sacrifice and train travel mean more than anything and are whole heartedly appreciated. How you put up with me I will never know! Thanks for being simply the best!

“Knowledge is knowing that a tomato is a fruit, wisdom is not putting it in a fruit salad.”

Miles Kington

Abstract

This thesis describes the development of nickel(I) complexes incorporating ring expanded N-heterocyclic carbene (RE NHC) ligands and examines their electronic characterisation, activation of O_2, reactivity and catalytic applications. A series of three coordinate, paramagnetic Ni(I) complexes of the form Ni(RE NHC)(PPh_3)Br **(1 – 10)** were prepared by comproportionation of $Ni(COD)_2$ and $Ni(PPh_3)_2Br_2$ in the presence of RE NHCs. The RE NHCs employed varied in the degree of ring expansion (6-, 7- and 8-membered), extent of N-substituent steric bulk (Mes, ^{o}Tol, ^{o}Anis) and the donor/acceptor properties of the carbene (diamino *vs.* diamido). EPR and DFT electronic characterisation of **1 – 10** confirmed that the unpaired electron was located on the nickel ion in a mixed orbital of predominantly $3d_{z2}$ character.

Yellow solutions of **1** or **6** (RE NHC = 6Mes and 7Mes respectively) immediately became purple in the presence of O_2 due to O_2 activation and incorporation of the oxygen atoms as bridging ligands resulting from C-H activation/oxygenation of an RE NHC N-substituent. This generated the dimeric Ni(II) complexes Ni(6/7Mes)Br(μ-OH)(μ-O-6/7Mes)'NiBr (6Mes = **13**; 7Mes = **14**). Mass spectrometry demonstrated that the doubly activated complexes [NiBr(μ-O-6/7Mes)']$_2$ (**15** and **16** respectively) were also formed in the reactions. UV-vis spectroscopy revealed the reactions took place rapidly, even at 190 K. Contrasting reactivity was observed when **2** or **7**, bearing the less sterically encumbered N-^{o}Tol substituents 6^{o}Tol and 7^{o}Tol respectively, were exposed to O_2, which led to the ligand redistribution products Ni^{II}(6/7^{o}Tol)(PPh_3)Br_2 (**17** and **18** respectively). The less electron rich diamido analogue containing 6MesDAC **(5)**, underwent dissociation and oxidation of the RE NHC and PPh_3 ligands.

Attempts to abstract the bromide from **1** generated novel two and three coordinate Ni(I) products. Reaction with additional 6Mes produced the two coordinate cation $[Ni(6Mes)_2]^+$ **(19)**, which could be reduced with KC_8 to $Ni(6Mes)_2$ **(20)**. SQUID analysis of **19** revealed it to be the first example of a nickel containing mononuclear single molecular magnet (SMM). Addition of $[Et_3Si]^+$ to **1** followed by work up in toluene led to the isolation of the Ni(I)-(η^2-toluene) complex $[Ni(6Mes)(\eta^2\text{-}C_6H_5CH_3)]^+$ **(21)**. Mesitylene generated the analogous $[Ni(6Mes)(\eta^2\text{-}C_6H_3(CH_3)_3)]^+$ **(23)**, but neither 1,4-xylene nor naphthalene gave isolable products. In all cases, cocrystallisation of $[6MesH]^{+\cdots}$arene was observed in variable amounts, which compromised reaction studies of the Ni-arene complexes. Removal of bromide from **1** with

$TlPF_6$ in THF generated the solvent coordinated cationic species $[Ni(6Mes)(PPh_3)(THF)]^+$ **(24)**. Attempts to remove the ligated THF molecule were unsuccessful, however, it could be directly substituted by CO to form $[Ni(6Mes)(PPh_3)(CO)]^+$ **(26)**. Similarly to **1**, complex **24** activated O_2, generating a dimer analogous to the singly activated complex **13** ($Ni(6Mes)(PPh_3)(\mu$-OH)(μ-O-6Mes)'NiBr **(25)**). Reactivity of **1** with $NaBH_4$ produced $[Ni(6Mes)(\kappa^2$-$BH_4)]_2$ **(28)**, a Ni(I) dimer bridged by two BH_4 ligands.

The catalytic efficiency of neutral **1** in Kumada cross-coupling of aryl halides and PhMgCl or MesMgBr was probed. Of note was the high activity towards both aryl chlorides and aryl fluorides. Comparisons with cationic **24**, larger 7- **(7)** and 8-membered ring (**8** and **9**) variants and the Ni(II) complexes $Ni(6Mes/6^o Tol/7^o Tol)(PPh_3)Br_2$ (**29**, **17** and **18** respectively) revealed that **1** exhibited the highest reactivity of all the precursors.

Contents

Appendices

Numbered Complexes

Abbreviations

Analytical

ac	Alternating current
BDE	Bond dissociation energy
br	Broad
COSY	Correlation spectroscopy
CT	Charge transfer
CV	Cyclic voltammetry
CW	Continuous wave
d	Doublet
dc	Direct current
DFT	Density functional theory
ENDOR	Electron nuclear double resonance
E_p	Potential voltage
$E_{p,a}$	Anodic voltage
$E_{p,c}$	Cathodic voltage
EPR	Electron paramagnetic resonance
ESI-TOF	Electrospray ionisation-time of flight
EXAFS	Extended X-ray absorption fine structure
EXSY	Exchange spectroscopy
g	***g*** factor in EPR (dimensionless magnetic moment)
GC-MS	Gas chromatography-mass spectrometry
g_e	***g*** factor of an electron with free spin in EPR
H	External reverse magnetic field
HMBC	Heteronuclear multiple bond correlation
HMQC	Heteronuclear multiple quantum coherence
HOMO	Highest occupied molecular orbital
HSQC	Heteronuclear single quantum coherence
I	Current
$i_{p,a}$	Anodic current
$i_{p,c}$	Cathodic current
IR	Infrared
$^nJ_{xy}$	Coupling constant of X to Y across n bonds
K_b	Cryoscopic constant
k_B	Boltzmann constant
m	Multiplet
M	Magnetisation value in SQUID
MS	Mass Spectroscopy
MW	Molecular weight
m/z	Mass to charge ratio
NHE	Normal hydrogen electrode
NMR	Nuclear magnetic resonance
q	Quartet
QTM	Quantum tunnelling of the magnetisation
quin	Quintet
RF	Radio frequency
s	Singlet

sept	Septet
SMM	Single molecular magnet
SOMO	Singly occupied molecular orbital
SQUID	Superconducting quantum interference device
t	Triplet
t	Time
T	Temperature
T_b	Blocking temperature
TOF	Turnover frequency (TON h^{-1})
$t_{1/2}$	Half life
U_{eff}	Anisotropy barrier
UV-vis	Ultraviolet-visible
VT	Variable temperature
X	Molecular fragment in mass spectrometry
XAS	X-ray absorption spectroscopy
δ	NMR chemical shift
ε	Molar extinction coefficient
λ	Wavelength
τ	Relaxation time
μ_{eff}	Effective magnetic moment
ν	Frequency
ν_L	IR shift of L
χT	Molar susceptibility per molecule defined as M/H (magnetic susceptability) at temperature T
$\%V_{Bur}$	Percentage of buried volume (for ligands)

Units

A	Amp
Å	Angström
atm	Atmosphere
cm	Centimetre
cm^{-1}	Wavenumber
dB	Decibel
dm	Decimetre
e^-	Electron
eV	Electron volt
g	Gram
GHz	Gigahertz
h	Hour(s)
Hz	Hertz
K	Kelvin
kcal	Kilocalorie
kHz	Kilohertz
kJ	Kilojoule
M	Molar concentration (mol dm^{-3})
mg	Milligram
MHz	Megahertz
min	Minute(s)

mL	Millilitre
mM	Millimolar
mmol	Millimole
mol	Mole
mV	Millivolt
mW	Milliwatt
nm	Nanometre
Oe	Oersted (unit of H)
ppm	Parts per million
s	Second(s)
T	Telsa
V	Volt
μA	Microamp
μB	Bohr magneton
μg	Microgram
μL	Microlitre
°	Degree

Chemical

Ac	Acetate
Ad	Adamantyl
Anis	2-Methoxyphenyl
Ar	Aryl group
BAr_4^F	$[B(C_6H_3\text{-}3,5\text{-}(CF_3)_2)_4]^-$
^{tBu}N4	N,N'-di*tert*butyl-2,11-diaza[3.3](2,6) pyridinophane
CAAC	Cyclic(alkyl)(amino)carbene
COD	Cycloocta-1,5-diene
COT	Cyclooctatetraene
Cp	Cyclopentadienyl
Cp*	1,2,3,4,5-Pentamethylcyclopentadienyl
Cy	Cyclohexyl
DAC	Diamidocarbene
d^{t}bpe	1,2-*bis*(di*tert*butylphosphino)ethane
dme	Dimethoxyethane
d^{i}pp	2,6-diisopropylphenyl
dppm	1,1-*bis*(diphenylphosphino)methane
dvtms	Divinyltetramethyldisiloxane
Fc	Ferrocene
Hal	Halide
i-	*Ipso*
I^{t}Bu	1,3-*bis*(*tert*butyl)imidazol-2-ylidene
IMe	1,3-*bis*(methyl)imidazol-2-ylidene
IMes	1,3-*bis*(2,4,6-trimethylphenyl)imidazol-2-ylidene
IMe_4	1,3,4,5-Tetramethylimidazol-2-ylidene
Ind	Indenyl
I^{i}Pr	1,3-*bis*(isopropyl)imidazol-2-ylidene
IPr	1,3-*bis* (2,6-diisopropylphenyl)imidazol-2-ylidene
L	Generic ligand
(L)'	C-H activated ligand

LB	Lewis base
LDA	Lithium diisopropylamide ($LiN(CH(CH_3)_2)_2$)
m-	*Meta*
M	Generic metal
MCR	Methyl-coenzyme M reductase
Mes	2,4,6-trimethylphenyl
N^N	β-diketiminate
Neopentyl	2,2-dimethylpropyl
Neophyl	(*tert*buty)benzene
NHC	N-heterocyclic carbene
o-	*Ortho*
OSET	Outer sphere electron transfer
p-	*Para*
Py	Pyridine
R	Alkyl or aryl
RE NHC	Ring expanded N-heterocyclic carbene
(RE NHC)'	Activated ring expanded N-heterocyclic carbene
SIMes	1,3-*bis*(2,4,6-trimethylphenyl)imidazolin-2-ylidene
SIPr	1,3-*bis*(2,6-diisopropylphenyl)imidazolin-2-ylidene
TBAH	Tetrabutylammonium hydroxide
THF	Tetrahydrofuran
TIME^{Me}	[1,1,1-*tris*(3-methylimidazol-2-ylidene)methyl]ethane
tmeda	Tetramethylethylenediamine
Tol	2-methylphenyl
Tp*	*Tris*(3,4,5-methylpyrazolyl)borate
tpy	Terpyridine
triphos	1,1,1-*tris*(diphenylphosphinomethyl)ethane
trop	*Bis*(tropylidenylamine); *bis*(5*H*-dibenzo[*a,d*]cyclohepten-5-yl)amine
X	Halide or other heteroatom
Xyl	Xylene
κ^n-L	Bonding/bridging ligand L through n atoms
η^n-L	Ligand hapticity (of number n)
μ-L	Bridging ligand *via* L
6^{o}Anis	1,3-*bis*(2-methoxyphenyl)-3,4,5,6-tetrahydro-[1,3]-pyrimid-2-ylidene
6^{o}AnisMes	1-(2-methoxyphenyl)-3-(2,4,6-trimethylphenyl)-3,4,5,6-tetrahydro-[1,3]-pyrimid-2- ylidene
6^{t}Bu	1,3-*bis*(*tert*butyl)-3,4,5,6-tetrahydro-[1,3]-pyrimid-2- ylidene
6Mes	1,3-*bis*(2,4,6-trimethylphenyl)-3,4,5,6-tetrahydro-[1,3]-pyrimid-2- ylidene
6MesDAC	1,3-*bis*(2,4,6-trimethylphenyl)-4,6-diketo-5,5-dimethyl-[1,3]-pyrimidin-2-ylidene
6Neo	1,3-*bis*(neopentyl)-3,4,5,6-tetrahydro-[1,3]-pyrimid-2- ylidene
6^{i}Pr	1,3-*bis*(isopropyl)-3,4,5,6-tetrahydro-[1,3]-pyrimid-2- ylidene
6^{o}Tol	1,3-*bis*(2-methylphenyl)-3,4,5,6-tetrahydro-[1,3]-pyrimid-2-ylidene
7Mes	1,3-*bis*(2,4,6-trimethylphenyl)-4,5,6,7-tetrahydro-[1,3]-diazepin-2- ylidene
7Neo	1,3-*bis*(neopentyl)-4,5,6,7-tetrahydro-[1,3]-diazepin-2- ylidene
7^{i}Pr	1,3-*bis*(isopropyl)-4,5,6,7-tetrahydro-[1,3]-diazepin-2- ylidene
7^{o}Tol	1,3-*bis*(2-methylphenyl)-4,5,6,7-tetrahydro-[1,3]-diazepin-2- ylidene
7^{m}Xyl	1,3-*bis*(2,5-methylphenyl)-4,5,6,7-tetrahydro-[1,3]-diazepin-2- ylidene
8Mes	1,3-*bis*(2,4,6-trimethylphenyl)-4,5,6,7,8-pentahydro-[1,3]-diazocin-2- ylidene
8^{o}Tol	1,3-*bis*(2-methylphenyl)-4,5,6,7,8-pentahydro-[1,3]-diazocin-2- ylidene
O-8^{o}Tol	1,3-*bis*(2-methylphenyl)-4,5,7,8-tetrahydro-6-oxa-[1,3]-diazocin-2- ylidene

NHC Structures

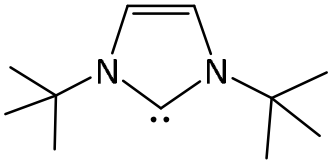

I^{t}Bu

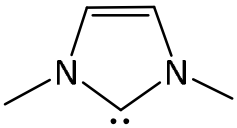

IMe

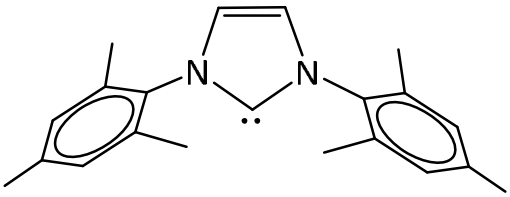

IMes

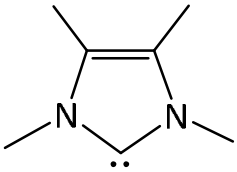

IMe$_4$

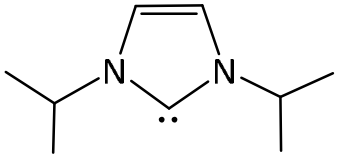

I^{i}Pr

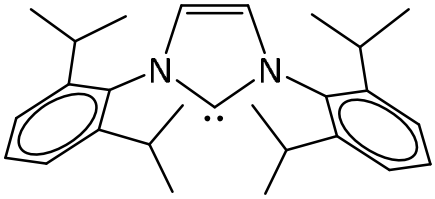

IPr

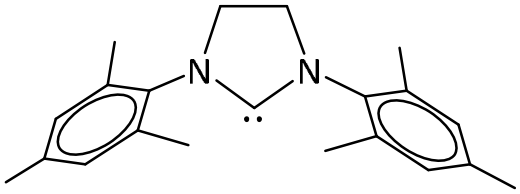

SIMes

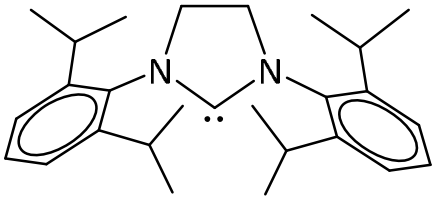

SIPr

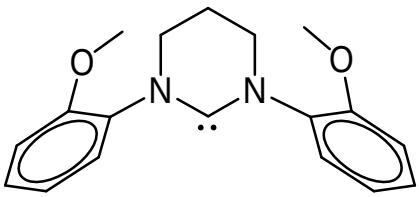

6^{o}Anis

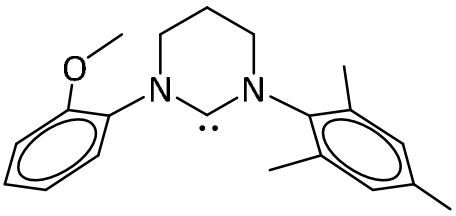

6^{o}AnisMes

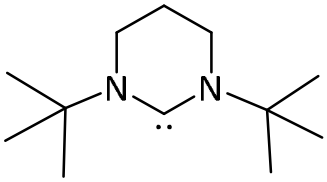

6^{t}Bu

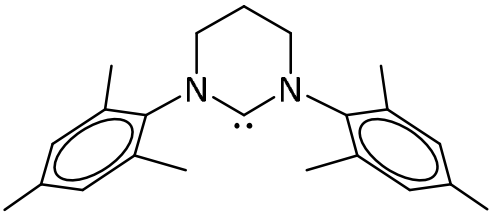

6Mes

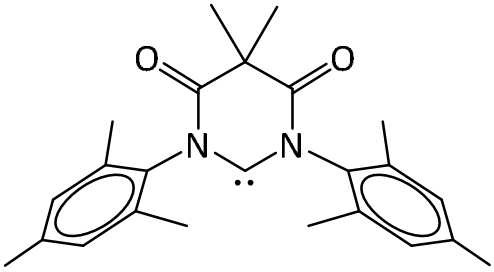

6MesDAC

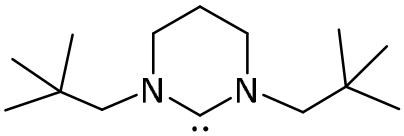

6Neo

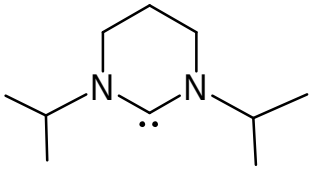

6^{i}Pr

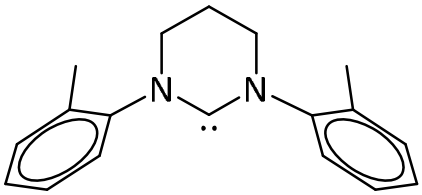

6^{o}Tol

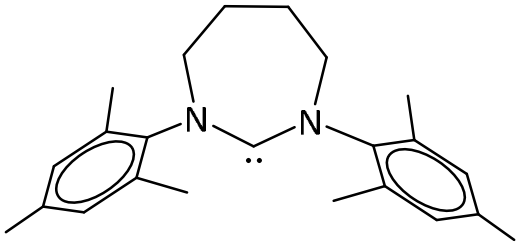

7Mes

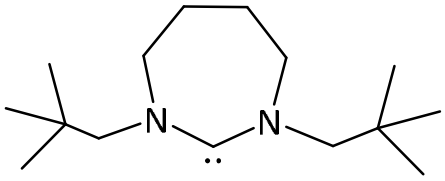

7Neo

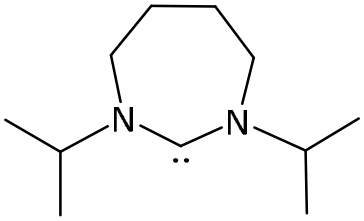

7^{i}Pr

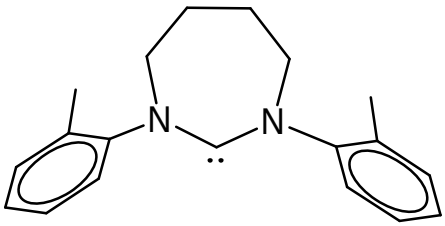

7^{o}Tol

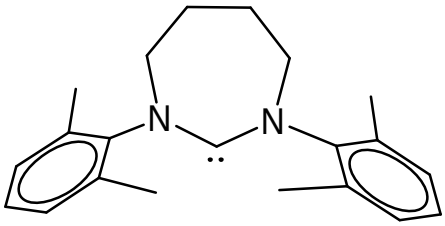

7^{m}Xyl

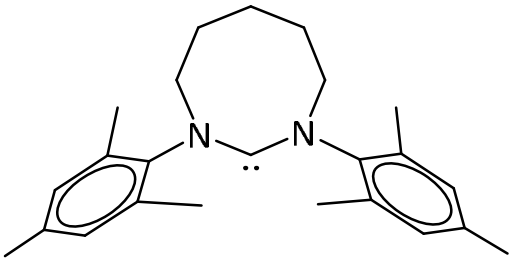

8Mes

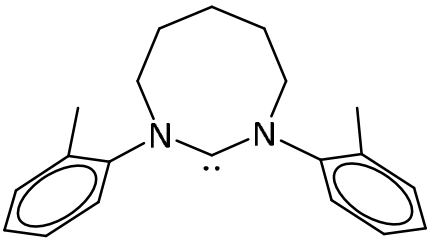

8^{o}Tol

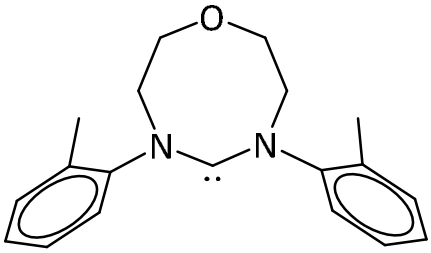

O-8^{o}Tol

CHAPTER 1

1 Introduction

1.1 Synthesis and Reactivity of Nickel(I) Complexes

The organometallic chemistry of nickel is extremely diverse and utilises a range of ligands to generate numerous complexes, varying in oxidation state, coordination number and geometry. Consequently, complexes of nickel are widely applied to several homogeneous catalytic processes[1-5] (*i.e.* cross-coupling, see **Chapter 5**), as well as being implicated as intermediates in many enzymatic cycles. For example, in physiological carbon cycling, where catalysts containing nickel active sites (carbon monoxide dehydrogenase (CODH) and acetyl coenzyme A synthase (ACS)) remove CO_2 and toxic CO from the surrounding environment of the cell, ultimately acting as a source of carbon and electrons for biological processes which take place in cells.[6-8] It is often well characterised complexes of Ni(0) or Ni(II), such as in CODH and ACS, that act as precursors for the transformations, with Ni(I) or Ni(III) species only ever occasionally observed or simply postulated. For instance, Ni(I) species have been implicated in the formation of methane released during the metabolism of bacteria (methanogenic archaea) which live in low oxygen concentrations. The final step in this process is catalysed by methyl-coenzyme M reductase (MCR) and converts two substrates, methyl coenzyme M and coenzyme B, into CH_4 and the corresponding heterodisulfide **(Scheme 1.1)**. MCR comprises of protein chains arranged around two active sites, each containing the nickel based cofactor F_{430} enzyme **(Figure 1.1)**. Isotopic labelling experiments indicated that these nickel centres pass through a Ni(I)-σ-CH_4 intermediate during this methane formation.[9-13]

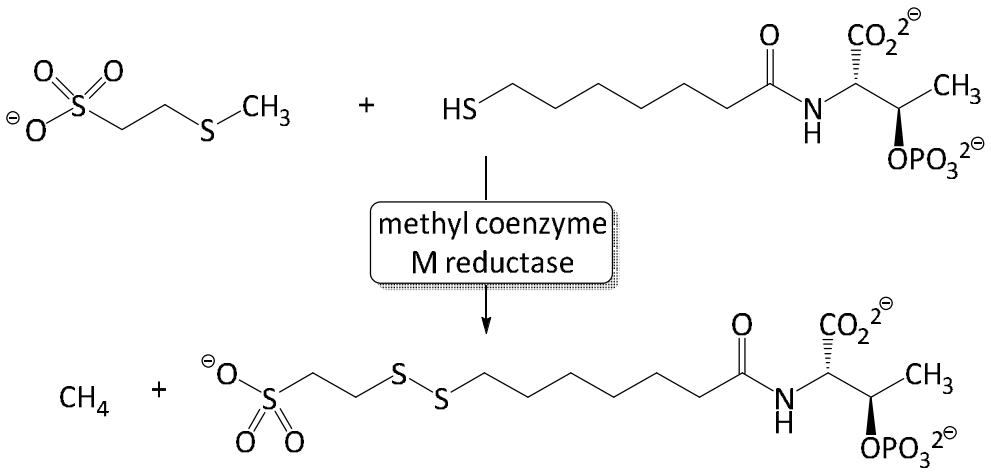

Scheme 1.1 The last step of methane formation in methanogenic archaea catalysed by MCR.

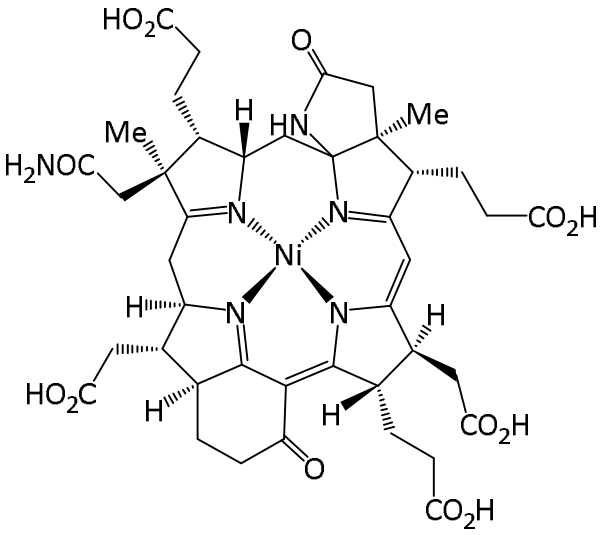

Figure 1.1 The nickel containing cofactor F_{430} in MCR.

Despite evidence for participation in central roles within enzymatic/biological processes, Ni(I) complexes are characteristically unstable. The nickel centre is often low coordinate and electron deficient, meaning that unless it is sterically protected, vacant coordination sites are open to attack allowing facile oxidation to a more stable state, frequently a 16 or 18e$^-$ Ni(II) complex. Isolation, and hence comprehensive characterisation, is also problematic, commonly leading to precipitation of metallic nickel. Ni(I) complexes are therefore far less abundant than those of either Ni(0) or Ni(II),[14,15] with most of the isolated examples containing bulky phosphines[16-18] and/or bidentate chelating ligands[17-19] such as β-diketiminates.[20-22] In these complexes, the nickel often resides in a three coordinate environment, with early examples indicating a geometric preference for T-shaped rather than trigonal planar as typically expected with tri-coordinate species. For example, Holland and coworkers[20] generated Ni(N^N)(CO) ***(Iii*; Chapter 4, 4.2.2.2)** (N^N = β-diketiminate), which displayed a T-shaped geometry that could be traced to the *trans* effect of the carbonyl ligand.

1.1.1 Mononuclear Nickel(I) Complexes

Early examples of Ni(I) species were reported by Bradley *et al.* in 1972. Upon probing the effects of phosphine stabilisation on nickel dialkylamides, they generated a series of three coordinate Ni(I)-*bis*(phosphine) complexes.[23] Reaction of $Ni(L)_nCl_2$ precursors (n = 2, L = PPh_3, PMe_2Ph, $PMePh_2$, $PEtPh_2$, PEt_2Ph, PEt_3; n = 1, L = $Ph_2PCH_2CH_2PPh_2$) with $LiN(SiMe_3)_2$ yielded air-sensitive crystals of the corresponding $Ni(L)_n(N(SiMe_3)_2)$ species **(Scheme 1.2)**.

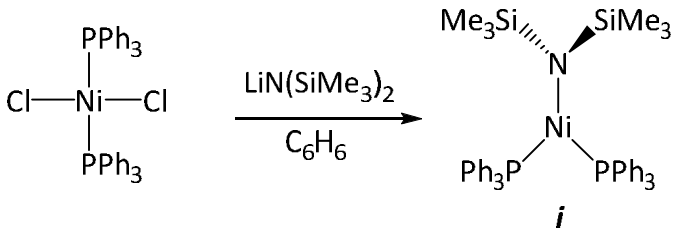

i

Scheme 1.2 Synthesis of a Ni(I)-*bis*(phosphine) complex ***(i)***.

These complexes all displayed typical EPR signals in accordance with the number of equivalent ^{31}P atoms present and magnetic moments (μ_{eff}) consistent with the presence of d^9 Ni(I) metal centres. Furthermore, X-ray crystallographic analysis led to $Ni(PPh_3)_2(N(SiMe_3)_2)$ ***(i)*** as the first fully characterised trigonal planar Ni(I) species and also confirmed there were no unusually short contacts between the *ortho*-C-H bonds of the phenyl rings and the nickel, suggesting no additional electronic stabilisation.

Building on the work of Bradley *et al.*, further three and four coordinate Ni(I)-phosphine complexes were reported, mainly formed from the *in situ* decomposition of Ni(II) species generated by stoichiometric oxidative addition reactions.[14,24] Unlike previous $15e^-$ complexes of formulation $Ni(PR_3)_2X$, which were reported to be dimeric with square planar nickel environments (R = Cy, X = Br, Cl)[25] or oligomeric (R = Ph, X = Br, Cl),[26] the distorted trigonal planar $Ni(PPh_3)_2Cl$[14] ***(ii)***, its corresponding THF solvated polymorph $Ni(PPh_3)_2Cl{\cdot}THF$[24] ***(iii)*** and the tetrahedral $Ni(PPh_3)_3Cl$[24,27] were all isolated and shown by X-ray crystallography to be monomeric species with no short intramolecular interactions. In contrast to ***i***, the greater distortion from trigonal planarity in ***ii*** leads to inequivalent phosphorus atoms, as confirmed in the crystallographic and EPR analyses. Common to all three complexes ***(i – iii)*** is the contraction of P-Ni-P angle relative to the 'ideal' 120°; 107.0(2), 114.94(2) and 111.52(2)° respectively. Steric considerations alone would predict the P-Ni-P angle to be greater than 120°, as observed in the copper(I) bromide analogue $Cu(PPh_3)_2Br$ (126.0(1)°).[28] Different explanations for this angular distortion have been postulated. Firstly, for ***ii*** and ***iii***, the lone pairs on the chloride ligand must be considered, as these bring the halide into closer proximity to the metal centre compared to the phosphorus atoms.[24,29] Secondly, the d^9 metal centre is thought to undergo Jahn-Teller distortions, destabilising the ML_3 structure from D_{3h} to C_{2v} symmetry.[14,30] The true cause of this angular distortion is most likely a composite effect.

Although a number of Ni(I) species featuring dative covalent ligands were reported in the literature, it was not until 2000 that the first structurally characterised Ni(I)-σ-C complex (and

indeed the first d^9 σ-bonded organometallic compound) was synthesised.[31] Addition of 2 eq of Li(C(SiMe$_3$)$_2$(SiMe$_2$C$_5$H$_4$-2-N)) to Ni(PPh$_3$)$_2$Cl$_2$ in THF gave the isolable, planar three coordinate species Ni(PPh$_3$)(C(SiMe$_3$)$_2$(SiMe$_2$C$_5$H$_4$-2-N)) ***iv*** **(Figure 1.2)**. Magnetic susceptibility (Evans method) and EPR analyses confirmed the presence of the d^9 metal centre. The unpaired electron was located on the nickel on the basis of a ***g*** value of 2.239 (similar to Ni(PPh$_3$)$_2$Br (2.209)) and a μ_{eff} of 1.55 μB.[27] The sum of the internal angles in ***iv*** was equal to 360°, with the bite angle of the bidentate ligand (98.0(1)°) and very wide P-Ni-C angle (155.67(11)°) reflecting the strong repulsion between the PPh$_3$ and SiMe$_3$ ligands. The shorter Ni-C (2.025(4) Å) and longer Ni-N (2.007(3) Å) bond distances relative to the Ni(II) complex Ni(C(SiMe$_3$)$_2$(C$_5$H$_4$-2-N))$_2$ **(*v*; Figure 1.2)** (2.078(3) and 1.887(2) Å),[32] mirror the lower metallacyclic strain in the 5-membered ring of ***iv*** compared to the 4-membered in ***v***. As attempts to isolate Ni(I)-organo compounds often lead to plating out of metallic nickel, it is thought that the steric demands of the bulky ligand in ***iv*** help to prevent any Ni-Ni aggregation and thus any unwanted reduction or oxidation.

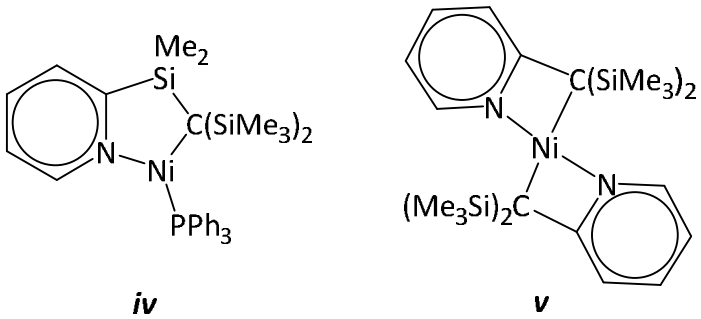

iv ***v***

Figure 1.2 The first structurally characterised Ni(I)-σ-C complex ***iv*** and a related Ni(II) species ***v***.

In 2004, Hillhouse and coworkers reported the synthesis of a range of monomeric Ni(I) species containing σ-bonded hydrocarbyl ligands.[33] As depicted in **Scheme 1.3**, alkyl lithium salts were reacted with Et$_2$O solutions of the Ni(I) dimer [Ni(d^{t}bpe)Cl]$_2$ at low temperature to afford the Ni(I)-alkyl complexes Ni(d^{t}bpe)(R) (R = CH$_2$CMe$_3$ ***(vi)***, CH$_2$SiMe$_3$ ***(vii)*** and CH$_2$CMe$_2$Ph ***(viii)***). X-ray crystallography revealed a planar three coordinate environment around the nickel in each case, while EPR spectra and magnetic moments were consistent with metal centres bearing a single unpaired electron.

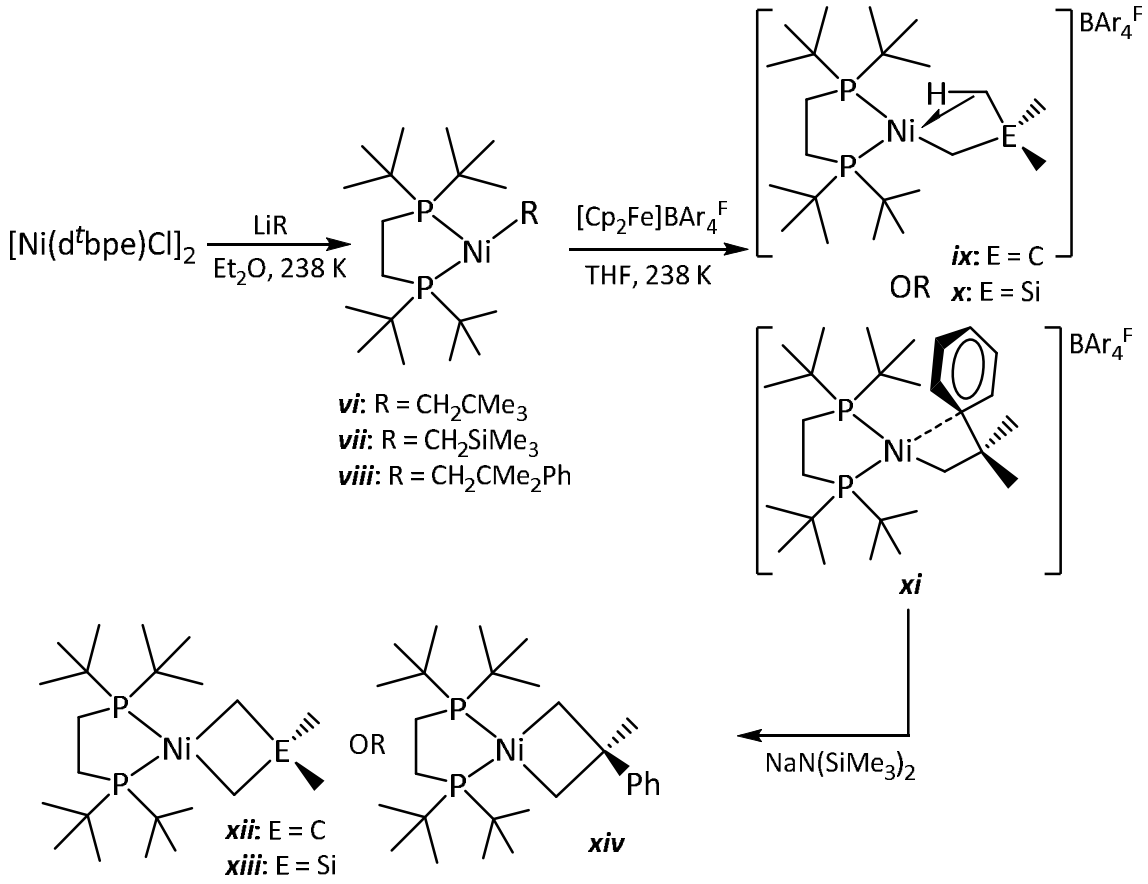

Scheme 1.3 Synthesis of a range of Ni(I)-alkyls **(*vi* – *viii*)** and their subsequent reactivity.

Oxidation by ferrocenium gave the corresponding γ-stabilised Ni(II) cations [Ni(d^{t}bpe)(R)]$^+$ **(*ix* – *xi*)**, indicating facile one electron oxidation can occur **(Scheme 1.3)**. This was confirmed by cyclic voltammetry with a reversible Ni(I)/Ni(II) couple at E = -1.25 V.[33] In each case, the nickel centres are in a pseudo-square planar environment, arising from γ-C-H agostic **(*ix, x*)** or γ-π,η^1 interactions to the *ipso* carbon on the phenyl in ***xi*** with the nickel centres. These are believed to stabilise the electron deficient 14e$^-$ alkyl cations. Similar β-C-H agostic interactions had previously been reported in [Ni(d^{t}bpe)(CH_2CH_3)]BF_4,[34] while *ipso* carbon stabilisation had been observed in related palladium complexes.[35,36] Interestingly, ^{1}H NMR spectroscopy indicated all the neopentyl protons in ***ix*** were equivalent, pointing to the weakness of the γ-interactions which allows rapid rotation of the ^{t}Bu group. It was proposed that these cationic Ni(II) species could act as synthons to nickel carbene complexes (d^{t}bpe)Ni=CR_2, on the basis of the susceptibility of amido and phosphido analogues to undergo one electron oxidation and subsequent α-deprotonation to imido and phosphinidene derivatives.[37] However, upon addition of $NaN(SiMe_3)_2$ to ***ix* – *xi***, deprotonation at the γ-Me C-H bond occurred instead, yielding the square planar Ni(II) nickellacyclobutane products **(*xii* – *xiv*; Scheme 1.3)**. In

benzene solution, ***xii*** and ***xiv*** reductively eliminated the corresponding cyclopropanes to form $[Ni(d^tbpe)]_2(C_6H_6)$, as previously reported for related platinum metallacyclobutanes.[38]

1.1.2 N-Heterocyclic Carbene (NHC) Ligands and Their Subclasses

N-Heterocyclic carbenes (NHCs) are a class of nucleophilic singlet state carbenes in which the carbenic carbon is traditionally positioned between two substituted nitrogen atoms in the 1 and 3 positions of a 5-membered imidazole derived ring **(Scheme 1.4)**. The N-substituents typically contain alkyl or aryl substituents, giving rise to tuneable stereoelectronic properties.[39] The carbon atoms in the 4 and 5 positions make up the backbone of the NHC and can either comprise a saturated (denoted by an 'Sl' preceding the nomenclature) or unsaturated bond (recognised with an 'I'). The first stable free NHC, IAd ***(xv)*** ('I' representing unsaturation and Ad signifying the adamantyl N-substituents), was only isolated by Arduengo *et al.*[40] in 1991 **(Scheme 1.4)**, but has already resulted in enormous interest in NHCs, particularly as alternative ligands to phosphines in organometallic homogeneous catalysis.

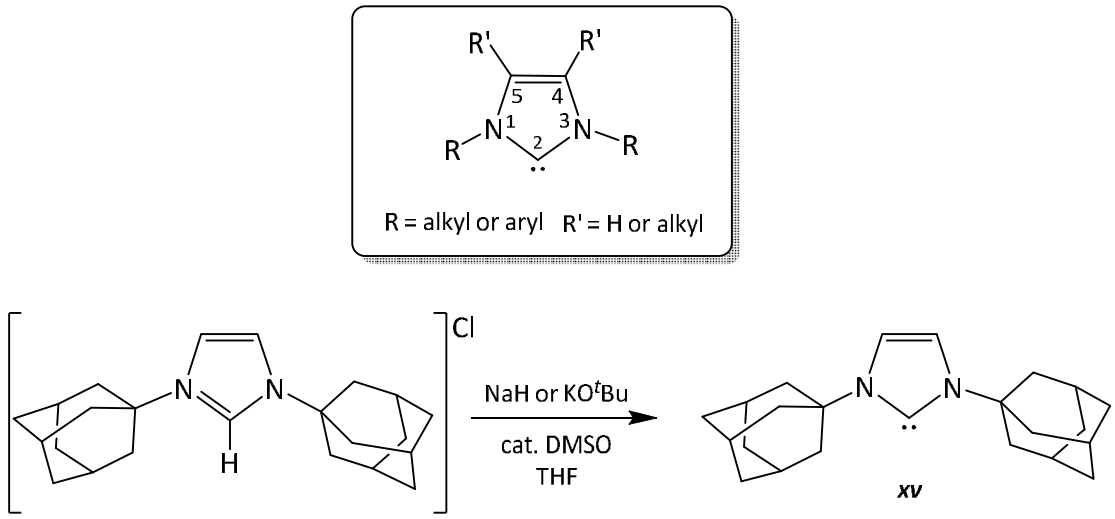

Scheme 1.4 Structure and nomenclature of a 5-membered NHC (above) and the isolation of the first stable free NHC ***xv*** (below).

NHCs possess a neutral, divalent carbenic carbon which houses only six electrons in its valence shell, thus failing to follow the octet rule. Two electrons (which can orientate to allow the carbene to exist in either a singlet or triplet state) are available for donation to an empty metal orbital. NHC bonding with a transition metal can be considered as a Fischer type interaction as the carbenic carbon bears π-donor nitrogen substituents and exists primarily as a nucleophilic singlet carbene.[41] However, a fundamental difference arises due to π-donation from the

nitrogen lone pairs into the empty p_π orbital of the carbenic carbon, which stabilises the NHC structure thus preventing or significantly reducing the level of backbonding normally associated with Fischer type carbenes **(Figure 1.3)**.[42-45] This is demonstrated by the difference in M-NHC bond lengths (> 2.1 Å) in comparison with metal to Fischer type carbenes (< 2.0 Å).[46] As a result, bonding is generally considered as arising primarily through σ-donation from the carbenic carbon and thus NHCs are considered as strong σ-donor ligands, represented by a single bond to the metal centre rather than the double bond representation often used in Fischer and Schrock type carbene complexes.

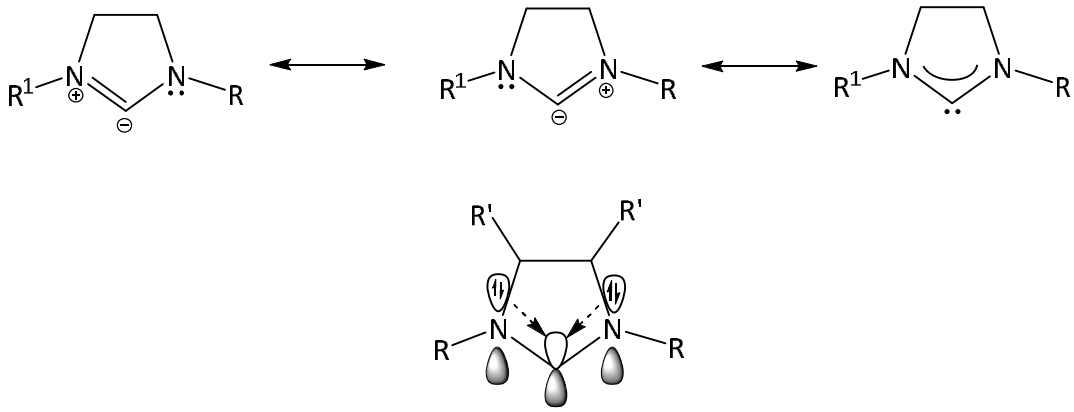

Figure 1.3 Stabilisation of the NHC structure through resonance forms arising from π-donation (above) and mesomeric induction (below) of the nitrogen atoms.

Whilst the traditional view of NHC bonding considers the ligand purely as a σ-donor, more recent studies have shown that filled and empty (including high energy lying) π and π^* orbitals on the 5-membered ring can contribute to the bonding interaction between an NHC and a metal centre.[44,45,47-50] Studies by Bertrand and coworkers[44] on carbene-phosphinidene adducts **(Figure 1.4)** revealed the structure, and hence electronic nature, of the carbene had a significant effect on the extent of π-acceptor character. Using ^{31}P NMR shifts as a measure of backbonding, unsaturated 5-membered NHCs, such as IMes, exhibited less backbonding (upfield ^{31}P signals) than the saturated (SIMes) or larger ring (6Pr) counterparts. NHCs incorporating π-accepting moieties, such as the 6Mes mono amide derivative (which has a C=O group on the C4 position withdrawing electron density from the carbenic *p* orbital), unsurprisingly demonstrated significantly downfield ^{31}P resonances, indicative of a greater level of backbonding. Meyer *et al.*[48] studied the tricationic portion of several electron-rich silver complexes ($[Ag_3(TIME^{Me})_2]^{3+}$) **(Figure 1.4)** incorporating a tridentate NHC $TIME^{Me}$ ($TIME^{Me}$ = [1,1,1-*tris*(3-methylimidazol-2-ylidene)methyl]ethane) using density functional theory (DFT). Calculations focussed on the metal to NHC bond and revealed a significant

overlap between the metal *d* orbitals and the carbene *p*-π hybrid orbitals. This indicated that stabilisation of the bond was at least part derived from π-interactions. The electron-poor doubly C-H activated complex [Ir(I^{t}Bu)'$_2$]PF$_6$ **(Figure 1.4)** was studied by Nolan and coworkers.[49] Although the two vacant coordination sites are positioned in close proximity to the C-H bonds of the ^{t}Bu moieties, the crystal structure showed no evidence of agostic interactions to stabilise the 14e$^-$ complex. Molecular orbital analysis revealed a strong electron density contribution from a filled NHC π orbital to the empty *d* orbitals on the metal centre, evidently preferred to σ-donation from a C-H bond of either ^{t}Bu group. Further work on NHC complexes with both electron-rich and electron-poor metal centres corroborated these findings, revealing that NHCs have the flexibility to either stabilise an electron-rich system as an acceptor *via* $d \rightarrow \pi^*$ back donation, or can contribute electron density into an electron-poor system *via* $\pi \rightarrow d$ donation.[49] These π-interactions may help to explain the added thermal stability of the metal-NHC bond over their phosphine containing analogues in many catalytic systems.

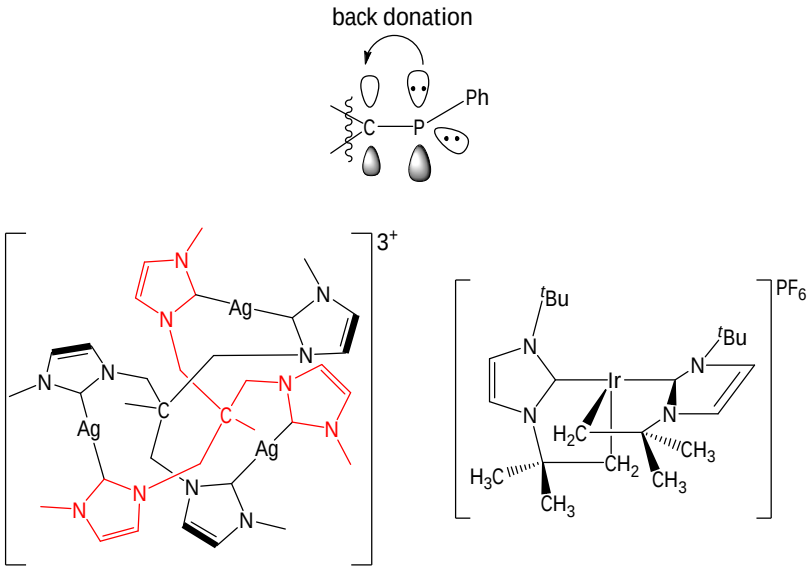

Figure 1.4 On the nature of the M-NHC interaction: a carbene-phosphinidene adduct (above), the electron-rich [Ag$_3$(TIME^{Me})$_2$]$^{3+}$ (below left) and electron-poor doubly C-H activated [Ir(I^{t}Bu)'$_2$]PF$_6$ (below right).

Initially, the inability of researchers to isolate NHCs cast doubt on their use as effective ligands for catalysis. However, following the isolation of ***xv*** the variety of NHCs developed increased significantly (often being synthesised from imidazolium salts *in situ* without ever isolating the free carbene)[51] and subsequently so did the research directed into their reactivity and applications. The electronic bonding properties of NHCs and phosphines are comparable as they are both neutral, two electron σ-donor ligands, with NHCs often being referred to as

'phosphine mimics' in the literature. However, a variety of studies have shown that NHCs possess superior Lewis basicity and nucleophilicity over phosphines and are thus classed as stronger σ-donors. Stronger metal-ligand bonds are therefore observed within NHC bearing complexes than even the most electron donating phosphines.[52-55] The added potential of π-interactions within M-NHC species (described above), further explains the enhanced thermal stability of the M-NHC bond, leading to recognition of NHCs as ancillary ligands in homogeneous catalytically active species which often outperform their phosphine counterparts.[46,56-59]

Percentage buried volume ($\%V_{Bur}$) calculations are typically used to compare the steric impact of ligands. Although this value is highly dependent on the metal in which the ligand is coordinated to and the geometry of the complex (*i.e.* in Au(NHC)Cl (NHC = I^{i}Pr, I^{i}PrMe (Me located on C4 and C5)) $\%V_{Bur}$ = 27.4 (I^{i}Pr) and 38.4 (I^{i}PrMe), whereas in Ir(NHC)(COD)(OH) they are 27.1 and 28.4 respectively),[60] comparisons of $\%V_{Bur}$ values between NHCs and phosphines have shown that in general NHCs are more sterically encumbered.[47,60] This suggests they provide greater steric crowding of the metal centre, which therefore increases the likelihood of kinetically stabilising low coordinate, potentially catalytically active species.[61] Nolan and coworkers[47,61] have revealed that in many instances a linear correlation exists between $\%V_{Bur}$ and the experimental bond dissociation energies (BDEs) of the NHC, indicating that steric demands play a large role in the control of BDE. Overall, the stronger bonding in NHC metal complexes enhances their thermodynamic stability, hopefully affording catalytic systems that can withstand elevated temperatures without degradation and exhibit enhanced efficiency.

1.1.2.1 Ring expanded N-heterocyclic carbenes (RE NHCs)

In recent years, considerable effort has been directed towards the syntheses of NHCs beyond the simple imidazole derived diaminocarbenes, as illustrated by the formation of cyclic(alkyl)(amino)carbenes (CAACs),[62,63] diamidocarbenes (DACs)[64,65] and ring expanded NHCs (RE NHCs)[66-70] **(Figure 1.5)**.

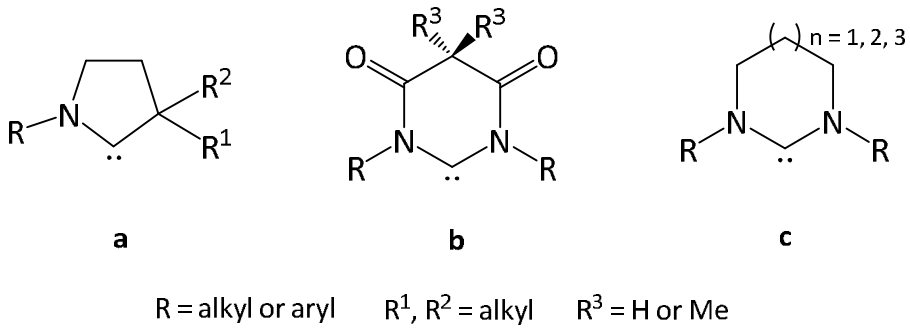

Figure 1.5 Examples of generalised CAACs (a), DACs (b) and RE NHCs (c).

RE NHCs is the name typically given to NHCs with ring sizes greater than the ubiquitous 5-membered species, most commonly six to eight. The increase in ring size affords carbenes that are more basic and display larger N-C_{NHC}-N angles. The wider angle allows the N-substituents to twist and reside closer to a bound transition metal, increasing steric shielding and thereby reducing the possibility of further ligand association to the metal. The potential for stabilising lower coordinate metal centres which may possess superior catalytic properties therefore increases, with a few examples showing such behaviour having been reported.[66,71-73] However, the close proximity of the increased steric bulk to the metal centre can enhance decomposition pathways such as cyclometallation, which in turn could hinder the efficiency of a catalyst.[74-76] For example, in 2010 Whittlesey and coworkers[74] showed that substitution of 6-membered NHCs such as 6Mes or 6^{i}Pr **(Scheme 1.5)** into Ru(PPh_3)$_3$(CO)(H)Cl resulted in intramolecular C-H activation and formation of Ru(6Mes)'(PPh_3)(CO)(H) and Ru(6^{i}Pr)'(PPh_3)$_2$(CO)(H) respectively. This highlights i) the influence the widened N-C_{NHC}-N has and ii) the importance of N-substituent steric bulk on the coordination geometry of transition metal RE NHC complexes.

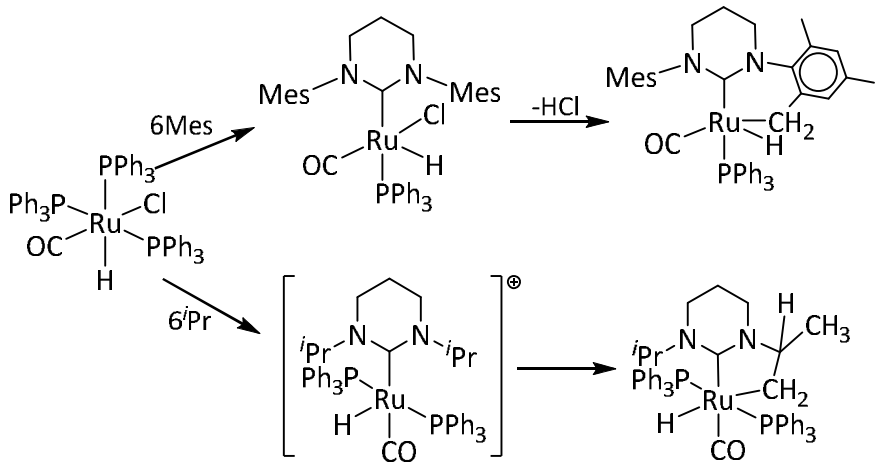

Scheme 1.5 Intramolecular C-H activation of 6Mes and 6^{i}Pr at ruthenium.

1.1.3 Mononuclear Nickel(I) NHC Complexes

Due to the properties described above in section **1.1.2**, NHCs have proven to be excellent ligands for transition metals and a wide variety of nickel-NHC complexes have been synthesised. However, Ni(I)-NHC complexes are relatively scarce with only a handful of examples reported, many of which have relevance to catalytic cycles **(Chapter 5)**. For example, studies on the ability of $Ni(IPr)_2$ ***(xvi)*** to catalyse the Negishi cross-coupling of aryl halides have led to isolation of the three coordinate, $15e^-$ species $Ni(IPr)_2Cl$ ***(xvii)***.[77] Complex ***xvi*** had previously displayed activity in a variety of cross-coupling reactions[78-80] and the mechanism was assumed to proceed through traditional oxidative addition of the aryl halide to form the four coordinate Ni(II) complex $Ni(IPr)_2(Ar)Cl$. However, during the reaction of equimolar *p*-chlorotoluene and ***xvi*** at room temperature, selective halide addition occurred generating ***xvii*** in 34 % yield **(Scheme 1.6)**. The presence of a bulky NHC results in steric clashes between the aryl electrophile and carbene. This prevents coordination of the aryl group and hinders complete oxidative addition, thus solely forming air-sensitive ***xvii***. As well as ***xvii***, the expected biaryl coupled product, 4,4'-dimethylbiphenyl (detected by NMR and GC-MS analysis), was generated as a result of radical coupling. The use of other aryl halides, including 2-chlorobenzaldehyde, 4-chlorobenzophenone and 4-chloroanisole, all afforded similar yields of ***xvii*** and the cross-coupled products.

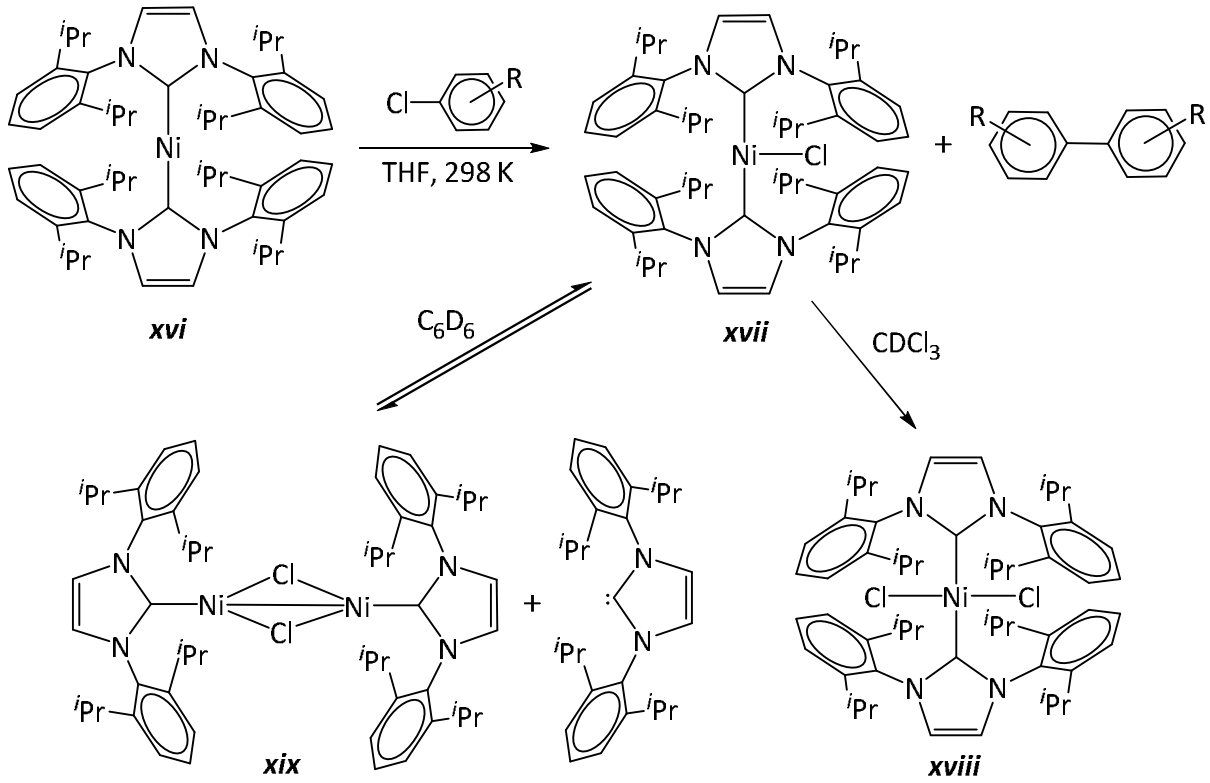

Scheme 1.6 Selective formation of a Ni(I) species **(*xvii*)** from ***xvi*** and subsequent reactivity.

Complex ***xvii*** represents the first example of a fully characterised three coordinate, monovalent nickel metal centre bearing NHC ligands. Magnetic susceptibility data, along with a broad ^{1}H NMR spectrum were testimony to its paramagnetic nature, while X-ray diffraction established a planar and T-shaped geometry. No Ni···H agostic nor Cl···H hydrogen bonding interactions involving the N-^{i}Pr substituents were observed, indicating some degree of inherent stability. The T-shaped geometry was confirmed by DFT calculations, which also showed that the unpaired electron was localised in a d_{x2-y2} non-bonding orbital with only 0.3 % distributed into the carbene π* and nickel-chloride σ* plane. This is in stark contrast to the Ni(I)-terpyridine complex, Ni(tpy)(CH_3) **(*lvi*; Chapter 5, 5.1.2.1)**, where the single unpaired electron was fully delocalised around the whole tpy ligand.[81]

When dissolved in $CDCl_3$, complex ***xvii*** formed divalent Ni(IPr)$_2$Cl$_2$ **(*xviii*)** in quantitative yield. However, no evidence of ***xviii*** was found upon addition of chloroarenes to ***xvii***, implying ***xvii*** is not prone to further reaction/oxidation with ArCl. Dissolution of ***xvii*** in C_6D_6 led to the formation of the chloro bridged dinickel complex **(*xix*)** along with free IPr **(Scheme 1.6)**.[16] When ***xvii*** was dissolved in C_6H_6 in the presence of excess IPr, ***xvii*** was the only detectable

species with no evidence of the halide bridged dimer, inferring a monomer-dimer equilibrium in solution.

Despite the assumption that oxidative addition to $Ni(NHC)_2$ (NHC = IPr) would occur, only two examples of $Ni^{II}(NHC)_n(Ar)X$ complexes bearing the relatively small IMe_4[82] and I^iPr[83] ligands have previously been reported. Based on the idea that Ni(I) halides may exhibit superior catalytic activities over their Ni(II) counterparts, Louie and coworkers[84] probed the effect of N-substituent bulk on aryl halide oxidative addition to zero-valent *bis*(NHC) nickel complexes and were able to show that this indeed does influence the nature of the observed products. Thus, treatment of $Ni(IMes)_2$ ***(xx)*** with PhX at room temperature gave the corresponding monovalent species $Ni(IMes)_2X$ (X = Br ***(xxi)***, Cl ***(xxii)***, I) in good yields (77 – 80 %). All three species showed distorted T-shaped geometries (C_{NHC}-Ni-C_{NHC} angle: 168.26(12), 166.46(16) and 166.47(10)^o respectively), with Ni-C_{NHC} bond lengths consistent with those seen in other Ni-NHC complexes.[16,77,83] Broad ^{1}H NMR spectra and archetypal ***g*** values for an unpaired spin (***g*** = 2.22 when X = I) in the EPR spectra were observed.

In order to try and promote the formation of $Ni^{II}(IMes)_2(Ar)X$, ligand displacement reactions of $Ni(PPh_3)_2(Ar)X$ with IMes at room temperature were attempted. A range of aryl groups were used: C_6H_5- (unactivated), *p*-CF_3-C_6H_4- (electron poor) and *p*-MeO-C_6H_4- (electron rich), but in all cases, $Ni^I(IMes)_2X$ species were immediately formed selectively upon addition of IMes **(Scheme 1.7)**.

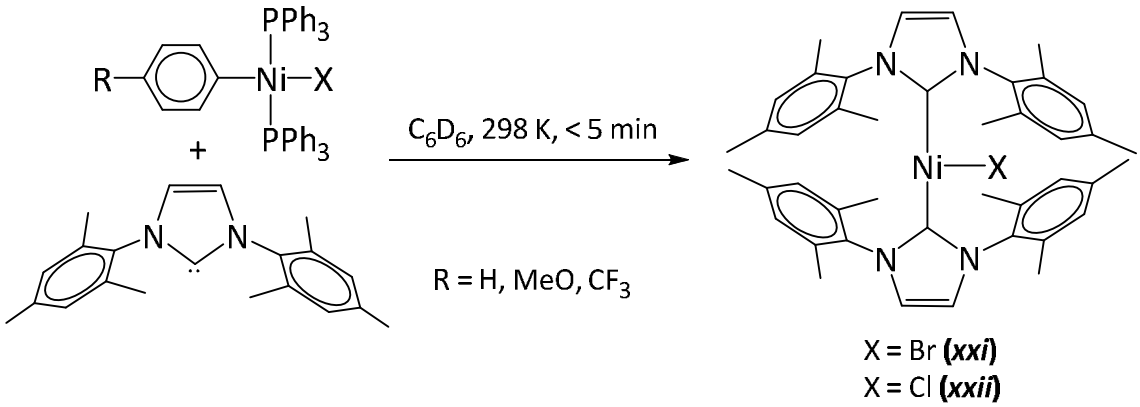

Scheme 1.7 Attempted generation of $Ni(IMes)_2(Ar)X$ (X = Br ***(xxi)***, Cl ***(xxii)***).

Treatment of $Ni(COD)_2$ with *p*-MeO-C_6H_4Br in the presence of the small IMe_4 ligand led to the isolation of $Ni(IMe_4)_2$(*p*-MeO-C_6H_4)Br (identical to a complex previously reported by Cavell)[82] in 47 % yield. The formation of a $Ni^{II}(IMe_4)_2(Ar)X$ species was observed with all electronic classes of aryl halide used: unactivated, electron poor and electron rich. The generation of Ni(I) halides is thus a feature of sterically encumbered NHC ligands (such as IMes and IPr), making the bulk of the NHC N-substituent an important consideration if a Ni(0) precatalyst is being employed in cross-coupling reactions. Smaller NHC ligands, for example those bearing N-^{i}Pr and N-Me substituents, tend to form the more conventional Ni(II)-aryl halide complexes. These findings suggests that reaction selectivity or degradation/decomposition of the assumed catalytically active Ni(0) species may alter the traditionally accepted Ni(0)/Ni(II) catalytic cycle from that in **Chapter 5 (Scheme 5.1)** to an alternative Ni(I) mediated pathway.

1.1.4 Dinuclear Nickel(I)-Nickel(I) Complexes

Nickel(I) initiated small molecule activation (described in more detail in section **1.2**) frequently features bridged dimeric Ni(I) intermediates, nearly exclusively generating a further dinuclear nickel complex as the ultimate product. Bimetallic complexes tend to contain multidentate ligands which saturate the coordination sphere and impede reactivity,[85,86] thus research into them is not as extensive as with monomeric complexes. Previous studies into Pd(I)-Pd(I) dimers and their use as initiators in catalytic redox coupling and C-H bond functionalisation have been reported,[87-90] however little has been published on dinuclear Ni(I)-Ni(I) species.[91,92] Those examples that have show catalytic potential. Thus, in 2010 Agapie and coworkers[93] reported the preparation of the Ni(I) dimer **(*xxiii*; Scheme 1.8)** from comproportionation of $Ni(COD)_2$ and $Ni(dme)Cl_2$ in the presence of a *p*-terphenyl-diphosphine. The Ni_2 core is coordinated to the phosphorus atoms creating a virtually linear P-Ni-Ni-P assembly and each nickel centre is involved in an η^2 interaction with the central ring of the terphenyl fragment. Metal aryl interactions have been previously shown to aid stabilisation of transition metal species[86,94-96] and are thought to be implicit in the stability of ***xxiii***.

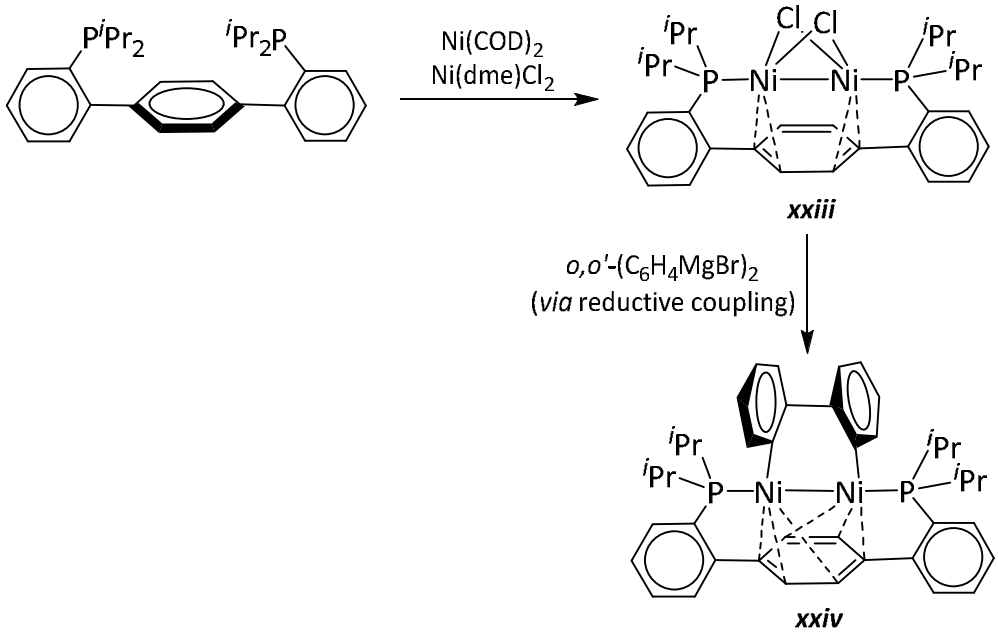

Scheme 1.8 Synthesis and reactivity of an arene stabilised Ni(I)-Ni(I) dimer ***(xxiii)***.

Within dinuclear structures, there is potential for oxidative addition to occur across both metal centres, increasing the oxidation state of each by one. These can then reductively couple and dissociate to form a cross-coupled organic compound. Reactions of ***xxiii*** with Grignard reagents were therefore carried out and the isolation of the expected Ni-hydrocarbyl species attempted in order to provide evidence for this oxidative addition process. Initial efforts with PhMgBr led to the production of the expected biphenyl cross-coupled product, although the intermediacy of '[Ni^I(Ph)(2-^{i}Pr$_2$P(*p*-terphenyl)-2-P^{i}Pr$_2$)Ni^I(Ph)]' could not be confirmed. The generation of biphenyl could also have arisen from dissociation of the Ni(I) dimer to monomeric species, which could then react *via* a monometallic route for C-C bond formation.

However, use of *o,o'*-biphenyldiyl magnesium bromide led to the isolable dinickel(I) biphenyl species **(*xxiv*; Scheme 1.8)**. The biphenyl ligand bridges the two nickel centres through two η^1 binding modes. Although the metal-arene interactions are still present between both the nickels and the central terphenyl ring, the nature of them has altered. These interactions now consist of each nickel interacting with a double bond (Ni–C: 1.98 – 2.06 Å) and a third carbon (the *ipso* carbon), although this exhibits a much longer distance (Ni-C$_{ipso}$: 2.20 – 2.30 Å). Analysis of the C=C$_{terphenyl}$ bond lengths indicates a partial loss of aromaticity of this ring. The Ni···Ni distances in ***xxiii*** (2.3658(2) Å) and ***xxiv*** (2.4426(2) Å) are believed to differ due to the steric restraints imposed by the bridging biphenyl ligand. However, they both lie in the range of reported Ni(I)-Ni(I) bond lengths (*ca.* 2.3 – 2.6 Å).[16,91-95]

The reactivity of ***xxiv*** provided an insight into potential catalytic applications. Exposure to excess CO at room temperature led to dissociation of the biphenyl bridging ligand and formation of fluorenone **(Scheme 1.9)**. Such functionalisation of biphenyl on a dimeric species is rare.[91,92] A pathway moderated by the dimeric structure (rather than a monomer) is shown in **Scheme 1.9** and involves a two electron reduction to a Ni(0)-Ni(0) dimer. This was supported experimentally by the generation of dinuclear Ni(0)-carbonyl species during the reaction.

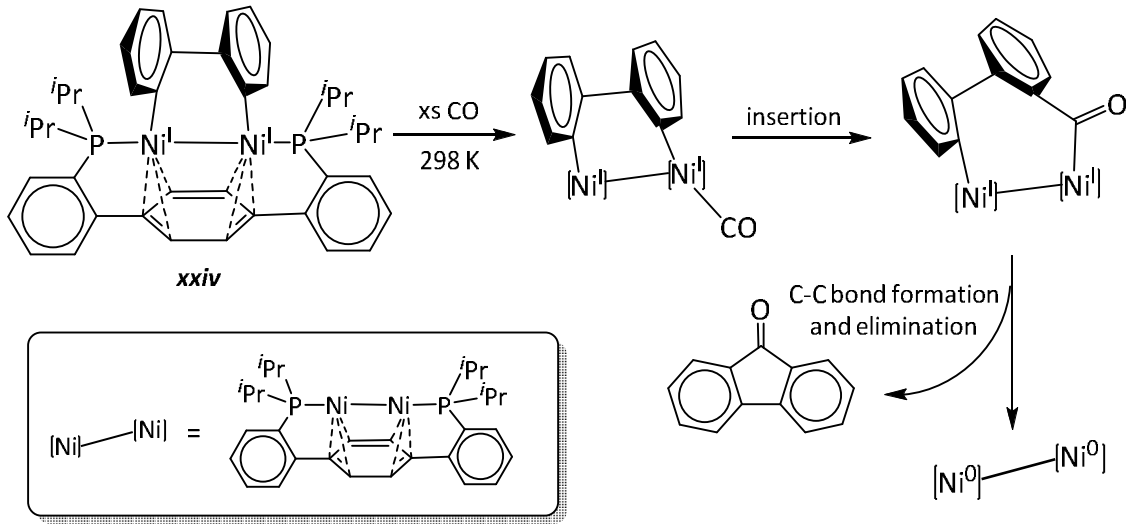

xxiv

Scheme 1.9 A proposed mechanism for reaction of the Ni(I) dimer ***xxiv*** with CO.

Reaction of ***xxiv*** with excess geminal dichloroalkanes (such as CH_2Cl_2) regenerated the initial Ni(I) dimer ***xxiii*** as well as fluorene derivatives, although this was dependent on the chloroalkane used **(Scheme 1.10)**. The intermolecular nature of this reaction suggests higher oxidation state intermediates (such as Ni(II)) are involved, despite previous studies showing stoichiometric intramolecular C-C couplings with Ni(I)-Ni(I) complexes proceeding *via* reduced Ni(0) species.[93] Thus, oxidative addition of a C-Cl bond across the two nickel centres takes place, generating a Ni(II)-Ni(II) species which can then undergo reductive elimination to form a C-C bond and a Ni(I)-Ni(I) dimer. If this process repeats itself intramolecularly, ***xxiii***, and subsequently ***xxiv***, are regenerated upon addition of more Grignard reagent. This mechanism **(Scheme 1.10)** has yet to be verified experimentally and other pathways are possible, including radical mechanisms generating partially oxidised nickel dimers (*i.e.* Ni(I)-Ni(II)) or dissociation to monomeric species. The reactivity of ***xxiv*** has hinted at the accessibility of both higher and lower oxidation state dinuclear nickel species, signifying their potential as precursors for catalytic transformations.

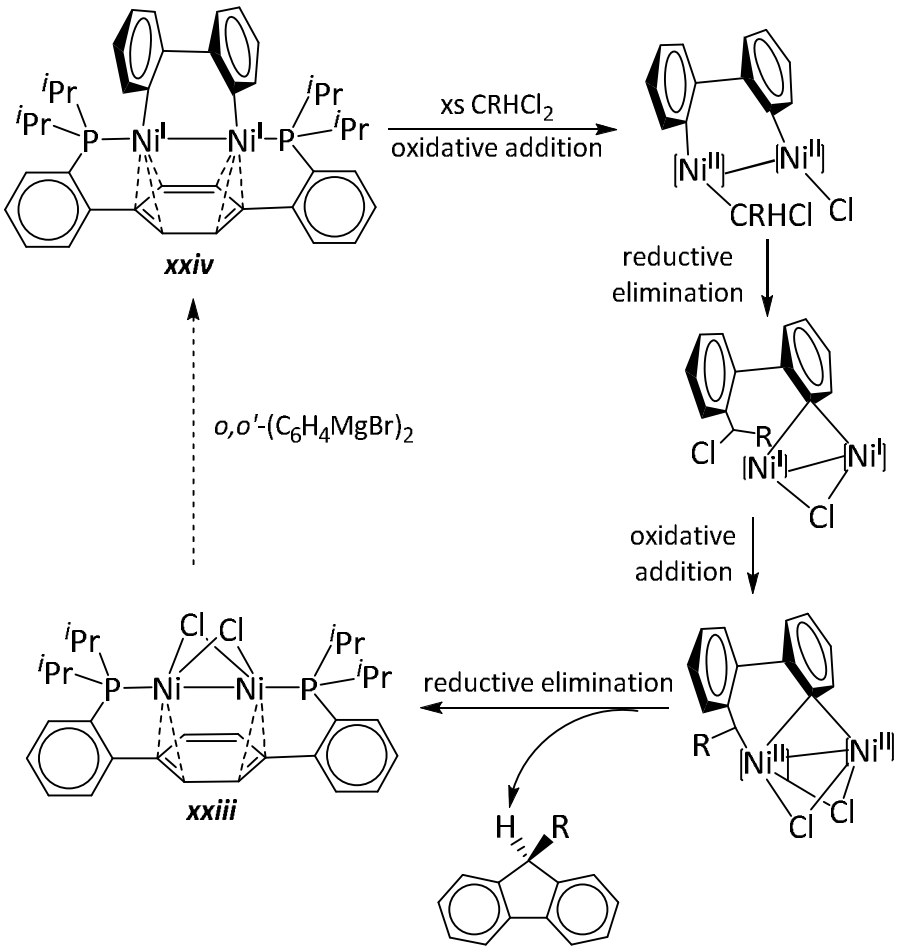

Scheme 1.10 A proposed mechanism for reaction of the Ni(I) dimer ***xxiv*** with dichloroalkanes.

In 2011, a related Ni(I)-Ni(I) dimer **(*xxvi*)** was prepared from reaction of P^iPr_3, $Ni(COD)_2$ and biphenylene, followed by reductive C-C coupling of the initially formed asymmetric Ni(III)-Ni(I) dimer ***xxv*** **(Scheme 1.11)**.[97] In ***xxv***, one biphenyl acts as a bidentate ligand bridging the two nickel metal centres *via* two η^1 σ-bonds, while the other is coplanar with one nickel metal centre (chelating to that nickel *via* two η^1 σ-bonds) and interacts with the second nickel *via* a π-interaction involving one double bond. This infers a Ni(III)-Ni(I) complex has been generated, support arising from structural features of the Ni(I) fragment conforming to previous dinuclear Ni(I)-Ni(I) species.[91,92] Upon standing for 6 h, C-C bond formation between the two biphenyl ligands in ***xxv*** took place, generating the isolable Ni(I) dimer ***xxvi***. Upon heating at 363 K, cyclic tetraphenylene was then released. $^{31}P\{^1H\}$ NMR spectroscopy showed that ***xxvi*** is the resting state for the reaction, implying ***xxvi*** is essentially converting biphenylene to tetraphenylene **(Scheme 1.11)**. Other analogues of ***xxvi*** with smaller phosphines (such as PEt_3) do not show any comparable activity for this conversion.

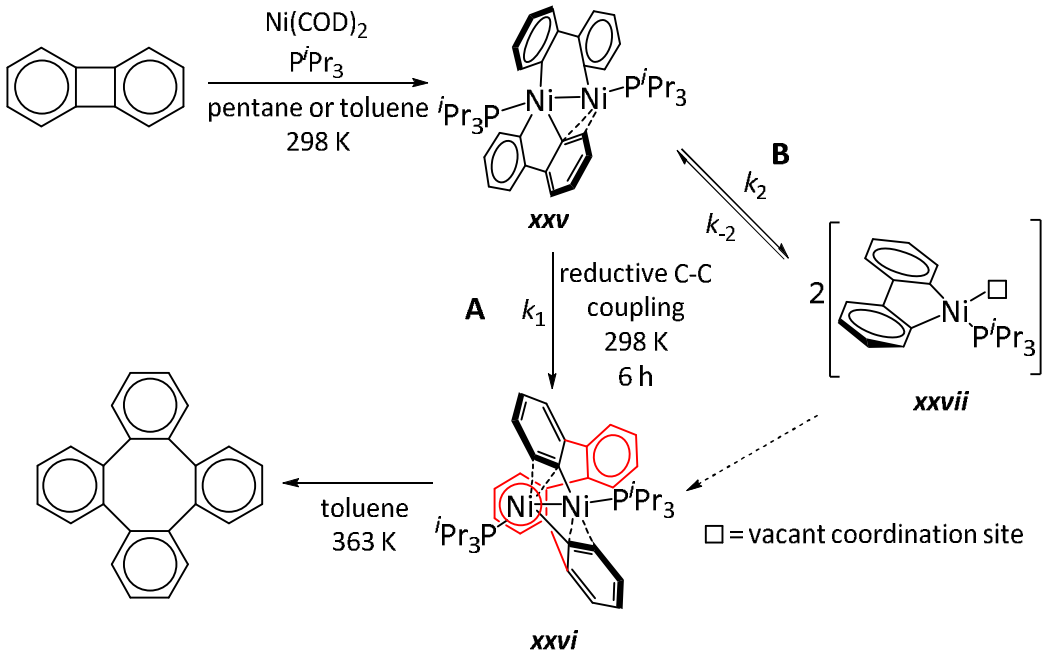

Scheme 1.11 Postulated pathways to the Ni(I)-Ni(I) dimer **(*xxvi*)**.

Reductive elimination of the *cis*-arranged biphenyl ligands at the Ni(III) metal centre in ***xxv*** was proposed as a possible mechanism for its transformation to ***xxvi*** (pathway **A**). This seemed the most logical pathway due to the highly asymmetric nature of ***xxv*** and the direct formation of ***xxvi*** without any additional metal-metal bond formations or σ-coordinated ligand rearrangements (from Ni(II)-Ni(0) intermediates) being required. Experimental support for this mechanism was provided by the calculated free energy activation barrier being a modest +8.1 ± 0.6 kcal mol^{-1}.[97] Mononuclear complexes of palladium and platinum have previously been shown to catalyse the conversion of biphenylene to tetraphenylene,[98] therefore an alternative mechanism (pathway **B**) involving a rate determining dissociation to the monomeric intermediate ***xxvii*** was postulated **(Scheme 1.11)**. DFT calculations (optimised using PMe_3 ligands) for this process gave $\Delta H_{298\ K}$ = +22.6 kcal mol^{-1}, easily attainable at room temperature. The increase in entropy upon monomer formation also makes it a favourable process. However, labelling studies with biphenylene-d_1 gave ***xxv-d*$_2$** and subsequently ***xxvi-d*$_2$**, while cross-over studies between *in situ* generated ***xxv*** and ***xxv-d*$_2$** yielded primarily ***xxvi*** and ***xxvi-d*$_2$** (with minor amount of ***xxvi-d*$_1$**), indicating that k_1 is larger than k_2. The intramolecular pathway **A** for the direct conversion of ***xxv*** to ***xxvi*** therefore appears to be supported more than the dissociative pathway **B**. The isolation of ***xxv*** and ***xxvi*** supplies evidence that asymmetric intermediates may have a key function in dinuclear nickel C-C coupling reactions

and within other associated catalytic cycles, providing further support for the importance of Ni(I) species, especially as catalytic entities.

1.1.5 Dinuclear Nickel(I)-Nickel(I) NHC Complexes

During research directed towards the formation of highly substituted π-allylnickel(II) chloride species incorporating NHC ligands, Sigman and coworkers[16] were able to synthesise the unusual Ni(I)-*bis*(μ-Cl) dimer ***(xix)***. This was later shown to be in an equilibrium with monomer ***xvii*** (section **1.1.3**).[77] $Ni(COD)_2$ was reacted with 4-chloro-2,4-dimethyl-2-pentene in the presence of IPr **(Scheme 1.12a)** and although a complex mixture of compounds was formed initially, ***xix*** was isolated (albeit in only *ca.* 20 % yield) and characterised as the major product of the reaction. It was thought that oxidative addition of the allyl chloride occurred to form a Ni(II) chloride species which, upon homolytic cleavage of the Ni(II)-carbon bond, generated the Ni(I) metal centres, a process promoted by the size of the allyl group and IPr ligands.

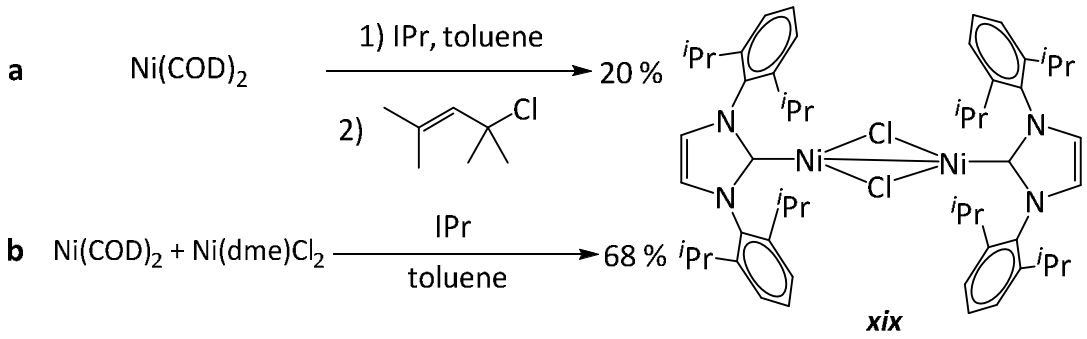

Scheme 1.12 Preparation of the Ni(I)-NHC dimer ***xix*** *via* oxidative addition/homolytic cleavage (a) and comproportionation (b) pathways.

The formation of ***xix*** initiated the development of more direct and generalised syntheses of Ni(I) complexes, accompanied by improved yields. A comproportionation reaction between equimolar quantities of Ni(0) and Ni(II) precursors, $Ni(COD)_2$ and $Ni(dme)Cl_2$, in the presence of IPr (2 eq) in toluene, was shown to give ***xix*** in a greatly enhanced yield of 68 % **(Scheme 1.12b)**. The Ni(II)-dme precursor is believed to initially chelate Ni(0) through the chlorine atoms to generate a Ni(I)-(μ-Cl) dimer, which is then trapped by the NHC ligand. X-ray crystallographic analysis of ***xix*** revealed asymmetry with regards to the IPr ligands (C_{NHC}-Ni-Ni-C_{NHC} torsion angle: 56.3(9)°), with a planar bridging structure and relatively short Ni-Ni distance (2.5194(9) Å). A single set of ligand proton resonances was observed in the solution ^{1}H NMR spectrum, suggesting that the inequivalence of the IPr groups observed in the solid-state is not

retained in solution, perhaps due to dissociation into a monomeric species.[77] Under identical reaction conditions, exchanging IPr for SIPr gave the analogous [Ni(SIPr)(μ-Cl)]$_2$ dimer, although a larger number of trace impurities were also detected.

Additional investigation into this Ni(I)-Ni(I) complex by Hillhouse and coworkers[99,100] alluded to its catalytic potential *via* the formation of further bridged species. **Scheme 1.13** shows ***xix*** reacts readily with excess N_3Mes to form a Ni(II)-Ni(II) bridging imido complex which can participate in the catalytic formation of carbodiimides (MesN=C=NR) from reaction of isocyanides. Activity was also observed for the formation of mesityl isocyanate (MesN=C=O) *via* reaction with CO.

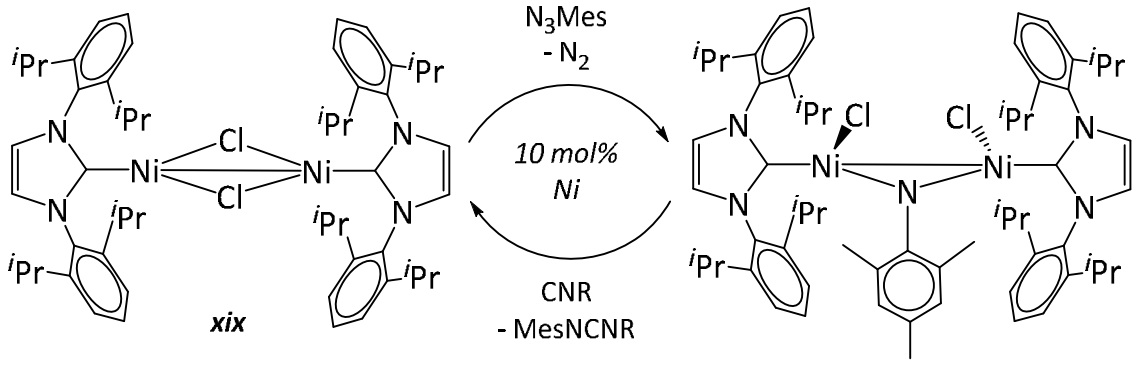

Scheme 1.13 Catalytic carbodiimide formation mediated by the dinuclear Ni(I)-IPr species ***xix***.

It was postulated that the presence of the sterically encumbered IPr ligands may provide enough stabilisation for the formation of a whole range of bridged dimers. If this bridging component is considered synthetically useful, it can then be applied to group transfer reactions. For example, reaction of ***xix*** with diazoalkanes formed the corresponding alkylidene bridged nickel systems, which acted as a carbene synthon for further reactivity. The stoichiometric reaction of ***xix*** with equimolar N_2CPh_2 in Et_2O resulted in the vigorous evolution of N_2 and formation of a complex mixture of products, including the desired Ni-(μ-CPh_2) dimer and unreacted ***xix***. Isolation of the Ni-(μ-CPh_2) intermediate could only be achieved when an equivalent of Na[BAr_4^F] was incorporated in the reaction, resulting in the clean formation of [Ni(IPr)(μ-CPh_2)(μ-Cl)Ni(IPr)]BAr_4^F ***(xxviii)*** as dark green crystals in 89 % yield **(Scheme 1.14)**. Several Ni-(μ-alkylidene) complexes had been reported previously by Carmona and coworkers,[101] however these were all formed *via* α-H elimination from cyclometallated neophyl ligands in Ni(PMe_3)$_2$(CH_2CMe_2-*o*-C_6H_4)'Ni(L) (L = a chelating phosphine *e.g.* $Me_2PCH_2CH_2PMe_2$). From X-ray crystallography, it was shown that ***xxviii*** is asymmetric in the solid-state, with the :CPh_2 functionality binding η^3 to one nickel through additional

interactions to the *ipso* carbon and an *ortho* carbon of a phenyl ring **(Scheme 1.14)**. Inspection of the Ni-$C_{alkylidene}$ bond lengths revealed that the distance between the η^1-alkylidene stabilised nickel (Ni_b) and carbon is shorter than the other Ni-$C_{alkylidene}$ bond (Ni_a-C: 1.958(3) Å; Ni_b-C: 1.831(5) Å). These values are close to those previously observed for the Ni-C single bond in [Ni(d^{t}bpe)(CH_2CMe_2Ph)]PF_6 (1.954(3) Å)[102] and Ni=C double bond in (d^{t}bpe)Ni=CPh_2[99] (1.836(2) Å) respectively. In contrast to crystallography, NMR characterisation was consistent with a symmetric C_{2v} geometry, indicating no *ipso*/*ortho* enhanced stabilisation in solution **(Scheme 1.14)**, and the ^{1}H NMR spectrum was indicative of a diamagnetic species.

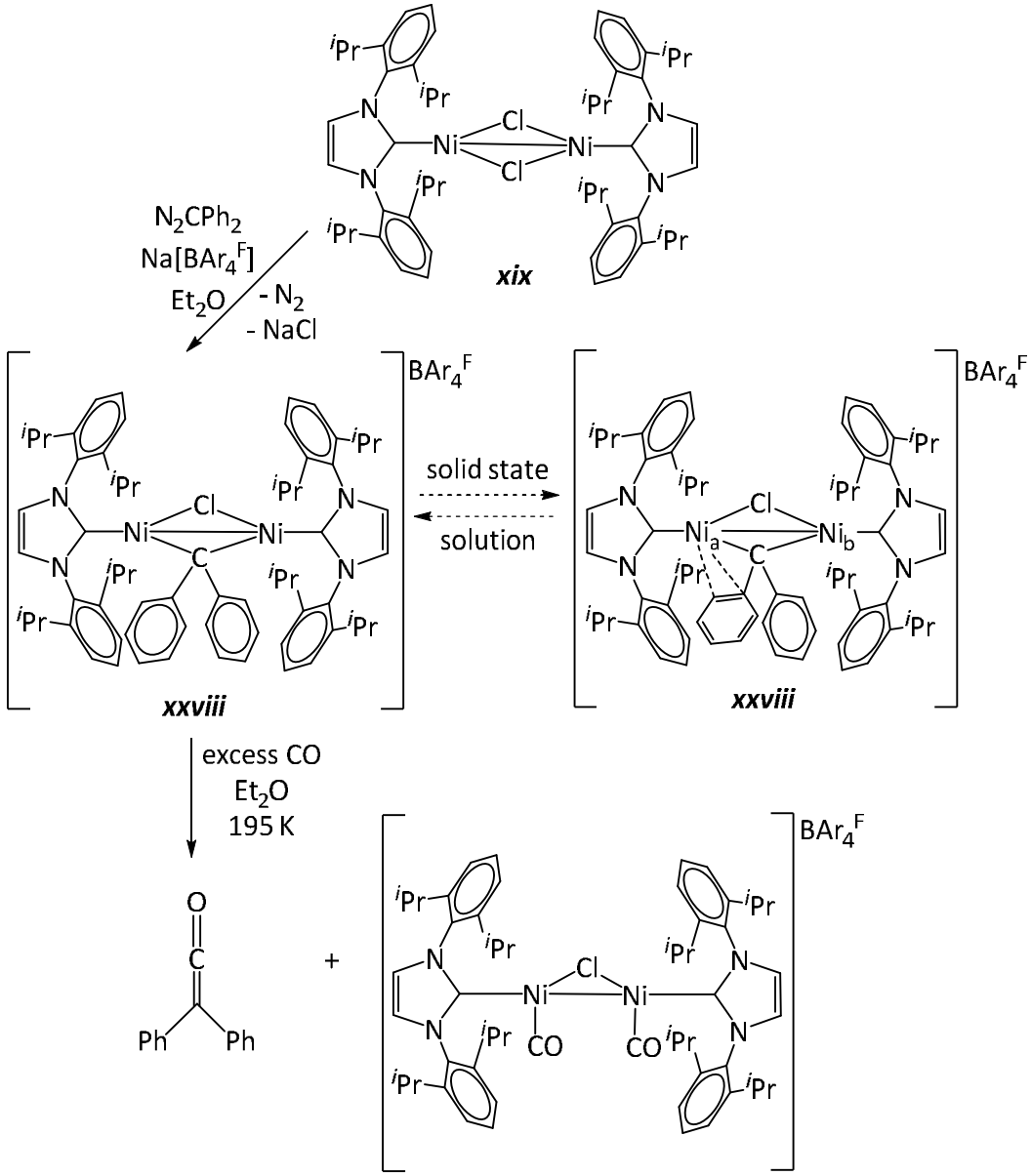

Scheme 1.14 Synthesis and reactivity of an alkylidene bridged nickel dimer ***(xxviii)***.

Related alkylidene bridged dicopper complexes have proven useful as a source of :CR_2 for addition to suitable nucleophiles.[103] Likewise, exposure of ***xxviii*** to excess CO readily and cleanly generated diphenylketene ($Ph_2C=C=O$) and the diamagnetic Ni(I)-Ni(I) carbonyl chloro bridged dimer, $[(Ni(IPr)(CO))_2(\mu\text{-}Cl)]BAr_4^F$ **(Scheme 1.14)**. This was stable in the presence of CO and no disproportionation to Ni(0) and Ni(II) was detected, contrary to the reaction of ***xix*** with CO which resulted in the formation of $Ni^0(IPr)(CO)_3$ and dimeric $[Ni^{II}(IPr)Cl(\mu\text{-}Cl)]_2$.[100] As expected for a cationic complex, the relatively short C-O bond distances in $[(Ni(IPr)(CO))_2(\mu\text{-}Cl)]BAr_4^F$ (1.134(3) and 1.145(3) Å) indicated limited backbonding from the nickel centre. This was supported by the high frequency of the ν_{CO} stretch in the IR spectrum (2023 cm^{-1}).

Successful :CR_2 transfer was also achieved in reactions of ***xxviii*** with N_3Mes and CN^tBu, which gave $Ph_2C=NMes$ and $Ph_2C=C=N^tBu$ respectively. However, the rates of reaction and fate of the nickel fragment differed significantly. Reactions with CO and CN^tBu proceed virtually instantaneously, whereas mesityl azide reacted very slowly, generating ketimine in 80 % yield over a three week period at room temperature. The reduced reaction rate is believed to arise from the decreased nucleophilicity of N_3Mes, inhibiting coordination to the sterically hindered nickel dimer and leading to only slow formation of bridging μ-N_3Mes or μ-NMes intermediates. Similarly to the reaction with CO, N_3Mes afforded a dimeric nickel product isostructural to ***xxviii***. In contrast, CN^tBu gave the monomeric Ni(I) complexes $[Ni(IPr)(CN^tBu)_3]BAr_4^F$ and $Ni(IPr)(CN^tBu)Cl$.[99,100]

1.2 Nickel(I) Mediated Small Molecule Activation

Small molecule activation by transition metal complexes is essential for a variety of stoichiometric and catalytic organic transformations, and typically involves metal centres with low oxidation states and low coordination numbers. Isolable, three coordinate Ni(I) species are therefore theoretically appealing precursors for small molecule activation, as they provide a redox active metal centre in combination with vacant coordination sites suitable for interacting with such molecules.[104]

Ni(I)-β-diketiminate complexes have shown huge affinity towards activation or functionalisation of small molecules, including H_2, N_2, SF_6, O_2, CO, P_4, S_8, N_2O and CO_2.[16,104-110] Nickel-hydride or –(η^2-H_2) coordinated complexes are of considerable interest, due to their postulated involvement in catalytic hydrogenation processes. For example, one of the main intermediates in the catalytic cycle of the mixed metallic dimer [Ni-Fe]-hydrogenase is

proposed to contain hydride ligands bridging the nickel and iron centres.[111,112] Pfirrmann *et al.*[105,113] employed nickel compounds based on β-diketiminate ligands to form Ni(I)-(μ-H)/(μ-N_2) species. Reduction of the Ni(II) dimer [Ni(N^N^{Me})(μ-Br)]$_2$ (N^N^{Me} = β-diketiminate [HC(C(Me)N(C$_6$H$_3$(^{i}Pr)$_2$))$_2$]$^-$) with KC_8 in toluene led to the isolation of [Ni(N^N^{Me})]$_2$ in 23 % yield **(*xxix*; Scheme 1.15)**. In ***xxix***, each nickel is bound to the nitrogen atoms of a β-diketiminate ligand, as well as in an η^2 fashion to an aryl ring on the second Ni-(N^N^{Me}) unit to give distorted T-shaped nickel centres (N_a-Ni-C_a: 149.56(6)°; N_b-Ni-C_a: 106.45(6)°).[22,113-115] The aryl rings interacting with the nickel atoms are close to parallel and, as a result, provide enhanced stabilisation of the Ni(I) dimer through π-π interactions. At room temperature, solid-state and solution magnetic measurements were consistent with the presence of two Ni(I) centres. However, at low temperatures (77 K), frozen hexane solutions and solid samples were EPR silent. This was attributed to antiferromagnetic coupling between the two Ni(I) metal centres, with DFT calculations confirming thermal energy disrupting this coupling at room temperature.

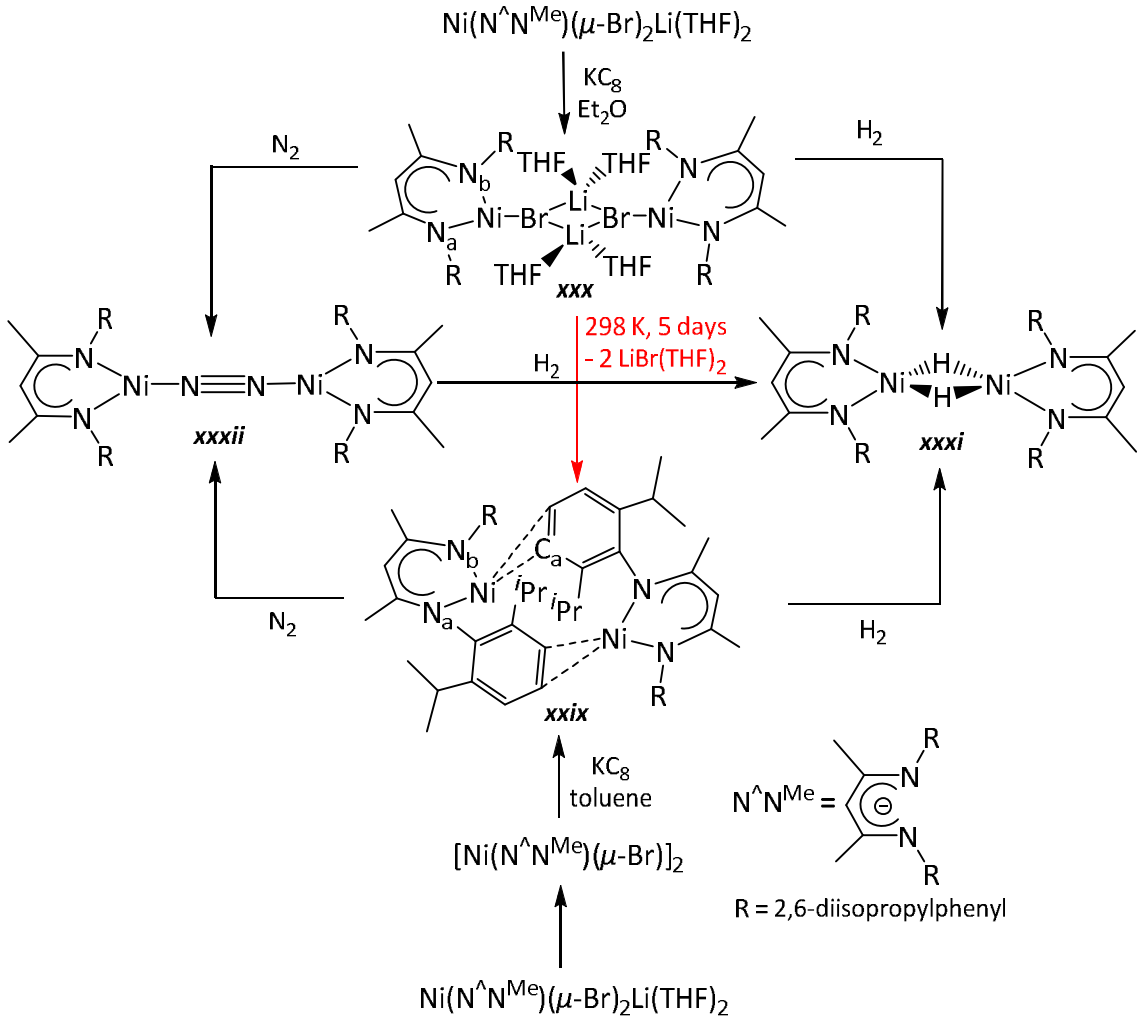

Scheme 1.15 N_2 and H_2 activation by Ni(I)-β-diketiminate dimers (***xxix*** and ***xxx***).

In contrast, direct reaction of the 'ate complex', Ni(N^N^{Me})(μ-Br)$_2$Li(THF)$_2$, with KC_8 in Et_2O gave [Ni(N^N^{Me})(μ-Br)Li(THF)$_2$]$_2$ **(*xxx*; Scheme 1.15)** instead. Crystallographic analysis of ***xxx*** showed two Ni(I)-(N^N^{Me}) moieties coordinated to a Br_2Li_2 central unit, again leading to a distorted T-shaped arrangement around the nickels (N_a-Ni-Br: 146.66(16)^o; N_b-Ni-Br: 114.28(15)^o). Each lithium ion was bound to two THF molecules to afford tetrahedral alkali metal centres. This coordination motif is similar to that in the known iron compound Fe(N^N^{tBu})(KCl){18-crown-6}.[116] EPR analysis (rhombic profile) and solution magnetic moments (μ_{eff} = 2.58 μB; μ_{eff} (calculated for two uncoupled Ni(I) units) = 2.45 μB) were as expected and confirmed a Ni(I) oxidation state. When concentrated solutions of ***xxx*** were stored at room temperature for several days, LiBr(THF)$_2$ precipitated out and crystalline ***xxix*** was produced, implying that ***xxx*** has only a metastable existence.

Exposure of both ***xxix*** and ***xxx*** to H_2 and N_2 formed Ni(II)-(μ-H)/(μ-N_2) bridged dimers. Addition of H_2 to a hexane solution of ***xxx*** led to the formation of a green solution over 16 h, which, upon simple work, afforded the hydride bridged dimer ***xxxi*** **(Scheme 1.15)** in 53 % yield. When ***xxix*** was reacted with H_2, an immediate colour change from brown to red-orange was observed followed by a gradual change to green over 12h. This also generated ***xxxi*** (86 % yield). The initial colour change was attributed to the formation of an intermediate species, which unfortunately could not be identified. It is believed that these reactions proceed due to weak ligation of the bridging atoms in ***xxix*** and ***xxx***, along with their strained structures. In contrast to relatively slow H_2 activation, hexane solutions of ***xxix*** and ***xxx*** both reacted instantaneously with N_2 precipitating out the end-on dinitrogen bridged complex (Ni(N^N^{Me}))$_2$(μ-N_2) **(*xxxii*; Scheme 1.15)**. Although analogous to the known iron complex, (Fe(N^N^{tBu}))$_2$(μ-N_2),[117] the N_2 unit appears to be more activated in ***xxxii*** since subsequent exposure to H_2 generated ***xxxi***, whereas no reaction was seen in the case of iron.

The N^N^{tBu} analogue of ***xxxii*** **(*xxxiii*; Scheme 1.16)** was synthesised and shown to react very readily with potent greenhouse gas SF_6.[118] Thus, exposure of a benzene solution of ***xxxiii*** to 1 eq of SF_6 generated two Ni(II) complexes, Ni(N^N^{tBu})F and (Ni(N^N^{tBu}))$_2$(μ-S), in a ratio of *ca.* 2:1 respectively **(Scheme 1.16)**. X-ray crystallography provided unequivocal evidence of the Ni(II)-F and bridging sulfide complexes, with Ni(N^N^{tBu})F being the first structurally characterised example of a three coordinate nickel fluoride complex and (Ni(N^N^{tBu}))$_2$(μ-S) exhibiting an extremely rare, almost linear, [Ni^{II}-(μ-S)-Ni^{II}]$^{2+}$ central core (Ni-S-Ni: 177.85(5)^o). When exposed to more than 5 eq of SF_6, the yield of the fluoride product increased, suggesting the simultaneous formation of gaseous sulfur fluorides (such as SF_4 or S_2F_{10}) or elemental

sulfur. This work is of interest due to the very few examples of SF_6 activation reactions. Those that are reported often involve the use of elevated temperatures and pressures or the reaction of strong reducing agents (most commonly elemental alkali metals).[118,119] The facile reactivity of ***xxix*** and ***xxx*** with H_2/N_2 and ***xxxiii*** with SF_6 highlights the potential application of reduced nickel atoms for activation reactions and the potential selective activation of extremely inert molecules and functional groups.

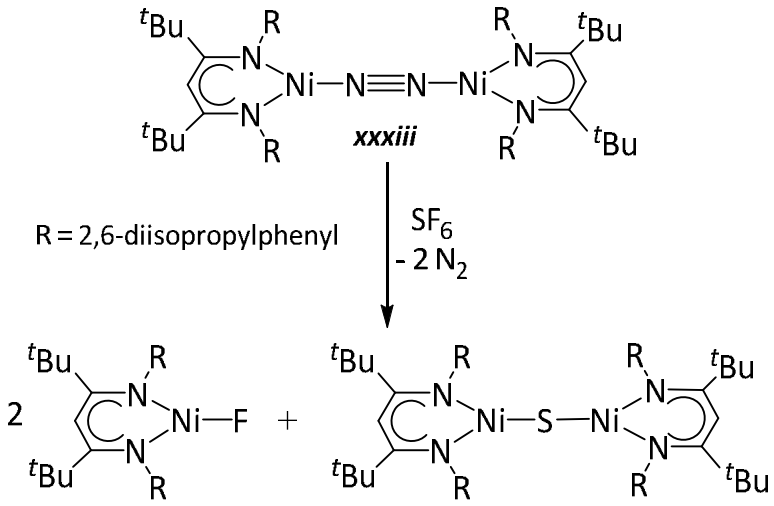

Scheme 1.16 Reaction of the Ni(I)-β-diketiminate dimer ***xxxiii*** with SF_6 to form Ni(II) species.

1.2.1 Activation of O_2

Previous studies of O_2 incorporation using H_2O_2 and Ni(II) salts have brought to light many nickel-dioxygen structural motifs, where the oxygen atoms can coordinate to the nickel as either terminal/bridging oxo (O), end-on/side-on superoxo ($[O_2]^-$) or end-on/side-on peroxo ($[O_2]^{2-}$) ligands **(Figure 1.6)**. Depending on the ancillary ligand environment and electronic composition, the nickel can reside in a variety of oxidation states, meaning any of these coordination modes are accessible for Ni(I) complexes.

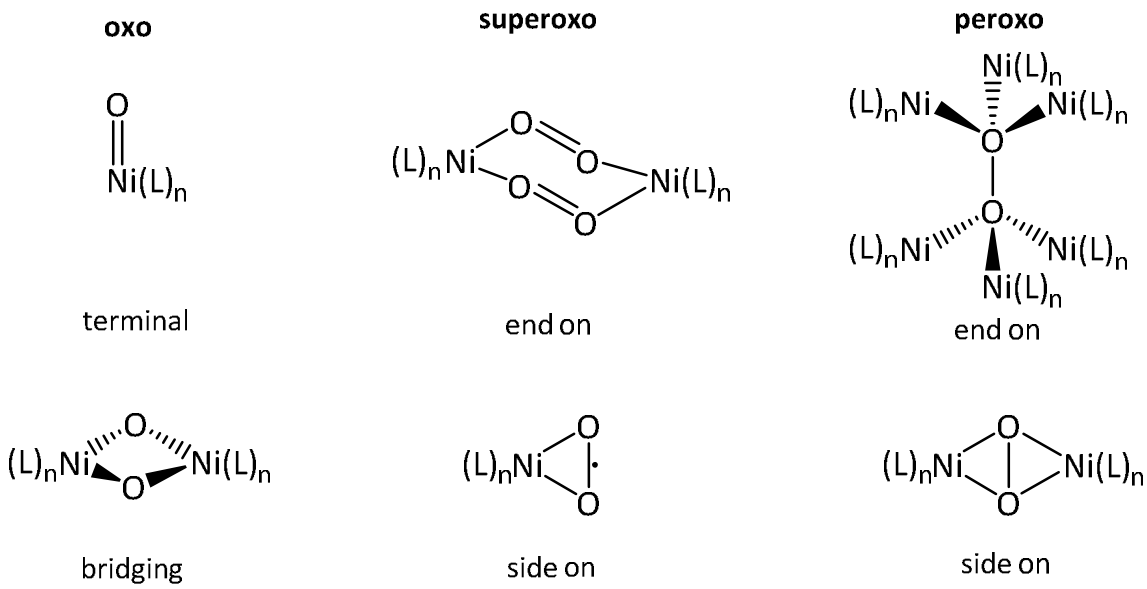

Figure 1.6 Coordination modes of oxo, superoxo and peroxo ligands in $Ni(L)_n$ complexes.

Driess and coworkers[104,120] reported the rapid, low temperature (195 K) reaction of the Ni(I)-β-diketiminate complex **(*xxxiv*; Scheme 1.17)** with O_2 to give the Ni(II)-superoxo complex ***xxxv***, which was isolated in 84 % yield. X-ray quality dark green crystals of ***xxxv*** confirmed the side-on coordination of the $[O_2]^-$ ligand, coplanar with the C_3N_2Ni ring. The O-O bond distance of 1.347(2) Å and ν_{OO} IR frequency of 971 cm^{-1} were consistent with assignment as a superoxo species (superoxo bond lengths: < 1.4 Å). EPR spectroscopy, in conjunction with DFT calculations, confirmed the paramagnetic nature of ***xxxv*** and an S = ½ ground state. The ***g*** values were consistent with that of $[O_2]^-$ dissolved in water,[121] while the SOMO was predicted to be the π^* orbital of the O_2 moiety, suggesting that the unpaired electron is located completely on the oxygen atoms. Complex ***xxxv*** is therefore thought to represent a genuine Ni(II)-superoxo complex. As anticipated for such a low coordinate species, oxygen transfer was facile, as shown with PPh_3 to give PPh_3=O. The Ni(II)-*bis*(μ-hydroxyl) dimer ***xxxvi*** **(Scheme 1.17)** was isolated as the nickel containing product of the reaction, presumably *via* a Ni=O oxo intermediate. Complex ***xxxvi*** was also formed upon treating ***xxxv*** with 0.5 eq ***xxxiv***. As with other doubly bridged dinuclear species, the d^8 Ni(II) metal centres in ***xxxvi*** adopt square plane geometries. An analogue of this hydroxyl bridged nickel dimer ($[Ni(N\hat{}N^{Et})(\mu\text{-}OH)]_2$) has been generated directly upon addition of O_2 to the $N\hat{}N^{Et}$ derivative of ***xxxiv***, showing that the N-substituents play no steric role in determining the pathway for O_2 activation.[104]

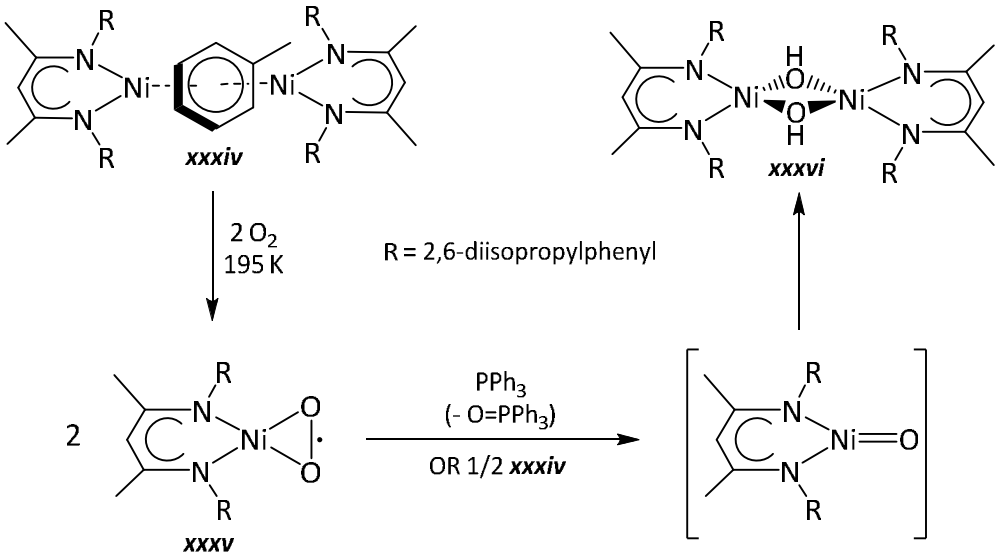

Scheme 1.17 Activation of O_2 with a Ni(I)-β-diketiminate complex ***(xxxiv)*** to generate the Ni(II)-superoxo species ***xxxv*** and its subsequent reactivity.

The versatility of ***xxxv*** as an oxidising agent has been investigated further. Although it was inert towards substrates bearing weak C-H bonds, such as 9,10-dihydroanthracene, it was active for the oxidation of O-H groups,[104,122] readily converting cyclohexanol and 1-phenylethanol to their corresponding ketones and 2,6-di-*tert*butylphenol to 2,6-di-*tert*butyl-1,4-benzoquinone **(Scheme 1.18)**. In the latter, an O-atom is transferred from the superoxo ligand to the *para* position of the phenol. N-H activation was also possible, with azobenzene formed as the sole oxidised product from 1,2-diphenylhydrazine. It is believed that the reactions proceed through initial abstraction of a hydrogen atom from either the O-H or N-H group in the substrates. Perhaps most surprisingly, ***xxxv*** acted as a dioxygenating agent when reacted with 2,4,6-tri-*tert*butylphenol, yielding an oxidation product incorporating two separate oxygen atoms from a single $[O_2]^-$ unit **(Scheme 1.18)**. Such results suggest great promise for providing organometallic complexes with selective oxygenating properties, making fundamental reactivity studies of great importance for understanding Ni(I) mediated O_2 activation.

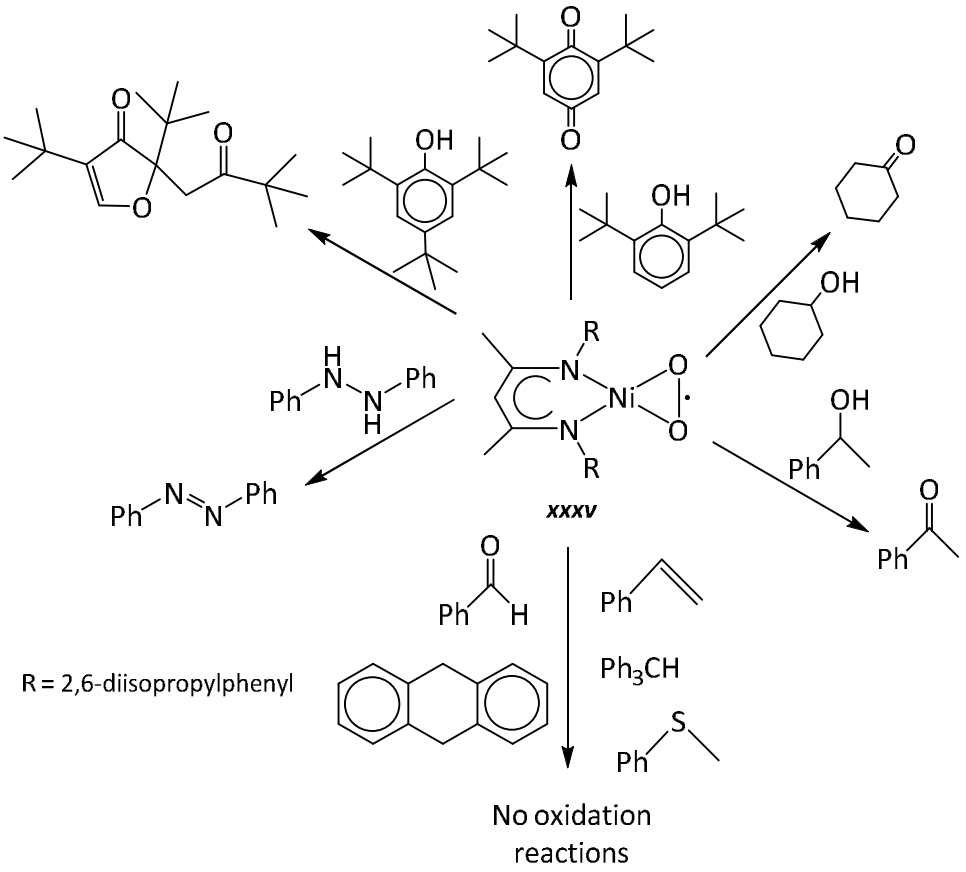

Scheme 1.18 Driess's reported use of ***xxxv*** for the oxidation of various substrates.

The 1e$^-$ reduction of THF solutions of ***xxxv*** with potassium bought about a colour change from green to brown-red and formation of a single diamagnetic product. Structural characterisation of brown crystals revealed a heterobimetallic peroxo dimer **(*xxxvii*; Scheme 1.19)** featuring a Ni(II) centre with a square planar geometry, along with a potassium coordinated crown ether bridged by a η^2:η^2-O_2 ligand. The planar Ni(μ-η^2:η^2-O_2)K core revealed an O-O distance significantly longer than in ***xxxv*** (***xxxvii*** 1.468(2) Å; ***xxxv*** 1.347(2) Å), but similar to the distances measured for other M-peroxo complexes (between 1.4 – 1.5 Å).[123] Complex ***xxxvii*** is a great deal more stable than ***xxxv*** and showed no activity towards the types of substrates shown in **Scheme 1.18**. Transmetallation of the potassium ion to form a direct Ni/Fe analogue *via* reaction of ***xxxvii*** with an iron(II)-β-diketiminate species proved unsuccessful, with scission of the O-O bond followed by hydrogen abstraction taking place to afford a heterobimetallic *bis*(μ-OH) bridged complex, Ni(L)(μ-OH)$_2$Fe(L) **(Scheme 1.19)**, analogous to ***xxxvi***. DFT calculations suggested the reaction proceeded *via* the intermediacy of ***xxxviii***, which featured two cleaved oxygen atoms generating a species with diradical character. However, this effect was diluted by the presence of the Ni(II) metal centre, polarising the Ni-O bonds and thus accounting for the observed H abstraction from any source in the surrounding reaction media.

This highlights the importance of any subtle electronic changes in the reactivity of heterobimetallic peroxo complexes, and probably accounts for why superoxo species are generally formed preferentially. Efforts to achieve the desired Ni/Fe peroxo product were attempted *via* the reverse synthesis, starting with oxidation of iron(I) precursors to form a superoxo complex. Despite leading to bimetallic μ-O_2 bridged complexes, these resulted in C-H activation of the ^{i}Pr groups on the β-diketiminate ligand coordinated to nickel **(*xxxix*; Scheme 1.19)**.

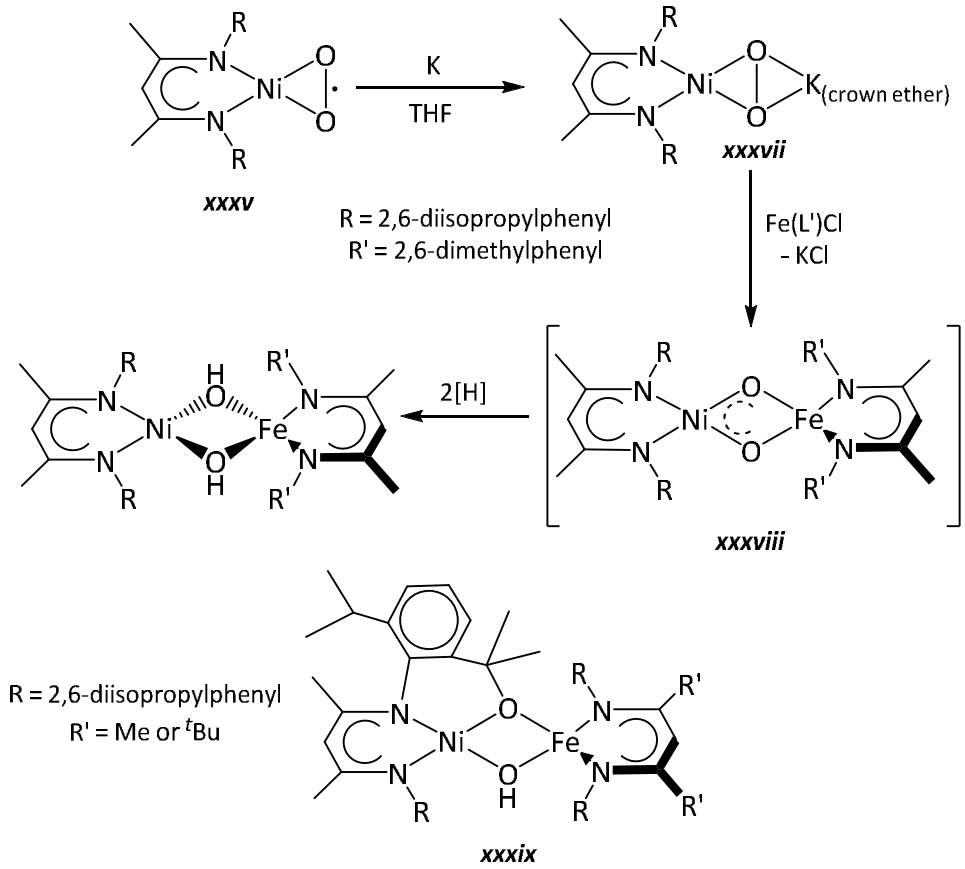

Scheme 1.19 Reactivity of nickel superoxo **(*xxxv*)** and peroxo **(*xxxvii*)** species to form the heterobimetallic dimer ***xxxviii***. ***xxxix***: a C-H activated analogue.

Early work by Riordan and coworkers[124] into O_2 activation with tripodal thioether supported Ni(I) complexes showed that purple crystals of a *bis*(μ-oxo) dimer, [Ni(PhTt$^{t\text{Bu}}$)(μ-O)]$_2$ **(*xl*)** (PhTt$^{t\text{Bu}}$ = phenyl(*tris*(*tert*butylthiomethyl))borate), were formed when toluene solutions of the ^{t}Bu substituted precursor were exposed to dry O_2 **(Scheme 1.20)**. The product was shown to be thermally unstable with a $t_{1/2}$ of only 5 min. X-ray crystallography confirmed the molecular connectivity, while UV-vis analysis afforded spectra consistent with bridging oxygen atoms and an oxygen to metal charge transfer (CT) band (565 nm). The Ni-O and Ni···Ni distances (1.82 and

2.83 Å respectively) were found to be typical of related species containing a $M_2(\mu\text{-}O)_2$ core (*e.g.* $Cu_2(\mu\text{-}O)_2$ derivatives with 1.90 and 3.48 Å).[125] No oxidation of alkenes or phosphines was observed, presumably due to the ^{t}Bu groups blocking access to the metal centre.

To promote formation of a monomeric species, the bulkier adamantyl precursor was synthesised. IR spectra suggested there was no electronic difference between the two Ni-CO complexes: Ni(PhTt^{tBu})(CO): 1999 cm^{-1}; Ni(PhTt^{Ad})(CO): 1997 cm^{-1}. When exposed to O_2 at low temperatures, the steric implications of the adamantyl ligand were apparent with oxygenation of Ni(PhTt^{Ad})(CO) affording the mononuclear adduct ***xli*** **(Scheme 1.20)**.

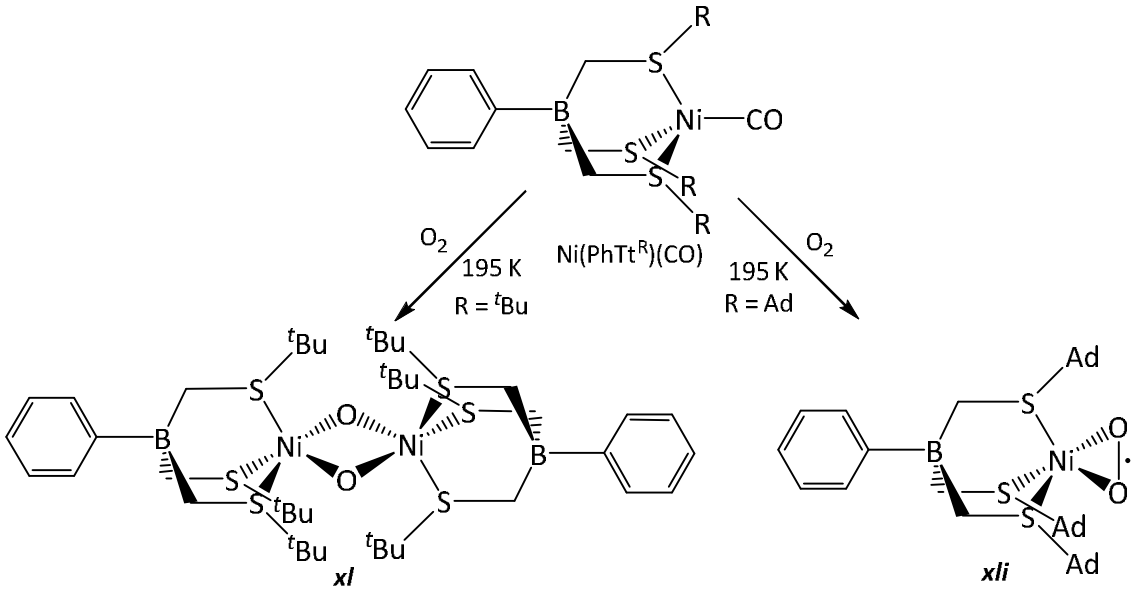

Scheme 1.20 Different O_2 activation pathways with R = ^{t}Bu or Ad for the tripodal stabilised Ni(I)-thioether complexes.

As with ***xl***, ***xli*** was only stable at low temperature, although it was shown conclusively to be monomeric on the basis of differences in the spectroscopic data and reactivity. Instead of a single UV-vis signal (565 nm for ***xl***), four absorption bands were found at 310, 386, 450 and 845 nm. DFT calculations, along with NMR and EPR spectra, were consistent with a paramagnetic compound containing one unpaired electron in a d_{z2} orbital. Although X-ray quality crystals were unattainable, computational and Ni EXAFS data fitted to a side-on bound O_2 motif, this geometry being *ca.* 10 kcal mol^{-1} more favourable than the end-on isomer. DFT analysis into the ν_{OO} stretches allowed further insight into the nature of the bond and extent of CT associated with O_2 ligation. The computed O-O distance of 1.38 Å is shorter than that expected for a peroxo compound (typically > 1.4 Å), suggesting that the monomer exhibits superoxo character. The nickel XAS displayed a pre-edge 1s → 3d transition at 8331.4 eV,

intermediate in value between Ni(I) and Ni(III). Complex ***xli*** is thus best considered as a Ni(II) superoxo species. As the oxidising core of the monomer is more accessible than in the sterically shielded dimer ***xl***, its reactivity is a lot more extensive, with PPh_3 readily oxidised to $O{=}PPh_3$.

1.3 Two Coordinate Transition Metal Complexes (ML_2)

Stable metal complexes with open shell electronic configurations (d^1 – d^9) in which the environment around the metal centre is strictly two coordinate or quasi-two coordinate are extremely rare, and are among the least researched in transition metal coordination chemistry.[126] Their paucity is mostly due to two factors. Firstly, such species nearly always exhibit extreme air and moisture instability, thus hindering simple experimentation and increasing the likelihood of side reactions with small molecules (such as O_2, N_2, N_2O and CO) or coordination to Lewis bases (*i.e.* phosphines, THF, pyridine). Secondly, the highly unsaturated coordination sphere raises the possibility of monomer association to produce aggregates or extended ionic lattices which display the more commonly observed and electronically more stable four or six coordinate metal environments.[126] The strategy of utilising sterically encumbered ligands to prevent such association, and hence stabilise low coordinate transition metal complexes at room temperature, has previously proven successful for the synthesis and isolation of ML_2 species. Most examples to date are based on the use of bulky amide, aryl, alkyl or alkoxo groups to stabilise first row (V – Ni) ML_2 complexes.

1.3.1 ML_2 Magnetic Properties and Single Molecular Magnets (SMMs)

In an extensive review of open-shell ML_2 complexes, Power[126] noted that within all the structurally characterised examples, a mere *ca.* 20 % displayed a highly linear geometry, with the rest greatly varying in their extent of deviation from linearity. The linear complexes are of specific interest because of the possibility of magnetic properties arising from unequal occupation of orbitals. The *d* orbital splitting arrangement for a typical linear ML_2 complex is shown in **Figure 1.7**. When an odd number of electrons reside in the degenerate $d_{x2\text{-}y2}/d_{xy}$ or d_{xz}/d_{yz} orbitals, this gives rise to a 1st order orbital magnetic moment and large magnetic anisotropy. In higher coordinate transition metal complexes, this magnetism is often quenched by the ligand field. However, for truly linear species where the ligands are positioned along just one of the axes (the z axis by convention), the magnetic moment remains unquenched due to the absence of any ligands directly interacting with these orbitals.

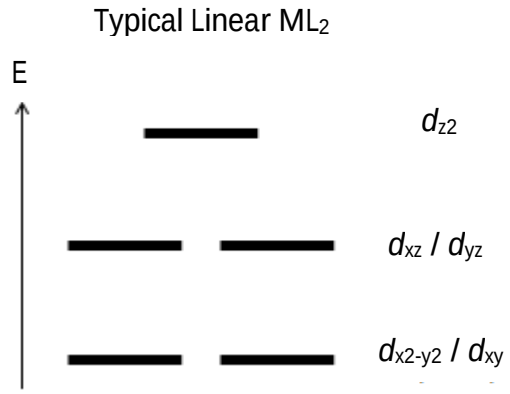

Figure 1.7 Splitting pattern for the metal based *d* orbitals in a typical linear ML_2 complex.

The presence of magnetic anisotropy is often related to complexes demonstrating single molecular magnetic (SMM) behaviour (although as demonstrated in **Chapter 2, 2.5**, this is not always the case). A SMM typically has at least one metallic ion (commonly a d- or f-block element) with an anisotropic electronic structure, which possesses the ability to retain magnetisation for relatively long periods of time in the absence of an applied magnetic field, invariably at low temperatures.[127] Within a bulk sample of material, each individual complex will display a magnetic moment of preferred orientation independent of an external field, ultimately leading to an overall net magnetisation. In an applied magnetic field, this net magnetisation will align itself along the field axis. However, when the applied field is removed or the orientation is lost through processes such as simple magnetic moment reversal, the level of magnetisation left (remanence magnetisation) is responsible for any SMM characteristics. This can only be achieved upon overcoming a thermal barrier known as the anisotropy barrier, U_{eff}. The magnitude of U_{eff} is therefore a metric by which to compare the success of different SMMs, with complexes which display a greater barrier usually exhibiting SMM properties at higher temperatures. A high degree of inherent orbital angular momentum (arising from unequal electronic configurations in the orbital splitting patterns in **Figure 1.7**) in a complex is a major contributor to its extent of zero-field splitting and hence influences its U_{eff} and SMM character. Any complexes with the potential for magnetic anisotropy should therefore be subject to magnetisation calculations.

The U_{eff} value is measured *via* magnetic susceptibility measurements in a small alternating current (ac) magnetic field, performed in either dc field (zero-static) or an applied dc field. In-phase (χ') and out-of-phase (χ'') components of magnetic susceptibility are produced as a function of both temperature and ac frequency (ν). Using the relationship shown in **Equation 1a**, the relaxation time (τ) of the complex can be extracted from the $\chi''(\nu)$ data.

U_{eff} values can then be determined from **Equation 1b** and the resulting ln τ *vs.* T^{-1} Arrhenius plot, thus describing a regime in which relaxation is thermally activated.[127]

a $\tau = 1/(2\pi\nu)$

ν = peak maximum

b $\tau = \tau_0 \exp(U_{eff}/k_B T)$

Equation 1 Equations to determine relaxation time (a) and anisotropy barrier (b) for SMMs.

Another method to determine SMM properties is to analyse the field dependence of magnetisation over a range of low temperatures (magnetic hysteresis). When subjected to a reverse magnetic field (H) and then subsequently returned to zero-field conditions, a 'magnetic' molecule will retain its magnetisation and thus display nonzero values of magnetisation (*M*). This phenomenon is called hysteresis, with a maximum temperature existing (the blocking temperature, T_b) at which this can occur. The extent of *M* is temperature and sweep width dependent, allowing further inferences to be made from the data.

Transition metal SMMs have been known for *ca.* 30 years and are extensively researched alongside lanthanide based SMMs.[127-131] However, low coordinate transition metal complexes are relatively new and have shown remarkable properties for the development of devices which produce electronic readouts of magnetic properties, such as nuclear spin of individual molecules.[127] In spite of this, the low T_b value associated with SMMs is the main limitation for them being utilised widely in industry. The major challenge is therefore to find SMMs with higher blocking temperatures for future development of device applications.

1.3.2 Two Coordinate Nickel Complexes (NiL_2)

Two coordinate nickel complexes are reported in the literature, however, the reaction chemistry is relatively under developed compared to other first row analogues.[126] In spite of this, the reactivity that has been described has displayed features that seem unique to nickel, especially regarding the ability to demonstrate two coordination in a range of different oxidation states: Ni(0), Ni(I) and Ni(II). The major constraint on developing NiL_2 chemistry is the lack of suitable low coordinate synthons with high hydrocarbon solubility at room temperature. For example, the early derived *bis*(amido) complex $Ni(N(SiMe_3)_2)_2$ was isolated from a salt metathesis reaction as a red oil. However, unlike its Fe, Mn and Co analogues, it

decomposes to a black gelatinous substance upon standing and when in contact with solvents at room temperature.[126,132]

The first structurally characterised two coordinate Ni(II) complexes were also synthesised *via* salt metathesis, in the form of the red borylamido species $Ni(N(Ar)(BMes_2))_2$ (Ar = Ph, Mes) **(Figure 1.8)**. Both complexes displayed bent structures, with the Ph analogue deviating most from linearity (N-Ni-N angle: 135.7(1)° (Ph) and 167.1(9)° (Mes)). As a result, the distance between the nickel and closest approaching ligand aryl groups, were, unsurprisingly, significantly shorter in the Ph variant ($Ni\cdots C_{aryl}$: 2.370(3) and 2.402(4) Å) than the Mes analogue ($Ni\cdots C_{aryl}$: 2.611(3) and 2.703(3) Å).[126,133,134] Derivatives bearing less bulky primary amides $(Ni(NH(Ar))_2$ (Ar = C_6H_3-2,6-($C_6H_m{}^iPr_n$) (when n = 2, m = 3; n = 3, m = 2)) were recently reported **(Figure 1.8)**.[135,136] In both cases, linear coordination was observed (N-Ni-N angle: 180.0(2) (n = 2) and 180.0(4)° (n = 3)), highlighting the importance of sterics in influencing the extent of bending.

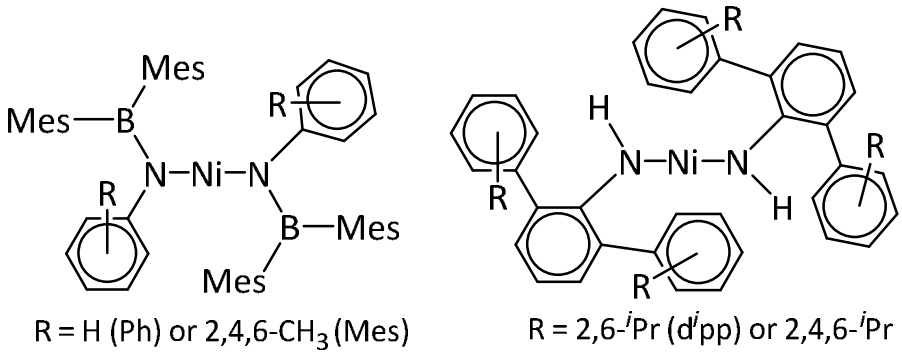

Figure 1.8 Ni(II) NiL_2 complexes $Ni(N(Ar)(BMes_2))_2$ (left) and $Ni(NH(Ar))_2$ (right).

Within the handful of NiL_2 species known, the monovalent oxidation state features heavily, often with the nickel coordinated to a neutral phosphine or carbene donor ligand in combination with anionic amido or thiolato coligands. The first examples of these were reported in 2008 by Hillhouse and coworkers.[137] The reaction of Sigman's dimer ***xix*** with 2 eq $NaN(SiMe_3)_2$ gave the $13e^-$, two coordinate, monomeric amide complex, $Ni(IPr)(N(SiMe_3)_2)$ **(*xlii*)**, as yellow crystals in 72 % yield **(Scheme 1.21)**.

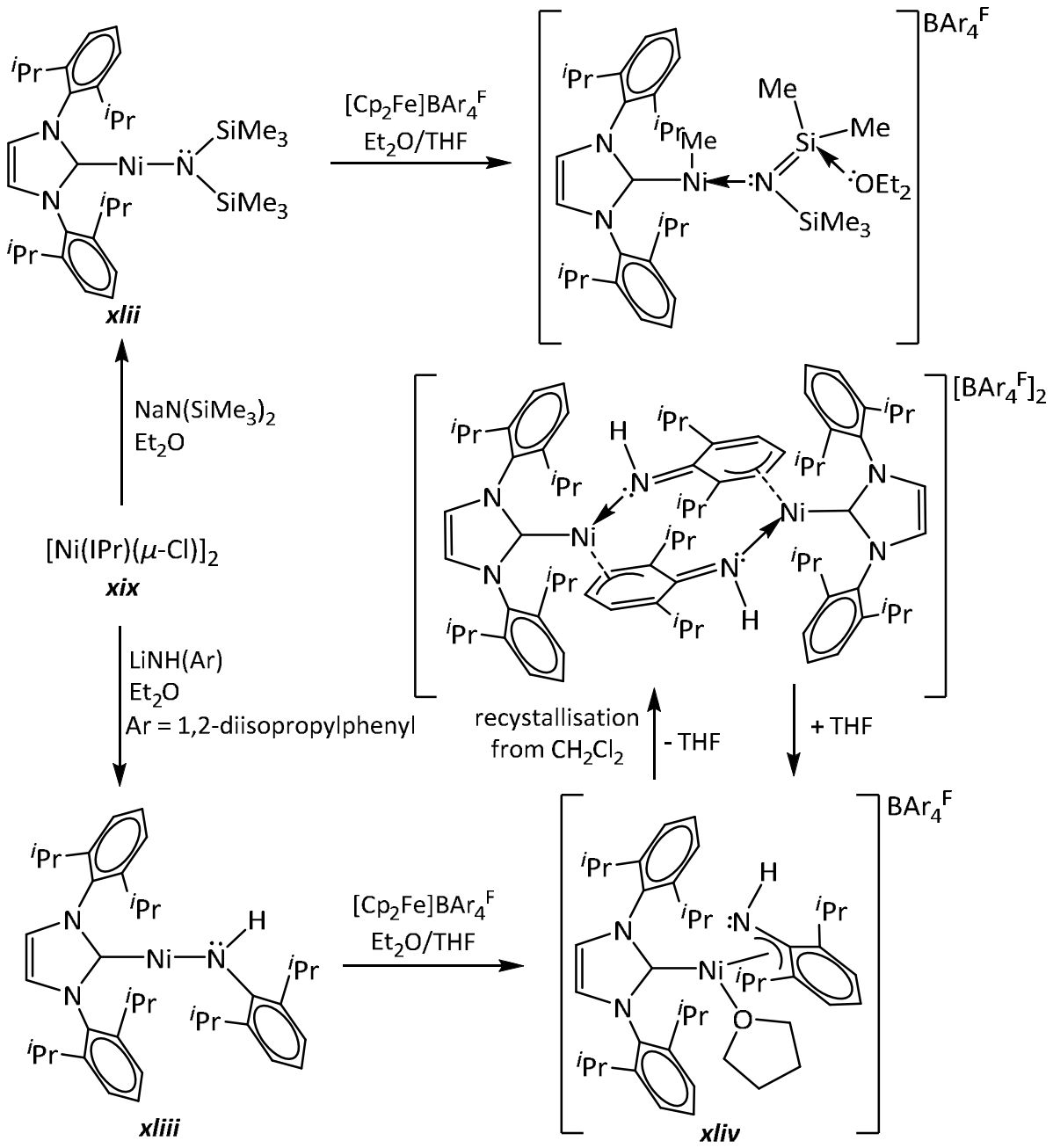

Scheme 1.21 Syntheses and reactivities of two coordinate Ni(I)-NHC amide species ***xlii*** and ***xliii***.

Solution magnetic susceptibility measurements (Evans) gave a μ_{eff} value of 1.9 μB, indicative of a single unpaired electron. Crystallographic analysis revealed the C_{NHC}-Ni-N bond angle to be close to linear (178.7(8)^o), with no significant intra- or intermolecular nonbonded interactions found to the surrounding ligands. The Ni-N distance (1.865(2) Å) was similar to that reported in the three coordinate phosphine derivative $Ni(PPh_3)_2(N(SiMe_3)_2)$ (1.881(2) Å).[137] Changing the base to LiNH(Ar) (Ar = 2,6-diisopropylphenyl) gave the corresponding purple Ni(I)-primary amide derivative, Ni(IPr)(NH(Ar)) ***(xliii*; Scheme 1.21)** in 84 % yield. In contrast to $Ni(NH(Ar))_2$

(Figure 1.8), ***xliii*** deviated from linearity with angles of 163.2(2) and 167.4(2)° found in the two independent molecules in the unit cell, although no evidence for any Ni-L stabilising interactions was found.

Cyclic voltammetry of ***xliii*** in THF/TBAH revealed a quasi-reversible oxidation wave for the Ni(I)/Ni(II) couple at E = -0.84 V and a quasi-reversible reduction for Ni(I)/Ni(0) at E = -2.41 V (*vs.* Fc/[Fc]$^+$). Chemical oxidation of ***xliii*** with $[Cp_2Fe]BAr_4^F$ in Et_2O generated the blue-green 16e$^-$ diamagnetic Ni(II) product [Ni(IPr)(η^3-NH(Ar))(THF)]BAr_4^F **(*xliv*)** in 76 % yield **(Scheme 1.21)**. Despite hopes that a two coordinate complex would be generated, the single crystal X-ray structure revealed ligation of the nickel to a molecule of THF as well as to the amide and carbene ligands. The coordination of the amide changed to an η^3-heterobenzylic mode involving the N, *ipso* and *ortho* carbon atoms on the aryl group. The lability of the THF ligand was confirmed by crystallisation of ***xliv*** from CH_2Cl_2 which gave the solvent free 16e$^-$ Ni(I) dimer $[(Ni(IPr)(\kappa^1\text{-}NH{=}\eta^3\text{-}C_6{}^iPr_2H_3))_2][BAr_4^F]_2$ **(Scheme 1.21)**. This reverted rapidly back to ***xliv*** in the presence of THF. Experimental attempts to obtain the reduction product of ***xliii***, d^{10} '[Ni(IPr)(NH(Ar))]', were unsuccessful, despite the isoelectronic Cu(I) complex Cu(IPr)(NH(Ar)) being known.[138,139]

In spite of the structural similarities of ***xlii*** and ***xliii***, ***xlii*** showed a remarkably different cyclic voltammogram, with only an irreversible oxidation wave at E = -0.21 V observed. Unexpectedly, one electron oxidation with $[Cp_2Fe]BAr_4^F$ was possible to form the diamagnetic iminosilane complex, $[Ni(IPr)(CH_3)(\kappa^1\text{-}N(SiMe_3){=}SiMe_2.Et_2O)]BAr_4^F$, which could be isolated in 74 % yield **(Scheme 1.21)**. This three coordinate species adopted a distorted T-shaped geometry (C_{NHC}-Ni-N = 166.0(2)°), with the iminosilane ligand N-coordinated *trans* to the NHC ligand. Despite a clear difference in the reaction pathways and ultimate oxidative products of ***xlii*** and ***xliii***, it is believed the iminosilane species arises *via* the expected d^8 cationic intermediate '$[Ni(IPr)(N(SiMe_3)_2)]^+$' which undergoes β-Me elimination.

Neutral, 14e$^-$, *bis*(NHC) nickel complexes were previously introduced in section **1.1.3** with discussion of the zero-valent $Ni(IPr)_2$ **(*xvi*)** and $Ni(IMes)_2$ **(*xx*)** as potential precursors to Ni(I) complexes. Early synthetic routes to ***xvi***, ***xx*** and $Ni(I^tBu)_2$ involved either laborious pathways comprising free NHC addition to $Ni(tmeda)(CH_3)_2$[140] or the more esoteric approach of metal vapour synthesis.[141] More straightforward preparative routes were therefore developed. Fort *et al*.[142] had previously postulated the formation of these complexes upon reaction of free NHC with the simple Ni(II) precursor $Ni(acac)_2$ in the presence of a hydrogen source, however the Ni(0) species were never isolated. Building on this, and the fact that Nolan was successful

in preparing *bis*(NHC) palladium analogues,[143] Matsubara *et al.*[79] were able to synthesise and isolate Ni(NHC)$_2$ (NHC = IPr, IMes) as well as the intermediate Ni(NHC)(acac)$_2$ species. Thus, addition of equimolar quantities of imidazolium chloride salts and NaO^{t}Bu to THF solutions of Ni(acac)$_2$ at room temperature gave Ni(NHC)(acac)$_2$ as light green crystals **(Scheme 1.22)**.[79] ^{1}H NMR measurements in C_6D_6 showed no evidence of Ni(acac)$_2$ or free IPr/IMes, supporting the stability of Ni(NHC)(acac)$_2$ in solution. Even at higher temperatures (373 K) or over extended reaction times (24 h), there was no evidence for Ni(NHC)(acac)Cl, in contrast to the analogous palladium chemistry.[143]

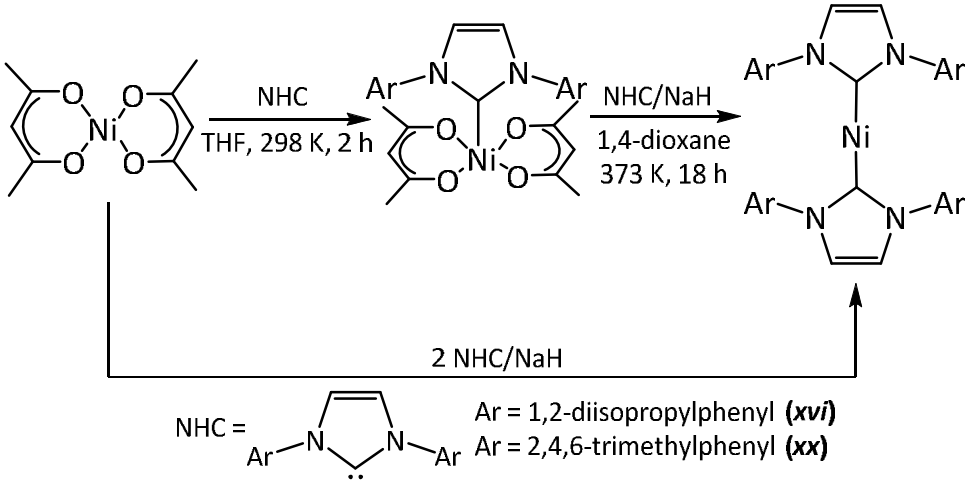

Scheme 1.22 Synthesis of the two coordinate Ni(NHC)$_2$ complexes.

Reduction of the mixed NHC/acac species to Ni(NHC)$_2$ could be achieved through addition of free IPr or IMes carbene and either NaH or Na (NaO^{t}Bu and ^{n}BuLi both proved ineffective, even in vast excess) leading to yields of up to 90 % for both ***xvi*** and ***xx***.[79] Interestingly, reduction by NaH in the absence of free carbene also generated the Ni(0)-*bis*(NHC) species (albeit in lower yields of *ca.* 43 %), indicating that within catalytic cycles incorporating nickel and NHCs, *in situ* generated Ni(0) complexes bearing two NHC ligands may exist as important entities. Free IPr/IMes was observed by ^{1}H NMR spectroscopy, suggesting that NHC dissociation occurs from the Ni(II) or Ni(0) complexes and later associates to the reduced Ni(0)-NHC species, thus providing further support for two coordinate formation even in the absence of additional NHC. It was later found that direct synthesis of ***xvi*** and ***xx*** in yields of 53 % could be achieved upon addition of 2 eq imidazolium chloride to Ni(acac)$_2$ in the presence of NaH.

	xvin[79]	***xx***[144]
Ni – C(1)	1.856(2)	1.827(6)
Ni – C(2)	1.872(2)	1.830(6)
C(1) – Ni – C(2)	177.78(10)	176.4(3)

Table 1.1 Selected bond lengths (Å) and angles (°) for $Ni(IPr)_2$ **(*xvi*)** and $Ni(IMes)_2$ **(*xx*)**.

Both ***xvi*** and ***xx*** were isolated as deep purple solids which displayed highly linear geometries **(Table 1.1)**. The Ni-C_{NHC} bond lengths in ***xvi*** (1.856(2) and 1.872(2) Å) were slightly longer than those in the IMes analogue ***xx*** (1.827(6) and 1.830(6) Å), which was attributed to steric repulsions between the two IPr ligands. The short Ni-C_{NHC} distances measured for ***xx*** are the smallest observed in comparison to other M-IMes species, for example Pt[79] (1.959(8) and 1.942(8) Å), Pd[145] (1.990(3) and 1.997(3) Å), Ag[146] (2.073 Å), Mg[147] (2.279 Å), Zn[147] (2.096 Å) and Al[148] (2.034 Å). This is believed to result from a combination of $d\pi$-$p\pi$ back donation and *sp* hybridisation at the linear two coordinate metal centre. The former factor is considered the most important as other linear complexes, such as the isostructural $14e^-$ Ag(I)-*bis*(carbene), do not show the same short distances, thus eliminating a strong hybridisation effect. Complex ***xvi*** also displayed two short contacts (3.844 and 3.624 Å *c.f.* the six other Ni-C_{Me} lengths at *ca.* 4.2 – 5.2 Å) between the unsaturated nickel and the methyl protons of two isopropyl groups located on the same IPr ligand. Analysis of the Ni···H-C angles (154.1 and 166.4°) indicated that these were largely electrostatic anagostic interactions. This is a rare example of agostic/anagostic stabilisation of low valent Ni(0) complexes, with C-H activation at the aromatic ring in a carbene ligand[149] or intermolecular agostic interactions[150] being more commonly observed.

1.4 Thesis Synopsis

This thesis describes the use of RE NHCs to stabilise Ni(I) species, particularly unsaturated two and three coordinate systems. **Chapter 2** provides details on the synthesis and characterisation of an array of $15e^-$, three coordinate Ni(I) complexes of the form Ni(RE NHC)(PPh_3)Br. A series of 6-, 7- and 8-membered RE NHCs were employed, all varying in steric bulk as a result of their differences in ring size and N-substituents.

Chapter 3 illustrates the instability of this class of compound, focussing on their reactivity towards O_2. The work highlights how subtle steric changes in the ligand environment can

dramatically affect the course of the reaction pathway with oxygen. The reactivity of Ni(RE NHC)(PPh_3)Br is explored further in **Chapter 4**, focussing primarily on attempts to generate lower coordinate Ni(I) species. Treatment with additional RE NHC gave a two coordinate *bis*(RE NHC) Ni(I) complex, which proved to be the first example of a nickel containing mononuclear SMM. This chapter also outlines attempts to remove bromide to generate unsaturated mixed RE NHC/phosphine complexes.

The potential application of Ni(RE NHC)(PPh_3)Br and a variety of subsequently synthesised nickel complexes as catalysts in Kumada cross-coupling reactions is probed in **Chapter 5**, accompanied by a brief introduction into the use of Ni(I) species in catalytic processes.

Future work regarding the chemistry in this thesis is described in **Chapter 6**, while experimental details for all the complexes synthesised are provided in **Chapter 7**.

1.5 References

1. M. L. H. Green and H. Munakata, *J. Chem. Soc. Dalton*, 1974, 269-272.
2. G. Wilke, *Angew. Chem., Int. Ed. Engl.*, 1988, **27**, 185-206.
3. W. Keim, *Angew. Chem., Int. Ed. Engl.*, 1990, **29**, 235-244.
4. C. A. Tolman, *Chem. Rev.*, 1977, **77**, 313-348.
5. C. A. Tolman, R. J. McKinney, W. C. Seidel, J. D. Druliner and W. R. Stevens, *Adv. Catal.*, 1985, **33**, 1-46.
6. D. J. Evans, *Coord. Chem. Rev.*, 2005, **249**, 1582-1595.
7. M. Can, F. A. Armstrong and S. W. Ragsdale, *Chem. Rev.*, 2014, **114**, 4149-4174.
8. S. W. Ragsdale, *Chem. Rev.*, 2006, **106**, 3317-3337.
9. J. Harmer, C. Finazzo, R. Piskorski, S. Ebner, E. C. Duin, M. Goenrich, R. K. Thauer, M. Reiher, A. Schweiger, D. Hinderberger and B. Jaun, *J. Am. Chem. Soc.*, 2008, **130**, 10907-10920.
10. X. Li, J. Telser, R. C. Kunz, B. M. Hoffman, G. Gerfen and S. W. Ragsdale, *Biochemistry*, 2010, **49**, 6866-6876.
11. S. Scheller, M. Goenrich, R. Boecher, R. K. Thauer and B. Jaun, *Nature*, 2010, **465**, 606-697.
12. J. Nishigaki, T. Matsumoto and K. Tatsumi, *Inorg. Chem.*, 2012, **51**, 5173-5187.
13. S. Scheller, M. Goenrich, S. Mayr, R. K. Thauer and B. Jaun, *Angew. Chem., Int. Ed.*, 2010, **49**, 8112-8115.
14. N. C. Norman, A. G. Orpen, M. J. Quayle and G. R. Whittell, *Acta. Crystallogr.*, 2002, **C58**, 160-161.
15. L. Sacconi, F. Mani and A. Bencini, *Nickel in Comprehensive Coordination Chemistry*, Pergamon Press, New York, 1987.
16. B. R. Dible, M. S. Sigman and A. M. Arif, *Inorg. Chem.*, 2005, **44**, 3774-3776.
17. J. Langer, R. Fischer, H. Goerls, N. Theyssen and D. Walther, *Z. Anorg. Allg. Chem.*, 2007, **633**, 557-562.
18. Y. Xiong, S. Yao, E. Bill and M. Driess, *Inorg. Chem.*, 2009, **48**, 7522-7524.
19. R. Melenkivitz, D. J. Mindiola and G. L. Hillhouse, *J. Am. Chem. Soc.*, 2002, **124**, 3846-3847.
20. N. A. Eckert, A. Dinescu, T. R. Cundari and P. R. Holland, *Inorg. Chem.*, 2005, **44**, 7702-7704.
21. G. Bai, P. Wei and D. W. Stephan, *Organometallics*, 2005, **24**, 5901-5908.

22. E. Kogut, H. L. Wiencko, L. B. Zhang, D. E. Cordeau and T. H. Warren, *J. Am. Chem. Soc.*, 2005, **127**, 11248-11249.
23. D. C. Bradley, M. B. Hursthouse, R. J. Smallwood and A. J. Welch, *J. Chem. Soc., Chem. Comm.*, 1972, 872-873.
24. D. D. Ellis and A. L. Spek, *Acta. Crystallogr.*, 2000, **C56**, 1067-1070.
25. M. Aresta, C. F. Nobile and A. Sacco, *Inorg. Chim. Acta.*, 1975, **12**, 167-178.
26. M. F. Lappert and G. Speier, *J. Organomet. Chem.*, 1974, **80**, 329-339.
27. M. J. Nilges, E. K. Barefield, R. L. Belford and P. H. Davies, *J. Am. Chem. Soc.*, 1977, **99**, 755-760.
28. P. H. Davis, R. L. Belford and I. C. Paul, *Inorg. Chem.*, 1973, **12**, 213-218.
29. L. Brammer and E. D. Stevens, *Acta. Crystallogr. Sect. C - Cryst. Struct. Commun.*, 1989, **45**, 400-403.
30. T. A. Albright, J. K. Burdett and M. H. Whangbo, *Orbital Interactions in Chemistry*, John Wiley and Sons, New York, 1985.
31. C. Eaborn, M. S. Hill, P. B. Hitchcock and J. D. Smith, *Chem. Commun.*, 2000, 691-692.
32. W. P. Leung, H. K. Lee, Z. Y. Zhou and T. C. W. Mak, *J. Organomet. Chem.*, 1998, **564**, 193-200.
33. K. D. Kitiachvili, D. J. Mindiola and G. L. Hillhouse, *J. Am. Chem. Soc.*, 2004, **126**, 10554-10555.
34. F. M. Conroylewis, L. Mole, A. D. Redhouse, S. A. Litster and J. L. Spencer, *J. Chem. Soc., Chem. Comm.*, 1991, 1601-1603.
35. J. Campora, J. A. Lopez, P. Palma, P. Valerga, E. Spillner and E. Carmona, *Angew. Chem., Int. Ed.*, 1999, **38**, 147-151.
36. J. Campora, E. Gutierrez-Puebla, J. A. Lopez, A. Monge, P. Palma, D. del Rio and E. Carmona, *Angew. Chem., Int. Ed.*, 2001, **40**, 3641.
37. D. J. Mindiola and G. L. Hillhouse, *J. Am. Chem. Soc.*, 2001, **123**, 4623-4624.
38. R. Dicosimo and G. M. Whitesides, *J. Am. Chem. Soc.*, 1982, **104**, 3601-3607.
39. F. E. Hahn and M. C. Jahnke, *Angew. Chem., Int. Ed.*, 2008, **47**, 3122-3172.
40. A. J. Arduengo, R. L. Harlow and M. Kline, *J. Am. Chem. Soc.*, 1991, **113**, 361-363.
41. E. O. Fischer and A. Maasbol, *Angew. Chem., Int. Ed.*, 1964, **3**, 580.
42. C. Boehme and G. Frenking, *J. Am. Chem. Soc.*, 1996, **118**, 2039-2046.
43. C. Heinemann, T. Muller, Y. Apeloig and H. Schwarz, *J. Am. Chem. Soc.*, 1996, **118**, 2023-2038.

44. O. Back, M. Henry-Ellinger, C. D. Martin, D. Martin and G. Bertrand, *Angew. Chem., Int. Ed.*, 2013, **52**, 2939-2943.
45. S. V. C. Vummaleti, D. J. Nelson, A. Poater, A. Gomez-Suarez, A. B. Cordes, A. M. Z. Slawin, S. P. Nolan and L. Cavallo, *Chem. Sci.*, 2015, **6**, 1895-1904.
46. W. A. Herrmann, *Angew. Chem., Int. Ed.*, 2002, **41**, 1290-1309.
47. S. Diez-Gonzalez and S. P. Nolan, *Coord. Chem. Rev.*, 2007, **251**, 874-883.
48. X. L. Hu, Y. J. Tang, P. Gantzel and K. Meyer, *Organometallics*, 2003, **22**, 612-614.
49. N. M. Scott, R. Dorta, E. D. Stevens, A. Correa, L. Cavallo and S. P. Nolan, *J. Am. Chem. Soc.*, 2005, **127**, 3516-3526.
50. X. L. Hu, I. Castro-Rodriguez, K. Olsen and K. Meyer, *Organometallics*, 2004, **23**, 755-764.
51. E. Peris and R. H. Crabtree, *C. R. Chim.*, 2003, **6**, 33-37.
52. A. M. Magill, K. J. Cavell and B. F. Yates, *J. Am. Chem. Soc.*, 2004, **126**, 8717-8724.
53. J. K. Huang, E. D. Stevens, S. P. Nolan and J. L. Petersen, *J. Am. Chem. Soc.*, 1999, **121**, 2674-2678.
54. W. A. Herrmann, T. Weskamp and V. P. W. Bohm, *Adv. Organomet. Chem.,* 2001, **48**, 1-69.
55. R. Dorta, E. D. Stevens, N. M. Scott, C. Costabile, L. Cavallo, C. D. Hoff and S. P. Nolan, *J. Am. Chem. Soc.*, 2005, **127**, 2485-2495.
56. S. Diez-Gonzalez, N. Marion and S. P. Nolan, *Chem. Rev.*, 2009, **109**, 3612-3676.
57. C. M. Crudden and D. P. Allen, *Coord. Chem. Rev.*, 2004, **248**, 2247-2273.
58. N. M. Scott and S. P. Nolan, *Eur. J. Inorg. Chem.*, 2005, 1815-1828.
59. E. Peris and R. H. Crabtree, *Coord. Chem. Rev.*, 2004, **248**, 2239-2246.
60. S. P. Nolan, *N-Heterocyclic Carbenes: Effective Tools for Organometallic Synthesis*, Wiley-VCH, Weinheim, 2013, pg 13-14.
61. A. C. Hillier, W. J. Sommer, B. S. Yong, J. L. Petersen, L. Cavallo and S. P. Nolan, *Organometallics*, 2003, **22**, 4322-4326.
62. V. Lavallo, Y. Canac, C. Prasang, B. Donnadieu and G. Bertrand, *Angew. Chem., Int. Ed.*, 2005, **44**, 5705-5709.
63. R. Jazzar, R. D. Dewhurst, J. B. Bourg, B. Donnadieu, Y. Canac and G. Bertrand, *Angew. Chem., Int. Ed.*, 2007, **46**, 2899-2902.
64. L. P. Spencer, S. Winston and M. D. Fryzuk, *Organometallics*, 2004, **23**, 3372-3374.
65. L. P. Spencer and M. D. Fryzuk, *J. Organomet. Chem.*, 2005, **690**, 5788-5803.

66. A. Binobaid, M. Iglesias, D. J. Beetstra, B. Kariuki, A. Dervisi, I. A. Fallis and K. J. Cavell, *Dalton Trans.*, 2009, 7099-7112.

67. M. Iglesias, D. J. Beetstra, J. C. Knight, L. L. Ooi, A. Stasch, S. Coles, L. Male, M. B. Hursthouse, K. J. Cavell, A. Dervisi and I. A. Fallis, *Organometallics*, 2008, **27**, 3279-3289.

68. W. Y. Lu, K. J. Cavell, J. S. Wixey and B. Kariuki, *Organometallics*, 2011, **30**, 5649-5655.

69. R. Jazzar, H. Liang, B. Donnadieu and G. Bertrand, *J. Organomet. Chem.*, 2006, **691**, 3201-3205.

70. M. Mayr, K. Wurst, K. H. Ongania and M. R. Buchmeiser, *Chem. Eur. J.*, 2004, **10**, 1256-1266.

71. S. K. Schneider, W. A. Herrmann and E. Herdtweck, *J. Mol. Catal. A: Chem.*, 2006, **245**, 248-254.

72. J. J. Dunsford, K. J. Cavell and B. Kariuki, *J. Organomet. Chem.*, 2011, **696**, 188-194.

73. J. J. Dunsford and K. J. Cavell, *Dalton Trans.*, 2011, **40**, 9131-9135.

74. R. Armstrong, C. Ecott, E. Mas-Marza, M. J. Page, M. F. Mahon and M. K. Whittlesey, *Organometallics*, 2010, **29**, 991-997.

75. C. J. E. Davies, M. J. Page, C. E. Ellul, M. F. Mahon and M. K. Whittlesey, *Chem. Commun.*, 2010, **46**, 5151-5153.

76. H. Tsurugi, S. Fujita, G. Choi, T. Yarnagata, S. Ito, H. Miyasaka and K. Mashima, *Organometallics*, 2010, **29**, 4120-4129.

77. S. Miyazaki, Y. Koga, T. Matsumoto and K. Matsubara, *Chem. Commun.*, 2010, **46**, 1932-1934.

78. K. Matsubara, K. Ueno and Y. Shibata, *Organometallics*, 2006, **25**, 3422-3427.

79. K. Matsubara, S. Miyazaki, Y. Koga, Y. Nibu, T. Hashimura and T. Matsumoto, *Organometallics*, 2008, **27**, 6020-6024.

80. K. Matsubara, K. Ueno, Y. Koga and K. Hara, *J. Org. Chem.*, 2007, **72**, 5069-5076.

81. G. D. Jones, J. L. Martin, C. McFarland, O. R. Allen, R. E. Hall, A. D. Haley, R. J. Brandon, T. Konovalova, P. J. Desrochers, P. Pulay and D. A. Vicic, *J. Am. Chem. Soc.*, 2006, **128**, 13175-13183.

82. D. S. McGuinness, K. J. Cavell, B. W. Skelton and A. H. White, *Organometallics*, 1999, **18**, 1596-1605.

83. T. Schaub, M. Backes and U. Radius, *J. Am. Chem. Soc.*, 2006, **128**, 15964-15965.

84. K. Zhing, M. Conda-Sheridan, S. R. Cooke and J. Louie, *Organometallics*, 2011, **30**, 2546-2552.

85. V. K. Jain and L. Jain, *Coord. Chem. Rev.*, 2005, **249**, 3075-3197.
86. T. Murahashi and H. Kurosawa, *Coord. Chem. Rev.*, 2002, **231**, 207-228.
87. U. Christmann, R. Vilar, A. J. P. White and D. J. Williams, *Chem. Commun.*, 2004, 1294-1295.
88. U. Christmann, D. A. Pantazis, J. Benet-Buchholz, J. E. McGrady, F. Maseras and R. Vilar, *J. Am. Chem. Soc.*, 2006, **128**, 6376-6390.
89. D. C. Powers and T. Ritter, *Nature Chem.*, 2009, **1**, 302-309.
90. N. R. Deprez and M. S. Sanford, *J. Am. Chem. Soc.*, 2009, **131**, 11234-11241.
91. J. J. Eisch, A. M. Piotrowski, K. I. Han, C. Kruger and Y. H. Tsay, *Organometallics*, 1985, **4**, 224-231.
92. T. V. V. Ramakrishna and P. R. Sharp, *Organometallics*, 2004, **23**, 3079-3081.
93. A. Velian, S. Lin, A. J. M. Miller, M. W. Day and T. Agapie, *J. Am. Chem. Soc.*, 2010, **132**, 6296.
94. Y. F. Chen, C. Sui-Seng and D. Zargarian, *Angew. Chem., Int. Ed.*, 2005, **44**, 7721-7725.
95. M. Ito, T. Matsumoto and K. Tatsumi, *Inorg. Chem.*, 2009, **48**, 2215-2223.
96. S. D. Walker, T. E. Barder, J. R. Martinelli and S. L. Buchwald, *Angew. Chem., Int. Ed.*, 2004, **43**, 1871-1876.
97. R. Beck and S. A. Johnson, *Chem. Commun.*, 2011, **47**, 9233-9235.
98. B. L. Edelbach, R. J. Lachicotte and W. D. Jones, *J. Am. Chem. Soc.*, 1998, **120**, 2843-2853.
99. C. A. Laskowski and G. L. Hillhouse, *Chem. Sci.*, 2011, **2**, 321-325.
100. C. A. Laskowski and G. L. Hillhouse, *Organometallics*, 2009, **28**, 6114-6120.
101. T. R. Belderrain, E. Gutierrez, A. Monge, M. C. Nicasio, M. Paneque, M. L. Poveda and E. Carmona, *Organometallics*, 1993, **12**, 4431-4442.
102. K. D. Kitiachvili, D. J. Mindiola and G. L. Hillhouse, *J. Am. Chem. Soc.*, 2004, **126**, 10554-10555.
103. Y. M. Badiei and T. H. Warren, *J. Organomet. Chem.*, 2005, **690**, 5989-6000.
104. S. Yao and M. Driess, *Acc. Chem. Res.*, 2012, **45**, 276-287.
105. S. Pfirrmann, S. Yao, B. Ziemer, R. Stoesser, M. Driess and C. Limberg, *Organometallics*, 2009, **28**, 6855-6860.
106. S. Pfirrmann, C. Limberg, C. Herwig, R. Stoesser and B. Ziemer, *Angew. Chem., Int. Ed.*, 2009, **48**, 3357-3361.
107. B. Horn, S. Pfirrmann, C. Limberg, C. Herwig, B. Braun, S. Mebs and R. Metzinger, *Z. Anorg. Allg. Chem.*, 2011, **637**, 1169-1174.

108. B. Horn, C. Limberg, C. Herwig and S. Mebs, *Angew. Chem., Int. Ed.*, 2011, **50**, 12621-12625.
109. B. Horn, C. Limberg, C. Herwig, M. Feist and S. Mebs, *Chem. Commun.*, 2012, **48**, 8243-8245.
110. B. Horn, C. Limberg, C. Herwig and B. Braun, *Chem. Commun.*, 2013, **49**, 10923-10925.
111. M. Brecht, M. van Gastel, T. Buhrke, B. Friedrich and W. Lubitz, *J. Am. Chem. Soc.*, 2003, **125**, 13075-13083.
112. B. E. Barton, C. M. Whaley, T. B. Rauchfuss and D. L. Gray, *J. Am. Chem. Soc.*, 2009, **131**, 6942.
113. S. Pfirrmann, C. Limberg and B. Ziemer, *Dalton Trans.*, 2008, 6689-6691.
114. N. A. Eckert, A. Dinescu, T. R. Cundari and P. L. Holland, *Inorg. Chem.*, 2005, **44**, 7702-7704.
115. G. C. Bai, P. R. Wei and D. W. Stephan, *Organometallics*, 2005, **24**, 5901-5908.
116. J. M. Smith, R. J. Lachicotte and P. L. Holland, *J. Am. Chem. Soc.*, 2003, **125**, 15752-15753.
117. T. R. Dugan and P. L. Holland, *J. Organomet. Chem.*, 2009, **694**, 2825-2830.
118. P. Holze, B. Horn, C. Limberg, C. Matlachowski and S. Mebs, *Angew. Chem., Int. Ed.*, 2014, **53**, 2750-2753.
119. H. C. Cowen, F. Riding and E. Warhurst, *J. Chem. Soc.*, 1953, 4168-4169.
120. S. Yao, E. Bill, C. Milsmann, K. Wieghardt and M. Driess, *Angew. Chem., Int. Ed.*, 2008, **47**, 7110-7113.
121. B. Ramdhanie, J. Telser, A. Caneschi, L. N. Zakharov, A. L. Rheingold and D. P. Goldberg, *J. Am. Chem. Soc.*, 2004, **126**, 2515-2525.
122. A. Company, S. Yao, K. Ray and M. Driess, *Chem. Eur. J.*, 2010, **16**, 9669-9675.
123. C. J. Cramer, W. B. Tolman, K. H. Theopold and A. L. Rheingold, *Proc. Natl. Acad. Sci. U.S.A.*, 2003, **100**, 3635-3640.
124. M. T. Kieber-Emmons and C. G. Riordan, *Acc. Chem. Res.*, 2007, **40**, 618-625.
125. L. M. Mirica, X. Ottenwaelder and T. D. P. Stack, *Chem. Rev.*, 2004, **104**, 1013-1045.
126. P. P. Power, *Chem. Rev.*, 2012, **112**, 3482-3507.
127. R. A. Layfield, *Organometallics*, 2014, **33**, 1084-1099.
128. P. H. Guo, Y. Meng, Y. C. Chen, Q. W. Li, B. Y. Wang, J. D. Leng, D. H. Bao, J. H. Jia and M. L. Tong, *J. Mater. Chem.*, 2014, **2**, 8858-8864.
129. L. Ungur, S. Y. Lin, J. Tang and L. F. Chibotaru, *Chem. Soc. Rev.*, 2014, **43**, 6894-6905.
130. S. K. Singh, T. Gupta and G. Rajaraman, *Inorg. Chem.*, 2014, **53**, 10835-10845.

131. M. Chen, E. Carolina Sanudo, E. Jimenez, S. M. Fang, C. S. Liu and M. Du, *Inorg. Chem.*, 2014, **53**, 6708-6714.
132. H. Buger and U. Wannagat, *Monatsh. Chem.*, 1964, **95**, 1099.
133. R. A. Bartlett, H. Chen and P. P. Power, *Angew. Chem., Int. Ed. Engl.*, 1989, **28**, 316-317.
134. H. Chen, R. A. Bartlett, M. M. Olmstead, P. P. Power and S. C. Shoner, *J. Am. Chem. Soc.*, 1990, **112**, 1048-1055.
135. A. M. Bryan, W. A. Merrill, W. M. Reiff, J. C. Fettinger and P. P. Power, *Inorg. Chem.*, 2012, **51**, 3366-3373.
136. J. Li, H. Song, C. Cui and J. P. Cheng, *Inorg. Chem.*, 2008, **47**, 3468-3470.
137. C. A. Laskowski and G. L. Hillhouse, *J. Am. Chem. Soc.*, 2008, **130**, 13846-13847.
138. L. A. Goj, E. D. Blue, C. Munro-Leighton, T. B. Gunnoe and J. L. Petersen, *Inorg. Chem.*, 2005, **44**, 8647-8649.
139. L. A. Goj, E. D. Blue, S. A. Delp, T. B. Gunnoe, T. R. Cundari, A. W. Pierpont, J. L. Petersen and P. D. Boyle, *Inorg. Chem.*, 2006, **45**, 9032-9045.
140. A. A. Danopoulos and D. Pugh, *Dalton Trans.*, 2008, 30-31.
141. P. L. Arnold, F. G. N. Cloke, T. Geldbach and P. B. Hitchcock, *Organometallics*, 1999, **18**, 3228-3233.
142. S. Kuhl, R. Schneider and Y. Fort, *Organometallics*, 2003, **22**, 4184-4186.
143. O. Navarro, N. Marion, N. M. Scott, J. Gonzalez, D. Amoroso, A. Bell and S. P. Nolan, *Tetrahedron*, 2005, **61**, 9716-9722.
144. A. J. Arduengo, S. F. Gamper, J. C. Calabrese and F. Davidson, *J. Am. Chem. Soc.*, 1994, **116**, 4391-4394.
145. M. M. Konnick, I. A. Guzei and S. S. Stahl, *J. Am. Chem. Soc.*, 2004, **126**, 10212-10213.
146. A. J. Arduengo, H. V. R. Dias, J. C. Calabrese and F. Davidson, *Organometallics*, 1993, **12**, 3405-3409.
147. A. J. Arduengo, H. V. R. Dias, F. Davidson and R. L. Harlow, *J. Organomet. Chem.*, 1993, **462**, 13-18.
148. A. J. Arduengo, H. V. R. Dias, J. C. Calabrese and F. Davidson, *J. Am. Chem. Soc.*, 1992, **114**, 9724-9725.
149. T. N. Tekavec and J. Louie, *Tetrahedron*, 2008, **64**, 6870-6875.
150. W. J. Youngs, J. D. Kinder, J. D. Bradshaw and C. A. Tessier, *Organometallics*, 1993, **12**, 2406-2407.

CHAPTER 2

2 Synthesis and Characterisation of Low Coordinate Nickel(I) RE NHC Complexes

2.1 Nickel(I) RE NHC Complexes

Compared to their 5-membered counterparts, RE NHCs have received very limited attention as ligands for organometallic complexes,[1-3] with little emphasis on nickel-RE NHC species. As outlined in **Chapter 1**, the advantageous steric and electronic properties of RE NHCs make them ideal candidates as ligands for the promotion and stabilisation of Ni(I) metal centres. Initial work to synthesise Ni(I)-RE NHC complexes by the Whittlesey group[4] were unsuccessful, but did highlight additional chemistry commonly observed with RE NHCs. Addition of the 6-membered N-mesityl NHC, 6Mes, to a toluene solution of zero-valent $Ni(COD)_2$ led to rapid formation of the deep red Ni(II) species ***(xlv)*** in a 40 % isolated yield, in which one of the bulky mesityl groups has undergone C-H activation at the *o*-Me position **(Scheme 2.1)**. X-ray crystallography showed the presence of a cyclooctenyl group which is proposed to arise through hydrogen transfer from a transient Ni-H species formed in the C-H activation step. An analogous η^3-cyclooctenyl nickel complex bearing a C-H activated 5-membered I^{t}Bu was previously reported by Cloke and Caddick.[5] X-ray analysis of ***xlv*** gave Ni-C_{NHC} and Ni-CH_2 distances of 1.8996(12) and 1.9796(14) Å, comparable to the metrics of the I^{t}Bu species (1.905(4) and 1.958(3) Å respectively).[5]

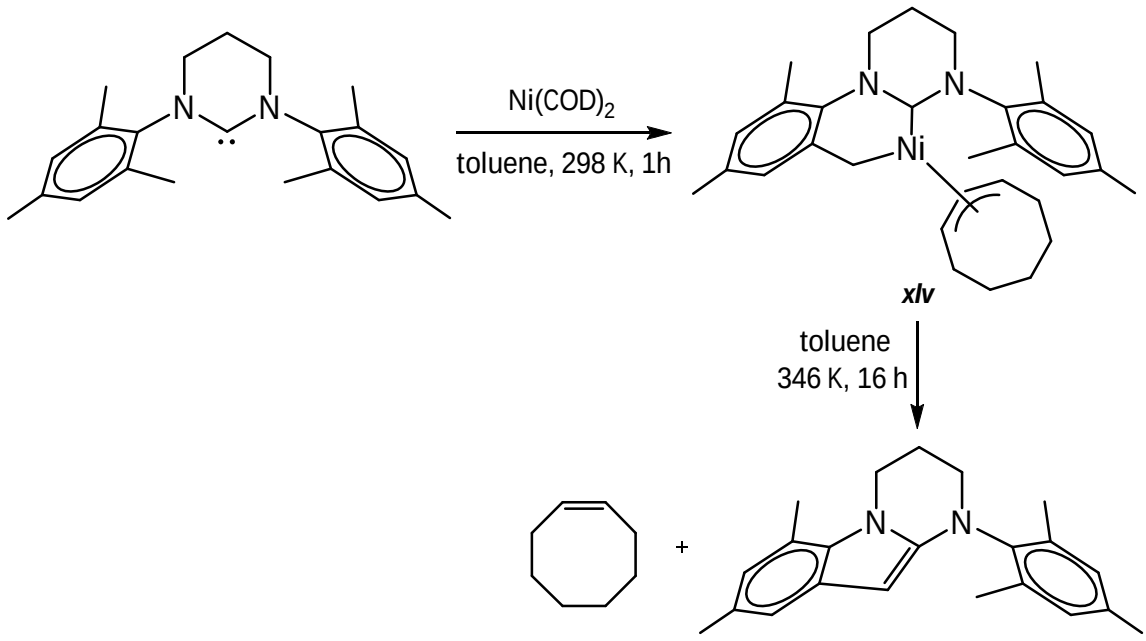

Scheme 2.1 Reaction of 6Mes with $Ni(COD)_2$ to generate the C-H activated Ni(II) complex ***xlv*** and subsequent indole formation.

Limited stability was established for ***xlv***, as heating at 346 K led to formation of the N-alkyl indole (62 % isolated yield) and cyclooctene. The presence of free cyclooctene corroborated the hydrogen transfer theory from the methylene activated arm, eliminating the indole derivative from the nickel metal centre. Furthermore, such degradation is facilitated by the presence of the cyclometallated/C-H activated arm in ***xlv***, induced from bulky N-substituents and their increased proximity to the metal centre (resulting from wider N-C_{NHC}-N angles) over their imidazolium based counterparts.

2.2 Synthesis and Characterisation of Ni(6Mes)(PPh_3)Br (1)

Following the success of Ni(I) synthesis *via* comproportionation by Sigman[6] **(Chapter 1, 1.1.5)**, it seemed plausible that Ni(I)-RE NHC complexes could also be formed in this manner. Adopting this approach, while building on the nickel/RE NHC work already carried out in the Whittlesey group **(Section 2.1)**, 6Mes (formed *in situ* from reaction of equimolar [6MesH]BF_4 and $KN(SiMe_3)_2$ in THF) was reacted at room temperature with $Ni(COD)_2$ and $Ni(PPh_3)_2Br_2$ in a ratio of 2:1:1 respectively, leading to a colour change from light brown to yellow. Precipitation with hexane allowed isolation of the Ni(I) species Ni(6Mes)(PPh_3)Br **(1)** as a bright yellow powder in 76 % yield after recrystallisation from THF/hexane. This neutral, three coordinate, $15e^-$ monomer **(Scheme 2.2)** was structurally characterised by X-ray crystallography, as shown

in **Figure 2.1**.[4] The compound was extremely sensitive to air, both in the solid-state and solution (THF, toluene, benzene), as apparent from the rapid colour change from yellow to purple, observed even upon exposure to trace levels of air (see **Chapter 3** for an in-depth discussion of this reaction).

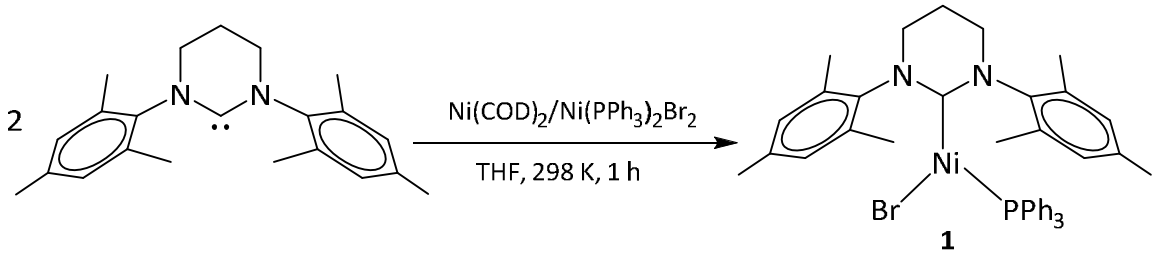

1

Scheme 2.2 Synthesis of **1** *via* comproportionation between $Ni(COD)_2$ and $Ni(PPh_3)_2Br_2$ in the presence of 6Mes.

The X-ray crystal structure of **1 (Figure 2.1)** displayed a distorted trigonal planar geometry, with the sum of the angles equalling 360.00(6)°. However, the internal angles were far from regular, with the C_{NHC}-Ni-Br angle being greater than the 'ideal' 120° (133.46(6)°), which can be accounted for, in part, by the steric requirements of the bromide ligand relative to the other two ligands (as noted in ***ii*** and ***iii*** **(Chapter 1, 1.1.1)**). Although this geometry is observed in other Ni(I) species (*i.e.* ***ii***),[7] it contrasts with other NHC bearing nickel complexes, such as the T-shaped *bis*(carbene) species ***xvii***,[8] ***xxi***[9] and ***xxii*** **(Chapter 1, 1.1.3)**.[9] It is likely that with the high steric demand of the 6Mes ligand, sterics play a major role in dictating the three coordinate geometry. However, Holland and coworkers[10] have reported that for other d^9 systems, ligand electronic effects can have a significant influence. In three coordinate β-diketiminate (N^N) substituted Ni(I) and Cu(II) complexes, they found that Y-shaped geometries are generally favoured (especially for Cu(II)). The bidentate nature of N^N naturally has a significant drive for the preference of this geometry, however, a T-shaped environment is instead observed when a highly electronegative ancillary ligand, or one with a strong *trans* influence is also ligated (*e.g.* CO in $Ni(N^{\wedge}N^{Me})(CO)$ **(*iii*; see Chapter 4, Figure 4.21)**).

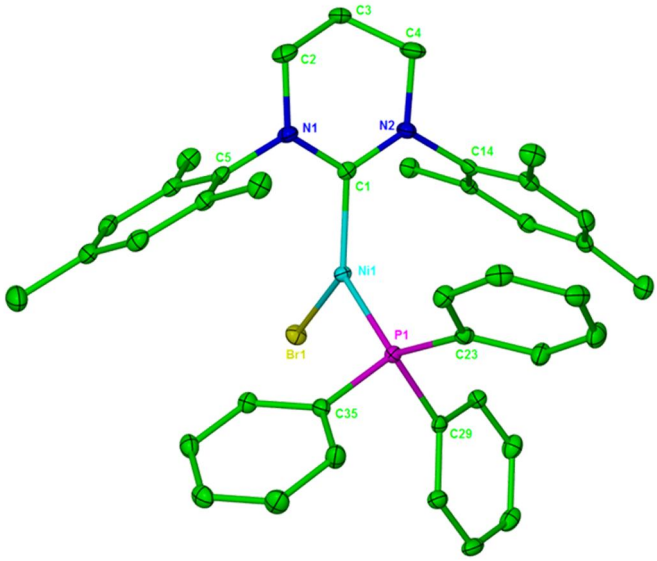

Figure 2.1 X-ray structure of **1**. Thermal ellipsoids are set at 30 % probability. All hydrogen atoms have been omitted for clarity.

The ^{1}H NMR spectrum of **1 (Figure 2.2)** showed a series of extremely broad and paramagnetically shifted resonances in the range of 30 to -17 ppm, consistent with paramagnetic Ni(I). The spectrum could be integrated, although assignment of individual peaks was not possible (see section **2.3** for further discussion). Despite single crystal X-ray analysis identifying the presence of a PPh_3 ligand, no phosphorus signal was observed in the $^{31}P\{^{1}H\}$ NMR spectrum, which along with the lack of any signal for free 6Mes in the ^{1}H NMR spectrum, indicated that no PPh_3 or 6Mes dissociation took place in solution. This excludes any monomer-dimer equilibrium as found for [Ni(IPr)(μ-Cl]$_2$ ***(xix)*** and monomeric Ni(IPr)$_2$Cl ***(xvii)***.[8,11] The room temperature solution magnetic moment was measured as 2.1 μB in C_6H_6 *via* the Evans method, consistent with the presence of a single unpaired electron.

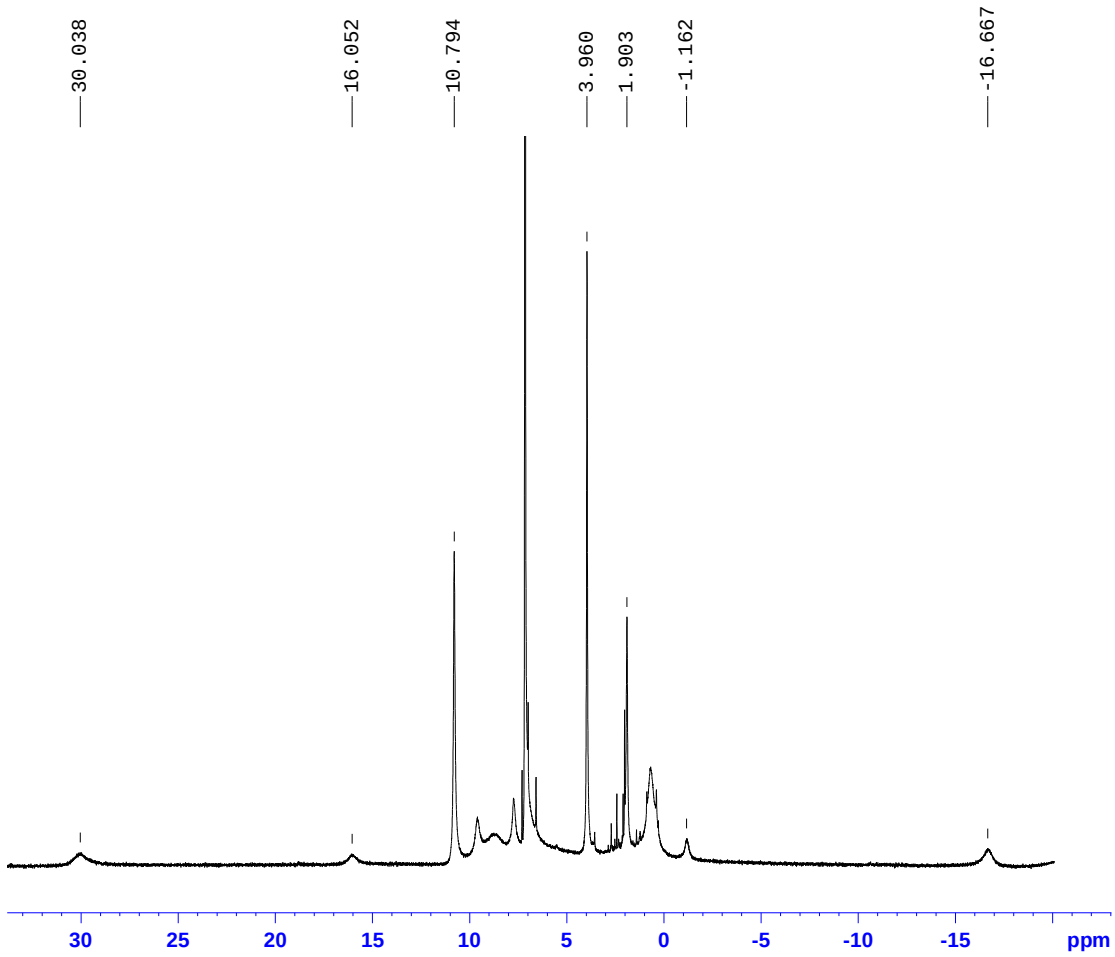

Figure 2.2 ^{1}H NMR spectrum of **1** (C_6D_6, 298 K, 500 MHz).

2.3 Synthesis and Characterisation of a Series of Ni(RE NHC)(PPh_3)X Complexes (X = Br, Cl)

The paucity of fully characterised three coordinate Ni(I) species[10,12-30] suggested that easy access to a range of analogues would provide an opportunity to gain an understanding of both fundamental properties (*i.e.* structure and bonding) as well as catalytic behaviour of low coordinate d^9 organometallics, especially if based upon a set of easily adapted and tuneable ligands such as RE NHCs. Adopting the same synthetic approach used for **1**, a series of isostructural Ni(RE NHC)(PPh_3)X (X = Br, Cl) complexes were prepared, incorporating 6-, 7- and 8-membered RE NHC ligands bearing a variety of N-aryl subsituents **(Scheme 2.3)**.[31] The 6- and 7-membered Ni(I) bromide analogues (**2 – 4**, **6** and **7**) were synthesised *via* the comproportionation reaction in the presence of 6^{o}Tol, 6^{o}Anis, 6^{o}AnisMes, 7Mes and 7^{o}Tol as the RE NHC ligands respectively (in all cases formed *in situ* from deprotonation of the corresponding pyrimidinium or diazepinium tetrafluoroborate salts with $KN(SiMe_3)_2$). Initial efforts (in collaboration with Cavell and coworkers at Cardiff University)[31] to prepare the

8-membered Ni(I) versions (8Mes, 8^{o}Tol, O-8^{o}Tol **(8 – 10)**) used $Ni(COD)_2$, $Ni(PPh_3)_2Cl_2$ and the appropriate RE NHC, formed *in situ* from the corresponding bromide salts and $KN(SiMe_3)_2$. X-ray crystallography showed mixed bromide/chloride occupancy of the halide site in a ratio of 70:30 respectively. Pure samples of both the bromide and chloride 8^{o}Tol derivatives $Ni(8^oTol)(PPh_3)Br$ and $Ni(8^oTol)(PPh_3)Cl$ were subsequently achieved by reacting $[8^oTolH]BF_4$ with $Ni(COD)_2$ and either $Ni(PPh_3)_2Br_2$ or $Ni(PPh_3)_2Cl_2$ as required. The closely related diamidocarbene analogue $Ni(6MesDAC)(PPh_3)Br$ **(5)** was synthesised *via* direct addition of free 6MesDAC to a mixture of the Ni(0)/Ni(II) precursors in the same 2:1:1 ratio (see **Abbreviations** for structures of the free RE NHCs).

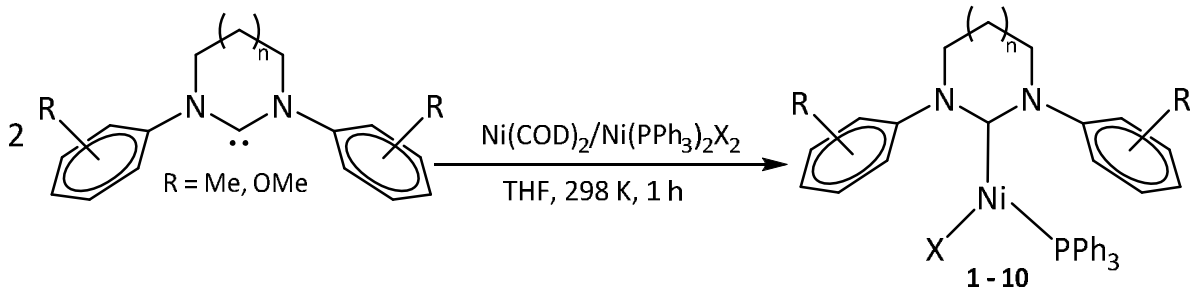

1: RE NHC = 6Mes, n = 1, X = Br
2: RE NHC = 6^{o}Tol, n = 1, X = Br
3: RE NHC = 6^{o}Anis, n = 1, X = Br
4: RE NHC = 6^{o}AnisMes, n = 1, X = Br

6: RE NHC = 7Mes, n = 2, X = Br
7: RE NHC = 7^{o}Tol, n = 2, X = Br
8: RE NHC = 8Mes, n = 3, X = Br/Cl
9: RE NHC = 8^{o}Tol, n = 3, X = Br, Cl, Br/Cl

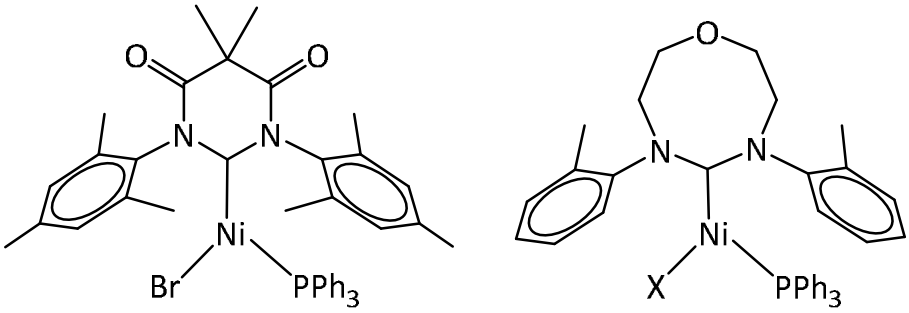

5

10: RE NHC = O-8^{o}Tol, X = Br/Cl

Scheme 2.3 Three coordinate Ni(I)-RE NHC complexes **1 – 4** and **6 – 10**, along with the diamido derivative **5**.

The Ni(RE NHC)(PPh_3)X complexes (**2 – 4** and **6 – 10**) were isolated as yellow microcrystalline powders in yields of 36 – 64 %, and were all characterised by X-ray crystallography. They shared the same level of air-sensitivity as the 6Mes containing **1**, rapidly turning purple upon exposure to air. By contrast, the 6MesDAC analogue **(5)** was orange in solution, but isolable as

dark purple crystals in 62 % yield from THF/hexane. Although it displayed similar levels of instability towards air, orange solutions of **5** instead turned virtually colourless.

Compounds **2 – 7** displayed paramagnetic ^{1}H NMR spectra, featuring broad and shifted resonances over the range 37 to -22 ppm. In all cases, the spectra of the compounds contained a relatively sharp singlet resonance between 9.5 and 11 ppm, as seen at 10.79 ppm for **1** in **Figure 2.2**. Unlike **1**, integration of the spectra for **2 – 7** was not possible. Solution stability towards PPh_3 or NHC dissociation, as found for **1**, was again apparent as none of the further nine compounds exhibited any $^{31}P\{^{1}H\}$ NMR resonances. No signals whatsoever were observed in the ^{1}H, $^{31}P\{^{1}H\}$ or $^{13}C\{^{1}H\}$ NMR spectra for the 8-membered ring analogues **(8 – 10)**. Solution magnetic measurements for compounds **3 – 7** were again consistent with the presence of a single unpaired electron in each complex, with values ranging from 1.2 – 2.6 μB (Evans method).

The further nine Ni(I)-RE NHC species proved isostructural to **1**, as shown by the X-ray structures in **Figure 2.3** and **Figure 2.4**. **Table 2.1** shows selected bond lengths and angles for complexes **1 – 10**. As described for **1**, all the internal angles in **2 – 10** are 360º (values range between 360±1º), with the C_{NHC}-Ni-Br angles substantially larger than the 120º expected for perfect trigonal planar environments (values between 127.66(5) – 139.22(7)º). Furthermore, the angle with which the two *ipso* carbons of the N-aryl substituents subtend the nickel atom generally increases with expansion of the NHC ring size (102.3, 102.9, 102.3, 101.9, 102.9, 104.3, 104.6, 106.9 and 106.4º for compounds **1 – 4, 6 – 10** respectively). This implies there is a small reduction in the steric demand of the RE NHC, which will also contribute to the ligand accommodation around the metal centre, presumably arising from increasing flexibility/puckering associated with larger rings (largest distance between puckered atom and mean plane of carbene backbone: **1**: 0.638 Å; **6**: 1.316 Å; **8**: 2.077 Å). The Ni-C_{NHC} bond lengths are all typical for a Ni-NHC complex, comparing well to ***xlv*** and $Ni(IMes)_2Br$ **(*xxi*)** (***xlv***: 1.8994(12) Å; ***xxi***: 1.913(4)/1.929(4) Å;[9] **1**: 1.942(2) Å; **6**: 1.9553(19) Å; **8**: 1.979(5) Å), and, as expected, the N-C_{NHC}-N bond angles widen with increasing ring size; this is readily demonstrated by closer analysis of the mesityl functionalised complexes (***xxi***: 102.9(3)/103.1(3),[9] **1**: 116.48(19), **6**: 118.49(17), **8**: 121.8(4)º). Additionally, expansion of ring size is accompanied by a slight Ni-C_{NHC} lengthening, which could be accounted for by increasing ring strain and hence instability of the RE NHC itself upon expansion from 6 to 7 and ultimately 8 atoms. This is echoed by the failure of all attempts by the Cavell group to form 9-membered RE NHCs and any subsequent Ni(I) complexes.

Interestingly, the metrics of the 6MesDAC complex **(5)** are perhaps contrary to expectations. Diamidocarbenes are less electron-donating[32-36] and so a lengthening of a Ni-C_{NHC} bond distance relative to **1** might be expected. In fact, there is a significant reduction (**1**: 1.942(2) Å; **5**: 1.8702(18) Å), most likely due to the enhanced π-accepting abilities that result from the presence of the carbonyl moieties at the C4 and C6 positions on the carbene backbone.[34,37,38] However, there are also changes between the Ni-Br and Ni-P distances, making a direct comparison between the diamino and diamido analogues difficult.

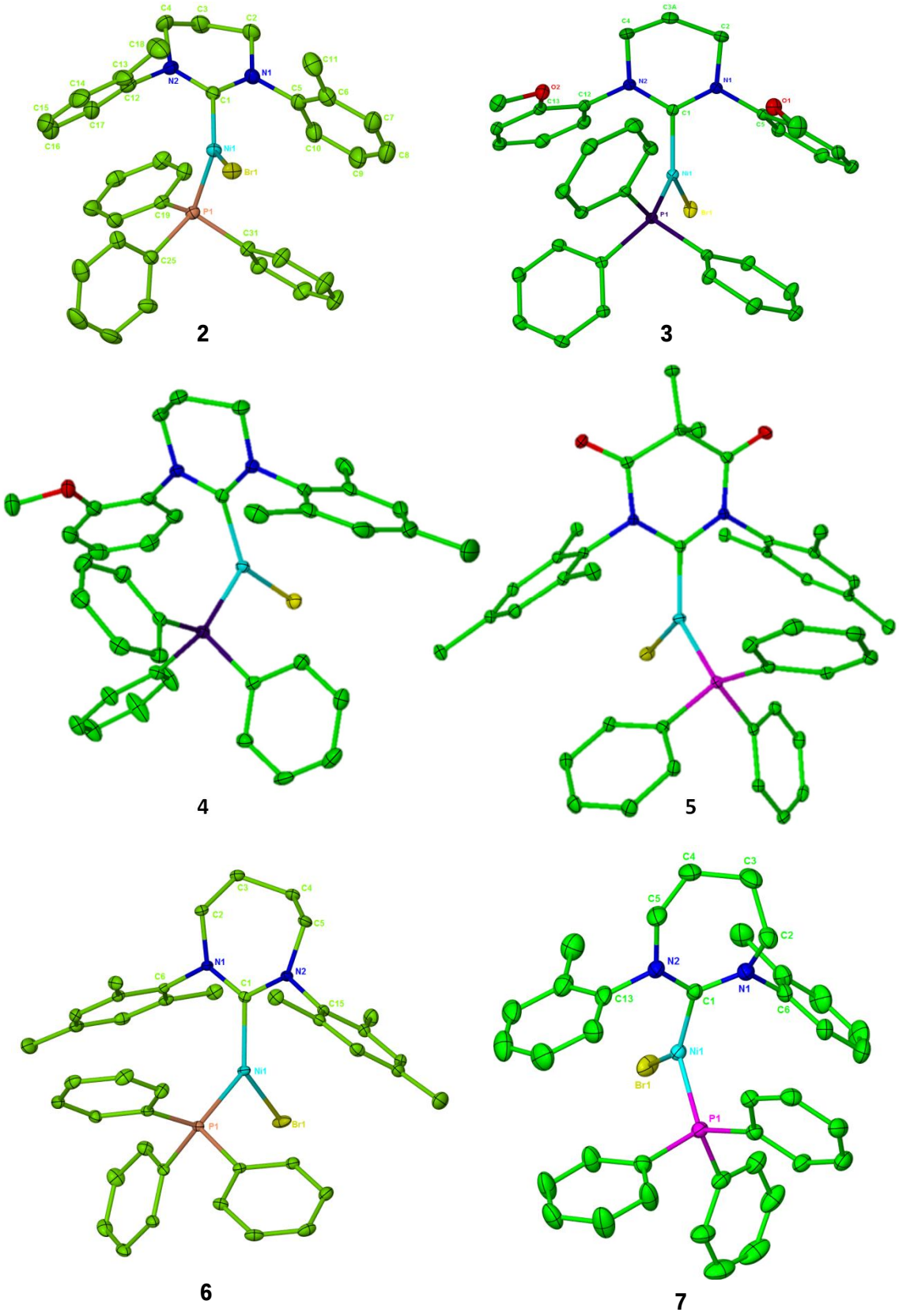

Figure 2.3 X-ray structures of the three coordinate 6- and 7-membered Ni(I)-RE NHC complexes **2 – 7**. Thermal ellipsoids are set at 30 %. All hydrogen atoms have been omitted for clarity.

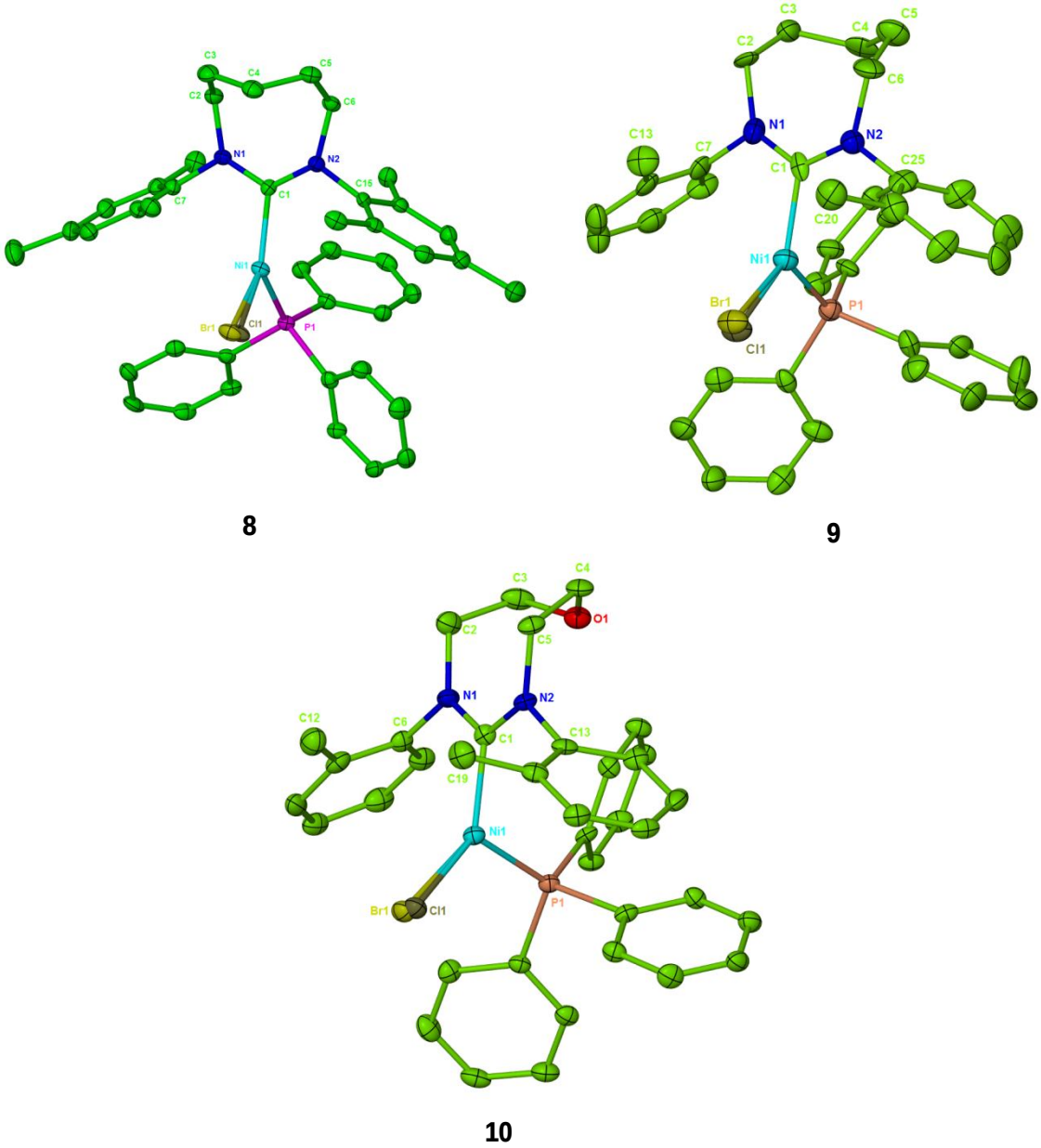

Figure 2.4 X-ray structures of the three coordinate 8-membered Ni(I)-RE NHC complexes **8 – 10**. Thermal ellipsoids are set at 30 %. All hydrogen atoms have been omitted for clarity. In all cases, there is partial occupancy by Br and Cl at the halide site.

	1	**2**	**3**	**4**	**5**	**6**	**7**	**8**	**9**	**10**
Ni – C_{NHC}	1.942(2)	1.926(4)	1.9346(19)	1.942(2)	1.8702(18)	1.9553(19)	1.925(3)	1.979(5)	1.949(4)	1.932(7)
Ni – P	2.2188(6)	2.1806(1)	2.1848(5)	2.1862(7)	2.2614(5)	2.2165(5)	2.1890(8)	2.2211(15)	2.1941(12)	2.193(2)
Ni – Br	2.3331(3)	2.3969(6)	2.3350(3)	2.3487(4)	2.3029(3)	2.3525(3)	2.3498(5)	2.3485(13)	2.328(3)	2.327(3)
N – C_{NHC} – N	116.48(19)	116.9(4)	117.06(17)	118.9(2)	115.68(15)	118.49(17)	118.5(2)	121.8(4)	121.0(4)	120.5(6)
C_{NHC} – Ni – P	117.01(6)	106.70(12)	106.39(5)	110.61(7)	118.99(5)	122.04(6)	110.07(8)	121.57(14)	111.83(13)	109.7(2)
C_{NHC} – Ni – Br	133.46(6)	138.82(12)	133.45(5)	139.22(7)	127.66(5)	134.00(5)	138.13(8)	135.0(2)	130.51(17)	133.8(2)
P – Ni – Br	109.531(19)	114.48(3)	120.123(17)	110.16(2)	113.352(16)	103.915(17)	111.66(2)	103.39(15)	117.64(11)	116.54(18)

Table 2.1 Selected bond lengths (Å) and angles (°) for **1 – 10**.

2.3.1 Attempted Synthesis of N-Alkyl Substituted Ni(RE NHC)(PPh$_3$)Br

Prompted by the success in generating N-aryl derived Ni(I)-RE NHC complexes efforts were made to employ sterically encumbering N-alkyl substituted RE NHCs. Following the same comproportionation pathway for the synthesis of **1 – 10**, a THF solution of 6^{t}Bu was formed *in situ*, reacted with Ni(COD)$_2$ and Ni(PPh$_3$)$_2$Br$_2$ in a ratio of 2:1:1 and stirred at room temperature for 2 h **(Scheme 2.4)**.

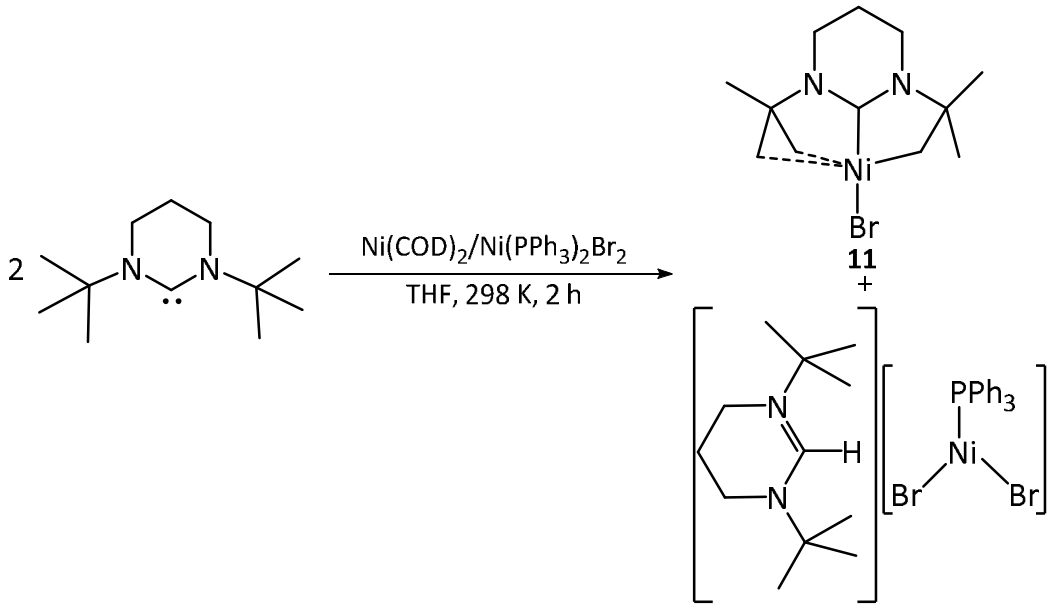

Scheme 2.4 Attempted comproportionation reaction of 6^{t}Bu with Ni(COD)$_2$ and Ni(PPh$_3$)$_2$Br$_2$.

The resulting orange solution was filtered and hexane added to yield a yellow precipitate. This showed no signals in the $^{31}P\{^1H\}$ NMR spectrum, while ^1H NMR analysis indicated the presence of paramagnetically shifted resonances in the range of 21.36 – -2.83 ppm. Recrystallisation from THF/hexane produced a mixture of orange block and yellow needle like crystals. X-ray crystallography showed the former to be Ni^{II}(6^{t}Bu)'Br **(11; Scheme 2.4, Figure 2.5)** in which the RE NHC displays one C-H activated and one agostically stabilised arm (through two separate agostic interactions). The structure appears best considered as a distorted trigonal bipyramidal Ni(II) species (C_{NHC}-Ni-Br: 178.58(5)^o; C_{NHC}-Ni-C(10): 83.48(7)^o; C(10)-Ni-H(6A): 159.67(9)^o; C(10)-Ni-H(6B): 148.17^o), in which the role of the agostic interactions is to stabilise what would otherwise be a highly electron deficient (14e$^-$) complex. This is commonly observed with 14e$^-$ *d*^{8} palladium[39,40] and platinum[41-43] systems. Selected metrics for **11** are displayed in **Table 2.2**. The second isolated product was the Ni(I) nickelate [6^{t}BuH][Ni(PPh$_3$)Br$_2$] (see **Appendix 2** for X-ray structure). Repeated attempts at this reaction afforded the same solution colour change

and similar ^{1}H NMR spectra. However, in spite of exhaustive efforts, further crystals or precipitation of **11** proved irreproducible, making additional characterisation or reactivity studies impossible to carry out (see **Appendix 7** for experimental).

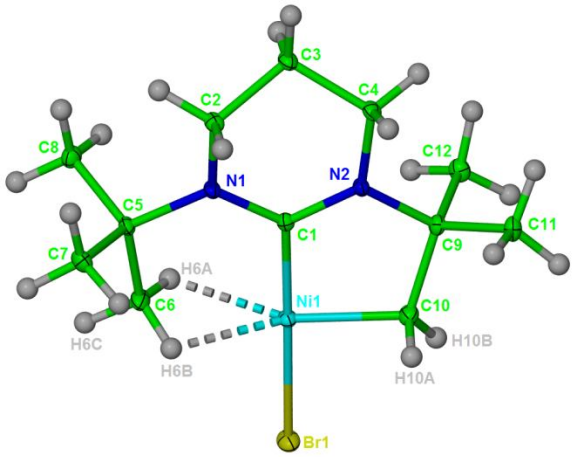

Figure 2.5 X-ray structure of **11**. Ellipsoids are shown at 30 % probability.

	11
Ni – C_{NHC}	1.8554(16)
Ni – C(10)	1.9148(18)
Ni – H(6A)	2.025(7)
Ni – H(6B)	1.975(8)
Ni – Br	2.3260(3)
N – C_{NHC} – N	119.74(15)
C_{NHC} – Ni – Br	178.58(5)
C_{NHC} – Ni – C(10)	83.48(7)
C(10) – Ni – H(6A)	159.67(9)
C(10) – Ni – H(6B)	148.17°

Table 2.2 Selected bond lengths (Å) and angles (°) for **11**.

Further experiments with other N-alkyl RE NHCs did prove more reliable, although less interesting. The smaller 6^{i}Pr (formed *in situ* from reaction of [6^{i}PrH]BF_4 with $KN(SiMe_3)_2$) was reacted with a 1:1 THF solution of $Ni(COD)_2$ and $Ni(PPh_3)_2Br_2$ for 2 h at 298 K. The resultant dark orange/red solution was filtered and hexane added to precipitate out a dark orange solid.

Analysis *via* ^{1}H NMR spectroscopy suggested the formation of a diamagnetic product that displayed resonances solely due to 6^{i}Pr ligands. Of most note, was a remarkably high frequency ^{i}Pr methine signal at 7.98 ppm (*c.f.* the C-H activated complex Ru(6^{i}Pr)'$(PPh_3)_2$(CO)(H) which displays methine signals at 6.08 (unactivated) and 5.14 ppm (activated)).[44] Recrystallisation from THF/hexane gave dark red crystals (13 % isolated yield) corresponding to the square planar Ni(II) complex Ni(6^{i}Pr)$_2$Br$_2$ **(12; Figure 2.6**). There was no indication of secondary products in the ^{1}H NMR spectrum of the reaction, suggesting that **12** is the major product of the reaction and that its low isolated yield results from high solubility. Formation of the same product was also achieved by reacting 6^{i}Pr with either Ni(dme)Br$_2$ or $Ni(PPh_3)_2Br_2$.

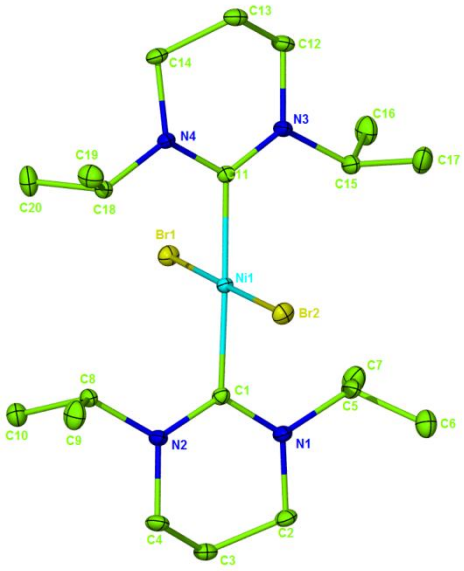

Figure 2.6 X-ray crystal structure of **12**. Thermal ellipsoids are set at 30 % probability. All hydrogen atoms have been omitted for clarity.

Table 2.3 shows selected bond lengths and angles for **12** and the related four coordinate Ni(II)-*bis*(carbene) species Ni(6Mes)$_2$Br$_2$[45] and Ni(IMe$_4$)$_2$I$_2$.[46] The N-C$_{NHC}$-N angles in **12** (117.87(16) and 118.14(16)^{o}) are about two degrees wider than in Ni(6Mes)$_2$Br$_2$ (115.87(14)^{o}). One result of this is the N-^{i}Pr substituents then reside in closer proximity to the nickel metal centre (**12**: Ni-C(5/8/15/18): 3.101(4)/3.085(4)/3.095(5)/3.081(5) Å; Ni(6Mes)$_2$Br$_2$: Ni-C$_{ipso}$: 3.281(6)/3.350(5) Å). The Ni-C$_{NHC}$ distances in **12** (1.9563(18) and 1.9534(18) Å) are comparable to the value in the 6Mes complex (1.9743(16) Å), although much longer than that in the IMe$_4$ derivative (1.897(3) Å). This seems counterintuitive given that 6-membered NHCs are considered to be the stronger σ-donors, which should shorten M-C$_{NHC}$. However, the proximity

of the N-substituents to the metal appears to push the NHC away. The failure to generate the three coordinate complex Ni(6^{i}Pr)(PPh_3)Br suggests that the N-^{i}Pr substituents are not bulky enough to stabilise a low coordinate Ni(I) species. Bromide coordination is possible into a vacant coordination site, thus generating the observed square planar Ni(II) complex.

	12	**Ni(6Mes)$_2$Br$_2$***[45]	**Ni(IMe$_4$)$_2$I$_2$***[46]
Ni – C(1)	1.9563(18)	1.9743(16)	1.897(3)
Ni – C(11)	1.9534(18)	-	-
Ni – X(1)	2.3381(3)	2.32623(17)	2.5180(3)
Ni – X(2)	2.3372(3)	-	-
N(1) – C(1) – N(2)	117.87(16)	115.87(14)	104.9(2)
N(3) – C(11) – N(4)	118.14(16)	-	-
C(1) – Ni – X(1)	91.86(5)	85.61(5)	90.79(8)
C(1) – Ni – X(2)	88.63(5)	94.39(5)	-

Table 2.3 Comparison of selected bond lengths (Å) and angles (°) in **12**, Ni(6Mes)$_2$Br$_2$ and Ni(IMe$_4$)$_2$I$_2$. X = halide (Br for **12**). * asymmetric unit = ½ of molecule with nickel atoms located on a crystallographic inversion centre.

The structures obtained from the attempts at forming N-alkyl RE NHC Ni(I) species indicate intrinsic differences between the use of N-aryl and N-alkyl substituents. N-aryl substituted NHCs seem to possess enough bulk, even with just one *o*-methyl group present (as in the cases of **2** and **7**) to stabilise three coordinate Ni(I). Conversely, N-alkyl substituted NHCs have shown no tendency thus far to form three coordinate species, but seem to give monomeric Ni(II) complexes and/or C-H activated ligands or nickelates. Even the bulkiest available ligand, 6^{t}Bu, appears not sterically encumbered enough to allow formation of the desired three coordinate Ni(I)-RE NHC products.

2.4 EPR and DFT Characterisation of Ni(RE NHC)(PPh_3)Br

Evans solution magnetic measurements had already confirmed the presence of a single unpaired electron in **1 – 10**, but EPR spectroscopy, in combination with DFT calculations, granted a more detailed understanding of the relationship between RE NHC ring size and the electronic properties of the d^9 Ni(I) centres.[31] X-band CW EPR (140 K) **(Figure 2.7)**, X-band FSED EPR (10 K), Q-band CW EPR (10K) and Q-band CW ^{1}H ENDOR spectra were recorded by

Dr. Emma Carter and Professor Damien Murphy at Cardiff University for **1, 5, 7 – 10** (**10**: only X-band FSED and Q-band CW EPR). To gain an insight into the effect of the halide, the mixed bromide/chloride complexes were measured for all the 8-membered RE NHC complexes, along with pure samples of the bromide and chloride 8^{o}Tol derivative **(9)**. Q-band EPR and ENDOR spectra are given in **Appendix 3**.

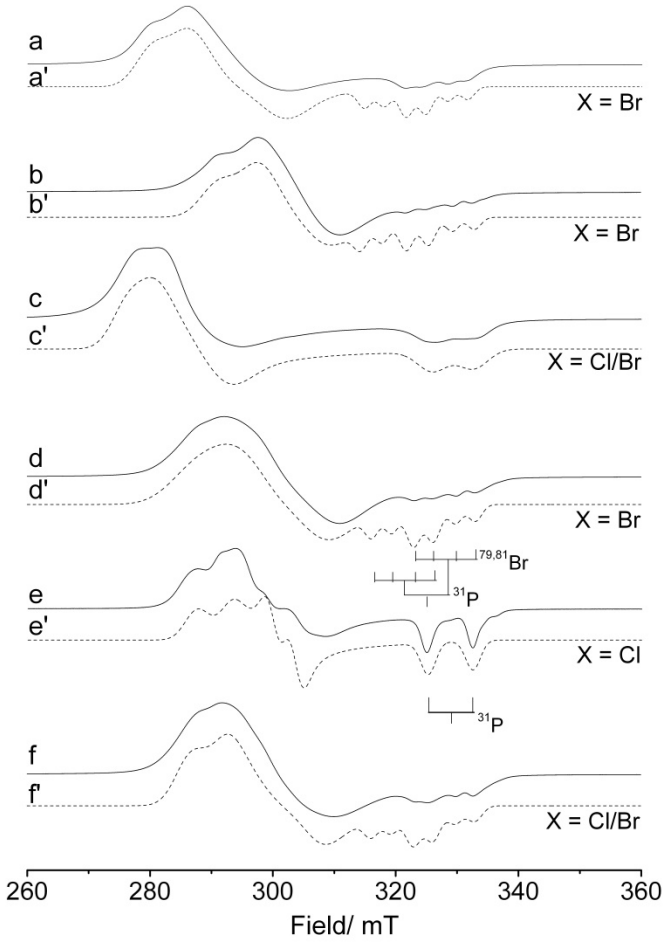

Figure 2.7 X-band CW EPR (140 K) spectra of Ni(RE NHC)(PPh_3)X (a – f) and the corresponding simulations (a' – f'). a: RE NHC = 6Mes, X = Br **(1)**; b: RE NHC = 7^{o}Tol, X = Br **(7)**; c: RE NHC = 8Mes, X = mixed Br/Cl **(8)**; d: RE NHC = 8^{o}Tol, X = Br **(9)**; e: RE NHC = 8^{o}Tol, X = Cl **(9)**; f: RE NHC = 8^{o}Tol, X = mixed Br/Cl **(9)**.

As seen in the X-band CW measurements **(Figure 2.7)**, all spectra display a rhombic ***g*** profile, with substantially broadened linewidths arising from the large superhyperfine coupling to the ^{31}P nucleus and, if present, the ^{79,81}Br nuclei (the *A* value was extracted more accurately from the ^{1}H ENDOR data). Rhombic spectra are not uncommon for Ni(I) metal centres, with four, five and six coordinate Ni(I) species being known to produce signals of this nature.[22,47-49] The ***g*** components for d^9 metal centres have been shown to be very sensitive to the coordination environment, easily allowing the theoretical parameters for any higher coordinated Ni(I)

species to be accounted for.[49-51] Conversely, due to their unstable nature and consequent lack of abundance, three coordinate Ni(I) metal centres are less well studied, making a strict theoretical description of them that incorporates vibronic interactions less straightforward.[22] Despite limited examples, the general trend of rhombic ***g*** tensor values observed in other three coordinate Ni(I) complexes, such as $[Ni(PPh_3)_3]BF_4$, $Ni(PPh_3)_2X$ (X = Br, Cl **(*ii*)**) and Ni(L)(N^N) (L = PCy_3, dppm; N^N = bulky β-diketiminate), is $\boldsymbol{g}_3 - \boldsymbol{g}_2 > \boldsymbol{g}_2 - \boldsymbol{g}_1$.[18,22,47,48] The opposite, less common trend, $\boldsymbol{g}_3 - \boldsymbol{g}_2 < \boldsymbol{g}_2 - \boldsymbol{g}_1$, is found in some examples such as $Ni(N\hat{}N)^{Me}(CO)$ ***(ii)***,[19,47] and is what is observed for **1 – 10**. Saraev *et al*.[47] reported that the ligand influences on the ***g*** tensor overide the effects of the vibronic interaction in ***ii***, thus leading to a reversal in the general trend. A similar explanation is therefore assumed for our RE NHC complexes, with the three ligands, specifically the RE NHC, outweighing any vibronic interactions. The ***g*** tensor components extracted from simulation of these Ni(RE NHC)(PPh_3)X complexes (**1**, **5**, and **7 – 10**), along with other reported three coordinate Ni(I) examples, are shown in **Table 2.4**

The trend and differences measured between the ***g*** values from EPR spectroscopy provide insight into the nature and location of the unpaired electron. In all the Ni(I)-RE NHC cases, $\boldsymbol{g}_2$ and $\boldsymbol{g}_3$ are considerably larger than $\boldsymbol{g}_1$ (which itself is close to free spin ($\boldsymbol{g}_e$)), indicating that the unpaired electron must be localised in a SOMO with predominantly $3d_{z2}$ character. The $\boldsymbol{g}_2$ and $\boldsymbol{g}_3$ values appear to be very sensitive to N-C_{NHC}-N bond angle variation and the increased NHC ring size (*i.e.* for the ^{o}Tol series: $\boldsymbol{g}_2$ = 2.275, $\boldsymbol{g}_3$ = 2.200 for the 7-membered complex **7** versus $\boldsymbol{g}_2$ = 2.312, $\boldsymbol{g}_3$ = 2.216 for the 8-membered species **9** (X = Br)). Previously, Pietrzyk *et al.*[49] used DFT to examine the ***g*** tensors for a variety of three coordinate Ni(I) centres of the form $[Ni(CO)_a(L)_b(L')_c]^{d+}$ (a = 1 – 4, L = H_2O (b = 0 – 2), L' = OH (c = 0 – 2), d = 0, 1), one of which was $[Ni(CO)(H_2O)_2]^+$, a T-shaped nickel cation with C_1 symmetry. Their calculations revealed an admixed SOMO of predominantly $3d_{z2}$ character mixed with some $3d_{x2-y2}$ and ***g*** tensor values of 2.357, 2.249 and 2.017 respectively, very similar to those observed for the RE NHC complexes **1**, **5** and **7 – 10** reported in **Table 2.4**. Comparative spectra and spin Hamiltonian parameters to those of **1** were obtained for the diamido complex **(5)**, suggesting that the differences in electronics between the NHC subclasses is not enough to change the orbital location of the unpaired electron or whether it is located solely on the nickel or not within this series of Ni(I)-RE NHC complexes.

Complex	g_1	g_2	$g_{3(z)}$	$g_3 - g_2$	$g_2 - g_1$	$^{P}A_1$ / MHz	$^{P}A_2$ / MHz	$^{P}A_3$ / MHz	Ref
1 (X = Br)	2.073	2.270	2.365	0.095	0.197	208 90	*206* *20*	*186* [a]*22*	t.w.
5 (X = Br)	2.035	2.220	2.373	0.153	0.185	249 50	*202* *47*	*68* [a]*97*	t.w.
7 (X = Br)	2.072	2.200	2.275	0.075	0.128	228 100	*169* *20*	*206* [a]*22*	t.w.
8 (X = Br/Cl)	2.034	2.322	2.405	0.083	0.288	188	*146*	*146*	t.w.
9 (X = Br)	2.066	2.216	2.312	0.096	0.150	208 90	*206* *20*	*186* [a]*22*	t.w.
9 (X = Cl)	2.037	2.216	2.307	0.091	0.179	208	*106*	*186*	t.w.
10 (X = Br/Cl)	2.072	2.216	2.322	0.106	0.144	228 100	*206* *20*	*186* [a]*22*	t.w.
$[Ni(PPh_3)_3]BF_4$	2.07	2.12	2.38	0.26	0.05	226 179	179 171	[b]171 [b]168	22,47
$Ni(PPh_3)_2Br$	2.112	2.209	2.435	0.226	0.097	216 105 21	159 105 93	159 102 [c]42	48
$Ni(PPh_3)_2Cl$ (*ii*)	2.111	2.167	2.446	0.279	0.056	201 123	165 117	[b]165 [b]105	48
$Ni(N^{\wedge}N)^{Me}$(dppm)	2.03	2.16	2.43	0.27	0.13				18
$Ni(N^{\wedge}N)^{Me}$(CO) (*iii*)	2.01	2.17	2.19	0.02	0.16				19
$[Ni(CO)(H_2O)_2]^+$	2.017	2.249	2.357	0.108	0.232				49

[a] Br couplings; [b] the two or three P nuclei are inequivalent in these literature complexes, hence the two ^{P}A values; [c] resolved Br coupling; t.w. = this work, all recorded in THF for direct comparison (***g*** values ±0.005). *N.B.: The italicised values of A_3/A_2 for the NHC complexes represent an estimated upper limit, as these couplings were not resolved in the broad experimental spectra.*

Table 2.4 Spin Hamiltonian parameters for Ni(RE NHC)(PPh_3)Br complexes **(1, 5, 7 – 10)** and other reported three coordinate Ni(I) complexes.

DFT calculations (performed by Dr. Andrés Algarra and Professor Stuart Macgregor at Heriot-Watt University) on complexes **1**, **7** and **8** (purely bromide containing) were used to explore the makeup of the SOMO in greater detail. The analysis revealed a SOMO admixture of $3d_{z2}$ and $3d_{x2-y2}$ for all the complexes studied, with predominant $3d_{z2}$ character for **1** and **8**. This agrees with the observed EPR data for all the Ni(I)-RE NHC complexes where $\boldsymbol{g}_{3,2} > \boldsymbol{g}_1 \approx \boldsymbol{g}_e$. In contrast, the calculated SOMO for **7 (Figure 2.8)** appears to contain a greater $3d_{x2-y2}$ component, which would be expected to produce a reversed ***g*** tensor profile, but was not observed. However, as reported by Pietrzyk *et al.*,[49] the mixed SOMO in $[Ni(CO)_a(L)_b(L')_c]^{d+}$ is heavily dependent on the geometry, changing from a $3d_{z2}$ ground state in a T-shape geometry to the $3d_{x2-y2}$ state for a trigonal planar environment. From **Table 2.1**, **7** does indeed have a

marginally larger C_{NHC}-Ni-Br angle, suggesting a greater T-shaped nature over the rest. This highlights how subtle alterations to the geometry of a complex can affect the admixed SOMO ground state in three coordinate Ni(I) complexes, and most likely explains the differences between complexes **1**, **7** and **8**. These calculations (pictorially shown in **Figure 2.8**) ultimately show that the single unpaired electron in these Ni(I)-RE NHC species is localised on the nickel metal centre and not delocalised around the ligand system as described earlier in the case of Ni(tpy)(CH_3) ***(lvi*; Chapter 1, 1.1.3, Chapter 5, 5.1.2.1)**.

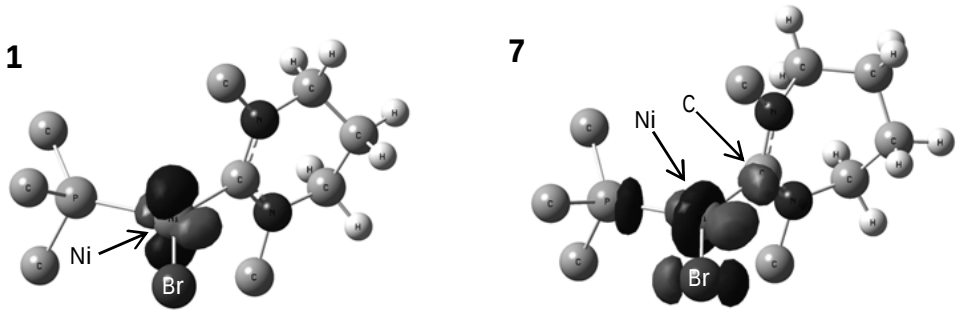

Figure 2.8 Computed SOMOs for **1** (left) and **7** (right). Isosurfaces are drawn at 0.07 probability and both the PPh_3 phenyl and NHC N-aryl substituents are truncated at the *ipso* carbon atoms for clarity.

It is expected that any $M(L)_n$ (L = phosphine) species with an unpaired electron will exhibit significant hyperfine coupling in an EPR spectrum. This is certainly true from the spin Hamiltonian parameters presented in **Table 2.4**, where all the three coordinate Ni(I) complexes bearing a coordinated phosphorus demonstrate large ^{P}A values with a predominant isotropic contribution, thus reflecting the expected high degree of Ni-P covalency. Although the $A_{2,3}$ components of the phosphine superhyperfine tensor were unresolved for Ni(RE NHC)(PPh_3)X due to the considerably broad line widths in the frozen solution spectra, the resolved A_1 component is of similar magnitude to other phosphorus containing three coordinate Ni(I) complexes.[22,48,52]

The inadvertent inclusion of mixed bromide/chloride, alongside the pure bromide and chloride measurements, has allowed analysis of the variation of the electronic state of Ni(RE NHC)(PPh_3)X as a function of halide X. The EPR spectra of the pure bromide containing complexes are shown in **Figure 2.7a**,**b** and **d** (for compounds **1**, **7** and **9** respectively), whereas **Figure 2.7e** shows the spectrum of the pure chloride containing Ni(8^{o}Tol)(PPh_3)Cl **(9)**. In the former, additional features are visible along the $\boldsymbol{g}_1$ component in the CW EPR spectra, which must arise from ^{79,81}Br couplings since the features are absent when X = Cl. Simulations carried

out on these spectra indicate that all the ***g*** values are very dependent on the nature of the halide, as shown experimentally in **Table 2.4** where there are significant differences in the ***g*** values for the Ni-8^{o}Tol derivative **(9)** when X = Br or Cl. This highlights the importance of the halide and again the ligand environment as a whole in influencing the ***g*** tensor values. Coupling to ^{79,81}Br in these types of complexes is not uncommon; Nilges *et al*.[48] has observed well resolved Br superhyperfine and quadrupole coupling in Ni(PPh$_3$)$_2$Br. They reported that the largest principal component of the quadrupole tensor was directed along the Ni-Br bond. However, as this was found to be of similar magnitude to the Br superhyperfine splitting, a complex EPR pattern resulted. The magnitude of the Br hyperfine couplings observed for the RE NHC complexes are similar to those reported by Nilges *et al.*, although, unsurprisingly, the quadrupole couplings could not be resolved in the frozen solution spectra. Furthermore, no Cl coupling was observed for the Ni-RE NHC complexes, analogous to the observations of Nilges *et al.* The EPR spectra of the mixed halide samples Ni(RE NHC)(PPh$_3$)Br/Cl shown in **Figure 2.7c** and **f** should therefore be regarded as composite spectra comprising of overlapping contributions from Ni(RE NHC)(PPh$_3$)Br and Ni(RE NHC)(PPh$_3$)Cl. Despite this, the mixed halide complex **8** (RE NHC = 8Mes, X = Br/Cl) appears to contain mostly chloride, whereas the mixed halide complex **9** (RE NHC = 8^{o}Tol, X = Br/Cl) appears to contain mostly bromide by comparison to the EPR spectra of the pure Br and Cl samples, **Figure 2.7d** and **e** respectively. Further DFT calculations taking into consideration the halide would be necessary to accurately quantify the SOMO and thus predict the ***g*** values of these complexes.

2.5 SQUID Magnetic Studies on Ni(RE NHC)(PPh$_3$)Br

The presence of an unpaired electron in these d^9 complexes gives rise to the possibility of interesting magnetic behaviour. The location of this electron, along with the ground state orbital angular momentum, can lead to the complex displaying SMM behaviour. In essence, SMMs are molecules which possess the ability to maintain magnetisation for relatively long periods of time in the absence of an applied magnetic field, invariably at low temperatures, and are described and discussed in further detail in **Chapter 1, 1.3.1** and **Chapter 4, 4.1.2**.[53] In complexes **1 – 10**, the free electron resides in a $3d_{z2}$ and $3d_{x2-y2}$ admixtured HOMO with predominantly $3d_{z2}$ character, allowing possible interconversion and rotation between the two. This gives rise to orbital angular momentum, which if it is unquenched by the ligand field, will lead to magnetic anistropy and possibly SMM characteristics. Analysis of these species *via*

a SQUID (superconducting quantum interferece device) allows for determination of magnetic properties from subtle magnetic field changes.

SQUID measurements were carried out in collaboration with Jennifer Le Roy and Professor Muralee Murugesu at the University of Ottawa on **1**, **3**, **4** and **6** with the intention of probing any effect of i) increasing carbene ring size (6Mes **(1)** and 7Mes **(6)**), ii) changing N-substituents (6Mes and 6^{o}Anis **(3)**) and iii) going from symmetric to asymmetric RE NHCs (6^{o}Anis and 6^{o}AnisMes **(4)**). The χT (magnetic susceptibility) values for all four complexes are shown in **Table 2.5**.

	1	**3**	**4**	**6**
χ**T**	0.76	0.90	0.67	1.03
M	1.16	1.08	1.03	1.06

Table 2.5 Magnetic susceptibility (χT) values (cm^3 K mol^{-1}) at room temperature and magnetisation saturation levels (*M*) at low temperatures (1.8 – 7 K) (μB) for **1**, **3**, **4** and **6**.

The room temperature χT values for all four species are slightly higher than the expected theoretical spin only value of 0.375 cm^3 K mol^{-1} for d^9 Ni(I) complexes (S = 1/2, $\boldsymbol{g}$ = 2, $\chi T = \boldsymbol{g}^2 S(S+1)/8$). The higher values can originate from significant inherent magnetic anisotropy expected in trigonal Ni(I) monomers.[54] The dependence of χT with temperature was investigated and, as shown in **Figure 2.9**, each complex shows a decrease in χT as the temperature is lowered. The decline in χT is constant from 300 K to 10 K, with a much sharper drop below 10 K to reach minimum values of 0.35, 0.34, 0.48 and 0.48 cm^3 K mol^{-1} (**1**, **3**, **4** and **6** respectively). This low temperature negative deviation of the χT product is most likely due to a combination of factors including antiferromagnetic intermolecular interactions, inherent magnetic anisotropy and/or the depopulation of excited states.

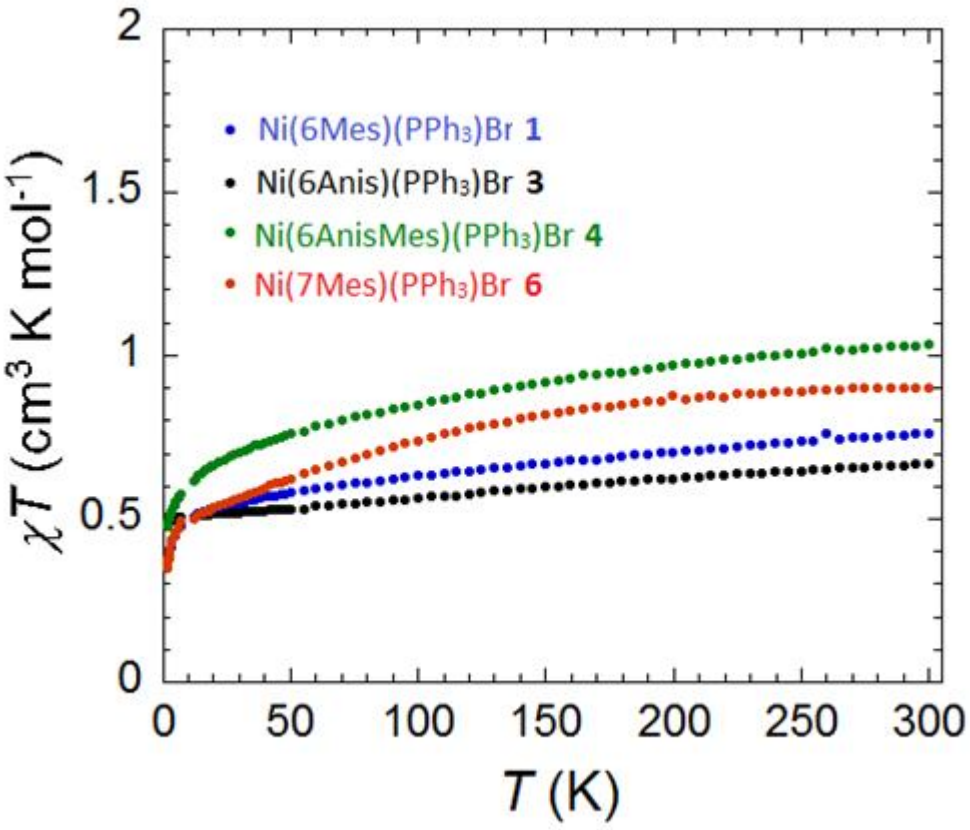

Figure 2.9 Temperature dependence of the χT value at 0.1 T for **1**, **3**, **4** and **6**.

To confirm the presence of magnetic anisotropy, field dependent magnetisation measurements were carried out between 1.8 and 7 K at fields ranging from 0 to 7 T. **Figure 2.10** shows the measurements for **1** and **3**. In each Ni(I) complex, the *M vs.* H data (H = external reversed magnetic field) below 7 K demonstrates a rapid increase in the magnetisation at low magnetic fields (< 2 T). Above 2 T, a more gradual increase is observed at 1.8 K, with the complexes reaching near saturation (*M*) at 1.8 K under 7 T **(Table 2.5)**. All four complexes also display similar *M vs.* H T^{-1} data, where at high fields there is no saturation nor overlay onto a single master curve (see *M vs.* H T^{-1} data for **1** in **Figure 2.10**). This indicates the presence of magnetic anisotropy and/or low-lying excited states. As observed in **Figure 2.10**, the 6^{o}Anis complex **3** displays near overlay of *M vs.* H T^{-1} data, indicative of less anisotropy in this system compared to the other complexes.

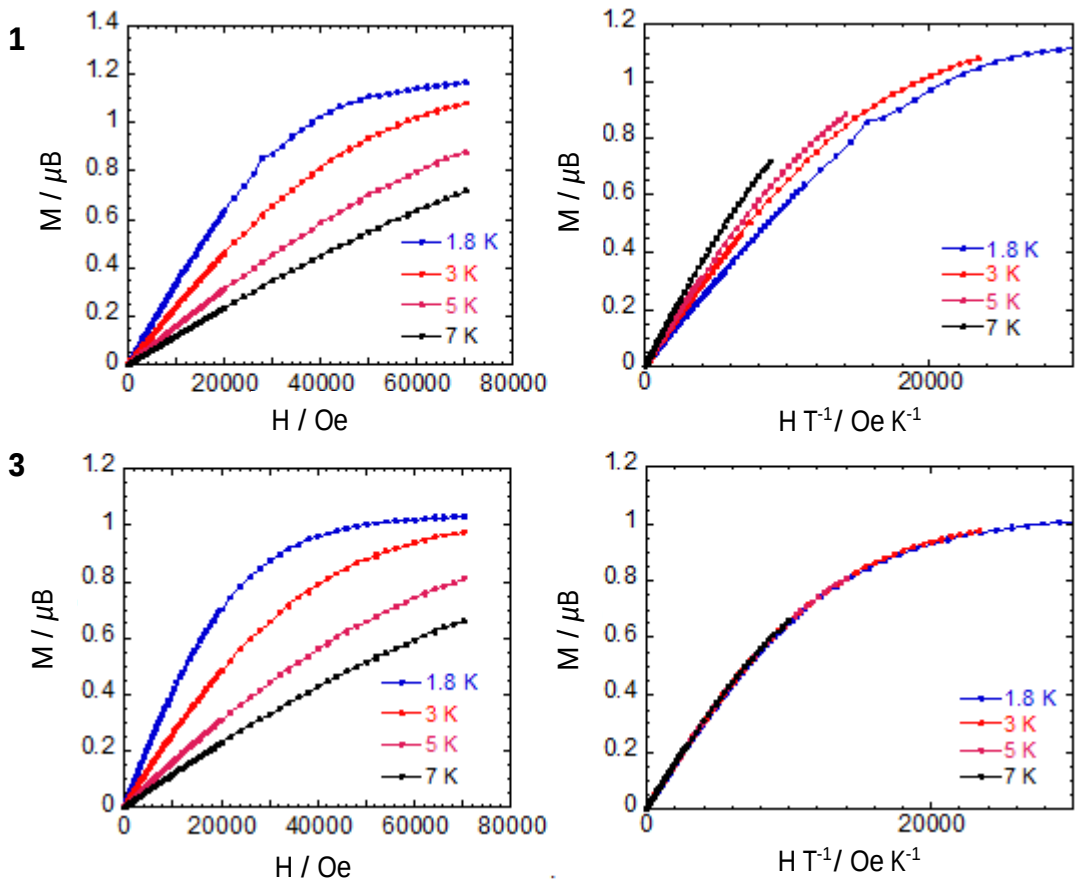

Figure 2.10 Field dependence of the magnetisation *M vs.* H (left) and reduced magnetisation *M vs.* H T^{-1} (right) for **1** (above) and **3** (below). 1 T = 10000 Oe.

To probe any SMM behaviour, the temperature dependence of the out-of-phase (χ'') magnetic susceptibility was investigated. Under both a zero applied dc field and a 0.1 T dc field, no temperature dependent signal was observed, precluding SMM behaviour in each of the three coordinate Ni(I) complexes. Therefore, despite the complexes displaying evidence for magnetic anisotropy, in these cases this does not lead to any SMM behaviour. This is not uncommon, with several nickel complexes in recent years being reported to have very large anisotropy values,[53,55-59] however none of these mononuclear complexes exhibited SMM characteristics. With these Ni(I) species providing additional examples, it further highlights the importance of measuring for remanence magnetisation.

2.6 Chapter Summary

Employing a comproportionation reaction, a series of 6-, 7- and 8-membered RE NHCs have been used to prepare a range of novel, trigonal planar nickel complexes of the form Ni(RE NHC)(PPh_3)Br. These compounds have been fully characterised through magnetic meaurements, ^{1}H NMR, EPR and ENDOR spectroscopy, as well as by X-ray diffraction. X- and Q-band EPR spectroscopy specifically revealed that the spin Hamiltonian parameters, especially ***g*** values, of these d^9 systems vary considerably as a function of i) RE NHC ring size (6-, 7- or 8-membered), ii) N-substituents (mesityl or tolyl) and iii) halide (Br or Cl), and, along with DFT calculations, verified that the single unpaired electron is localised on the nickel metal centre in a mixed SOMO of predominantly $3d_{z2}$ character. However, this admixture (of $3d_{z2}$ and $3d_{x2-y2}$) varies between complexes (*e.g.* Ni-6Mes **(1)** and Ni-7^{o}Tol **(7)**), revealing the sensitivity of the SOMO to the ligand environment emcompassing the Ni(I) metal ion. Large ^{13}P and ^{79,81}Br couplings were also detected in the EPR spectra, with magnitudes comparable to other $Ni^I(PPh_3)_nBr$ complexes. SQUID analysis showed that despite measurable magnetic susceptibility, these systems were not SMMs.

2.7 References

1. A. Binobaid, M. Iglesias, D. J. Beetstra, B. Kariuki, A. Dervisi, I. A. Fallis and K. J. Cavell, *Dalton Trans.*, 2009, 7099-7112.
2. M. Iglesias, D. J. Beetstra, J. C. Knight, L. L. Ooi, A. Stasch, S. Coles, L. Male, M. B. Hursthouse, K. J. Cavell, A. Dervisi and I. A. Fallis, *Organometallics*, 2008, **27**, 3279-3289.
3. M. Mayr, K. Wurst, K. H. Ongania and M. R. Buchmeiser, *Chem. Eur. J.*, 2004, **10**, 1256-1266.
4. C. J. E. Davies, M. J. Page, C. E. Ellul, M. F. Mahon and M. K. Whittlesey, *Chem. Commun.*, 2010, **46**, 5151-5153.
5. S. Caddick, F. G. N. Cloke, P. B. Hitchcock and A. K. D. Lewis, *Angew. Chem., Int. Ed.*, 2004, **43**, 5824-5827.
6. B. R. Dible, M. S. Sigman and A. M. Arif, *Inorg. Chem.*, 2005, **44**, 3774-3776.
7. M. S. Khan, S. J. Davies, A. K. Kakkar, D. Schwartz, B. Lin, B. F. G. Johnson and J. Lewis, *J. Organomet. Chem.*, 1992, **424**, 87-97.
8. S. Miyazaki, Y. Koga, T. Matsumoto and K. Matsubara, *Chem. Commun.*, 2010, **46**, 1932-1934.
9. K. Zhing, M. Conda-Sheridan, S. R. Cooke and J. Louie, *Organometallics*, 2011, **30**, 2546-2552.
10. N. A. Eckert, A. Dinescu, T. R. Cundari and P. R. Holland, *Inorg. Chem.*, 2005, **44**, 7702-7704.
11. S. Nagao, T. Matsumoto, Y. Koga and K. Matsubara, *Chem. Lett.*, 2011, **40**, 1036-1038.
12. D. C. Bradley, M. B. Hursthouse, R. J. Smallwood and A. J. Welch, *J. Chem. Soc. - Chem. Comm.*, 1972, 872-873.
13. C. Eaborn, M. S. Hill, P. B. Hitchcock and J. D. Smith, *Chem. Commun.*, 2000, 691-692.
14. D. D. Ellis and A. L. Spek, *Acta. Crystallogr. Sect. C - Cryst. Struct. Commun*, 2000, **C56**, 1067-1070.
15. D. J. Mindiola and G. L. Hillhouse, *J. Am. Chem. Soc.*, 2001, **123**, 4623-4624.
16. N. C. Norman, A. G. Orpen, M. J. Quayle and G. R. Whittell, *Acta. Crystallogr. Sect. C - Cryst. Struct. Commun*, 2002, **C58**, 160-161.
17. R. Melenkivitz, D. J. Mindiola and G. L. Hillhouse, *J. Am. Chem. Soc.*, 2002, **124**, 3846-3847.
18. K. D. Kitiachvili, D. J. Mindiola and G. L. Hillhouse, *J. Am. Chem. Soc.*, 2004, **126**, 10554-10555.

19. G. Bai, P. Wei and D. W. Stephan, *Organometallics*, 2005, **24**, 5901-5908.
20. Z. Weng, S. Teo, L. L. Koh and T. S. A. Hor, *Angew. Chem., Int. Ed.*, 2005, **44**, 7560-7564.
21. H. Y. Wang, X. Meng and G. X. Jin, *Dalton Trans.*, 2006, 2579-2585.
22. V. V. Saraev, P. B. Kraikivskii, I. Svoboda, A. S. Kuzakov and R. F. Jordan, *J. Phys. Chem. A*, 2008, **112**, 12449-12455.
23. D. Adhikari, S. Mossin, F. Basuli, B. R. Dible, M. Chipara, H. Fan, J. C. Huffman, K. Meyer and D. J. Mindiola, *Inorg. Chem.*, 2008, **47**, 10479-10490.
24. S. Pfirrmann, C. Limberg, C. Herwig, R. Stösser and B. Ziemer, *Angew. Chem., Int. Ed.*, 2009, **48**, 3357-3361.
25. C. A. Laskowski and G. L. Hillhouse, *Organometallics*, 2009, **28**, 6114-6120.
26. V. M. Iluc and G. L. Hillhouse, *J. Am. Chem. Soc.*, 2010, **132**, 11890-11892.
27. V. M. Iluc and G. L. Hillhouse, *J. Am. Chem. Soc.*, 2010, **132**, 15148-15150.
28. S. T. Chao, N. C. Lara, S. Lin, M. W. Day and T. Agapie, *Angew. Chem., Int. Ed.*, 2011, **50**, 7529-7532.
29. C. Liu, S. Tang, D. Liu, J. Yuan, L. Zheng, L. Meng and A. Lei, *Angew. Chem., Int. Ed.*, 2012, **51**, 3638-3641.
30. M. J. Ingleson, B. C. Fullmer, D. T. Buschhorn, H. Fan, M. Pink, J. C. Huffman and K. G. Caulton, *Inorg. Chem.*, 2008, **47**, 407-409.
31. M. J. Page, W. Y. Lu, R. C. Poulten, E. Carter, A. G. Algarra, B. M. Kariuki, S. A. Macgregor, M. F. Mahon, K. J. Cavell, D. M. Murphy and M. K. Whittlesey, *Chem. Eur. J.*, 2013, **19**, 2158-2167.
32. T. W. Hudnall, A. G. Tennyson and C. W. Bielawski, *Organometallics*, 2010, **29**, 4569-4578.
33. T. W. Hudnall, J. P. Moerdyk and C. W. Bielawski, *Chem. Commun.*, 2010, **46**, 4288-4290.
34. T. W. Hudnall and C. W. Bielawski, *J. Am. Chem. Soc.*, 2009, **131**, 16039.
35. J. P. Moerdyk and C. W. Bielawski, *Chem. Commun.*, 2014, **50**, 4551-4553.
36. M. Braun, W. Frank, G. J. Reiss and C. Ganter, *Organometallics*, 2010, **29**, 4418-4420.
37. V. Cesar, N. Lugan and G. Lavigne, *J. Am. Chem. Soc.*, 2008, **130**, 11286.
38. V. Cesar, N. Lugan and G. Lavigne, *Eur. J. Inorg. Chem.*, 2010, 361-365.
39. J. Campora, E. Gutierrez-Puebla, J. A. Lopez, A. Monge, P. Palma, D. del Rio and E. Carmona, *Angew. Chem., Int. Ed.*, 2001, **40**, 3641.
40. J. P. Stambuli, R. Kuwano and J. F. Hartwig, *Angew. Chem., Int. Ed.*, 2002, **41**, 4746-4748.

41. M. J. Ingleson, M. F. Mahon and A. S. Weller, *Chem. Commun.*, 2004, 2398-2399.
42. L. Mole, J. L. Spencer, N. Carr and A. G. Orpen, *Organometallics*, 1991, **10**, 49-52.
43. W. Baratta, S. Stoccoro, A. Doppiu, E. Herdtweck, A. Zucca and P. Rigo, *Angew. Chem., Int. Ed.*, 2003, **42**, 105-108.
44. R. Armstrong, C. Ecott, E. Mas-Marza, M. J. Page, M. F. Mahon and M. K. Whittlesey, *Organometallics*, 2010, **29**, 991-997.
45. M. Page, *Unpublished Results*.
46. D. S. McGuinness, K. J. Cavell, B. W. Skelton and A. H. White, *Organometallics*, 1999, **18**, 1596-1605.
47. V. V. Saraev, P. B. Kraikivskii, P. G. Lazarev, G. Myagmarsuren, V. S. Tkach and F. K. Schmidt, *Russ. J. Coord. Chem.*, 1996, **22**, 615-621.
48. M. J. Nilges, E. K. Barefield, R. L. Belford and P. H. Davies, *J. Am. Chem. Soc.*, 1977, **99**, 755-760.
49. P. Pietrzyk, K. Podolska and Z. Sojka, *J. Phys. Chem. A*, 2008, **112**, 12208-12219.
50. J. Telser, *J. Braz. Chem. Soc.*, 2010, **21**, 1139-1157.
51. J. Pilbrow, *Transition Ion Electron Paramagnetic Resonance*, Clarendon Press, Oxford, 1990.
52. V. V. Saraev, P. B. Kraikivskii, P. G. Lazarev, G. Myagmarsuren, V. S. Tkach and F. K. Shmidt, *Koordinats. Khim.*, 1996, **22**, 648-654.
53. R. A. Layfield, *Organometallics*, 2014, **33**, 1084-1099.
54. M. Franks, A. Gadzhieva, L. Ghandhi, D. Murrell, A. J. Blake, E. S. Davies, W. Lewis, F. Moro, J. McMaster and M. Schroeder, *Inorg. Chem.*, 2013, **52**, 660-670.
55. F. Neese and D. A. Pantazis, *Farad. Discuss.*, 2011, **148**, 229-238.
56. G. Rogez, J. N. Rebilly, A. L. Barra, L. Sorace, G. Blondin, N. Kirchner, M. Duran, J. van Slageren, S. Parsons, L. Ricard, A. Marvilliers and T. Mallah, *Angew. Chem., Int. Ed.*, 2005, **44**, 1876-1879.
57. R. Ruamps, R. Maurice, L. Batchelor, M. Boggio-Pasqua, R. Guillot, A. L. Barra, J. Liu, E.-E. Bendeif, S. Pillet, S. Hill, T. Mallah and N. Guihery, *J. Am. Chem. Soc.*, 2013, **135**, 3017-3026.
58. R. Ruamps, L. J. Batchelor, R. Maurice, N. Gogoi, P. Jimenez-Lozano, N. Guihery, C. de Graaf, A. L. Barra, J. P. Sutter and T. Mallah, *Chem. Eur. J.*, 2013, **19**, 950-956.
59. J. Krzystek, J. H. Park, M. W. Meisel, M. A. Hitchman, H. Stratemeier, L. C. Brunel and J. Telser, *Inorg. Chem.*, 2002, **41**, 4478-4487.

CHAPTER 3

3 Instability of Ni(RE NHC)(PPh_3)Br

As briefly described in **Chapter 1**, Ni(I) complexes show reactivity towards a whole range of small molecules, leading to bond activation and in some cases, further functionalisation. The resultant nickel complexes are often bridged dimeric species consisting of $Ni_2(\mu\text{-}L)_2$ cores. The preparation and characterisation of **1 – 10** bearing the easily modified RE NHC ligand set affords a complete series of three coordinate Ni(I) complexes, in which the stereoelectronic properties of the metal centre can be altered in a controlled manner. This provides an opportunity for extensive research into Ni(I) reactivity, allowing for the possibility of correlating Ni(I) structure with small molecule activation/reactivity.

3.1 Reactivity of Ni(RE NHC)(PPh_3)Br with O_2 (RE NHC N-Substituent = Mesityl)

During efforts to prepare the N-Mes substituted complexes **1** and **6**, their air-sensitivity in both solid-state and solution was apparent by a rapid change in colour from yellow to purple upon even inadvertent exposure of trace levels of air/oxygen. In an effort to address this reactivity, THF solutions of **1** and **6** were opened to 1 atm O_2 at 298 K to bring about the anticipated colour change. Upon removal of the solvent and recrystallisation of the resultant purple residues from CH_2Cl_2/hexane or THF/hexane, dark purple crystals were obtained. Single crystal X-ray analysis indicated that activation of O_2 had occurred to generate the Ni(II) dimers Ni(6Mes)Br(μ-OH)(μ-O-6Mes)'NiBr **(13)** and Ni(7Mes)Br(μ-OH)(μ-O-7Mes)'NiBr **(14)**, which were isolated in low yields of 10 % and 14 % respectively **(Scheme 3.1)**.[1] Yields of > 50 % were achieved for both **13** and **14** upon drying the crude reaction mixture *in vacuo*, redissolving in C_6H_5F and then vigorously stirring overnight with hexane to afford the products as purple precipitates.

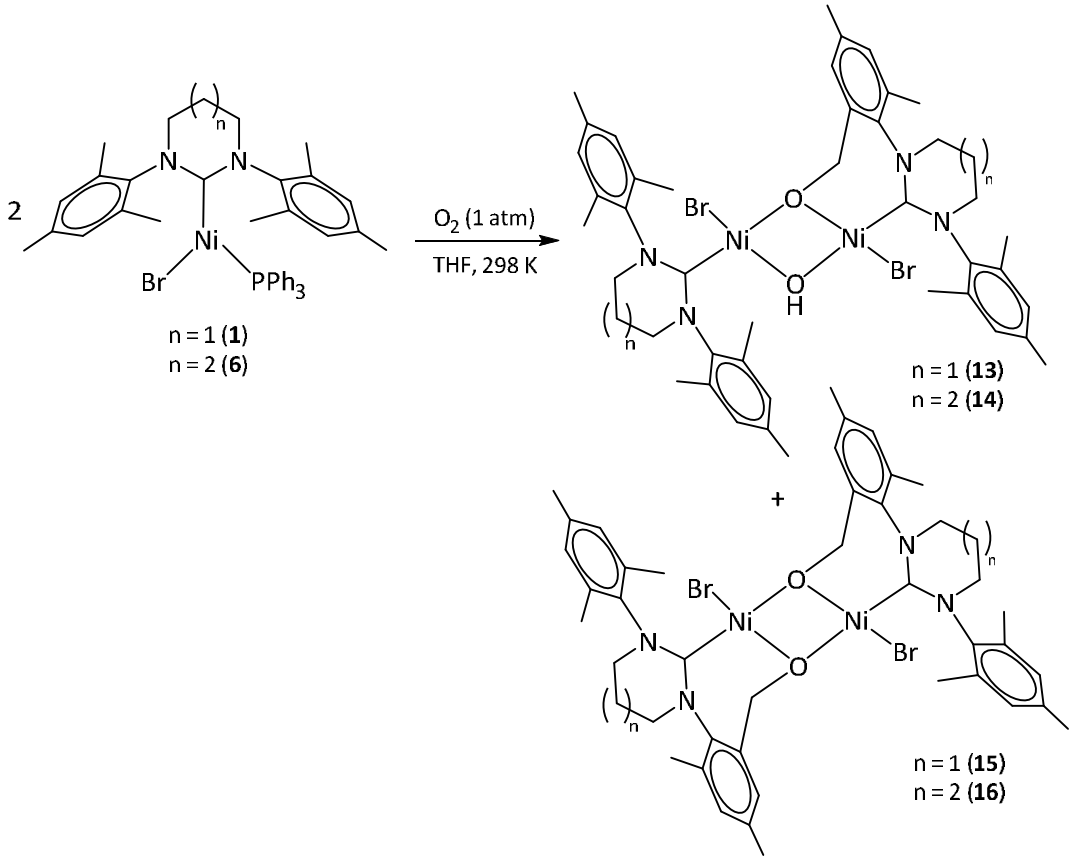

Scheme 3.1 Activation of O_2 by **1** and **6** to form singly C-H activated (**13** and **14**) and doubly C-H activated (**15** and **16**) Ni(II) dimers.

The ^{1}H NMR spectra of both the crude reaction mixtures and isolated samples of **13** and **14** contained numerous overlapping broad signals which could not be assigned to specific groups, as shown in the case of **13** in **Figure 3.1**. The signals of most interest were singlets which resonated at -6.19 ppm in CD_2Cl_2 **(Figure 3.1)** and -8.36 ppm in C_6D_6 for **13** and at -8.84 ppm in CD_2Cl_2 for **14**. On the basis of subsequent X-ray analysis, these were attributed to the hydroxyl protons. As expected, they disappeared upon addition of D_2O.* Such a low frequency for the hydroxyl proton in the ^{1}H NMR spectra is not uncommon with [Ni(IPr)Cl(μ-OH)]$_2$ ***(xlvii)*** exhibiting an upfield singlet resonance at -7.80 ppm.[2,†] The remainder of the ^{1}H NMR spectrum of **13** yielded very little interpretable information. The spectrum of **14** was much broader and therefore even less diagnostic. These spectra are discussed further in section **3.1.1**. Neither complex proved to be soluble enough in acetone, MeCN, C_6H_6, toluene, CH_2Cl_2 or even C_6H_5F to provide samples strong enough to record diagnostic ^{13}C NMR spectra. In particular, it was not

* Likewise, μ-OH stretches for **13** and **14** in their IR spectra vanished after exchange with D_2O (**13**: ν_{NiO-H} = 3412 cm^{-1}; **14**: ν_{NiO-H} = 3436 cm^{-1}).
† ***xlvii*** displays a sharp IR stretch at 3645 cm^{-1}.[2]

possible to observe the Ni-$^{13}C_{NHC}$ resonances in either case. Only free PPh_3 was observed by $^{31}P\{^1H\}$ NMR spectroscopy of crude reaction mixtures.

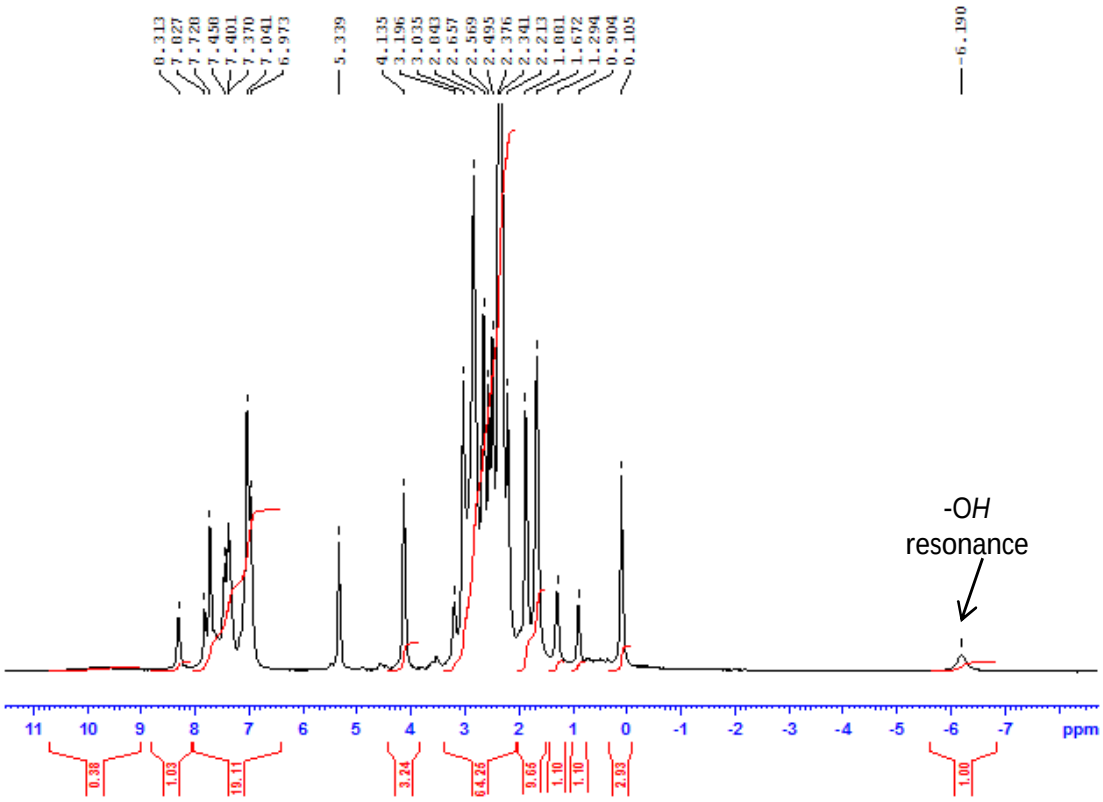

Figure 3.1 ^1H NMR spectrum of **13** (CD_2Cl_2, 500 MHz, 298 K).

The X-ray structures of **13** and **14** are shown in **Figure 3.2**. For both complexes, each nickel centre is in a square planar environment coordinated to one bromide and one carbene ligand, while bridged by two –OR groups. One bridge consists of a hydroxyl group, while the other is formed from oxidation of a C-H bond in one of the *o*-methyl groups of a 6/7Mes ligand. The most likely source of hydrogen in the hydroxyl ligands is that released upon activation of the 6Mes methyl arm.[3]

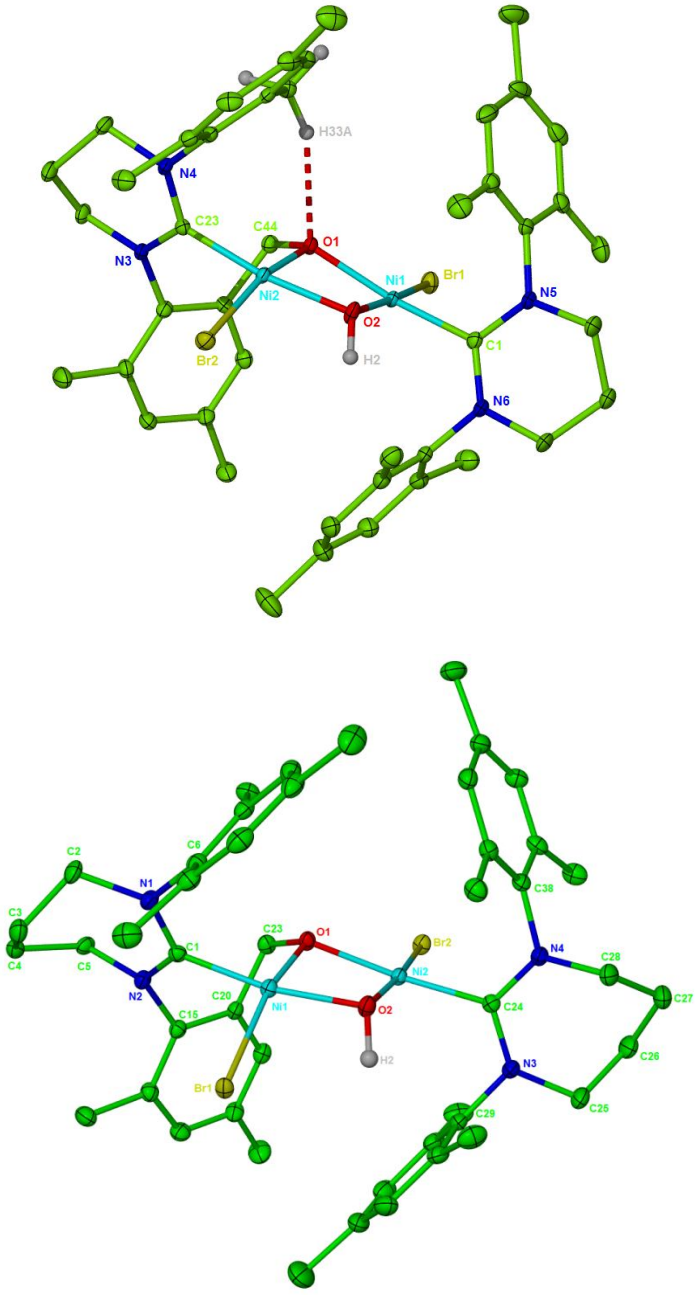

Figure 3.2 X-ray structures of **13** (above) and **14** (below). Thermal ellipsoids are set at 30 % probability. All hydrogen atoms have been omitted for clarity, apart from H(2) and H(33A) in **13** and H(2) for **14**.

Metrics for **13** and **14** are given in **Table 3.1**. All bond lengths and angles in **13** and **14** are similar with no noteworthy exceptions. The strain imposed by the bridging -OCH_2-aryl group contributes to the acute O-Ni-O bond angles observed (**13**: 80.18(10), 80.55(10)°; **14**: 80.13(13), 79.40(13)°). The central $Ni_2(\mu$-OH)(μ-OCH_2) cores are asymmetric, with all four of the Ni-O bond lengths in each complex being marginally different to one another. The longest distances are found between the non-activated NHC bound nickel and the μ-O-CH_2-aryl oxygen

(**13**: Ni(1)-O(1) 1.926(2) Å; **14**: Ni(2)-O(1) 1.936(3) Å), while the shortest are from the same nickel centres to the *μ*-OH bridge (**13**: Ni(1)-O(2) 1.869(3) Å; **14**: Ni(2)-O(2) 1.878(4) Å).

	13	**14**
Ni(1) – C(1)	1.883(4)	1.878(4)
Ni(2) – C(23)	1.856(3)	1.896(4)
O(1) – C(44)	1.443(4)	1.437(5)
Ni(1) – O(1)	1.926(2)	1.889(3)
Ni(1) – O(2)	1.869(3)	1.896(3)
Ni(2) – O(1)	1.892(2)	1.936(3)
Ni(2) – O(2)	1.890(2)	1.878(3)
Ni(1) – Br(1)	2.3299(6)	2.4139(7)
Ni(2) – Br(2)	2.3083(6)	2.3264(7)
Ni(1)···Ni(2)	2.8713(6)	2.8871(8)
O(1) – O(2)	2.445(5)	2.436(5)
N(5) – C(1) – N(6)	116.5(3)	118.3(4)
N(3) – C(23) – N(4)	118.2(3)	120.7(4)
Ni(1) – O(1) – Ni(2)	97.53(11)	98.00(13)
Ni(1) – O(2) – Ni(2)	99.63(12)	99.83(14)
O(1) – Ni(1) – O(2)	80.18(10)	80.13(13)
O(1) – Ni(2) – O(2)	80.55(10)	79.40(13)

Table 3.1 A comparison of selected bond lengths (Å) and angles (°) in **13** and **14**. The atom numbers refer to complex **13**, with the metrics for the corresponding bond/angle in **14** shown in the same row.

The orientation of the C-H activated *o*-methyl substituent is such that, as expected, the N-C_{NHC}-N bond angle for the activated RE NHC ligand (**13**: 118.2(3)°; **14**: 120.7(4)°) is wider than that of the unactivated 6/7Mes groups (**13**: 116.5(3)°; **14**: 118.3(4)°). The O-$C_{activated}$ bond distances (**13**: 1.443(4) Å; **14**: 1.437(5) Å) are unexceptional, falling in the range of a typical O-CH_n bond length.[4] On inspection, the activated mesityl mean plane in both complexes intersects the RE NHC backbone mean plane at a much more acute angle (**13**: 61.22(9)°; **14**: 52.12(8)°) than observed for either the unactivated mesityl located on the same RE NHC (**13**: 77.12(8)°; **14**: 64.34(7)°) or the other carbene ligand (**13**: 73.71(7) and 88.25(10)°;

14: 71.57(9) and 71.43(9)°). This suggests that the presence of the C-O moiety pulls in the mesityl substituent closer to the nickel metal centre bearing the activated RE NHC, which potentially sterically stabilises it from further attack. It is notable that in **13**, deviation of the carbene nitrogen atoms from the mean plane of the surrounding bonded carbon atoms is maximised in the case of that bonded to the hydroxylated mesityl ring (0.11 Å for N(3) relative to an average of 0.02 Å for N(4), N(5) and N(6)). These data reflect a distortion from the idealised sp^2 geometry at N(3), about which strain is optimal. A comparative observation is evident in **14** where the distance of the N-hydroxylated mesityl nitrogen from the mean plane of the surrounding bonded carbon atoms is 0.16 Å.

3.1.1 Detection of Double Oxygenative C-H Activated Ni(II) Dimers [NiBr(μ-O-RE NHC)']$_2$

Although **13** showed limited solubility in most solvents (section **3.1**), it did exhibit slightly greater solubility in C_5H_5N or CH_2Cl_2 doped with 5 eq C_5H_5N. In both cases, this resulted in the formation of orange rather than purple solutions. Upon layering a CH_2Cl_2/C_5H_5N sample with hexane, a small number of purple crystals were formed, which were shown by X-ray crystallography to be the double C-H functionalised product [NiBr/Cl(μ-O-6Mes)']$_2$ **(15; Scheme 3.1, Figure 3.3)**. The coordination spheres of the two identical square planar nickel centres consist of a C-H activated 6Mes ligand, two μ-O-CH_2 bridges and a halide which comprised of an 80:20 mixture of disordered Cl and Br respectively, the former presumably arising from the CH_2Cl_2 used as solvent. Only a small quantity of **15** could be isolated and attempts to identify any further components from the orange solution were unsuccessful.

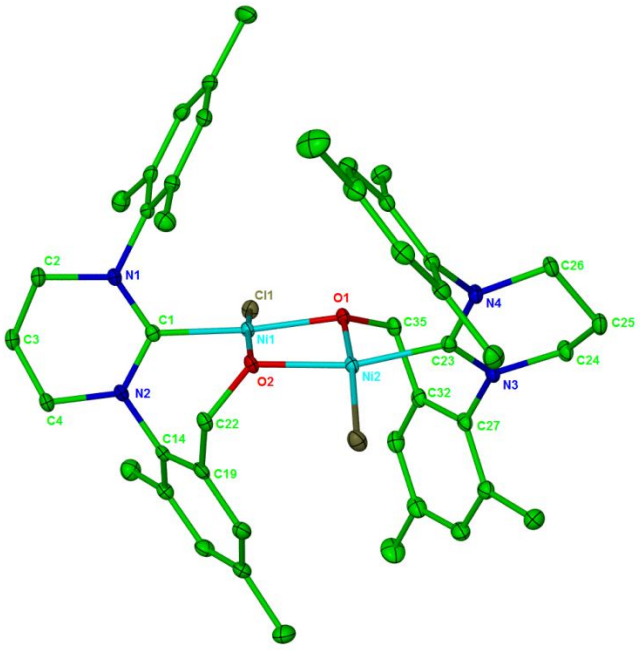

Figure 3.3 X-ray structure of **15**. Thermal ellipsoids are set at 30 % probability. All hydrogen atoms have been omitted for clarity.

Bond lengths and angles for **15** and a related IPr based dimer (***xlviii***; see section **3.1.2**, **Scheme 3.2** for more detail) are compared in **Table 3.2**. The activated arms of the ligands in both complexes are in *syn* arrangement about the planar $Ni_2(\mu\text{-}O\text{-}CH_2)_2$ core with O-Ni-O angles similar to those of **13 (Table 3.1)**, although the 5-membered double C-H activated ***xlviii*** is the most acute at 77.74(12)° (**13**: 80.18(10), 80.55(10)°; **15**: 79.67(6), 79.60(6)°). In contrast to **13** and **14**, structural distortions of the nitrogen atoms attached to the oxidised mesityl groups in **15** were marginal.

	15	***Xlviii****[,5]
Ni(1) – C(1)	1.868(2)	1.876(4)
Ni(2) – C(23)	1.872(2)	-
Ni(1) – O(1)	1.9204(14)	1.914(3)
Ni(1) – O(2)	1.8806(15)	1.868(3)
Ni(2) – O(1)	1.8873(15)	-
Ni(2) – O(2)	1.9166(14)	-
Ni(1) – O(1) – Ni(2)	99.86(7)	102.26(12)
Ni(1) – O(2) – Ni(2)	99.48(6)	-
O(1) – Ni(1) – O(2)	79.67(6)	77.74(12)
O(1) – Ni(2) – O(2)	79.60(6)	-

Table 3.2 A comparison of selected bond lengths (Å) and angles (º) in **15** and ***xlviii***.
* asymmetric unit = ½ of molecule with dimer centre located on a crystallographic inversion centre.

Despite many efforts, **15** could not be produced in higher yields for a more complete characterisation. However, ESI-QTOF mass spectral analysis of MeCN solutions of crystalline material produced upon reacting **1** with O_2 gave an isotope pattern consistent with the presence of both **13** and **15** in the initial reaction.[1] As **13** and **15** contain nickel and bromine atoms, both existing with naturally occurring isotopes, a $[M - X + H]^+$ signal with a predictable isotope pattern and *m/z* can be simulated for the mass spectra of pure **13** or **15**. For example, if only **13** was present in solution, the isotope pattern shown in **Figure 3.4b** simulated for $[M - HBr + H]^+$ gives an accurate mass of 869.2267 *m/z*. As the double oxygenative C-H activated complex **15** structurally differs from **13** by only two hydrogen atoms, the same isotope pattern would be expected for a sample of solely **15**, but at a $[M - HBr + H]^+$ of 867.2110 *m/z* **(Figure 3.4c)**. Thus, for a solution containing a mixture of **13** and **15**, an amalgamation of the two predicted signals would be expected with the intensities being the sum of both. This was indeed observed in the mass spectrum **(Figure 3.4a)**.

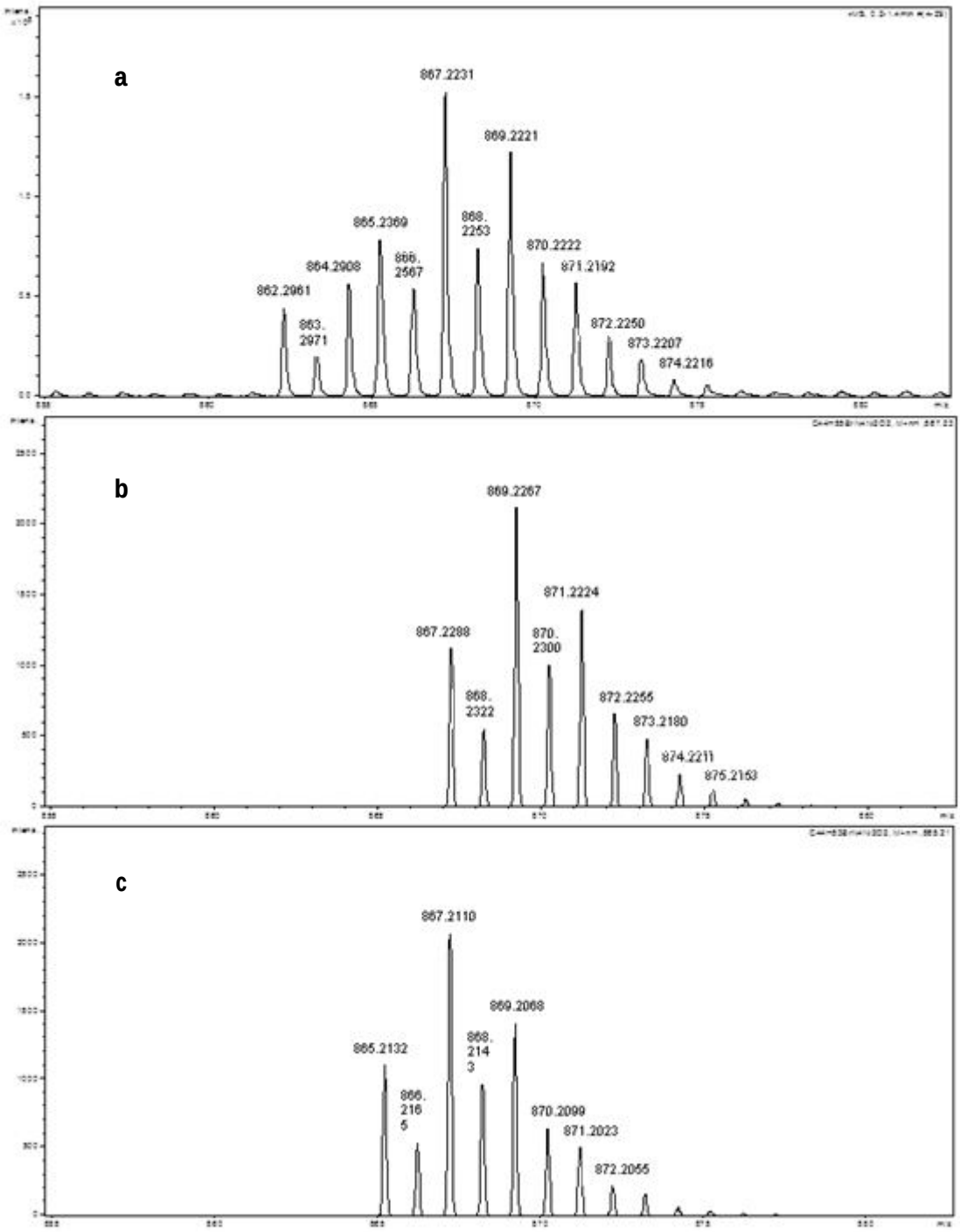

Figure 3.4 the ESI-QTOF mass spectrum of a MeCN solution of crystalline material from reaction of **1** with O_2 (*m/z* corresponds to $[M_{(13)} – HBr + H]^+$) (a), simulated isotope signal for $[M – HBr + H]^+$ for **13** (b) and simulated isotope signal for $[M – HBr + H]^+$ for **15** (c).

When the ^{1}H NMR spectrum of **13** described above in section **3.1** was analysed further, it was noted that integration of the remainder of the spectrum relative to the Ni-O*H* resonance afforded a greater number of protons than could be accounted for by the presence of **13** alone; O*H*:rest of spectrum = 1:103 (expected 1:55). Thus, while **13** can be isolated and

characterised as a pure material in the solid-state, it appears to be prone to further functionalisation of a second mesityl substituent to also form **15** in solution. In an effort to confirm this, X-ray unit cell parameters for six separate crystals from a crude batch of material isolated from the reaction of **1** and O_2 were measured. As the cell parameters in all cases matched those of just **13**, it would appear that the crystalline material consists overwhelmingly of this one compound. However, the ^{1}H NMR spectrum recorded upon dissolution of the remaining crystals again integrated to too many protons than could be accounted for by just **13** alone.

Identical observations were seen with the 7Mes analogue **14**. Mass spectra of MeCN solutions of **6** + O_2 again showed an isotope pattern consistent with the presence of **14** and the double oxygenative C-H activated analogue **(16; Scheme 3.1)** for $[M_{(16)} - HBr + H]^+$ at 897.2520 *m/z* (see **Appendix 4** for mass spectral data for **14/16** mixture). Unfortunately, no synthetic route could be established to generate **16** for full structural characterisation. The same crystal picking method of analysis used for **13** once more pointed only to the presence of **14** in the solid-state, whereas integration of the ^{1}H NMR spectrum indicated the presence of more than this one species in solution. A 55:45 ratio of the two products (single activation:double activation) for both **13/15** and **14/16** was achieved by analysis of the ^{1}H NMR spectra. These ratios did not change over time, suggesting that the second hydroxylation process occurs readily in solution and then proceeds no further.

3.1.2 Comparisons to Literature

As briefly discussed in **Chapter 1, 1.2.1**, the $Ni_2(\mu\text{-}O_2)_2$ core motif seen in **13**, **14** and **15** is a common feature of nickel chemistry,[2,3,5-11] but in most cases where the ancillary ligand is an extremely large β-diketiminate. Such examples include the mixed Ni/Fe dimer ***xxxix***[8] (**Scheme 3.2** and **Chapter 1, 1.2.1**), where, like in **13** and **14**, oxygenative C-H bond activation is observed. Several nickel complexes have been shown to promote either intermolecular[12,13] or intramolecular[2,14-16] C-H functionalisation with either O_2 or H_2O_2 as the oxidant. Starting with Ni(I) or Ni(II) complexes, it is believed that these C-H bond activations proceed through Ni(III) superoxide intermediates[13-15] as opposed to a direct interaction between the C-H bond and nickel atom. Decomposition of these Ni(III) species then tends to lead to ligand oxygenation. Extensive DFT calculations were carried out on ***xxxix*** to determine whether the bulk of the N-substituents and their proximity to the oxygen atoms affected the selectivity of

functionalisation. However, no rationalisation of why only one oxygenative C-H activation took place could be made.

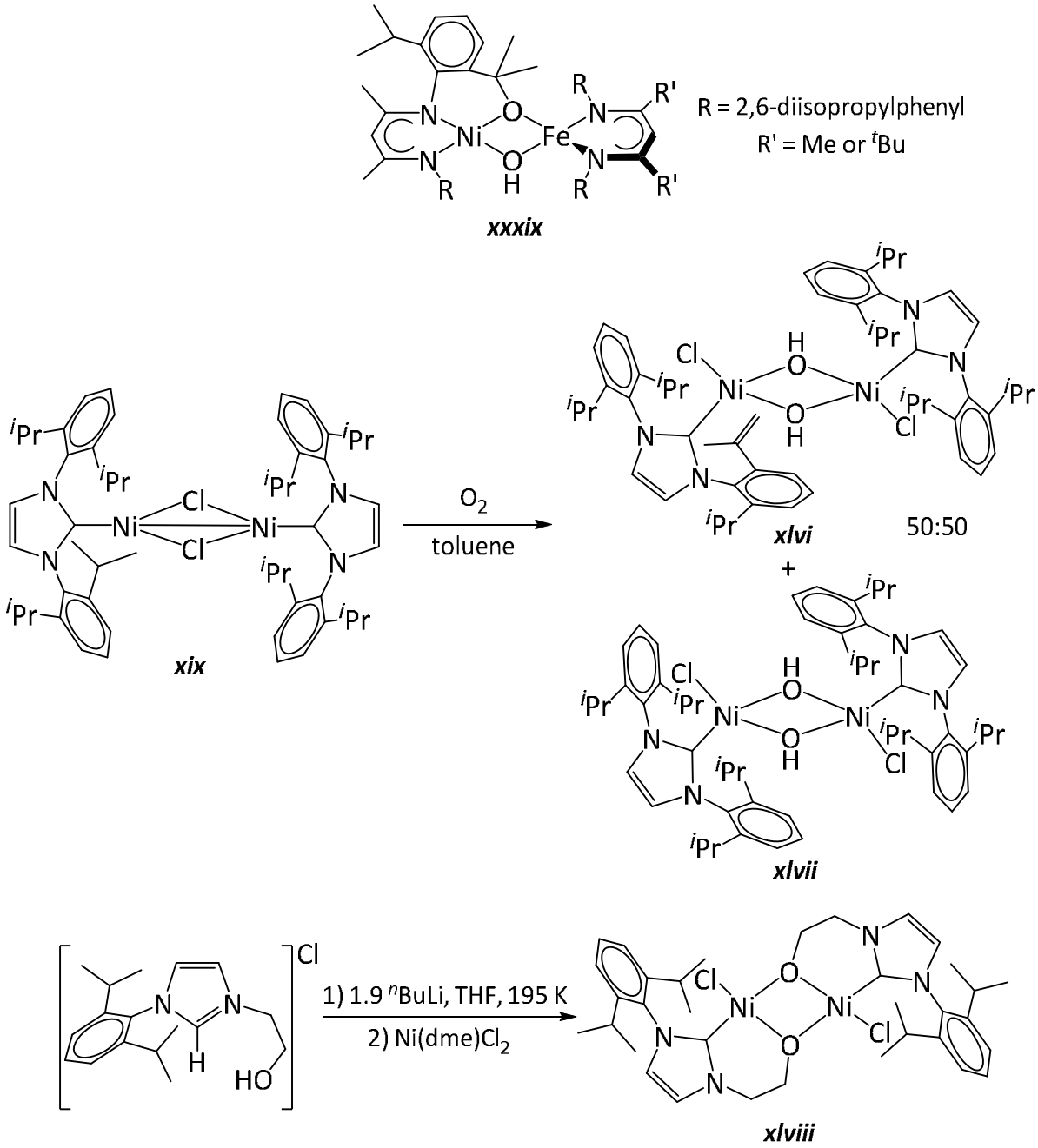

Scheme 3.2 A selection of μ-O dinuclear species with varying degrees of functionalisation. ***xxxix***: single oxygenative C-H activation (above); ***xlvi***: a dehydrogenated IPr dimer and the saturated analogue ***xlvii*** (middle); ***xlviii***: double oxygenative activation (below).

The isolation of **13** and **14** upon employment of RE NHCs does share some parallels to earlier work with Ni-NHC dimers from Sigman's group,[9] who reported that addition of O_2 to the Ni(I) dinuclear complex ***xix*** resulted in oxidation of the N-substituent. However in this case, dehydrogenation of one ^{i}Pr substituent was observed giving rise to ***xlvi***, a complex very similar to the previously reported *bis*(μ-OH) dimer [Ni(IPr)Cl(μ-OH)]$_2$ ***xlvii*** **(Scheme 3.2)**.[2,9] Detection of the alkene moiety in ***xlvi*** with X-ray crystallography was not initially possible and the proposed structure was originally thought to be ***xlvii***. This was further supported by the presence of a crystallographic inversion centre. Both complexes appear to give the same UV-vis (λ_{max} = 502 nm) and IR spectra (***xlvi*** and ***xlvii***: $\nu_{\mu\text{-OH}}$ = 3645 cm^{-1} and ν_{NiO} = 546 cm^{-1}). However, for ***xlvii*** a single set of resonances was observed in the ^{1}H NMR spectrum, consistent with a symmetric geometry, whereas ***xlvi*** clearly displayed a large number of overlapping resonances indicative of asymmetry. In addition, signals at 5.07 and 5.16 ppm (C_6D_6) for ***xlvi*** were observed, suggesting the possibility of a terminal double bond. Shifts in the IR spectra were seen in μ-^{18}OH samples of ***xlvi*** and ***xlvii*** (both displaying $\nu_{\mu\text{-}^{18}OH}$ = 3632 cm^{-1} and $\nu_{Ni\text{-}^{18}O}$ = 529 cm^{-1}). However, an additional absorbance at 893 cm^{-1}, regardless of the isotope used, was observed for ***xlvi***, consistent with a geminal vinylidene C-H bending mode. Upon more extensive analysis of the X-ray structure, a terminal C=C bond of a reduced ^{i}Pr group was detected, disordered 1:1 with ***xlvii***, thus providing an explanation for the crystallographic inversion centre. Isopropyl ligand dehydrogenation had previously been reported in [Ir(IPr)(COD)]$^{+}$ and Pt-β-diketiminate species.[17,18] When left in solution, both ***xlvi*** and ***xlvii*** slowly decomposed generating imidazolium and unidentifiable nickel products, suggestive of discrete ligand dissociation. No such degradation was observed for **13** and **14**.

Doubly activated bridged dinuclear complexes are not widely known. However, an imidazol-2-ylidene bearing dimer **(*xlviii*)** analogous to **15** has very recently been reported, synthesised *via* double deprotonation of an alcohol functionalised [IPrH]Cl salt with ^{n}BuLi in the presence of Ni(dme)Cl_2 **(Scheme 3.2)**.[5] The Ni-C_{NHC} and Ni-O lengths in ***xlviii*** **(Table 3.2)** are comparable to those in **13**, **14** and **15**, with the Ni-O distance *trans* to the carbene (Ni(1)-O(1) and Ni(2)-O(2) in **15**) being longer than that *trans* to the halide (Ni(1)-O(2) and Ni(2)-O(1)) in all cases. This presumably results from the strong *trans* effect of the RE NHC.

3.2 Attempts to Probe O_2 Activation by Ni(6Mes)(PPh_3)Br (1) Using UV-Visible Spectroscopy

As mentioned previously, it is postulated that during the formation of $Ni_2(\mu\text{-OR})_2$ dimers upon activation of O_2 with Ni(I), the reaction may pass through Ni(III) superoxide intermediates.[2,5,8-11] In an attempt to probe the formation for **13** – **16** in more detail, low temperature UV-visible spectroscopic studies were performed in collaboration with Isidoro López and Professor Antoni Llobet at ICIQ in Tarragona, Spain.

The room temperature electronic absorption spectrum of **13** measured in THF showed a single absorption band at λ_{max} = 362 nm (ε = 474 M cm^{-1}; this value is based on the assumption that **13** is the only species present).[1] As the colour change associated with the reaction of **1** and O_2 was observed within seconds, **1** was dissolved in THF and cooled to 190 K. 1 mL of air was added at this temperature and the reaction monitored by UV-vis spectroscopy every 18 s **(Figure 3.5)**. After 6 min reaction time, no further change was observed in the UV-vis spectrum. Two isosbestic points were observed at 290 and 420 nm suggesting a simple A → B or equilibrium reaction. The final spectrum obtained is very similar to that of **13**, suggesting that this is the major species in the reaction. However, it is likely that the *bis*(μ-alkoxy) complex **15** would have a very similar UV-vis spectrum to that of **13** due to the similar set of chromophores. Indeed, evidence for the formation of multiple species in the reaction was suggested by singular value decomposition (SVD) analysis, which revealed the presence of at least three eigenvectors. It is therefore not possible to develop a simple kinetic model, even if at first sight simple isosbestic points are observed.

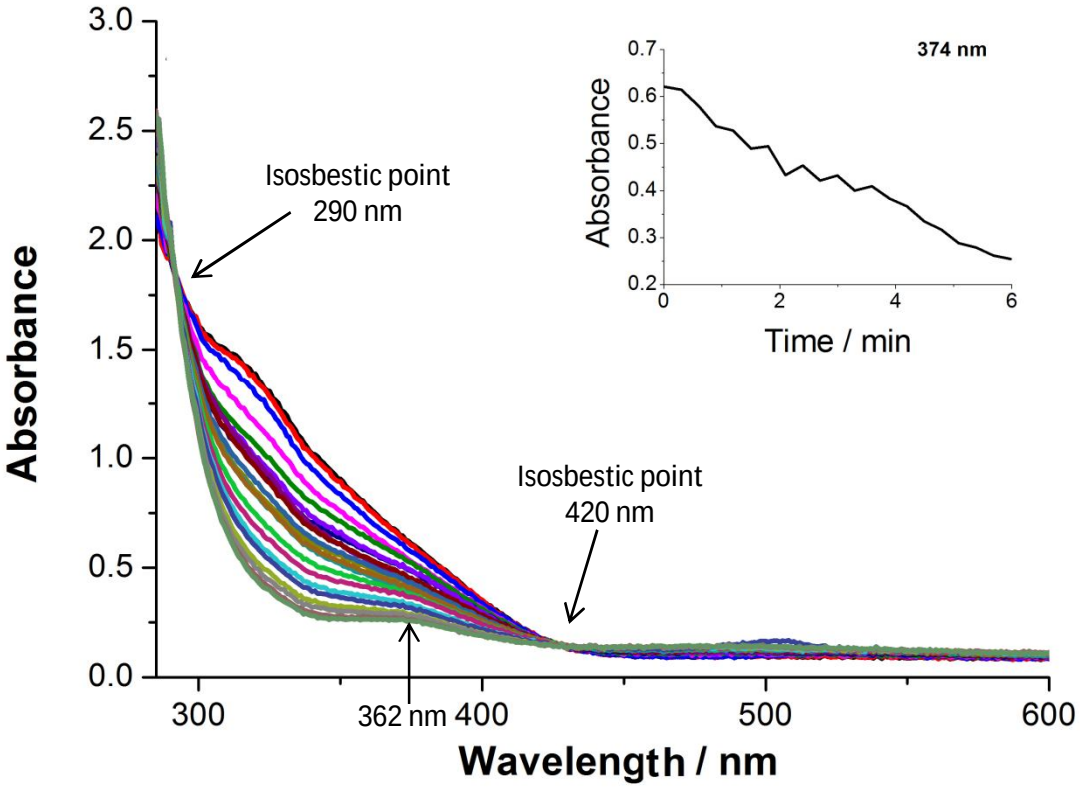

Figure 3.5 UV-vis monitoring for the reaction of 0.5 mM **1** with 1 mL of air at 190 K in THF over a period of 6 min. Measurements were taken every 18 s (red: 0 s, green: 6 min). The inset shows the absorbance *vs.* time plot at 374 nm.

The reaction of **1** and O_2 suggest the production of highly reactive, high oxidation state Ni-*bis*(oxo), –superoxo or –peroxo species that further evolve in the formation of **13** and **15**. Attempts to detect such intermediates by carrying out the reaction at different temperatures ultimately proved unsuccessful, with the reaction at 190 K still proceeding too fast to determine any mechanistic information. Similar findings were reported by Sigman and coworkers[9] upon UV-vis analysis of the IPr dimer ***xix*** oxidation to form ***xlvi/xlvii*** (section **3.1.2**). They found that toluene and THF solutions reacted to completion with O_2 at both 298 and 190 K in < 15 s even at low concentrations of < 1 mM, without providing evidence of any Ni(III), or indeed any other, intermediates.

3.3 Reactivity of Ni(6MesDAC)(PPh_3)Br (5) With O_2

In an attempt to retard the rate of mesityl group oxidation and allow the observation of intermediates, the less electron rich diamidocarbene Ni(I) complex Ni(6MesDAC)(PPh_3)Br **(5)** was reacted with O_2. Dark orange solutions of **5** became virtually colourless instantaneously upon the addition of 1 atm O_2. Attempted crystallisation from either CH_2Cl_2/hexane or THF/hexane afforded a creamy-green precipitate, from which a small number of green and colourless crystals were isolated and manually separated. These were shown by X-ray crystallography to be the known tetrahedral Ni(II)-phosphine oxide complex, Ni(O=PPh_3)$_2$$Br_2$,[19] and urea, (6MesDAC)=O,[20,21] respectively **(Scheme 3.3)**. The latter was also characterised by ^{1}H and ^{13}C{^{1}H} NMR spectroscopy through comparison to the data reported by Bielawski and coworkers.[19] Details of the X-ray structure of Ni(O=PPh_3)$_2$$Br_2$ are given in **Appendix 2**. Thus, rather than impeding the rate of C-H functionalisation of the N-Mes group, the change from 6Mes to 6MesDAC completely alters the oxidation path that is observed.

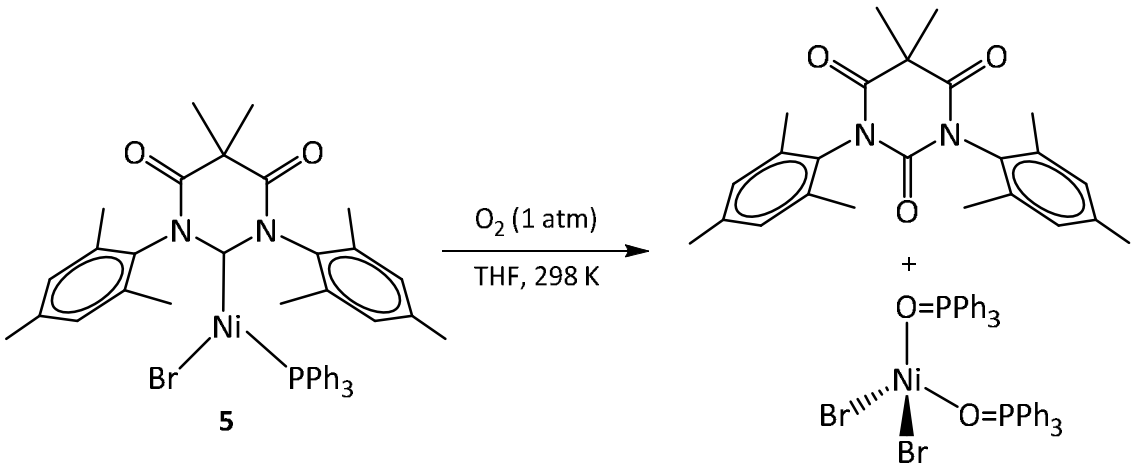

Scheme 3.3 Reaction of **5** with O_2.

3.4 Reactivity of Ni(RE NHC)(PPh_3)Br With O_2 (RE NHC N-Substituent = Less Bulky *o*-Tolyl)

As the change of diamino- to diamidocarbene is clearly too dramatic to allow the oxidation chemistry to be retained, diamino NHCs were considered again, though with different N-substitution patterns. This also allowed the influence of steric bulk to be determined and compared to what was observed in the reactions of Ni(PhTt$^{tBu/Ad}$)(CO) with O_2 described in **Chapter 1, 1.2.1**.

When the less sterically bulky *o*-tolyl complexes **2** and **7** were exposed to 1 atm O_2, immediate colour changes from yellow to red-pink were observed. Upon work up, the purple mononuclear Ni(II)-dihalide complexes Ni(6/7^{o}Tol)(PPh_3)Br_2 (6^{o}Tol **(17)**; 7^{o}Tol **(18)**) were isolated **(Scheme 3.4)**,[1,22] albeit in low yields of 20 and 38 % respectively. For mass balance, other unidentified products must also be formed.

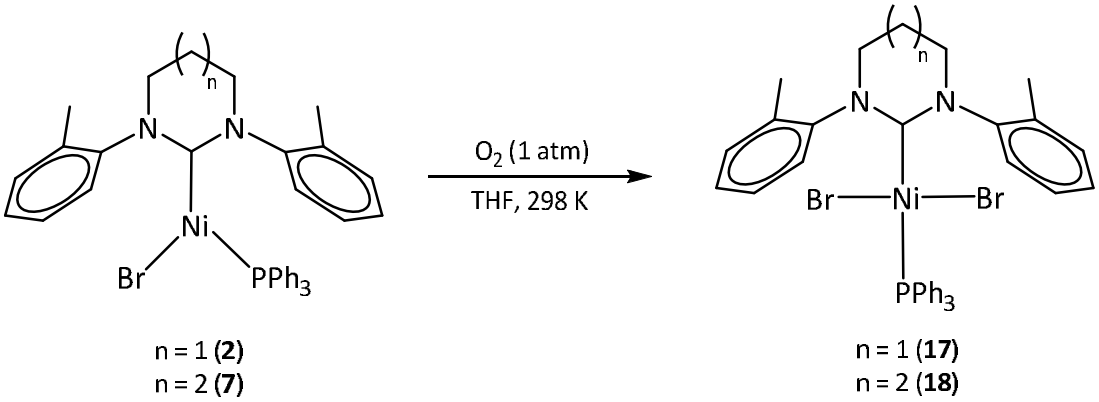

n = 1 (**2**)
n = 2 (**7**)

n = 1 (**17**)
n = 2 (**18**)

Scheme 3.4 Reaction of **2** and **7** with O_2 to form Ni(RE NHC)(PPh_3)Br_2 (**17** and **18** respectively).

Both **17** and **18** could also be made by simple ligand substitution reactions of Ni(PPh_3)$_2Br_2$ with 6^{o}Tol or 7^{o}Tol. Unfortunately, this synthetic route also afforded significant quantities of the corresponding pyrimidinium or diazepinium salts of [Ni(PPh_3)Br_3]$^-$, [6^{o}TolH][Ni(PPh_3)Br_3] and [7^{o}TolH][Ni(PPh_3)Br_3], respectively (see **Appendix 2** for X-ray structure of the former), which reduced the yields to < 15 %. The relative facile formation of this Ni(II) impurity strongly indicates the preference for oxidation and hence the Ni(II) state, as well as the highly nucleophilic nature of RE NHCs with its regeneration of pyrimidinium/diazepinium from a proton source in the surrounding reaction media.

The crystal structures of **17** and **18 (Figure 3.6)** displayed the expected square planar nickel geometries with *trans*-bromide ligands. Selected bond lengths and angles are given in **Table 3.3**. The Ni-C_{NHC} distances of 1.910(5) Å **(17)** and 1.905(3) Å **(18)** were comparable to that reported in *trans*-Ni(IPr)(PPh_3)Cl_2 (1.912(4) Å), which is one of the few other examples of Ni(NHC)(PR_3)(halide)$_2$ complexes reported in the literature.[22] One interesting note is that compared to **17** and **18**, Ni(IPr)(PPh_3)Cl_2 has a far more acute C_{NHC}-Ni-P angle (**17**: 179.26(18)^o; **18**: 178.26(17)^o; Ni(IPr)(PPh_3)Cl_2: 165.9(1)^o). Comparison to the related Ni(II)-*bis*(phosphine) or –*bis*(NHC) complexes suggest that this is a stereoelectronic effect associated with the presence of PPh_3, as Ni(PPh_3)$_2Cl_2$ shows a tetrahedral structure (P-Ni-P angle = 111.42(1)^o),[23,24] while Ni(IPr)$_2Cl_2$ ***(xviii*; Chapter 1, 1.1.3)** is square plane with a near linear C_{NHC}-Ni-C_{NHC} angle

(178.9(7)°).[22] Furthermore, the Ni-P bond length in Ni(IPr)(PPh_3)Cl_2 (2.2541(1) Å) was 0.07 Å shorter than in Ni(PPh_3)$_2Cl_2$ (2.3180(2) Å),[23,24] indicating the stronger σ-donor ability of the NHC ligand over PPh_3. However, the difference in geometry between the complexes has to be considered and most likely also contributes to this decrease. The Ni-P distances in **17** and **18** (**17**: 2.2505(15) and **18**: 2.2912(16) Å) are of similar magnitude to Ni(IPr)(PPh_3)Cl_2 and therefore also shorter than the Ni(II)-*bis*(phosphine) complex, consistent with the enhanced donor capabilities of NHC/RE NHC ligands.

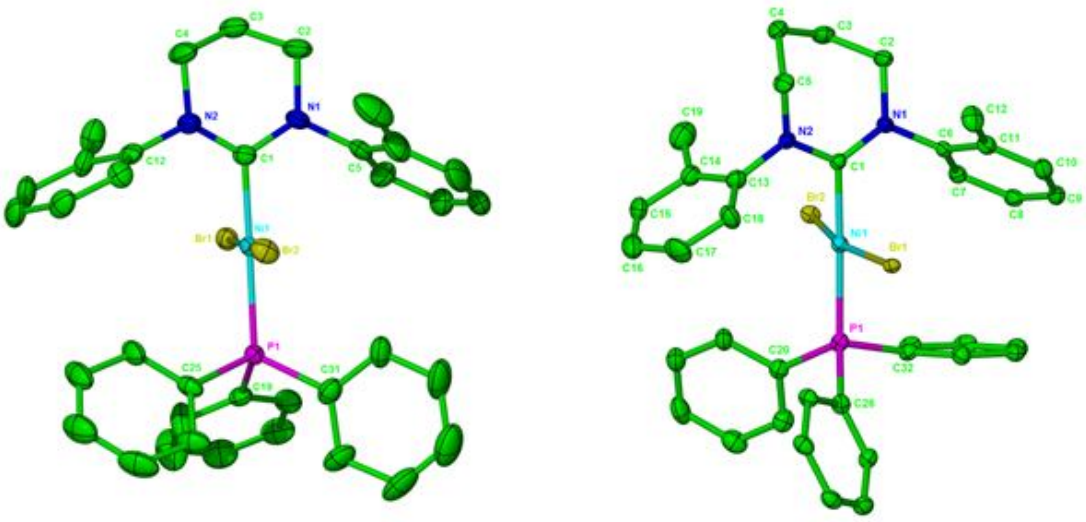

Figure 3.6 X-ray crystal structures of **17** (left) and **18** (right). Thermal ellipsoids are set at 30 % probability. All hydrogen atoms have been omitted for clarity.

	17	**18**	**Ni(IPr)(PPh_3)Cl_2** [22]
Ni – C_{NHC}	1.910(5)	1.911(5)	1.912(14)
Ni – X(1)	2.3026(8)	2.3982(8)	2.146(1)
Ni – X(2)	2.3122(9)	2.3949(8)	2.277(1)
Ni – P	2.2505(15)	2.2912(16)	2.2541(1)
N – C_{NHC} – N	177.0(5)	199.3(5)	-
X(1) – Ni – X(2)	175.82(4)	166.48(4)	165.78(6)
C_{NHC} – Ni – P	179.26(18)	178.26(17)	165.9(1)

Table 3.3 Selected bond lengths (Å) and angles (°) for **17**, **18** and the related IPr example Ni(IPr)(PPh_3)Cl_2. X = Br (**17** and **18**), Cl (Ni(IPr)(PPh_3)Cl_2).

The ^{1}H NMR spectra of **17** and **18** unexpectedly displayed quite broad, unresolved and overlapping resonances, which could not be integrated. Moreover, **17** showed two resonances in the $^{31}P\{^{1}H\}$ NMR spectrum at 17.3 and 16.6 ppm (CD_2Cl_2) in a ratio of *ca.* 1:1.9, which along with the complicated ^{1}H spectrum, was interpreted as showing the possible existence of isomers. Unlike in the case of Ni(IPr)(PPh_3)Cl_2[22] and previously studied palladium analogues (Pd(NHC)(PR_3)I_2 (NHC = IMe, I^{t}Bu; R = Ph, ^{o}Tol, ^{t}Bu, Cy)),[25] assignment of the two signals to *cis*-/*trans*-isomers was excluded by the appearance of large (122 Hz) *trans*-^{13}C-^{31}P coupling on both of the carbene resonances in the $^{13}C\{^{1}H\}$ NMR spectrum. It seems more reasonable to suggest the formation of rotamers, arising due to hindered rotation of the RE NHC. Indeed, in the case of **18**, five phosphorus signals were seen (21.4, 21.3, 20.3, 17.5 and 16.7 ppm (C_6D_6)) in a ratio of 1:2:1:38:13, which cannot be explained by *cis*-/*trans*- isomerisation. $^{31}P\{^{1}H\}$-$^{31}P\{^{1}H\}$ EXSY **(Figure 3.7)** revealed exchange between the two most intense resonances at 17.5 and 16.7 ppm, and a separate exchange process involving the three smaller signals at 21.4, 21.3 and 20.3 ppm.

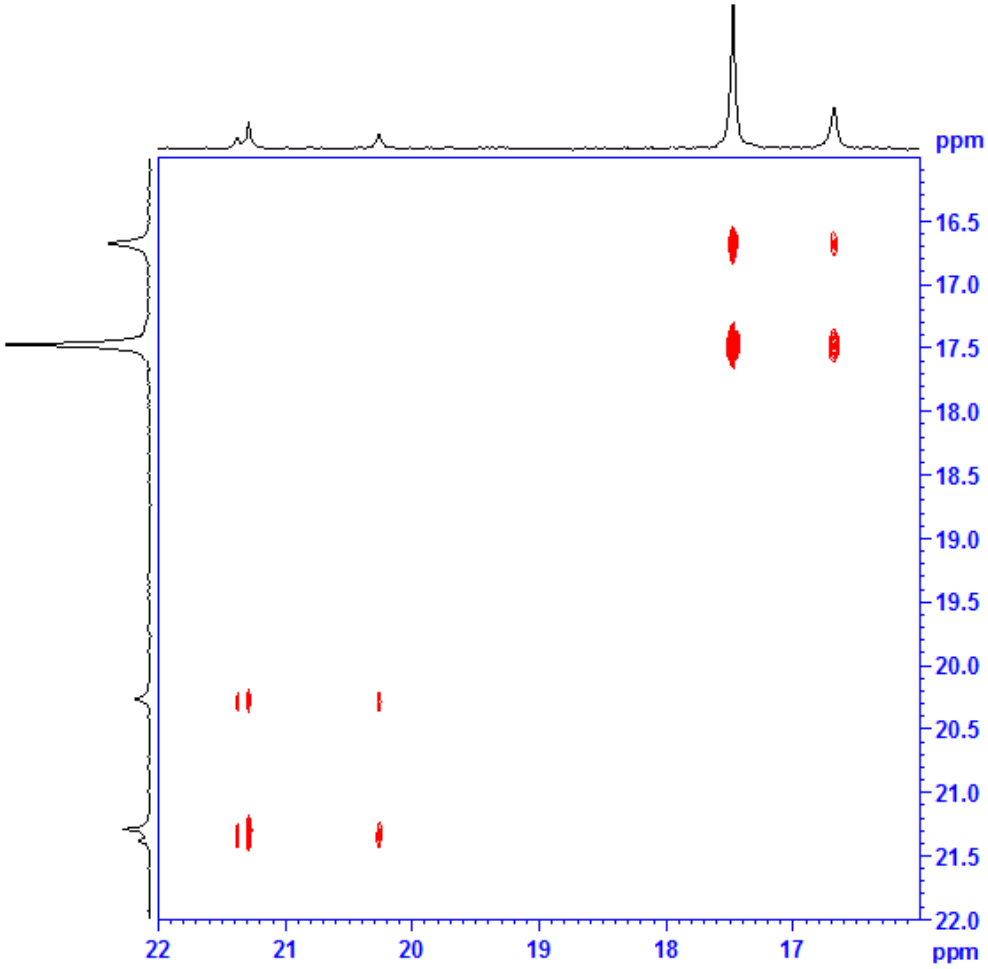

Figure 3.7 $^{31}P\{^{1}H\}$-$^{31}P\{^{1}H\}$ EXSY spectrum of **18** (C_6D_6, 162 MHz).

Rotamer formation was also proposed in the case of Rh(7^{o}Tol)(COD)Cl by Cavell and coworkers.[26] They postulated rotameric structures differing in *syn*- versus *anti*-arrangements of the *o*-Me groups on the RE NHC to account for the appearance of multiple signals in the ^{1}H NMR spectrum. In comparison, ^{1}H and ^{13}C spectroscopic analysis of Rh(IMes)(CO)$_2$Cl implied free rotation about the N-mesityl bonds due to the reduced steric demands of IMes.[26]

Using this argument, **Figure 3.8** shows possible rotamers for **18**. The direction of the carbene backbone bend, either above or below the plane indicated in **Figure 3.8**, also lends to the formation of further *syn*- and *anti*-isomers, possibly explaining the observation of more than four resonances in the ^{31}P spectrum. The X-ray structure of **18** actually has two molecules of Ni(7^{o}Tol)(PPh$_3$)Br$_2$ in the unit cell, one with the top of the 7-membered ring pointing directly over one phenyl ring of the *trans*-PPh$_3$ ligand (as seen in **Figure 3.6**) and the other with the top bent in the opposite direction residing over the gap of two phenyl rings. In both cases, they display an *anti*-*o*-Me arrangement, suggesting these as the two main candidates for the major signals detected in the ^{31}P{^{1}H} NMR spectrum. This also could provide an explanation for why these two isomers interconvert with each other at room temperature in the ^{31}P{^{1}H}-^{31}P{1H} EXSY spectrum.

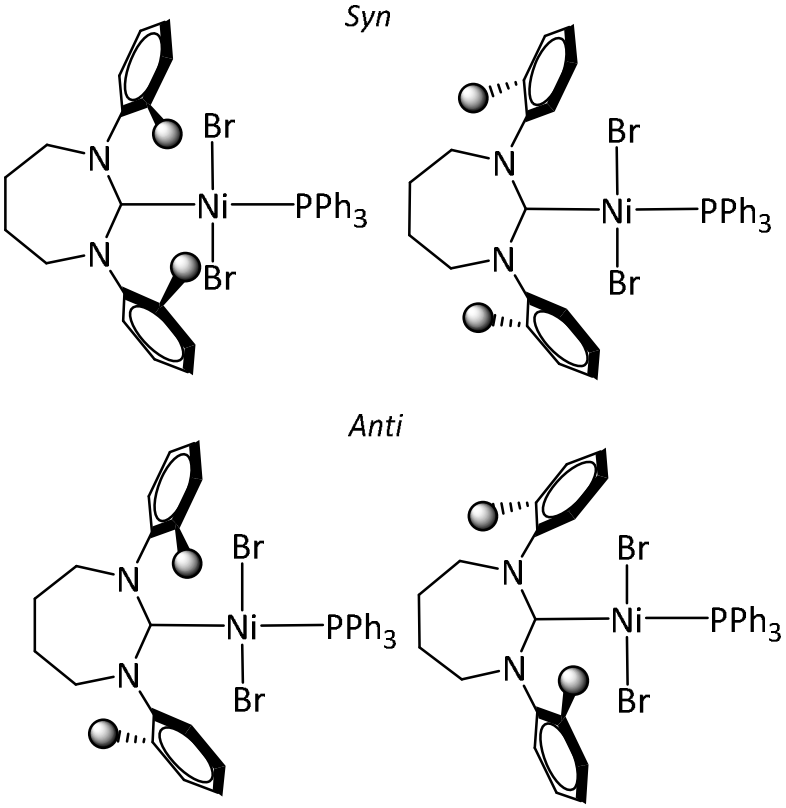

Figure 3.8 Possible rotameric structures for **18**, where the *o*-methyl N-substituents reside in a *syn*- (above) or *anti*- (below) arrangement.

3.5 Attempted Rationalisation of Differing O_2 Reactivity *via* Electrochemistry

In an effort to try to rationalise the different reactivities of **1/6** (N-Mes), **2/7** (N-^{o}Tol) and **5** (6MesDAC) towards O_2, the redox properties of the complexes were probed by cyclic voltammetry (CV). The CVs of the N-Mes substituted complexes, **1** and **5**, showed the presence of a chemically irreversible oxidation wave in the anodic region and a chemically irreversible reduction in the cathodic region **(Figure 3.9a)**. Similar behaviour was observed for **6**, while **2** and **7** (Ni-6/7^{o}Tol respectively) showed two irreversible reductions **(Figure 3.9b)**.

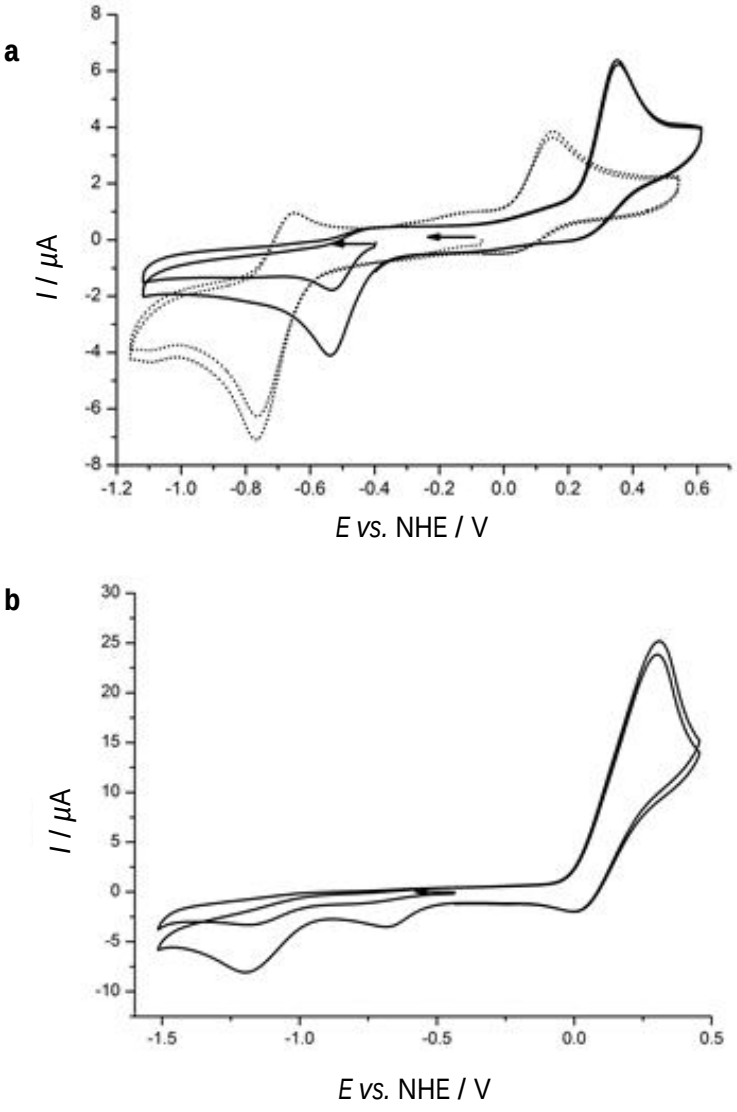

Figure 3.9 Cyclic voltammogram for complexes **1** (solid line) and **5** (dashed line) (a) and **2** (b). All were run at 100 mV s^{-1} scan rate *vs.* NHE. The arrow indicates the initial scanning potential and the scan direction.

The $E_{p,a}$ and $E_{p,c}$ values found for the five complexes are listed in **Table 3.4**. As the redox processes measured were chemically irreversible in all cases, this precludes the extraction of accurate thermodynamic potentials. However, since all the mononuclear complexes studied have very similar molecular structures in terms of the ligand environment around nickel, trends can be deduced. The anodic potentials shown in **Table 3.4** do not follow a regular trend based on the induction effects expected by increasing the number of methylene units in the carbene ligand backbones or by increasing the number of methyl groups (tolyl to mesityl) in the N-substituents. It is also surprising that **5**, containing the diamidocarbene 6MesDAC, displays one of the lowest $E_{p,a}$ values, together with **2** and **7**. However, the most interesting feature that can be extracted from these measurements is the fact that complexes **1** and **6**, which have the highest redox potentials by far, are the ones that undergo oxidation *via* O atom transfer from O_2. The rest of the complexes with much lower redox potentials undergo oxidation primarily by outer sphere electron transfer (OSET) giving simple Ni(II) complexes with no oxygen incorporated into the final products. This suggests that complexes that are much more difficult to oxidise by OSET (**1** and **6**) find a lower energy pathway involving O-atom transfer from O_2, hence the formation of the hydroxyl/aryloxy bridged Ni(II) dimers (**13** and **14**).

Ni(I) complex	$E_{p,a}$ (V *vs.* NHE)	$E_{p,c}$ (V *vs.* NHE)
1 (6Mes)	0.35	-0.54
6 (7Mes)	0.48	-0.49
5 (6MesDAC)	0.15	-0.77
2 (6^{o}Tol)	0.25	-0.68, -1.19
7 (7^{o}Tol)	0.20	-0.72, -1.08

Table 3.4 Anodic and cathodic redox waves measured for complexes **1**, **2**, **4**, **5 – 7**.

3.6 Chapter Summary

The three coordinate Ni(I)-RE NHC complexes **1**, **2**, **5 – 7** exhibit different reaction pathways upon exposure to O_2, generating markedly different oxidation products. In the complexes bearing N-Mes substituted RE NHCs (**1** and **6**), oxidation of an *o*-Me C-H bond leads to dimeric Ni(II) products containing μ-hydroxyl and μ-alkoxy ligands (**13** and **14** respectively). This reactivity appears to correlate with the high redox potentials of **1** and **6** determined by CV. Attempts to probe the mechanism of oxidation and detect potential intermediates by UV-vis

spectroscopy were precluded by the remarkably facile nature of the oxidation reaction, which was shown to be complete within a few minutes, even at 190 K. Analysis of the low temperature UV-vis data taken together with NMR and mass spectrometry evidence revealed the formation of secondary products resulting from functionalisation of the second RE NHC ligand. This was confirmed by the structural characterisation of the 6Mes derivative $[NiBr(\mu\text{-O-6Mes})']_2$ **(15)**, although the exact circumstances under which this secondary reaction takes place are unclear.

In an effort to slow down the rate of oxidation through the use of less bulky N-^{o}Tol or more π-accepting diamidocarbene containing precursors, different products were found. Although this resulted in the isolation of Ni(II) complexes, they were generated by ligand redistribution or degradation reactions. In the diamido Ni(I) complex **5**, both the RE NHC and PPh_3 dissociated and were oxidised to give (6MesDAC)=O and $Ni(O{=}PPh_3)_2Br_2$ respectively. The N-^{o}Tol analogues **2** and **7** both underwent simple ligand redistribution reactions to form the monomeric square planar Ni(II) species Ni(RE NHC)$(PPh_3)Br_2$ (**17** and **18**).

The stark contrast in C-H activated products from the use of N-Mes and N-^{o}Tol substituted RE NHCs provides an interesting insight into the effect of N-substituent bulk on Ni(I) reactivity. The large size of the mesityl substituents seems to promote activation and incorporation of dioxygen into a Ni(II) dimeric structure. The widened N-C_{NHC}-N angle of these 6- and 7-membered analogues over their 5-membered counterparts appears to position the mesityl groups in close enough proximity to the oxygen bridges, facilitating oxidation/C-H activation of these substituents and essentially sterically trapping the $Ni_2(\mu\text{-OR})_2$ core. On the other hand, complexes with the *o*-tolyl substituents do not incorporate O_2 into a nickel coordinating environment, with no rotation of the tolyl group ensuing to allow trapping of an oxygen atom. The reduced steric bulk associated with this class of RE NHC is therefore not enough to promote dimer formation, and a simple ligand rearrangement reaction instead proceeds with direct oxidation of the metal centre to Ni(II) *via* OSET. As dehydrogenation of IPr was observed in ***xlvi*** (section **3.1.2**), it implies that if the N-substituent always has an alkyl group pointing directly towards the metal, *i.e.* N-Mes or N-d^{i}pp, activation of some sort will ensue. In cases where there is a choice of alkyl group orientation, such as in N-^{o}Tol, the N-substituent will rotate to preferentially direct the alkyl group away from the metal.

It seems surprising that such different reactivity can occur upon making the relatively small change of N-Mes to N-^{o}Tol groups. However, the CV measurements do show some marked differences in redox properties to support this.

3.7 References

1. R. C. Poulten, I. Lopez, A. Llobet, M. F. Mahon and M. K. Whittlesey, *Inorg. Chem.*, 2014, **53**, 7160-7169.
2. B. R. Dible and M. S. Sigman, *J. Am. Chem. Soc.*, 2003, **125**, 872-873.
3. A. Kunishita, Y. Doi, M. Kubo, T. Ogura, H. Sugimoto and S. Itoh, *Inorg. Chem.*, 2009, **48**, 4997-5004.
4. T. L. Cottrell, *The Strengths of Chemical Bonds*, 2nd edn., Buttersworth, London, 1958.
5. S. Hameury, P. de Fremont, P. A. R. Breuil, H. Olivier-Bourbigou and P. Braunstein, *Inorg. Chem.*, 2014, **53**, 5189-5200.
6. I. Garcia-Bosch, X. Ribas and M. Costas, *Eur. J. Inorg. Chem.*, 2012, 179-187.
7. A. Gunay and K. H. Theopold, *Chem. Rev.*, 2010, **110**, 1060-1081.
8. S. Yao and M. Driess, *Acc. Chem. Res.*, 2012, **45**, 276-287.
9. B. R. Dible, M. S. Sigman and A. M. Arif, *Inorg. Chem.*, 2005, **44**, 3774-3776.
10. M. T. Kieber-Emmons and C. G. Riordan, *Acc. Chem. Res.*, 2007, **40**, 618-625.
11. B. S. Mandimutsira, J. L. Yamarik, T. C. Brunold, W. W. Gu, S. P. Cramer and C. G. Riordan, *J. Am. Chem. Soc.*, 2001, **123**, 9194-9195.
12. E. Kimura, A. Sakonaka, R. Machida and M. Kodama, *J. Am. Chem. Soc.*, 1982, **104**, 4255-4257.
13. E. Kimura and R. Machida, *J. Chem. Soc., Chem. Comm.*, 1984, 499-500.
14. K. Haas, H. Dialer, H. Piotrowski, J. Schapp and W. Beck, *Angew. Chem., Int. Ed.*, 2002, **41**, 1879.
15. S. Itoh, H. Bandoh, M. Nakagawa, S. Nagatomo, T. Kitagawa, K. D. Karlin and S. Fukuzumi, *J. Am. Chem. Soc.*, 2001, **123**, 11168-11178.
16. S. Itoh, H. Bandoh, S. Nagatomo, T. Kitagawa and S. Fukuzumi, *J. Am. Chem. Soc.*, 1999, **121**, 8945-8946.
17. C. Y. Tang, J. Lednik, D. Vidovic, A. L. Thompson and S. Aldridge, *Chem. Commun.*, 2011, **47**, 2523-2525.
18. U. Fekl and K. I. Goldberg, *J. Am. Chem. Soc.*, 2002, **124**, 6804-6805.
19. K. M. Wiggins, J. P. Moerdyk and C. W. Bielawski, *Chem. Sci.*, 2012, **3**, 2986-2992.
20. F. A. Cotton and D. M. L. Goodgame, *J. Am. Chem. Soc.*, 1960, **82**, 5771-5774.
21. W. E. Daniels, *Inorg. Chem.*, 1964, **3**, 1800.
22. K. Matsubara, K. Ueno and Y. Shibata, *Organometallics*, 2006, **25**, 3422-3427.
23. B. Corain, B. Longato, R. Angeletti and G. Valle, *Inorg. Chim. Acta.*, 1985, **104**, 15-18.

24. L. Brammer and E. D. Stevens, *Acta. Crystallogr. Sect. C - Cryst. Struct. Commun*, 1989, **45**, 400-403.

25. W. A. Herrmann, V. P. W. Bohm, C. W. K. Gstottmayr, M. Grosche, C. P. Reisinger and T. Weskamp, *J. Organomet. Chem.*, 2001, **617**, 616-628.

26. M. Iglesias, D. J. Beetstra, B. Kariuki, K. J. Cavell, A. Dervisi and I. A. Fallis, *Eur. J. Inorg. Chem.*, 2009, 1913-1919.

CHAPTER 4

4 Reactivity of Ni(6Mes)(PPh_3)Br

Following the success of using sterically bulky RE NHCs to promote the formation of unique, low coordinate complexes of Ni(I), it raises the question of how much further the increased size of RE NHC ligands can help stabilise these highly unstable complexes and prevent additional attack into the large number of available vacant coordination sites. Further studies incorporating RE NHCs were therefore carried out with the ultimate aim of forming even lower coordinate Ni(I) complexes. The most logical approach to this was to utilise the newly synthesised **1 – 10** as precursor species. The degradation chemistry demonstrated in **Chapter 3** highlights **1** as a potential reactive fragment. Thus, the reactivity of **1** was explored in a more constructive manner through ligand substitution and halide abstraction reactions, with the aim of forming a two coordinate Ni(I) environment, or alternatively, more examples of chemically and structurally interesting low coordinate nickel complexes.

4.1 Ligand Substitution Reactions of Ni(6Mes)(PPh_3)Br (1)

4.1.1 Reaction of Ni(6Mes)(PPh_3)Br (1) with RE NHCs

RE NHCs have previously shown they can substitute nickel bound PPh_3 in the reaction of $Ni(PPh_3)_2Br_2$ with 6/7^{o}Tol to form the Ni(II) products Ni(6/7^{o}Tol)(PPh_3)Br_2 (**17** and **18** respectively) **(Chapter 3, 3.4)**.[1] It was therefore reasoned that the same could happen with **1**, simultaneously promoting bromide association and ultimately leading to a NiL_2 complex. As depicted in **Scheme 4.1**, a THF solution of **1** was reacted overnight with 1.5 eq of 6Mes at room temperature. The yellow coloured solution synonymous with the three coordinate Ni(I) starting material was replaced by a light brown solution and beige precipitate. Isolation of the precipitate gave a cream coloured solid in 62 % yield, which upon X-ray analysis of crystals grown from CH_2Cl_2/hexane, proved to be the *bis*(NHC) Ni(I) product [Ni(6Mes)$_2$]Br **(19)**.[2]

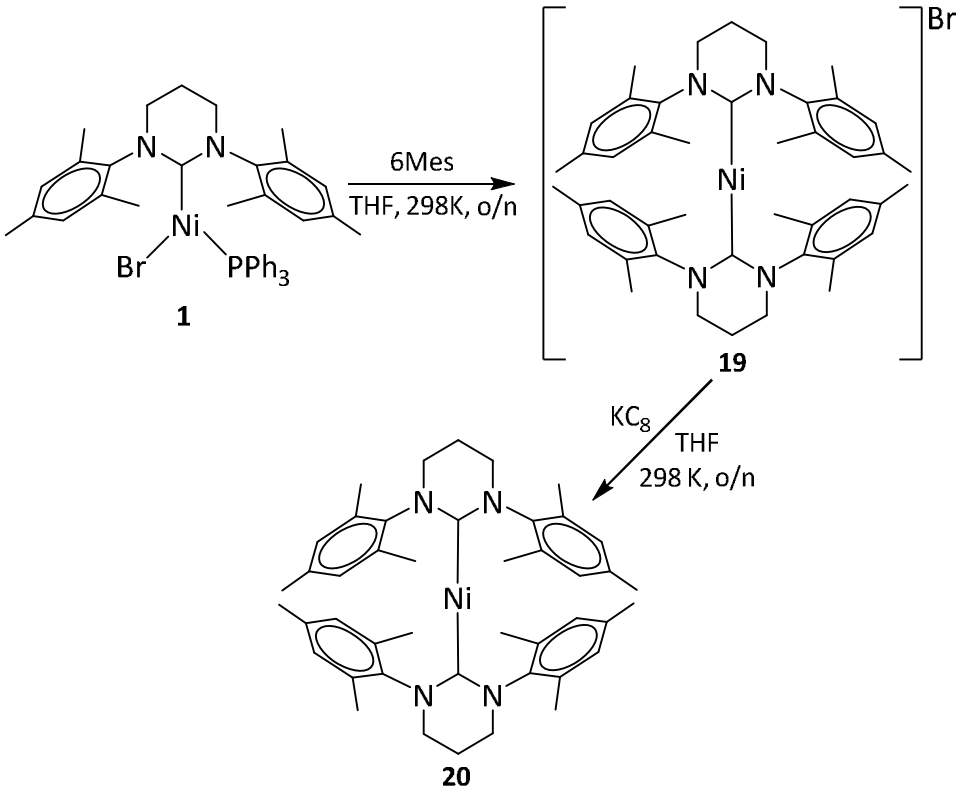

Scheme 4.1 Reactivity of **1** with 6Mes to generate **(19)** and its subsequent reduction to **20**.

The X-ray structure of **19** is shown in **Figure 4.1**. The central nickel atom is directly coordinated to two 6Mes ligands, enforcing a highly linear geometry (C_{NHC}-Ni-C_{NHC}: 179.27(13)°) with Ni-C_{NHC} lengths of 1.939(3) and 1.941(3) Å. Further bond lengths and angles are given in **Table 4.1**. The bromide counterion was solvated by two molecules of CH_2Cl_2. Anion exchange reactions on **19** were carried out to generate $[Ni(6Mes)_2]X$ (X = $[PF_6]^-$, $[BF_4]^-$, $[BPh_4]^-$, $[BAr_4^F]^-$. In all cases, X-ray analysis showed the existence of one cation and one anion.

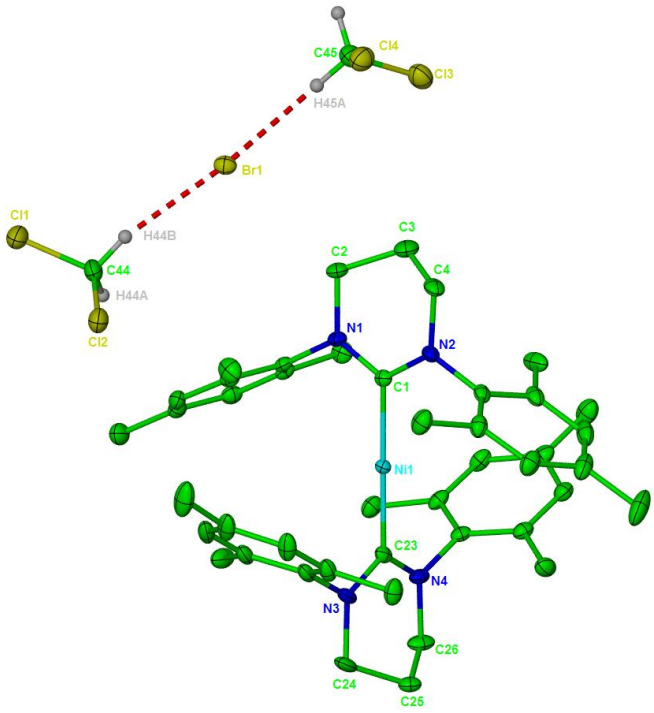

Figure 4.1 X-ray structure of **19**. Thermal ellipsoids are set at 30 % probability. All hydrogen atoms have been omitted for clarity, apart from in the two molecules of CH_2Cl_2 solvent crystallised in the lattice.

Despite being highly electron deficient (formally $13e^-$), no short contacts were apparent between any of the C-H moieties and the nickel metal centre in **19**, excluding any activation or stabilising agostic interactions with the carbene. The two 6Mes ligands reside at roughly right angles to each other (the mean planes of the two RE NHC backbones intersect each other at 80.95(15)º), presumably as a result of steric interactions of the mesityl substituents. Thus, the Ni(I) ion is almost completely encapsulated by the mesityl N-substituents in a cage like structure, as evident from the space filling diagram of **19** in **Figure 4.2**. The high level of encapsulation is attributed to the widened N-C_{NHC}-N angles associated with RE NHCs, which leads to the extremely bulky N-Mes substituents being pulled in and residing much closer to the nickel atom compared to the standard 5-membered NHCs. This was reflected experimentally by the unsuccessful attempts to generate the analogous $[Ni(6Mes)(IMes)]^+$ or $[Ni(6Mes)(6^oTol)]^+$ cations upon reaction of **1** with either IMes or 6^oTol respectively.

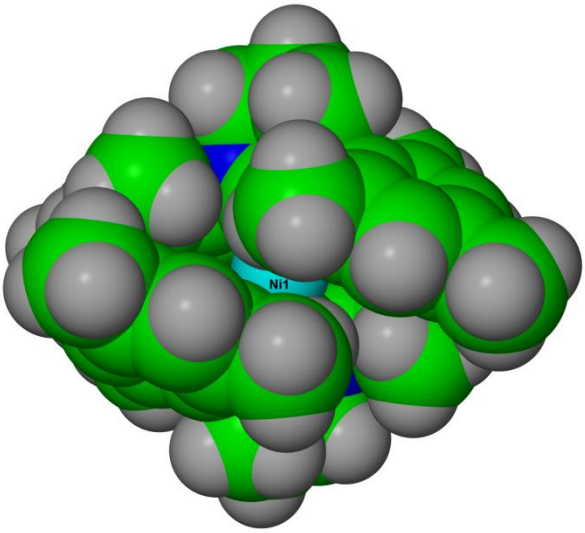

Figure 4.2 Space filling diagram of the cation in **19**.

^{1}H NMR spectroscopy corroborated that **19** was paramagnetic, although in contrast to **1**, full integration and signal assignment could be made. The extremely broad and shifted resonances associated with the methyl protons were observed at -12.70 (24 H, *ortho*) and 10.51 ppm (12H, *para*), while the carbene backbone signals appeared at 49.94 (8H, NCH_2) and 52.52 ppm (4H, NCH_2CH_2) in CD_2Cl_2. Cryoscopic calculations highlighted that the solid-state structure of **19** was retained in solution (see **Appendix 5**). A 0.53 molecular weight fraction of **19** was measured in nitrobenzene and confirmed a monomer species (0.5 is expected due to the presence of a cation and anion in **19**), precluding any association or aggregation. In fact, **19** was so stable that it could be openly handled in air for several minutes without any observable colour change or modifications to the ^{1}H NMR spectrum.‡

Electrochemistry was carried out on THF solutions of **19**, employing a carbon rod (working), Pt wire (counter) and $Ag/AgNO_3$ solution (reference) as the electrodes. Scanning cathodically, the cyclic voltammogram **(Figure 4.3)** revealed the presence of a chemically reversible ($i_{p,a}/i_{p,c}$ = 1.0) and electrochemically quasi-reversible ($E_{p,a} - E_{p,c}$ = 171 mV) wave associated with a one electron reduction of Ni(I) to Ni(0) at -1.32 V *vs.* NHE. Bulk electrolysis at an applied potential of -1.66 V verified the process was one electron in nature. When scanned in the anodic direction, a chemically irreversible wave was observed at $E_{p,a}$ = +1.21 V. In comparison to two other two coordinate (albeit neutral) Ni(I) complexes, Ni(IPr)(N(SiMe$_3$)$_2$) ***(xlii)*** and Ni(IPr)(NH(d^{i}pp)) ***(xliii)*** **(Chapter 1, 1.3.2)**, the reduction and oxidation peaks for **19** are at markedly different potentials (both the Ni(I)/Ni(II) potentials for ***xlii*** and ***xliii*** were negative,

‡ Exemplified when a CD_2Cl_2 solution of **19** was left open to air for 30 min.

E = -0.21 and -0.84 V respectively). Despite being referenced to two different potentials, the large difference between them (*e.g.* 1.4 V for the Ni(I)/Ni(0) couple between **19** and ***xliii***) highlights potentially significant different reactivity.

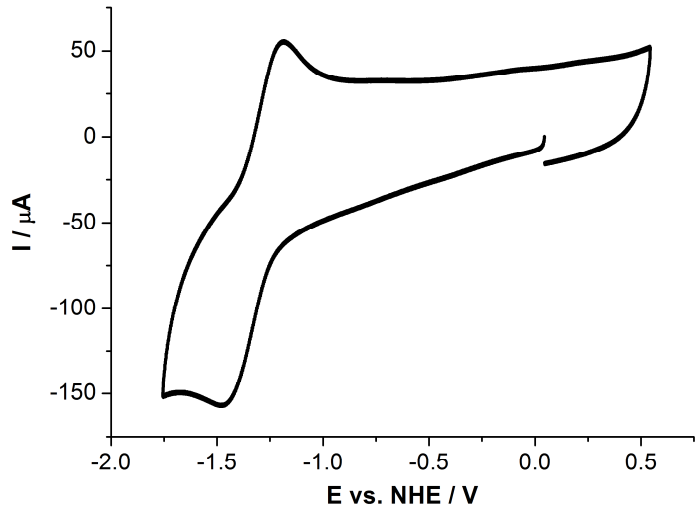

Figure 4.3 Cyclic voltammogram before electrolysis of a solution of **19** (0.5 mM) in 0.1 M THF/[^{n}Bu$_4$N]PF$_6$. The working electrode was a carbon rod, counter electrode a Pt wire and the reference electrode a Ag/AgNO$_3$ solution (0.01 M in MeCN). Scan rate = 150 mV s^{-1}.

Chemical reduction of **19** to Ni(6Mes)$_2$ **(20)** was achieved upon reaction with 4 eq of KC$_8$ in THF at room temperature **(Scheme 4.1)**. **20** was isolated as extremely air-sensitive dark purple crystals (consistent with other neutral Ni(NHC)$_2$ species: ***xvi*** and ***xx***[3] **(Chapter 1, 1.1.3, 1.3.2)**) that instantly decolourised in the presence of air. The structure of **20** is shown in **Figure 4.4** with selected bond lengths and angles given in **Table 4.1**.

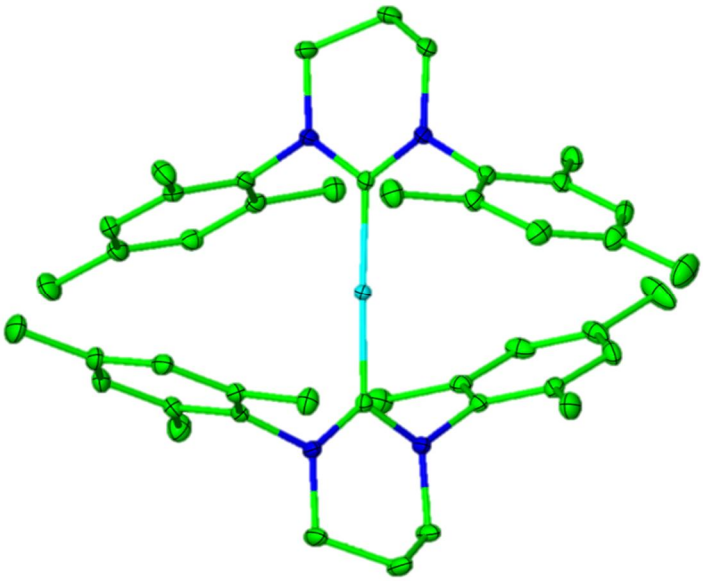

Figure 4.4 X-ray structure of **20**. Thermal ellipsoids are set at 30 % probability and all hydrogen atoms have been omitted for clarity.

	19	**20**
Ni – C(1)	1.941(3)	1.852(2)
Ni – C(23)	1.939(3)	1.868(3)
N(1) – C(1) – N(2)	117.6(2)	114.2(2)
N(3) – C(23) – N(4)	117.3(3)	114.6(2)
C(1) – Ni – C(23)	179.27(13)	177.71(10)

Table 4.1 Selected bond lengths (Å) and angles (°) for **19** and **20**.

Of most note is the surprising decrease in Ni-C_{NHC} bond lengths upon reduction from Ni(I) (1.941(3) and 1.939(3) Å) to Ni(0) (1.852(2) and 1.868(3) Å). The simplest explanation for this could relate to a change in the level of M → RE NHC backbonding, *i.e.* there is greater M → RE NHC back donation in Ni(0) and therefore a shorter Ni-C_{NHC} bond length is observed. DFT calculations reproduced this shortening perfectly for a 6Mes ligand (average Ni-C_{calc} for 6Mes: 1.945 Å in **19**; 1.869 Å in **20**), but moreover, showed analogous behaviour in $[Ni(NH_3)_2]^+/Ni(NH_3)_2$.[4] This cannot be due to backbonding as NH_3 is a pure σ-donor. In Ni(0), the DFT calculated molecular orbital diagram revealed a *sd* hybridised orbital, which was non-bonding with respect to the ligands. However, upon oxidation to Ni(I), the level of

s contribution decreases and the orbital becomes a lot more antibonding in character, thus elongating the N-C_{NHC} bond. A similar trend was noted by Matsubara *et al.*[5] in their studies of Ni(IPr)$_2$ ***(xvi)*** and Ni(IMes)$_2$ ***(xx)*** **(Chapter 1, 1.1.3, 1.3.2)**. They compared DFT calculated bond dissociation energies (BDEs) for ***xvi***, and two Ni(II) complexes, Ni(IPr)$_2$Cl$_2$ ***(xviii)*** and Ni(IPr)(PPh$_3$)Cl$_2$. Although they are hard to directly compare due to changes in coordination number and geometry, the Ni(0)-C_{NHC} BDE was +53 kcal mol^{-1}, 6 – 16 kcal mol^{-1} higher than for Ni(II)-C_{NHC} **(Table 4.2)**. This suggests why 'Ni(IPr)' was never observed in any manipulations of ***xvi*** and why only a small concentration of Ni(IMes)$_2$ was formed when free IMes was reacted with ***xvi***. The higher BDE associated with the low valent Ni(0) complex ***xvi*** is consistent with the short bond lengths observed (Ni-C_{NHC}: 1.865(2) and 1.872(2) Å), which are of similar magnitude to those in Ni(6Mes)$_2$ (**20**: 1.852(2) and 1.868(3) Å). In contrast, Pd(0) complexes, Pd(NHC)$_2$ (NHC = I^{t}Bu, IPr), have been shown to have weaker Pd-NHC bonds than their divalent analogues.[6]

	BDE
xvi	+53
xviii	+37
Ni(IPr)(PPh$_3$)Cl$_2$	+47

Table 4.2 Calculated BDEs (kcal mol^{-1}) of Ni(0) ***(xvi)*** and Ni(II) (***xviii*** and Ni(IPr)(PPh$_3$)Cl$_2$).

Comparisons of the N-C_{NHC}-N bond angle in **20** with that in **19 (Table 4.1)** show there is a noticeable decrease for **20**, implying the mesityl substituents are pulled in less tightly around the nickel centre. This might be one factor in the increased air-sensitivity observed for the complex compared to **19**. All other metrics are similar to those found for the neutral Ni-*bis*(imidazol-2-ylidene) complexes (***xvi*** and ***xx***).[5]

The reactivity of **1** with RE NHCs is not limited to the formation of symmetric *bis*(RE NHC) Ni(I) complexes. Upon reaction of **1** with an excess of the 7-membered RE NHC 7Mes, the asymmetric cationic Ni(I) complex [Ni(6Mes)(7Mes)]Br was isolated. As for **19**, [Ni(6Mes)(7Mes)]Br was isolated as a cream solid which exhibited reasonable stability towards air. The paramagnetic ^{1}H NMR spectrum was consistent with the d^9 Ni(I) formulation. [Ni(6Mes)(7Mes)]Br could be reduced to the extremely air sensitive zero-valent neutral counterpart Ni(6Mes)(7Mes) *via* reaction with KC_8 (see **Appendix 2** for the X-ray structures and selected metrics of [Ni(6Mes)(7Mes)]$^+$ and Ni(6Mes)(7Mes)). Comparable bond lengths and angles were observed to **19** and **20**, including the same shortening of Ni-C_{NHC} distances upon reduction (Ni(I): Ni-C_{6Mes} 1.9427(18), Ni-C_{7Mes} 1.9353(18) Å; Ni(0): Ni-C_{6Mes} 1.89(5),

Ni-C_{7Mes} 1.83(5) Å). This reactivity was not transferrable to other RE NHCs. As briefly mentioned previously, no analogous two coordinate complexes could be isolated from reactions of **1** with less sterically encumbered NHCs, such as IMes and 6^{o}Tol.

4.1.2 DFT and Magnetisation Studies on [Ni(6Mes)$_2$]Br (19) and Ni(6Mes)$_2$ (20)

Despite overwhelming evidence in the form of the ^{1}H NMR spectra and X-ray crystallography for the presence of a Ni(I) metal centre in complex **19**, two pieces of data contradicted this. Firstly, room temperature magnetic moment determinations in solution (Evans method) and the solid-state (Gouy balance) gave μ_{eff} values corresponding to the presence of two unpaired electrons; 3.3 and 2.7 μB respectively. More interestingly, X-band and Q-band EPR spectra showed no evidence for any unpaired electron, either at low temperature (4 K) or in the solid-state. This conundrum was answered upon examination of DFT calculations. DFT reproduced the near linear geometry of **19** and **20** and predicted the electronic arrangement of the molecules (calculated for **20** and then applied to **19**) to have five occupied metal based *d* orbitals split in an approximate 2:1:2 pattern **(Figure 4.5)**.[2] This is in contrast to the expected 2:2:1 splitting previously observed for other linear ML_2 transition metal complexes described by Power **(Chapter 1, 1.3.1)**.[7]

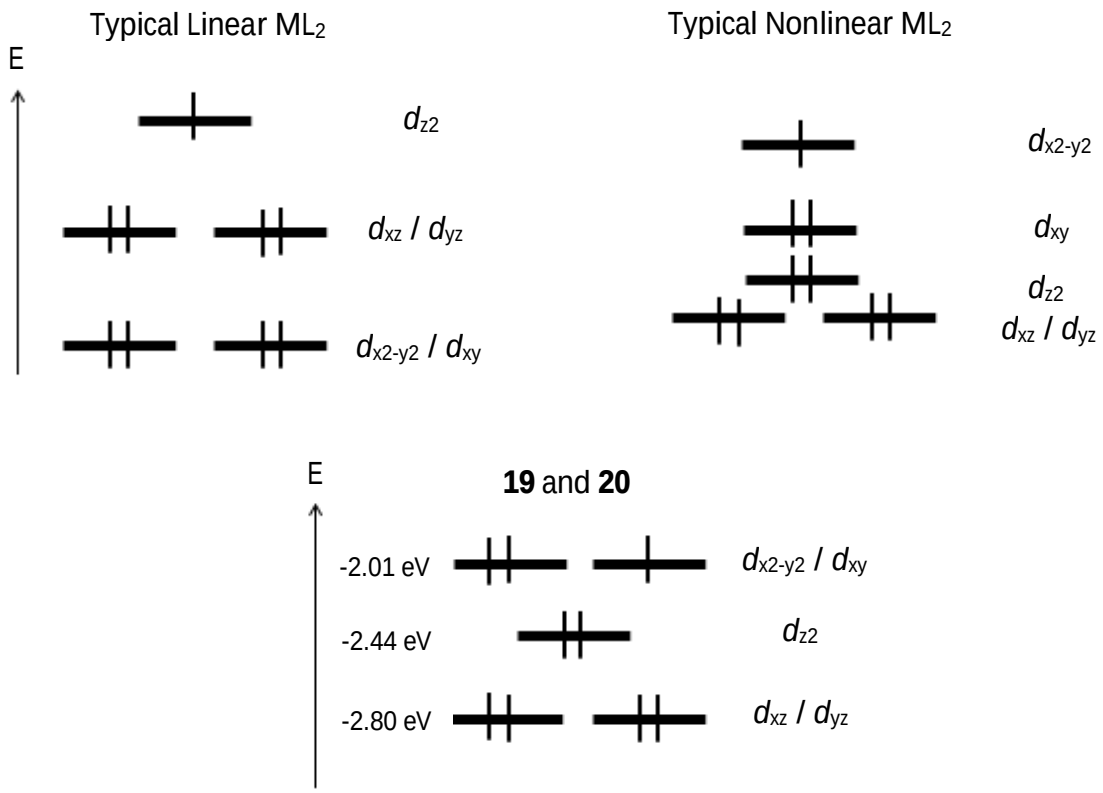

Figure 4.5 The relative *d* orbital splitting pattern for a typical linear and nonlinear (90° bend) ML_2 complex (above), along with the DFT calculated pattern for $Ni(6Mes)_2$ **(20)** and hence **19** (below). All are occupied in accordance to the electronic configuration for a d^9 Ni(I) complex.

Moreover, this splitting pattern observed for **19** and **20** actually bears greater resemblance to the splitting associated with nonlinear ML_2 species with a 90° L-M-L angle **(Figure 4.5)**, only differing in the magnitude of energy difference between the d_{x2-y2} and d_{xy} orbitals. In a standard nonlinear species, these lay far enough apart from each other in energy to be classed as non-degenerate orbitals, therefore the HOMO would consist mainly of d_{x2-y2} character when applied to a d^9 electronic configuration. However for **19** and **20**, the d_{x2-y2} and d_{xy} orbitals lie close enough in energy to be considered degenerate, meaning the unpaired electron associated with a Ni(I) d^9 complex would reside in a near degenerate HOMO corresponding to these nickel *d* orbitals. This HOMO lies *ca.* 0.43 eV above a σ-type orbital at -2.44 eV which is dominated by nickel d_{z2} and *s* character, with the last two near degenerate metal orbitals d_{xz} and d_{yz} at -2.80 eV. A very similar set of orbitals was observed for $Pd(NHC)_2$ (NHC = I^{t}Bu, IMe) species, however in that case, a 1:2:2 splitting was computed and confirmed by photoelectron spectroscopy.[8,9] A comparison of the splitting diagrams for standard linear and nonlinear ML_2

complexes, along with the pattern computed for **19** and **20**, are shown in **Figure 4.5**. They are filled in accordance to an electronic configuration for a d^9 system.

As described in **Chapter 1, 1.3.1**, partially filled degenerate orbitals can give rise to interesting molecular magnetic properties in the form of SMMs. The orbital degeneracy calculated for **19** and **20** are therefore central to understanding any magnetic characteristics **19** may possess. To elucidate these magnetic properties, solid-state SQUID measurements were performed on crushed polycrystalline samples of **19**. The dc magnetic properties were investigated under a 1000 Oe dc field in the temperature range 1.8 – 300 K. The room temperature χT value of 1.12 cm^3 K mol^{-1} is much higher than the expected theoretical spin-only value of 0.375 cm^3 K mol^{-1} for a d^9 Ni(I) complex (S = 1/2, $\boldsymbol{g}$ = 2, $\chi T = \boldsymbol{g}^2 S(S+1)/8$), however it is consistent with the observed room temperature values measured *via* the Evans or Gouy balance methods. This atypically high value may originate from significant inherent anisotropy of the Ni(I) ion apparent from the *d* orbital splitting in **Figure 4.5**. Partial occupancy of the higher energy d_{x2-y2} and d_{xy} orbitals allows them to interconvert, resulting in spin-orbit coupling. Therefore, in the ground state, the orbital angular momentum is not quenched by the ligand field, leading to 1st order orbital angular momentum and a sizeable intrinsic magnetic anisotropy.[10,11] It has been previously postulated that unquenched orbital angular momentum can lead to extremely large and broadened $\boldsymbol{g}$ shifts in EPR spectroscopy,[12,13] which may explain the absence of any detectable signal in the EPR spectrum of **19**. Use of high field EPR would provide support for this, although such measurements have not been possible thus far.

If the theoretical orbital contribution is subsequently taken into consideration, the observed χT of 1.12 cm^3 K mol^{-1} is in better agreement with the revised expected value of 1.57 cm^3 K mol^{-1} for a Ni(I) ion with unquenched orbital angular momentum. Upon decreasing the temperature, the χT value remains near linear until a slight decrease below 10 K reaching a minimum value of 1.00 cm^3 K mol^{-1}. This is indicative of a non-interacting mononuclear complex, consistent with the large Ni···Ni distances measured from X-ray crystallography (10.3 Å), leading to inherent anisotropy. The presence of magnetic anisotropy was further confirmed from field dependent magnetisation measurements of **19**, which were carried out between temperatures of 1.8 and 7 K at applied external fields ranging from 0 to 7 T **(Figure 4.6)**. The magnetisation data below 7 K displays a rapid increase of the magnetisation as the field is increased when low magnetic fields are employed (< 2 T). Above 2 T, a more gradual increase is observed with near saturation reached at low temperatures; M = 2.45 μB at 1.8 K, under 7 T (T_b < 7K). The

non-saturation as well as the non-superimposition of temperature lines in the *M vs.* H T^{-1} plot (unlike for **3** in **Figure 2.10**) again verify the existence of magnetic anisotropy in **19** **(Figure 4.6 (right))**. The data measured is similar to the field dependent studies carried out on **1**, **3**, **4** and **6**, however the saturation level reached for **19** is a lot higher, suggesting, as expected, a greater level of magnetic anisotropy.

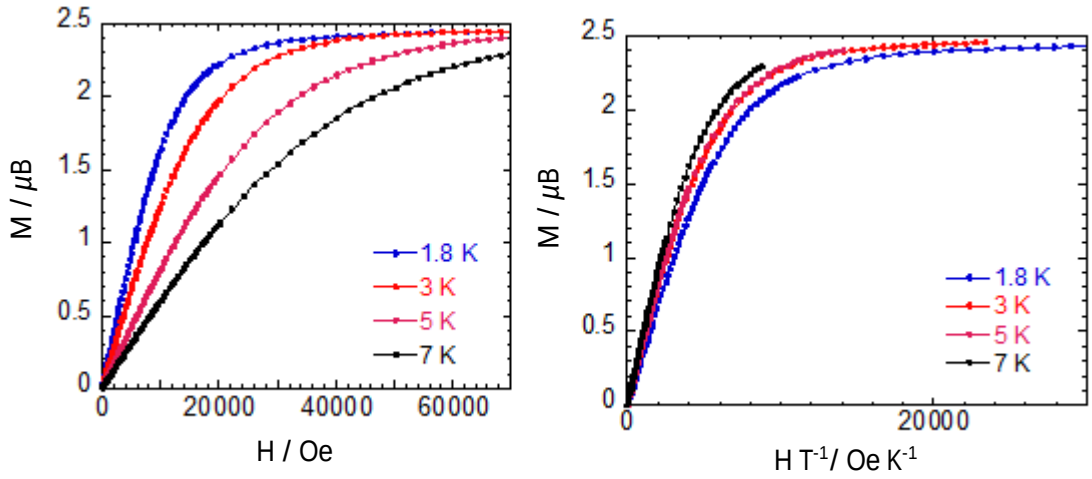

Figure 4.6 Field dependence of the magnetisation *M vs.* H (left) and reduced magnetisation *M vs.* H T^{-1} (right) for **19**. 1 T = 10000 Oe.

To probe the magnetic relaxation dynamics of **19**, ac magnetic susceptibility measurements were performed. Under zero applied dc field no out-of-phase (χ") signal was observed. However, under a 600 Oe applied dc field, **19** displayed both a strong frequency and temperature dependent χ" signal. Such slow relaxation of the magnetisation is consistent with field-induced SMM behaviour. Temperature dependent χ" data revealed full frequency dependent peaks with peak maxima shifting towards lower temperatures **(Figure 4.7 (right))**. Similarly, the frequency dependent data **(Figure 4.7 (left))** reveals χ" decreases with increasing temperature and frequency over the temperature range of 1.8 – 9 K, further indicating SMM behaviour.

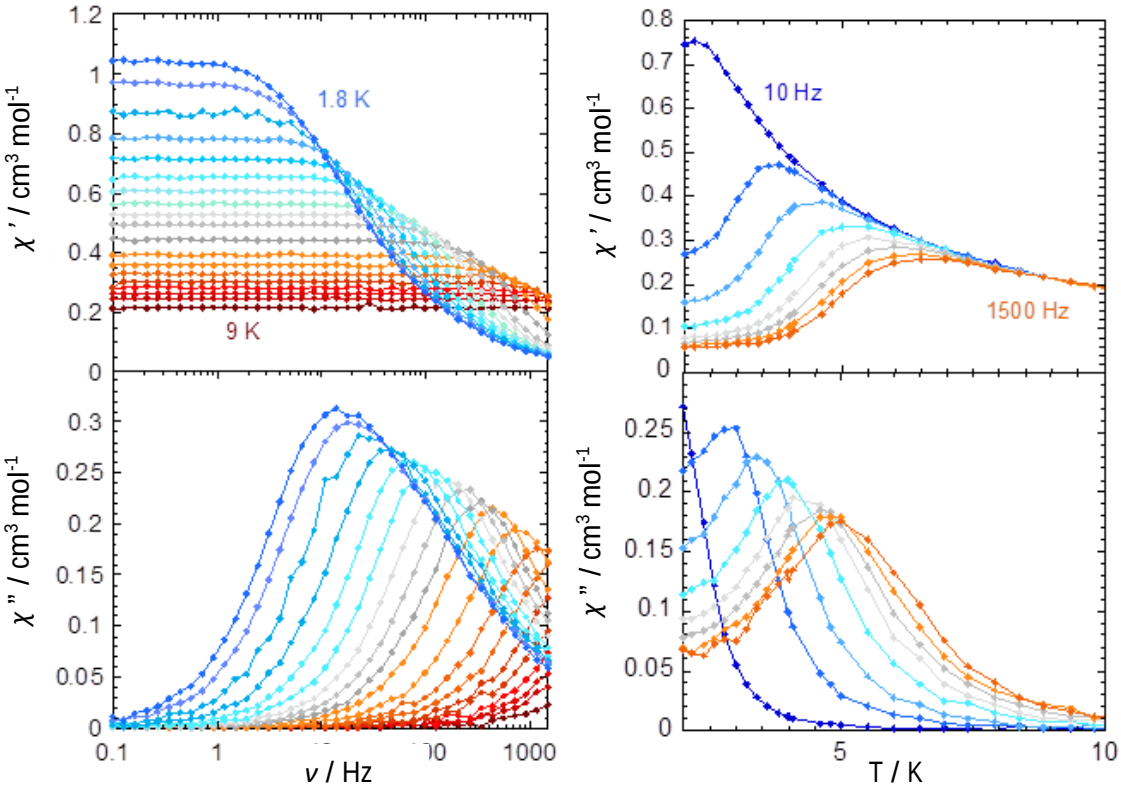

Figure 4.7 Frequency dependence (left) and temperature dependence (right) of the in-phase χ' (top) and out-of-phase χ'' (bottom) susceptibility of **19** under 600 Oe applied dc field.

The frequency dependent data ($\chi''(\nu)$) was used to extract the anisotropic barrier for **19**, U_{eff} = 12 cm^{-1}; τ_0 = 4.6 x10^{-6} s. Typical U_{eff} values lie in the region of 2 – 653 cm^{-1}.[14] Although relatively small, this energy barrier signifies **19** as the first mononuclear nickel complex to display SMM behaviour. Surprisingly, the energy barrier was only observed under an applied dc field, not zero-static. This is due to the occurrence of quantum tunnelling of the magnetisation (QTM) in the ground state, an efficient relaxation process leading to fast relaxation dynamics which cannot be detected in zero-field. A bias towards utilising an applied field is necessary to suppress QTM and allow any thermally activated relaxation processes to be observed. This effect has been observed numerous times, for example, upon applying a 6000 Oe external field, Dy(η^8-COT)(η^5-Cp*) and Ho(η^8-COT)(η^5-Cp*) both exhibited U_{eff} values (25 and 23.5/17.0 cm^{-1} respectively)[15] which were previously a lot smaller when measured in zero-field. The origins of this unexpected fast QTM within the ground state of complex **19** at zero-field are not immediately apparent. One rationale is that, as it possess half-integer spin and significant anisotropy, there is mixing between the degenerate ground state and thermally accessible excited electronic states.[2] Alternatively, examination of the packing in the crystal structure suggests that the bromide anion could interact with a further molecule of **19**,

bringing it into close enough proximity (Ni···Ni distance of 10.3 Å) to allow intermolecular dipolar fields to influence the relaxation behaviour.[15]

In recent years, several Ni complexes with very large anisotropy values have been reported,[15-20] however **19** is the first mononuclear complex to exhibit SMM characteristics. This highlights the importance and intriguing chemistry of ML_2 complexes and the role of the bulky RE NHCs which make this possible.

4.2 Attempted Halide Abstraction From Ni(6Mes)(PPh_3)Br (1)

A straightforward method to obtain a two coordinate species originating from **1** is to remove the halide. Typical halophiles include Ag^+, Tl^+, $[Et_3Si]^+$, $B(C_6F_5)_3$ and other Lewis acids, and a variety of these were reacted with **1**. In all cases, no simple abstraction of the bromide was achieved. AgX reagents (X = $[BF_4]^-$, $[NO_3]^-$, $[SO_3CF_3]^-$) led to the formation of [6MesH]X and the plating out of metallic nickel. The ^{19}F and ^{11}B NMR spectra of the reaction with $B(C_6F_5)_3$ provided some suggestion for the formation of a four coordinate boron species, indicating potential B-Br bonding. However, this reaction was evidently not clean and despite numerous efforts, no products could be isolated. The reactions with $[Et_3Si]^+$ and Tl^+ on the other hand led to the isolation and characterisation of unique nickel complexes.

4.2.1 Reaction of Ni(6Mes)(PPh_3)Br (1) with $[Et_3Si]^+$

$[R_3Si]^+$ existing alongside non-coordinating anions are a highly exploited range of electrophiles in both stoichiometric and, more impressively, catalytic reactions.[21] $[Et_3Si][B(C_6F_5)_4]$ (the true nature of which will be discussed later) is an extremely versatile reagent for abstraction of halide ions, proving highly successful towards both main group and transition metal complexes.[21] The ultimate metallic fragment thus formed is a coordinatively unsaturated, highly reactive cationic complex with $[B(C_6F_5)_4]^-$ as the counterion. The exceptionally high electrophilic nature of $[Et_3Si]^+$ unfortunately results in problematic synthesis, with the majority of solvents, even weakly coordinating ones such as C_6H_6,[22] CH_2Cl_2 and liquid SO_2,[23] coordinating to $[Et_3Si]^+$ to form $[Et_3Si(solvent)]^+$ cations.[21] However, it can be readily prepared by reaction of two commercially available compounds, the trityl salt of $[B(C_6F_5)_4]^-$ and triethylsilane.[22] Excess Et_3SiH acts as solvent and the intense bright yellow colour of $[Ph_3C][B(C_6F_5)_4]$ is transformed to colourless $[Et_3Si][B(C_6F_5)_4]$ **(Scheme 4.2)**.[21] The generated triphenylmethane can be removed by washing with hexane and drying *in vacuo*.

$$[Ph_3C][B(C_6F_5)_4] + Et_3SiH \xrightarrow{o/n,\ 298\ K} [Et_3Si][B(C_6F_5)_4] + Ph_3CH$$

Scheme 4.2 Synthesis of the highly reactive $[Et_3Si]^+$ electrophile.

Upon addition of a yellow C_6H_5F solution of **1** to equimolar quantities of $[Et_3Si]^+$, an instantaneous change in colour from yellow to an intense deep red was observed, consistent with the formation of Et_3SiBr.[24] The solvent suppressed ^1H NMR spectrum of the solution recorded in C_6H_5F (discussed *vide infra*) was broadened and highly shifted (although to a lesser extent than **1**), with the most noteworthy new resonances being two broad singlets at 17.25 and 17.06 ppm. Upon layering with toluene, light green crystals were formed. X-ray crystallography disclosed that instead of just simple bromide extraction to form the expected two coordinate '$[Ni(6Mes)(PPh_3)]^+$' complex, loss of PPh_3 ligand had also taken place along with the coordination of toluene to give the cationic Ni(I) complex $[Ni(6Mes)(\eta^2\text{-}C_6H_5CH_3)][B(C_6F_5)_4]$ **(21; Scheme 4.3; Figure 4.8)**. $[6MesH]^{\cdot\cdot}(C_6H_5CH_3)[B(C_6F_5)_4]$ cocrystallised alongside **21**. The formation and implications of this is discussed later in more detail.

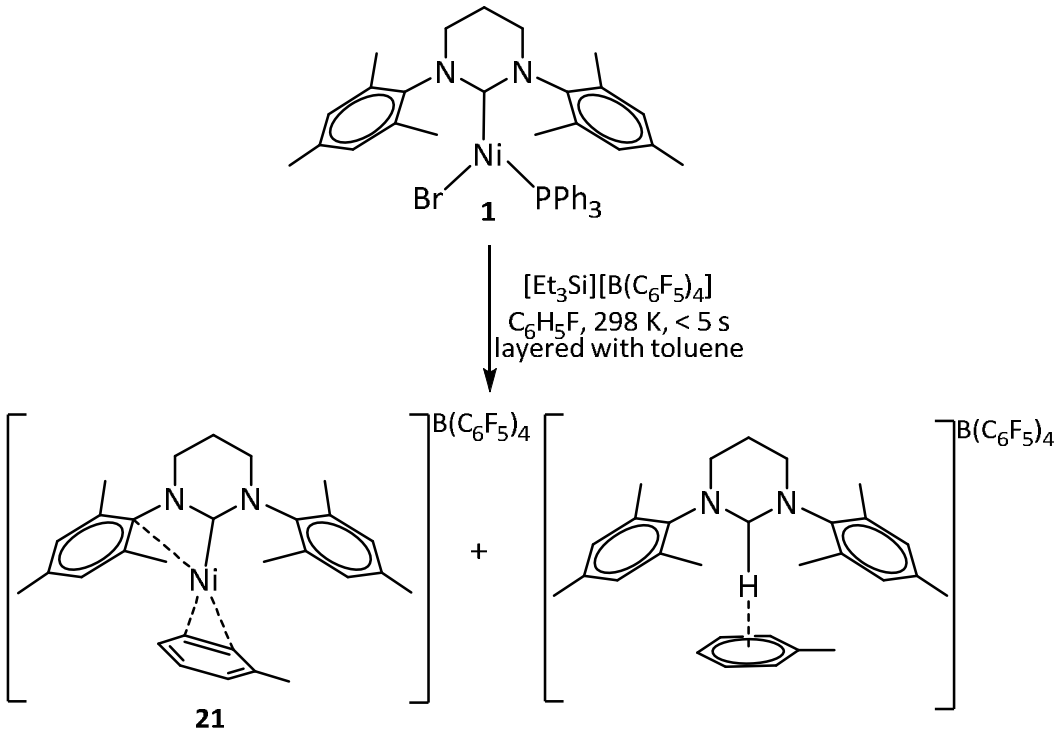

Scheme 4.3 Reaction of **1** with $[Et_3Si]^+$ to cocrystallise **21** and $[6MesH]^{+\cdot\cdot}(C_6H_5CH_3)$.

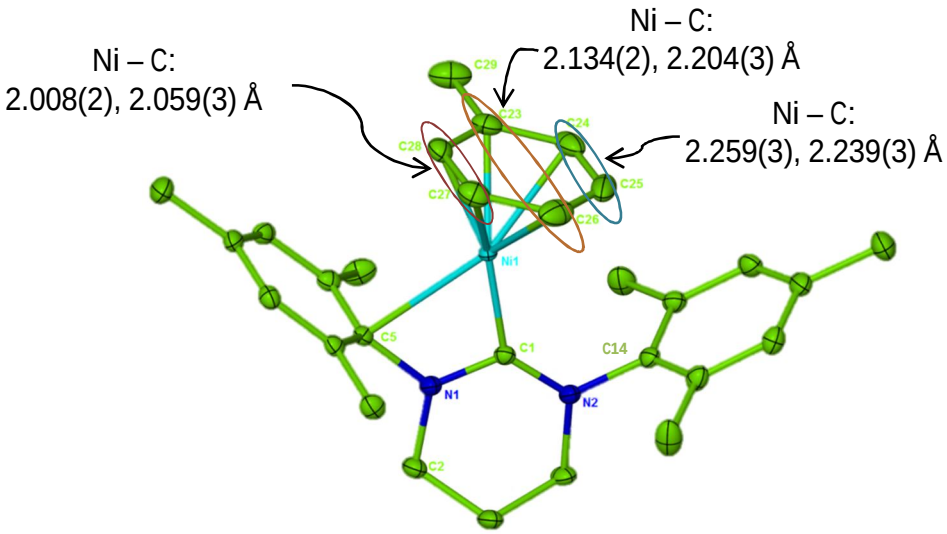

Figure 4.8 X-ray crystal structure of the cation in **21** with the Ni-C_{tol} bond lengths highlighted. Thermal ellipsoids are set at 30 % probability. All hydrogen atoms have been omitted for clarity.

	21		**21**
Ni – C(27)	2.059(3)	**Ni – C_{NHC}**	1.914(2)
Ni – C(28)	2.008(2)	**Ni – C(5)$_{ipso}$**	2.1510(2)
Ni – C(23)	2.134(2)	**Ni – C(14)$_{ipso}$**	3.363(9)
Ni – C(26)	2.204(3)	**Ni – C_{NHC} – N(1)**	103.48(13)
Ni – C(24)	2.259(3)	**Ni – C_{NHC} – N(2)**	134.07(15)
Ni – C(25)	2.239(3)		

Table 4.3 Selected bond lengths (Å) and angles (º) in **21**.

Structural determination of **21** revealed a central nickel atom coordinated to a single 6Mes ligand. The Ni-C_{NHC} bond length (1.914(2) Å) is much shorter than that found in either **1** or **19** (**1**: 1.942(2) Å; **19**: 1.941(3), 1.939(3) Å), presumably due to both the nature of the *trans* ligand and the geometry. Analysis of the Ni-C_{tol} bond distances shown in **Table 4.3**, along with other selected metrics, provided greater detail into the binding mode of the solvent molecule, revealing two short contacts to C(27) and C(28) (2.059(3) and 2.008 (2) Å), intermediate distances to C(23) and C(26) (2.134(2) and 2.204(3) Å), while even longer Ni-C(24) and -C(25) interactions (2.259(3) and 2.293(3) Å) (also shown in **Figure 4.8**). This implies toluene interacts

with nickel through η^2 coordination, instead of *via* the more symmetrical η^6 fashion. There is also a close interaction with an *ipso* carbon of one of the mesityl substituents; the Ni-C(5) distance of 2.1510(2) Å is much shorter than the next closest interaction to C(14) of 3.363 Å. Complex **21** can thus be considered as a 13e$^-$ fragment in a distorted T-shaped geometry with a C_{NHC}-Ni-C(28) angle of 165.10(10)^o (C(28) is the toluene carbon with the shortest Ni-C_{tol} distance) and C_{NHC}-Ni-C(5) of 63.23(7)^o. The lack of ligand bulk and hence more open space around the coordinatively unsaturated nickel centre presumably allows this *ipso* stabilisation to occur which, in conjunction, also pulls the nickel atom to much closer proximity to the stabilising N-mesityl group. This significantly offsets the position of the nickel atom with regards to the RE NHC, disturbing the near perfect sp^2 hybridisation of the carbenic carbon seen in the majority of Ni-6Mes complexes described in this thesis, including the precursor to **21**, **1** (**21**: Ni-C_{NHC}-N(1): 103.48(13), Ni-C_{NHC}-N(2): 134.07(15)^o; **1**: Ni-C_{NHC}-N(1): 121.34(16), Ni-C_{NHC}-N(2): 121.69(15)^{o25}). Relief of coordinative unsaturation by *ipso* carbon stabilisation has been observed elsewhere, but is unusal.[26-29] In the Rh(I)-diamidocarbene complex [Rh(6MesDAC)(COD)]$^+$ synthesised by Cesar *et al.*,[26] the rhodium is coordinated to one 6MesDAC and one η^2:η^2-COD ligand, as well as bonding to the *ipso* carbon of one of the mesityl rings on the 6MesDAC ligand (Rh-C_{ipso}: 2.346(2) Å). A similar distance (2.377(4) Å) was found in the IMes analogue [Rh(IMes)(COD)]$^+$,[27] although both distances are much larger than that measured in **21**.

Further analysis shows that the toluene ring lies almost parallel to a pentafluorophenyl ring in [B(C_6F_5)$_4$]$^-$ **(Figure 4.9)**, with the angle between the relevant least-squares aromatic ring mean planes being 9.9^o. Moreover, the centroid-centroid distance between these rings (3.78 Å) and the shortest distance from the centroid of one ring to the mean plane of the other (3.27 Å) suggests the presence of offset π-π stacking and hence additional π-stabilisation to the complex, affording further rationale for alignment of the toluene throughout the crystal.

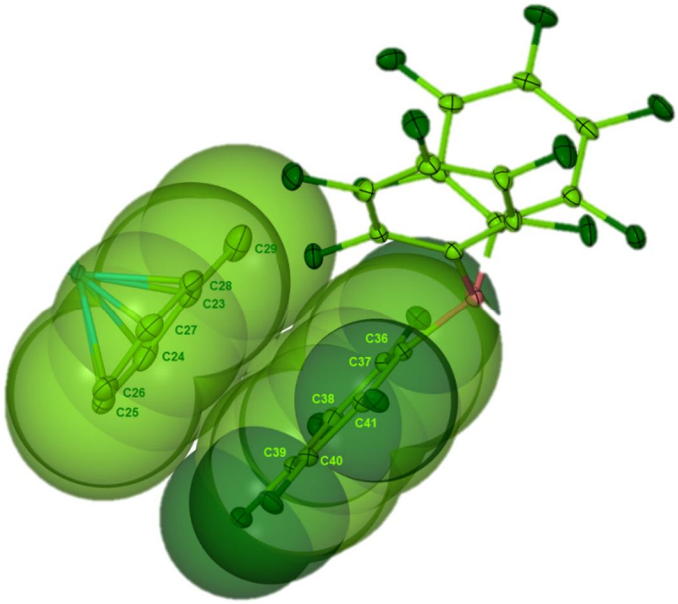

Figure 4.9 Full X-ray crystal structure of **21** showing the alignment of cation to anion thought to give rise to π-π interactions. Thermal ellipsoids are set at 30 % probability and all hydrogen atoms have been omitted for clarity.

Complex **21** is believed to be the first example of a strictly mononuclear Ni(I) complex containing a neutral π-coordinated arene ligand. All previous examples (some of which are shown in **Scheme 4.4**) contain either anionic ligands such as $[Cp]^-$ and $[B(C_6H_5)_4]^-$,[59] are dimeric in structure (such as ***xxiii*** **(Chapter 1, 1.1.4)**)[30] and/or interact with flanking aryl fragments which comprise the coordinated ligand. Tatsumi and coworkers[31] reported the isolation of a Ni(I)-thiolate complex **(*xlix*)** which showed short interactions to the *ipso* and *ortho* carbons of the sulfur bound terphenyl group (Ni-C_{ipso}: 2.129(3) Å; Ni-C_{ortho}: 2.147(2) Å). Pfirrmann *et al.*[32] synthesised the dimeric Ni(I)-β-diketiminate complex **(*xxix*; Chapter 1, 1.2)**, which showed short Ni-C contacts (2.20747(15) and 2.1337(15) Å) to *meta* and *para* carbon atoms respectively of one of the d^{i}pp groups. A toluene stabilised Ni(I) dinuclear system **(*l*)** was reported by Jones *et al*.,[33] in which two nickel guanidinato fragments are bridged by a toluene molecule with interactions of each nickel to three aromatic carbons (1.937(2), 2.089(2), 2.105(2) Å). As expected for a directly coordinated ligand, the Ni-$C_{toluene}$ (to the η^2-diene moiety) bond lengths in **21** (2.059(3) and 2.008(2) Å) are shorter than the majority of those seen in the above examples.

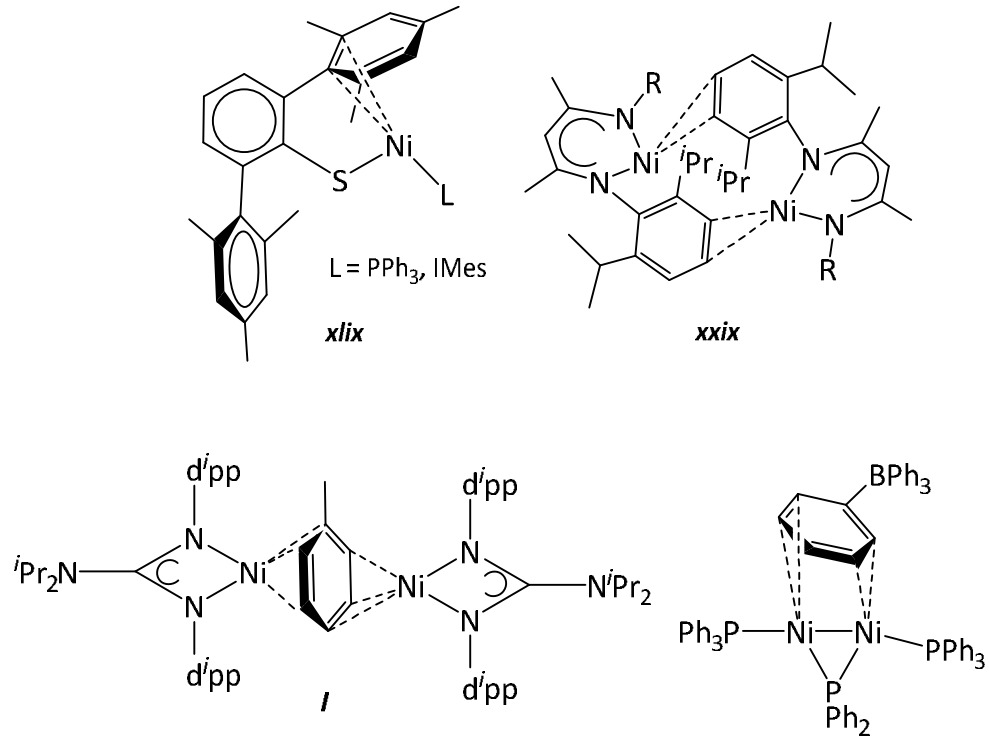

Scheme 4.4 Examples of Ni(I) monomeric/dimeric complexes π-stabilised by non-directly coordinated aryl groups (above) or dinuclear species interacting with arenes (below).

Ni-arene complexes where the arene coordinates in a neutral manner are widely known,[34-37] however, the nickel is almost exclusively in a zero oxidation state. Driess and coworkers[34] synthesised a series of silylene Ni(0)-η^6-arene complexes with toluene, 1,4-xylene and mesitylene **(Figure 4.10)**. Many other examples involve Ni-NHC fragments,[36,37] such as the very recent report of Ni(IPr)(η^6-C_6H_5R) (R = H or CH_3) **(Figure 4.10)**.[37]

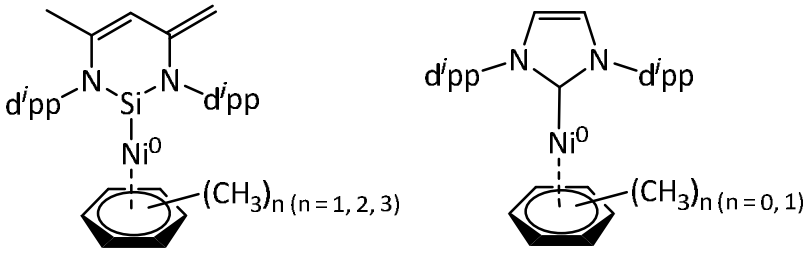

Figure 4.10 Examples of Ni(0)-η^6-arene species.

Despite the formation of **21**, initial X-ray crystallographic analysis revealed only 25 % occupancy by the nickel ion. For the remaining 75 %, a hydrogen atom was present instead, yielding the pyrimidinium cation $[6MesH]^{+}\cdots(C_6H_5CH_3)$ **(Figure 4.11)**. The $[B(C_6F_5)_4]^-$ acts as the counterion and is thus present in the unit cell 100 % of the time. The C-H bond points towards a molecule of toluene, with H(1) at a distance of 2.468 Å from the mean plane of the toluene

ring and 2.49 Å from the centroid of the same ring. This is indicative of a C-H···π interaction, based on similar distances being previously computed in benzene clusters.[38]

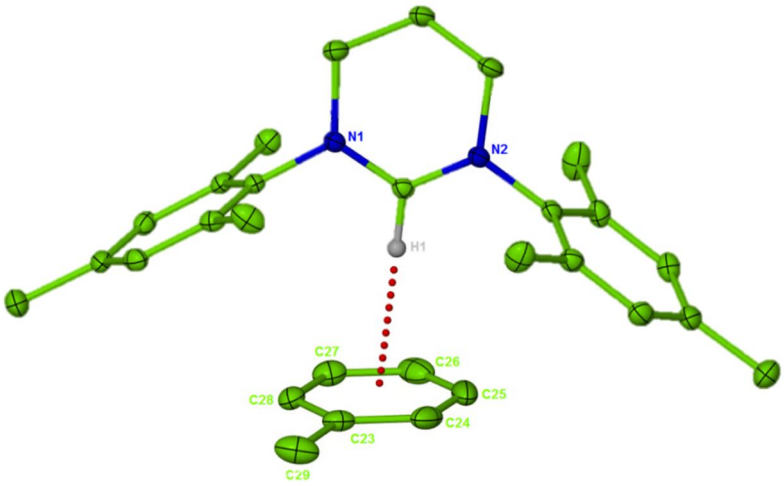

Figure 4.11 X-ray crystal structure of the cation in $[6MesH]^{\cdots}(C_6H_5CH_3)[B(C_6F_5)_4]$. Thermal ellipsoids are set at 30 % probability. All hydrogen atoms have been omitted for clarity, except for H(1).

The most likely source of the pyrimidinium proton was thought to be either residual Et_3SiH or Ph_3CH, but even upon prolonged evaporation of all traces of unreacted Et_3SiH and hexane washing to remove Ph_3CH, $[6MesH]^{\cdots}(C_6H_5CH_3)[B(C_6F_5)_4]$ was still detected. When the whole reaction ($[Et_3Si]^+$ synthesis and addition of **1**) was carried out in a glove box, the number of hexane washings increased to five and drying times lengthened to overnight, a best ratio of 65:35 for **21**:$[6MesH]^{\cdots}(C_6H_5CH_3)[B(C_6F_5)_4]$ in the cocrystal lattice was achieved. NMR studies were carried out to establish whether Et_3SiH or Ph_3CH were a source of H^+. ^1H NMR spectra of C_6H_5F solutions of i) free 6Mes with a) Et_3SiH or b) Ph_3CH and ii) **1** with a) Et_3SiH or b) Ph_3CH followed by addition of free 6Mes were recorded. In all cases, there was no spectroscopic evidence for formation of $[6MesH]^+$, implying that neither Et_3SiH or Ph_3CH were the H^+ sources.

An alternative proton source may result from considering the exact structure of $[Et_3Si][B(C_6F_5)_4]$ reported by Reed and coworkers.[21] During characterisation of isolated samples of their assumed $[Et_3Si][B(C_6F_5)_4]$ pair, they recorded IR spectra consistent with the formation of a silane adduct, $[Et_3Si–H–SiEt_3][B(C_6F_5)_4]$ (ν_{SiHSi} = 1900 cm^{-1} (broad)), where once again, solvent has coordinated to the highly reactive $[Et_3Si]^+$ fragment. When isolated, $[Et_3Si–H–SiEt_3]^+$ is then dissolved in solvents such as arenes or ethers for reactions to commence, forming $[Et_3Si(solvent)]^+$ and thus initiating the electrophile towards halide abstraction. During the

reaction with **1**, if $[Et_3Si–H–SiEt_3]^+$ is indeed generated, upon dissolution into C_6H_5F 'Et_3SiH' like fragments would be liberated and provide a source of H^+.[§]

Crystalline samples of **21** were insoluble in all nonpolar solvents (as well as C_6H_5F), but dissolution in THF followed by layering with toluene, still gave crystals of the complex, suggestive that toluene coordination is retained in THF solution. As mentioned previously, the ^1H NMR spectrum of the crude reaction mixture formed in C_6H_5F before addition of toluene was paramagnetic in nature and showed two broad resonances at 17.25 and 17.06 ppm **(Figure 4.12a)**. In contrast, the THF-d_8 spectrum of **21** after recrystallisation displayed signals which were less paramagnetic in character and the two broad singlets had disappeared **(Figure 4.12b)**. There was however a singlet of significant intensity (integral of 1H) at 8.48 ppm, which was later assigned to the C_{NHC}-*H* proton from isolated samples of [6MesH][$B(C_6F_5)_4$]. The ^1H spectrum in THF-d_8 showed no evidence of bound THF-h_8 from residual protio THF, and integration and assignments of all the resonances were possible to the solid-state structure of **21**, including toluene signals at 7.08 (C*H*) and *ca.* 2.29 ppm (CH_3). The extreme change in NMR spectra suggest that the initial nickel fragment formed upon reaction with $[Et_3Si]^+$ is not retained in solution with addition of toluene. Moreover, as the ^1H NMR spectrum of dissolved **21** is surprisingly diamagnetic in nature, it implies **21** exists slightly differently in solution than compared to its solid state structure, perhaps as aggregates. The $^{11}B\{^1H\}$ spectrum of **21** in THF-d_8 was consistent with crystallography, displaying two singlets at -18.4 and -16.6 ppm. The former has a different chemical shift from the signal associated with the $[CPh_3][B(C_6F_5)_4]$ starting material (-15.8 ppm), while the latter corresponds to [6MesH][$B(C_6F_5)_4$].

[§]As the exact structure and nature of the electrophilic silylium fragment is unknown under the reaction conditions used, it will still be referred to as $[Et_3Si]^+$ for the remainder of this thesis.

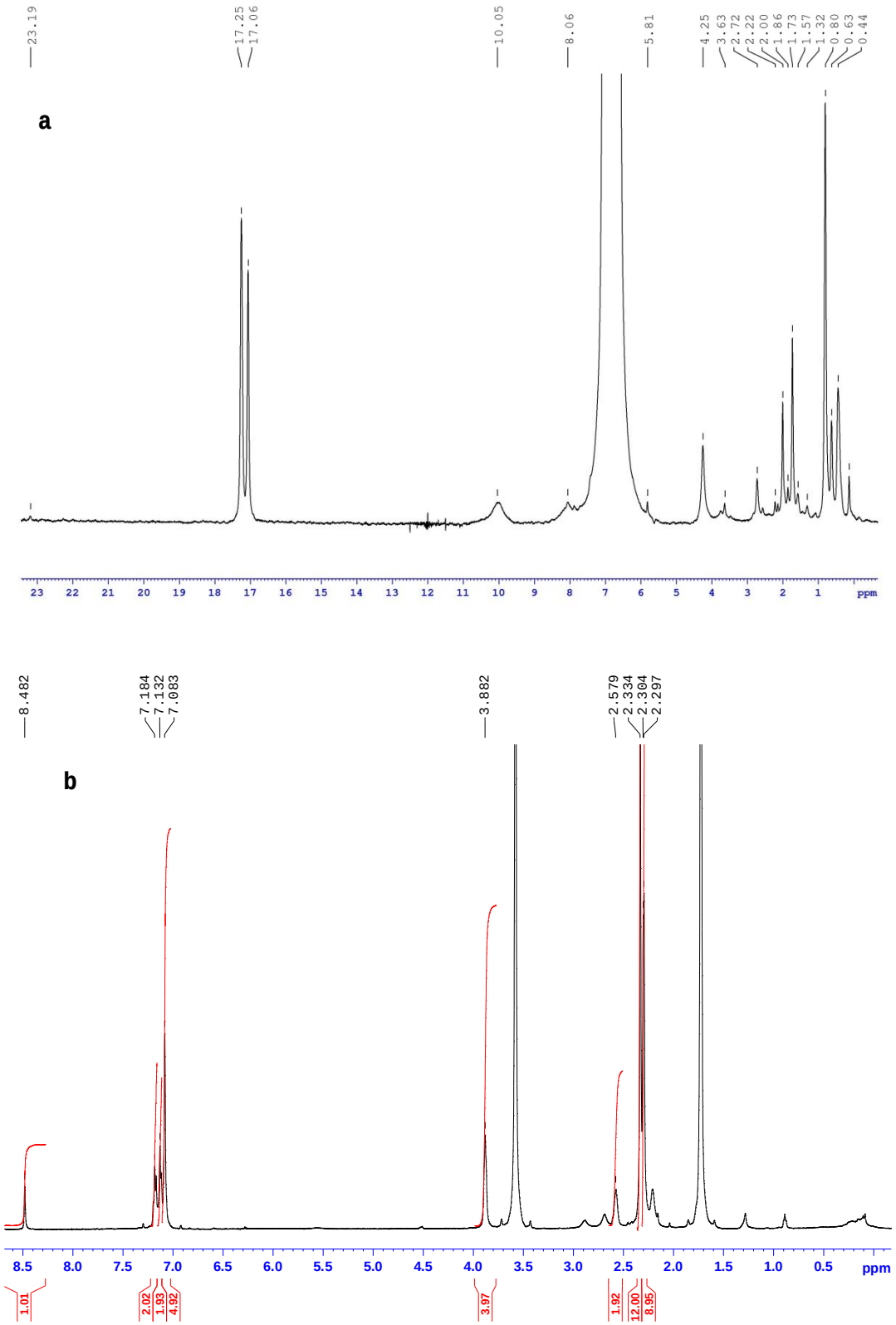

Figure 4.12 ^{1}H NMR spectra of **1** + $[Et_3Si]^+$ (before layering with toluene) (C_6H_5F, 298 K, 500 MHz) (a) and recrystallised samples of **21** (THF-d_8, 298 K, 400 MHz) (b).

*4.2.1.1 EPR spectroscopic analysis of [Ni(6Mes)(η^2-$C_6H_5CH_3$)][$B(C_6F_5)_4$] **(21)***

As the composition of **21**:[6MesH]$^{\cdot\cdot}$($C_6H_5CH_3$)[$B(C_6F_5)_4$] varied from sample to sample, the Evans method (which relies on known mass) could not be used to determine the magnetic susceptibility of **21**. The pyrimidinium impurity is expected to be EPR silent, therefore the paramagnetism of **21** was probed by X-band EPR measurements at 140 K **(Figure 4.13)**. A preliminary report of this is given below, although as will become clear, a more extensive investigation is required.

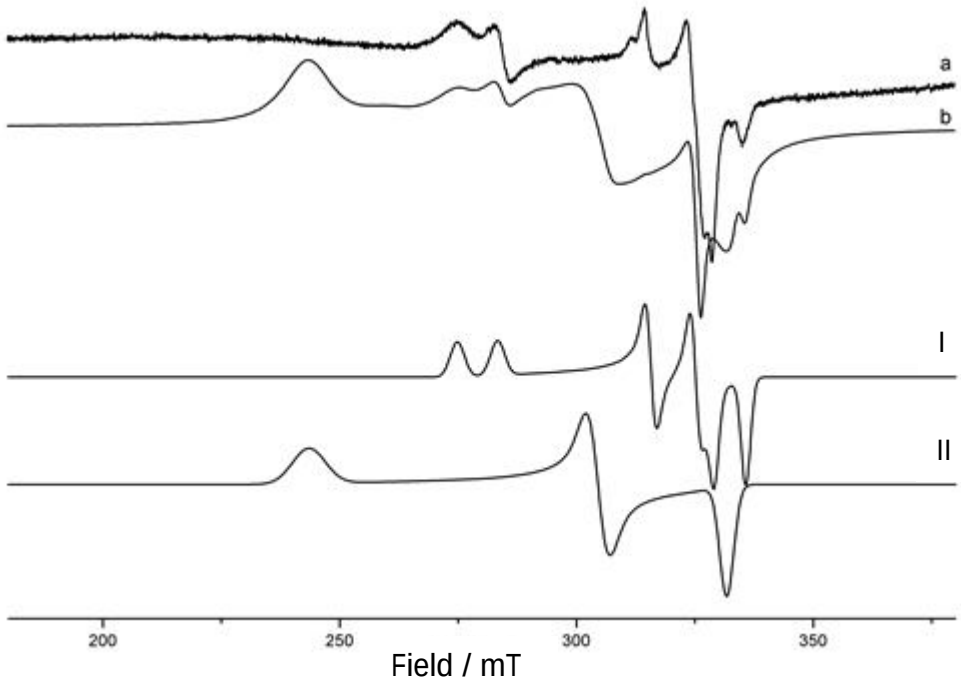

Figure 4.13 X-band EPR (140 K) spectra of [Ni(6Mes)(η^2-$C_6H_5CH_3$)][$B(C_6F_5)_4$] **(21)** after 2 h at 298 K (a) and fresh sample (b). I and II represent the simulations of the two species contributing to the fresh sample shown in b.

Complex	g_1	g_2	g_3	$g_3 - g_2$	$g_2 - g_1$	A_1 / MHz	A_2 / MHz	A_3 / MHz
21, species I	2.015	2.090	2.399	0.309	0.075	189	278	285
21, species II	2.02	2.20	2.75	0.55	0.18	-	-	-

Table 4.4 Spin Hamiltonian parameters for complex **21**. ***g*** values ±0.005 for species I and ±0.05 for species II.

Two independent spin species (I = ½) were observed in the spectra of freshly prepared samples of **21**, labelled species I and II in **Figure 4.13**. These were deconvoluted to allow simulation of each of them, resulting in the spin Hamiltonian parameters listed in **Table 4.4**. Due to the disappearance of signals originating from species II in the EPR spectrum collected after 2 h, it suggests that this species is less stable than species I. The presence of two individual species suggests that the isolated solid of **21** is i) not paramagnetically pure (despite numerous recrystallisations) or ii) forms a secondary species in solution during the EPR sample preparation. Both species I and II displayed a rhombic profile consistent with a true Ni(I) metal centre, which rules out the possibility of a Ni(II) species with an electron delocalised onto the ancillary ligands, as potentially indicated by the diamagnetic nature of the THF-d^8 ^{1}H NMR spectrum in **Figure 4.12b**. The $\boldsymbol{g}$ values obtained show a trend of $\boldsymbol{g}_3 - \boldsymbol{g}_2 > \boldsymbol{g}_2 - \boldsymbol{g}_1$ (0.309 > 0.075), opposite to that measured for the Ni(RE NHC)(PPh_3)X complexes studied **(1, 5, 7 – 10)**. This is the more commonly established trend for Ni(I) species, which indicates a ground state SOMO that is principally $3d_{x2-y2}$ in character. This differs from the calculated SOMO for Ni(6Mes)(PPh_3)Br **(1)** (admixture of predominantly $3d_{z2}$ character), an alteration most likely arising from a change in geometry of the complex (from Y-shaped **1** to a more T-shaped **21**).

Hyperfine coupling to a nucleus with I = ½ was observed for species I, with the largest hyperfine coupling now observed along the A_3 component instead of A_1 as with **1, 5, 7 – 10**. This is again probably due to the change in ground state structure. The exact identity of this I = ½ nucleus is unknown, although it is presumed to be to a ^{31}P atom in a PPh_3 containing impurity. ^{1}H ENDOR measurements are needed to confirm this assignment to ^{31}P. No hyperfine coupling could be resolved in any of the principal directions for species II, which could be a result of inaccurate simulation due to overlapping features from the presence of multiple spin species. There is also an unusually high $\boldsymbol{g}_3$ value associated with species II (2.75). Typical $\boldsymbol{g}_3$ values for Ni(I) complexes are *ca.* 2.3 – 2.4, with **1, 5, 7 – 10** all falling into this range (**1**: 2.365 (See **Table 2.4**)). Determination of the exact identity of the two species is required in order to understand the origin for the high $\boldsymbol{g}_3$ value. Some small unassigned resonances are observed in the ^{1}H NMR spectrum of recrystallised samples of **21**, which may be responsible for a second species **(Figure 4.12b)**.

4.2.1.2 Analogues of [Ni(6Mes)(η²-C₆H₅CH₃)][B(C₆F₅)₄] ***(21)***

The synthesis of **21** prompted efforts to prepare other derivatives to determine whether there was any effect of changing the ring size and N-substituents of the RE NHC or in altering the coordinated arene. **Scheme 4.5** shows the results of trying to prepare analogues with the larger Ni(7Mes)(PPh_3)Br **(6)** and less bulky 6-membered Ni(6^{o}Tol)(PPh_3)Br **(2)**. Interaction of the nickel in **21** with *ortho* and *meta* carbon atoms of the toluene directed attempts to investigate arenes with no substituents (C_6H_6) and other methyl substitution patterns (1,4-xylene and mesitylene), as well as polyarene systems like naphthalene. These results are summarised in **Scheme 4.6**.

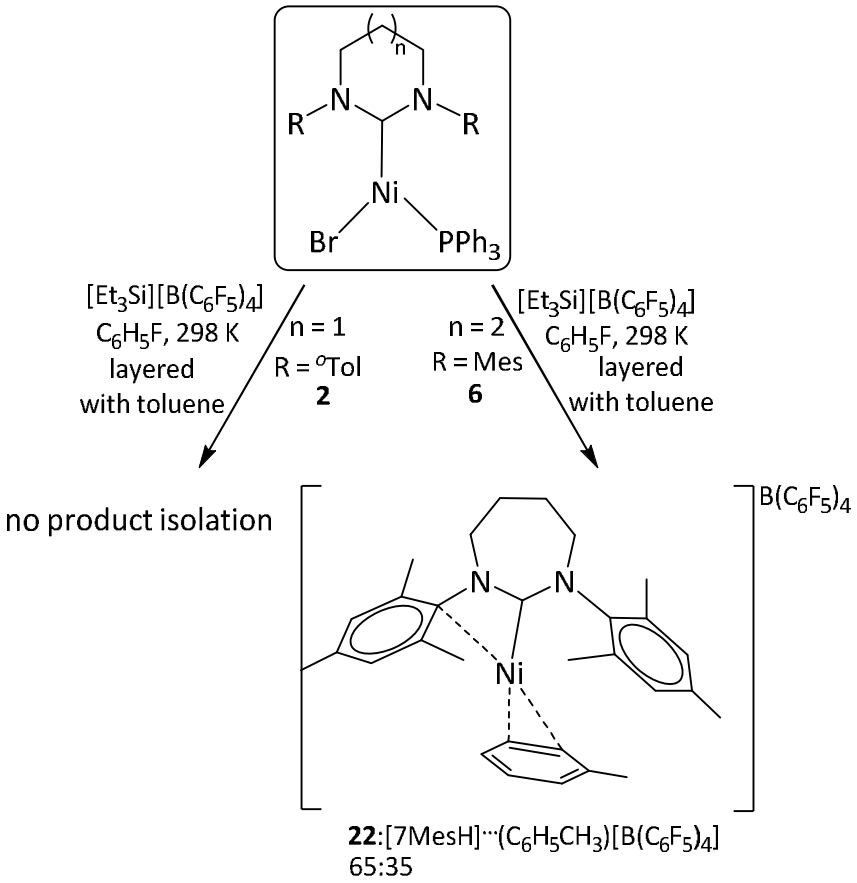

Scheme 4.5 Attempted reactions of $[Et_3Si]^+$ with **2** and **6** to establish the role of RE NHC sterics.

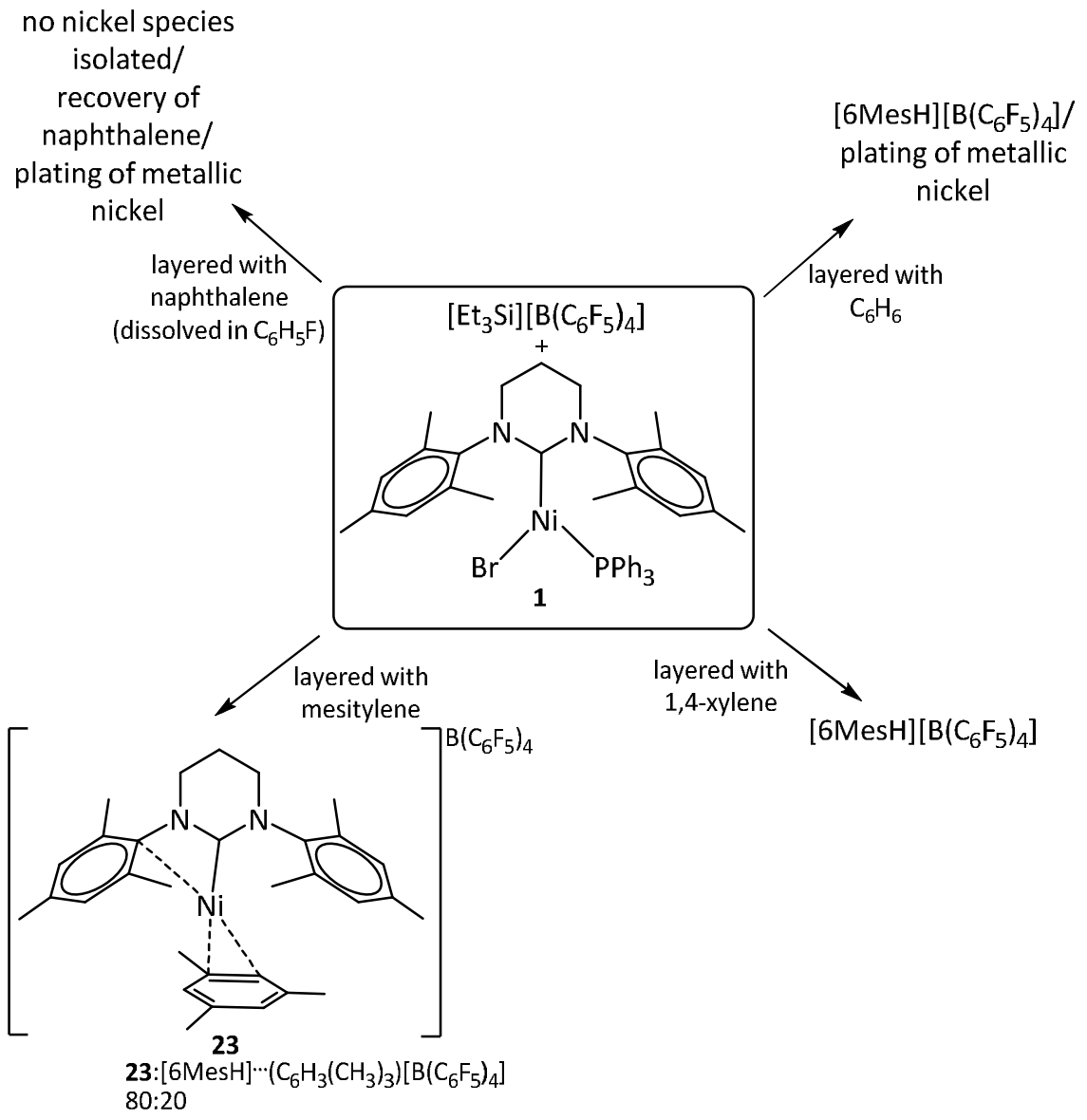

Scheme 4.6 Attempted isolation of other Ni(I)-arene species following reaction of **1** with $[Et_3Si]^+$.

Only **6** + $[Et_3Si]^+$/toluene **(Scheme 4.5)** and **1** + $[Et_3Si]^+$/mesitylene **(Scheme 4.6)** gave crystals of nickel containing products, [Ni(7Mes)(η^2-$C_6H_5CH_3$)][$B(C_6F_5)_4$] **(22)** and [Ni(6Mes)(η^2-$C_6H_3(CH_3)_3$)][$B(C_6F_5)_4$] **(23)** respectively, both isostructural and isoelectronic to **21**. These are shown in **Figure 4.14**, with selected metrics in **Table 4.5** alongside those of **21** for comparison. In both cases, the corresponding arene coordinated diazepinium/pyrimidinium salts cocrystallised with the Ni(I)-arene species, with a maximum ratio of 65:35 for **22**:[7MesH]···($C_6H_5CH_3$)[$B(C_6F_5)_4$]. X-ray crystallography revealed a large level of disorder in **23**, where the nickel atom was disordered over two sites along with the hydrogen atom from [6MesH]···($C_6H_3(CH_3)_3$)[$B(C_6F_5)_4$]. The overall **23**:[6MesH]···($C_6H_3(CH_3)_3$)[$B(C_6F_5)_4$] ratio was 80:20,

where the **23** component is made up of the sum occupancies of both the disordered nickel atoms. The metrics for **23** in **Table 4.5** correspond to the location of the nickel with the highest occupancy (75 %). In the other attempted reactions, either no crystalline material could be achieved (*i.e.* for reaction of **2** with $[Et_3Si]^+$/toluene) or only $[6MesH]^{+\cdots}$arene could be structurally characterised, as with **1** + $[Et_3Si]^+$/benzene and **1** + $[Et_3Si]^+$/1,4-xylene. This was especially surprising for 1,4-xylene given the relatively minor modification to toluene.

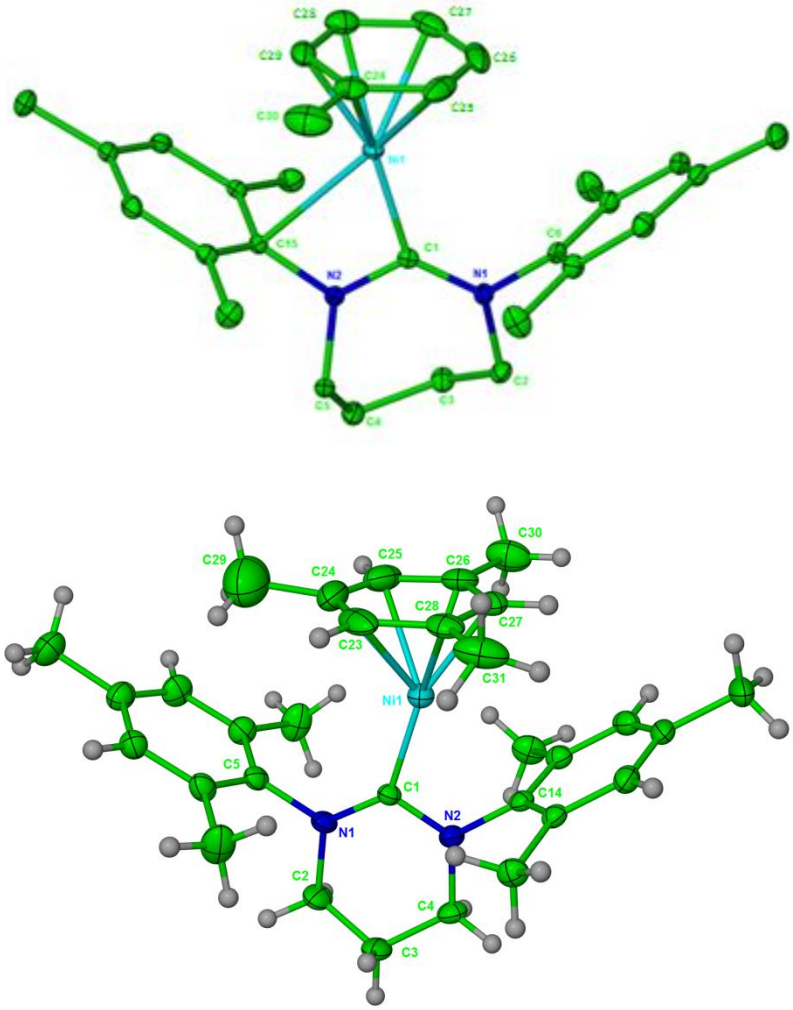

Figure 4.14 X-ray structures of the cations in **22** (above) and **23** (below). Thermal ellipsoids are set at 30 % probability. All hydrogen atoms have been omitted for clarity in **22**.

Entry		21	22	23
1	**Ni – C(28)**	2.059(3)	2.075(3)	2.111(6)
2	**Ni – C(29)**	2.008(2)	2.062(3)	2.159(5)
3	**Ni – C(24)**	2.134(2)	2.186(3)	2.238(6)
4	**Ni – C(27)**	2.204(3)	2.192(3)	2.190(6)
5	**Ni – C(25)**	2.259(3)	2.267(3)	2.303(7)
6	**Ni – C(26)**	2.239(3)	2.270(3)	2.254(7)
7	**Ni – C_{NHC}**	1.914(2)	1.932(2)	1.936(4)
8	**Ni – C(15)$_{ipso}$**	2.1510(2)	2.490(2)	2.570(11)
9	**Ni – C(6)$_{ipso}$**	3.363(9)	3.325(2)	3.400(12)
10	**C_{NHC} – Ni – C(29)$_{toluene}$**	165.57(5)	162.71(6)	161.2(2)
11	**C_{NHC} – Ni – C(15)$_{ipso}$**	56.49(8)	63.24(9)	60.69(10)
12	**Ni – C_{NHC} – N(1)**	134.07(15)	133.22(17)	133.6(3)
13	**Ni – C_{NHC} – N(2)**	103.48(13)	102.89(15)	106.7(3)
14	**N(1) – C_{NHC} – N(2)**	122.69(3)	123.9(2)	119.6(4)

Table 4.5 Selected bond lengths (Å) and angles (°) for **22** and **23** alongside **21** as a comparison. The atom numbers refer to complex **22**, with the metrics for the corresponding bond/angle in **21** and **23** shown in the same row.

The Ni-C_{arene} bond lengths in **22** and **23** follow the same pattern as that observed for **21**; three distinct sets of Ni-C_{arene} bonding can be established according to their magnitude, leading to a Ni-arene interaction that is still best considered as being η^2 in nature (*c.f.* entries 1 and 2 displaying the shortest lengths, 3 and 4 intermediate distances and 5 and 6 the longest Ni-C_{arene} bond lengths). The groupings are however less distinctive in **22** and even less so in **23**, as shown by the smaller difference between the longest and shortest Ni-C_{arene} bond distance when compared to **21** (**22**: Δ(Ni-C_{arene}) = 0.223 Å; **23**: Δ(Ni-C_{arene}) = 0.192 Å; **21**: Δ(Ni-C_{arene}) = 0.284 Å) and the lesser extent to which the carbenic carbon deviates from trigonal planarity (**22**: N(2/1)-C_{NHC}-Ni: 102.89(15)/133.22(17)°; **23**: N(2/1)-C_{NHC}-Ni: 106.7(3)/133.6(3)°; **21**: N(1/2)-C_{NHC}-Ni: 103.48(13)/134.07(15)° (entries 12 and 13)). As for **21**,

entry 8 shows shorter interactions between the nickel and *ipso* carbon of one N-Mes substituent (**22**: 2.4980(2) Å; **23**: 2.570(11) Å) compared to the other located on the second mesityl (**22**: 3.325(2) Å; **23**: 3.400(12) Å (entry 9)). However, in both cases this *ipso* interaction is a lot longer than the corresponding distance in **21** (2.1510(2) Å) and [Rh(NHC)(COD)]$^+$ (NHC = 6MesDAC[26] (2.346(2) Å), IMes[27] (2.377(4) Å)). This suggests the extent of additional stabilisation of the 13e$^-$ Ni(I) centre is less in **22** and **23**, possibly due to the increased RE NHC or arene ligand steric bulk that restricts orientation towards the *ipso* carbon. Thus, distorted T-shaped environments are again observed around the nickel metal centres (entries 10 and 11). The Ni-C_{NHC} bond lengths in **22** and **23** (**22**: 1.932(2) Å; **23**: 1.936(4) Å (entry 7)) are also slightly longer than in **21** (1.914(2) Å), again most likely due to the increased steric requirements of the higher substituted mesitylene and RE NHC backbone.

As in **21**, the packing of the cation and anion in **22** and **23** arrange themselves such that π-interactions between the coordinated arene and a pentafluorophenyl group on the anion can provide additional stability. The two aromatic rings were again nearly parallel with each other (least-squares mean planes intersect each other at 9.2 and 11.9^o respectively for **22** and **23** (**21**: 9.9^o)), with the shortest distance between one centroid to the other mean plane being 3.49 and 3.22 Å (**21**: 3.27 Å). The centroid-centroid distance between the two aromatic rings was again short at 3.63 and 3.76 Å (**21**: 3.78 Å).

The ^{1}H NMR spectra of complexes **22** and **23** in THF-d_8 were similar in nature to that of **21**, displaying a diamagnetic like spectrum which could be fully integrated and assigned to the solid-state structure. There was again a singlet resonance at 8.13 and 8.46 ppm respectively, assigned as the $C_{NHC}H$ proton in the cocrystallised diazepinium/pyrimidinium salt. Both ^{11}B{^{1}H} spectra revealed two singlet resonances, corresponding to the boron in the [$B(C_6F_5)_4$]$^-$ counterion of i) the Ni(I)-arene complex (**22** or **23**) and ii) protonated RE NHC.

Attempts to trap any low coordinate nickel species from the reaction of **1** and [Et_3Si]$^+$ with naphthalene were unsuccessful. No isolation of any nickel containing products was possible and ^{1}H NMR spectroscopy showed no evidence for naphthalene coordination. As depicted in **Scheme 4.6**, only naphthalene was crystallised out of solution along with the plating of metallic nickel. Naphthalene had previously been shown to be an effective polyarene ligand for group 4 and 5 transition metal complexes and more recently with iron, but only in the presence of a crown ether.[39] For example, Wolf *et al.*[39] have reported the formation of Fe(Cp*)(η^4-$C_{10}H_8$){K(18-crown-6)} **(Figure 4.15)**, where the naphthalene molecule is coordinated to the metal centre through one of its aromatic rings (stabilising the low valent

iron to form 18e$^-$ Fe(0)), while the other is in η^6-coordination with the K^+ of the crown ether, causing folding of the naphthalene by 35.1°. Success of naphthalene ligation with more electron rich transition metals, *i.e.* nickel, is however scarce. Unlike with the more aromatic toluene in **21**, π-interactions instigated by the presence of the $[B(C_6F_5)_4]^-$ anion with naphthalene may not be enough to stabilise any Ni-naphthalene complex formed. Thus, the addition of better stabilising agents, such as crown ethers, may be needed in order to promote this.

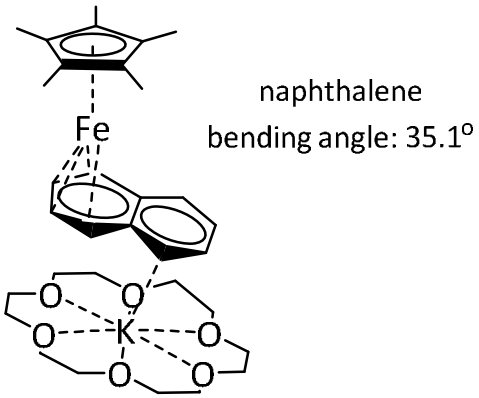

Figure 4.15 An example of a bent naphthalene coordinated Fe(0) complex.

Unsurprisingly, just pyrimidinium salt was identified upon layering a mixture of **1** + $[Et_3Si]^+$ with cyclohexane, indicating the necessity for a π-aromatic system for stabilisation of this low oxidation state and highly coordinatively unsaturated metal centre.

Due to the variable level of pyrimidinium/diazepinium contamination in batches of **21**, **22** and **23**, studies to probe the reactivity of these complexes have not been attempted at this time.

4.2.2 Halide Abstraction From Ni(6Mes)(PPh$_3$)Br (1) With Tl$^+$

A yellow THF solution of **1** (1 eq) was reacted with a slight excess of $TlPF_6$ (1.2 eq) at room temperature for 30 min, leading to a very light yellow coloured solution. Insoluble white powder (presumably TlBr) was filtered off and addition of hexane to the light yellow filtrate generated a pale yellow precipitate. X-ray quality crystals were obtained from THF/hexane, which crystallographic analysis revealed to be a three coordinate THF stabilised Ni(I) cation, $[Ni(6Mes)(PPh_3)(THF)]PF_6$ **(24; Scheme 4.7)**.

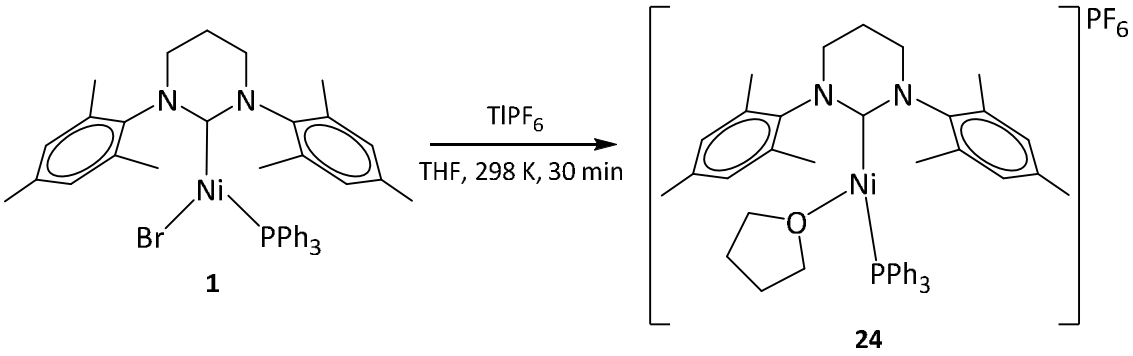

Scheme 4.7 Reaction of **1** with $TlPF_6$ to generate the Ni(I)-RE NHC cation **24**.

The nickel metal centre is bonded to the 6Mes, PPh_3 and THF in a distorted T-shaped arrangement, as depicted in **Figure 4.16**, with C_{NHC}-Ni-P and C_{NHC}-Ni-O_{THF} angles of 158.59(6) and 102.65(8)° respectively **(Table 4.6)**. The Ni-C_{NHC} distance (1.968(2) Å) is slightly longer than that in **1** (1.942(2) Å), whereas the Ni-P distances are identical in the two complexes (**24**: 2.2190(5) Å; **1**: 2.2188(6) Å).

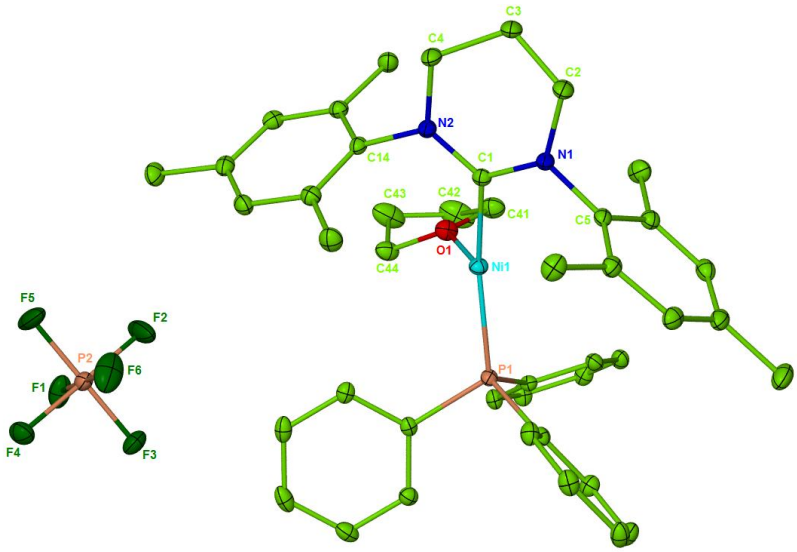

Figure 4.16 X-ray crystal structure of **24**. Thermal ellipsoids are set at 30 % probability. All hydrogen atoms have been omitted for clarity.

	24	***xliv*** [40]
Ni – C_{NHC}	1.968(2)	1.907(6)
Ni – O_{THF}	2.0956(17)	1.947(4)
Ni – P	2.2190(5)	-
C_{NHC} – Ni – L	158.59(6)	145.21(6)
C_{NHC} – Ni – O_{THF}	102.65(8)	-
N – C_{NHC} – N	117.55(18)	-

Table 4.6 Selected bond lengths (Å) and angles (°) for **24** and the related [Ni(IPr)(η^3-NHAr)(THF)]BAr_4^F ***xxxii***. L = P **(24)**, N **(*xliv*)**.

Complex **24** is somewhat structurally similar to the cationic Ni(II) amide complex ***xliv*** ([Ni(IPr)(η^3-NHAr)(THF)]BAr_4^F) introduced in **Chapter 1, 1.3.2**, with selected bond lengths for comparison shown in **Table 4.6**. In ***xliv***, the ligated THF molecule displayed a relatively long Ni-O_{THF} bond length of 1.947(4) Å and was shown to be labile as recrystallisation from CH_2Cl_2 gave a solvent free dimeric derivative of ***xliv*** in which each nickel was stabilised by the amide nitrogen atom on a neighbouring Ni-(IPr)(amide) fragment **(Scheme 1.22)**. Although a direct comparison to **24** is limited due to differences in oxidation state, the Ni-O_{THF} distance in **24** is longer (2.0956(17) Å) compared to that in ***xliv***, suggestive of even greater lability (discussed further in section **4.2.2.1**). The geometry of ***xliv*** is much more bent (C_{NHC}-Ni-N_{amide}: 145.21(6)°) when compared to **24** (C_{NHC}-Ni-P: 158.59(6)°). This is further illustrated by a less *trans* affected Ni-C_{NHC} bond length in ***xliv*** (***xliv***: 1.947(4) Å; **24**: 1.968(2) Å) and closer proximity of THF to the metal centre.

*4.2.2.1 Spectroscopic analysis of [Ni(6Mes)(PPh_3)(THF)]PF_6 **(24)***

The ^{1}H NMR spectrum of **24** displayed extremely broad resonances between 16.94 and 0.12 ppm in THF-d_8. The signals could not be integrated and so the bound THF could not be identified. Attempts to prove THF removal were therefore thwarted, especially as after any manipulations on **24** to achieve this required re-dissolution into THF for spectroscopic analysis. The best evidence obtained was *via* X-ray crystallography, which repeatedly revealed the presence of THF in **24** upon numerous recrystallisation attempts (from CH_2Cl_2, C_6H_5F, C_6H_6, toluene), suggesting the THF molecule could not be easily dissociated from the nickel.

The X-band EPR (140 K) spectrum of **24** is displayed in **Figure 4.17** along with the simulated spectrum. The spin Hamiltonian parameters extracted from this rhombic spectrum are given in **Table 4.7**. In contrast to **1**, $\boldsymbol{g}_3 - \boldsymbol{g}_2 > \boldsymbol{g}_2 - \boldsymbol{g}_1$, which can again be attributed to the T-shaped like

geometry. Hyperfine coupling to two ^{31}P nuclei were detected, which may indicate weak interaction to the $[PF_6]^-$ counterion. Simulation of the spectrum was unfortunately not optimised and further EPR studies are necessary to provide a more detailed analysis.

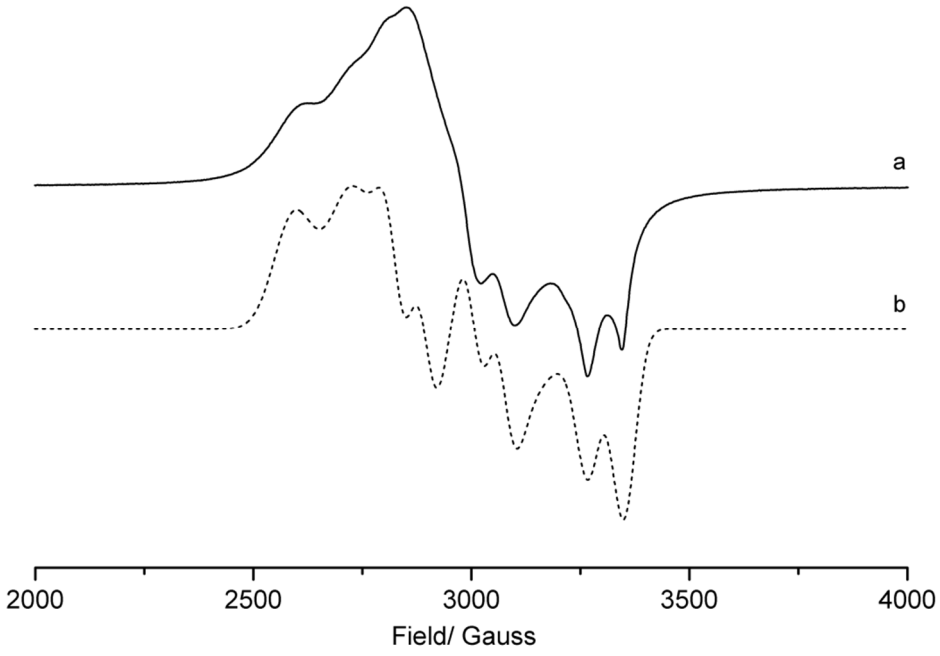

Figure 4.17 Measured (a) and simulated (b) X-band EPR (140 K) spectra of **24**.

Complex	g_1	g_2	g_3	$g_3 - g_2$	$g_2 - g_1$	A_1 / MHz	A_2 / MHz	A_3 / MHz
24	2.025	2.277	2.522	0.250	0.247	227	572	441
						[a]57	[a]222	[a]53

Table 4.7 Spin Hamiltonian parameters for **24**. ***g*** values ±0.005. [a] ^{31}P hyperfine coupling.

A μ_{eff} value of 1.4 μB was determined by the Evans method and was consistent with that expected for the presence of a single unpaired electron. The variable temperature magnetic susceptibility measured by SQUID magnetometry between 1.8 and 300 K, gave a room temperature χT value of 1.04 cm^3 K mol^{-1}. As found for **1, 3, 4** and **6** and two coordinate **19** (range between 0.67 – 1.12 cm^3 K mol^{-1}), this is higher than the expected theoretical spin-only value of 0.375 cm^3 K mol^{-1} for a d^9 Ni(I) complex. This enhanced χT value can again originate from significant inherent anisotropy and it is worth noting that the cationic complexes (**19** and **24**) generally display values greater than the neutral complexes. When orbital contributions are taken into consideration, the observed room temperature χT value lies half

way between the expected value of 1.57 cm^3 K mol^{-1} for a Ni(I) ion with unquenched orbital angular momentum and the spin-only value. As for **19**, the χT value shows a negative dependence with decreasing temperature, accompanied with a much sharper drop below 10 K to reach a minimum value of 0.458 cm^3 K mol^{-1} (half the value of that determined for SMM **19**). This low temperature negative deviation of the χT product most likely results from a combination of factors; antiferromagnetic intermolecular interactions, inherent magnetic anisotropy and depopulation of excited states.

To confirm the presence of magnetic anisotropy, field dependent magnetisation measurements **(Figure 4.18)** were carried out between 1.8 and 7 K at fields ranging from 0 to 7 T. The *M vs.* H data below 7 K demonstrates a rapid increase in the magnetisation at low magnetic fields. Above 2 T, a more gradual increase is observed at 1.8 K, with near saturation being reached (M = 1.15 μB) at low temperature (1.8 K) under 7 T (M = 2.45 μB for **19**). The *M vs.* H T^{-1} measurements reveal that at high fields there is no saturation or overlay onto a single master curve, indicative of low-lying excited states and/or the presence of large magnetic anisotropy, albeit to a lesser extent than in **19**.

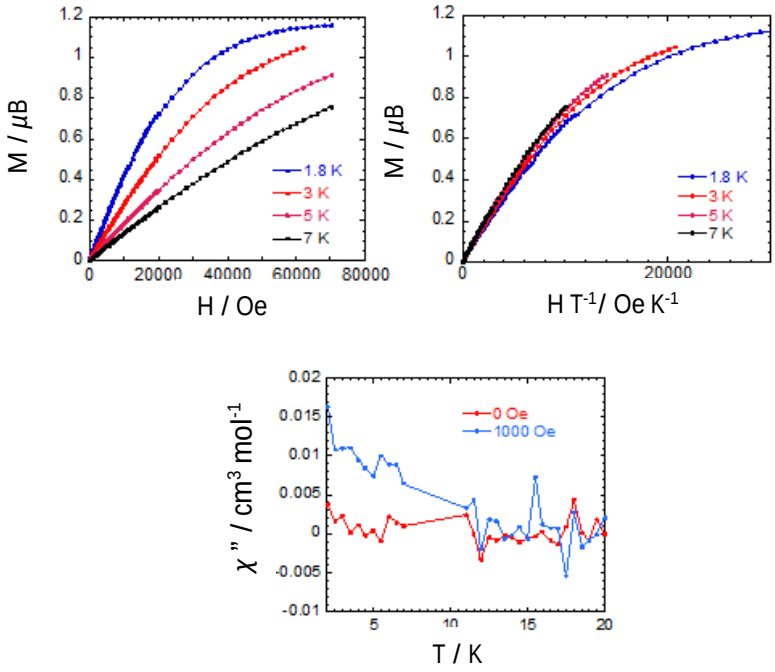

Figure 4.18 SQUID measurements on **24**. Above: field dependent magnetisation (left) and reduce magnetisation (right) at 1.8, 3, 5 and 7 K. Below: Temperature dependent ac susceptibility between 1.8 – 20 K.

To probe any potential SMM behaviour, the temperature dependence of the out-of-phase (χ'') magnetic susceptibility was investigated. Under zero applied dc field and a 0.1 T field, no temperature dependent signal was observed **(Figure 4.18)** ruling out SMM behaviour in **24**.

4.2.2.2 Reactivity of [Ni(6Mes)(PPh_3)(THF)]PF_6 (24)

Preliminary studies of the reactivity of **24** were explored by exposing THF solutions of the complex to H_2, O_2 and CO **(Scheme 4.8)**. Although a colour change from pale yellow to green was observed upon addition of 1 atm H_2, ^{1}H NMR analysis showed only the presence of starting material **24**, although some plating out of what appeared to be metallic nickel was apparent.

Upon exposure of a pale yellow THF solution of **24** to 1 atm O_2, an immediate colour change to deep purple was observed, similar to that seen in the reaction of Ni(RE NHC)(PPh_3)Br **(1, 2, 6, 7)** with O_2. Recrystallisation from THF/hexane, led to the formation of purple crystals of [Ni(6Mes)Br(μ-OH)(μ-O-6Mes)'Ni(PPh_3)]PF_6 **(25; Scheme 4.8)**. The X-ray crystal structure **(Figure 4.19)** revealed a dimeric structure analogous to that in **13**, but now with a PPh_3 rather than a bromide bound to the nickel bearing the activated 6Mes ligand. The replacement of a $1e^-$ donor for a neutral $2e^-$ donor ligand is compensated for by the presence of a $[PF_6]^-$ counterion that retains the overall Ni(II) oxidation state at each metal centre. The presence of bromide on the second nickel centre was initially a quandary, though mass spectrometry of isolated samples of **24** (even those recrystallised multiple times) revealed the presence of traces of TlBr, which is presumably the source of the bromide ligand in **25**.

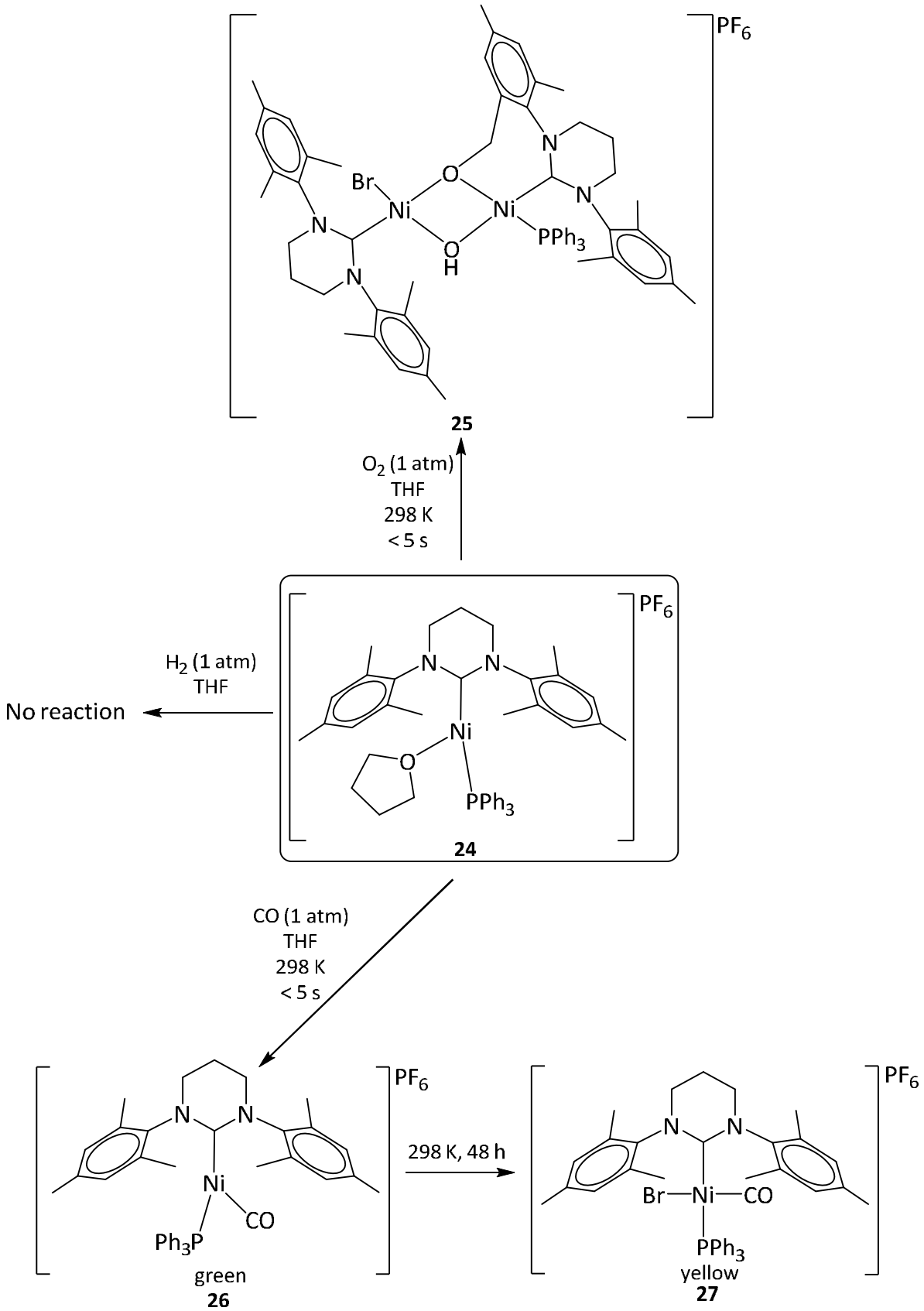

Scheme 4.8 Reactivity of **24** with H_2, O_2 and CO.

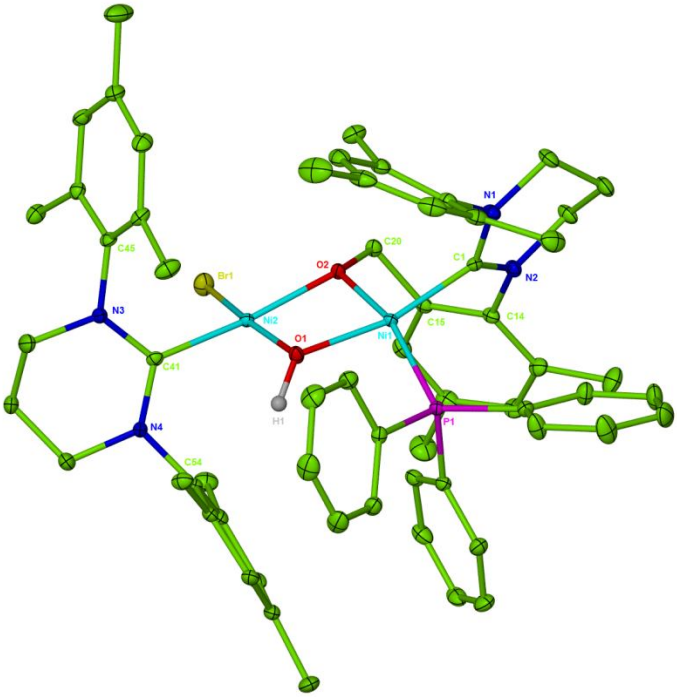

Figure 4.19 X-ray structure of the cation in **25**. Thermal ellipsoids are set to 30 % probability. All hydrogen atoms have been omitted for clarity, except for H(1).

Table 4.8 displays selected metrics for **25**, alongside those of **13** for a comparison. It seems that the strain imposed by increased ligand sterics and the μ-O-aryl group in **25**, causes the central asymmetric $Ni_2(\mu\text{-}OR)_2$ core to open up, leading to less acute Ni-O-Ni angles (**25**: 101.24(12) and 99.78(11)º; **13**: 96.63(12) and 97.53(11)º) and greater Ni···Ni separation (**25**: 2.9208(6) Å; **13**: 2.8712(6) Å). The lengthening of the Ni-C_{NHC} distances (**25**: 1.902(4) and 1.901(4) Å; **13**: 1.856(3) and 1.883(4) Å), particularly at Ni(1), would be consistent with greater congestion resulting from the presence of PPh_3 (**25**: Ni-Br: 2.2866(6) and Ni-P: 2.1769(10) Å; **13**: Ni-Br: 2.3299(6)/2.3083(6) Å; **24**: Ni-P: 2.2190(5) Å). The same trends in N-C_{NHC}-N bond angles, Ni-O distances and nitrogen atom deviation from the mean plane of its bonded atoms described for **13** in **Chapter 3, 3.1** are observed for **25**.

	25	**13**
Ni(1) – C_{NHC}	1.902(4)	1.856(3)
Ni(2) – C_{NHC}	1.901(4)	1.883(4)
O(2) – C(20)	1.421(4)	1.443(4)
Ni(1) – O(1)	1.897(2)	1.878(3)
Ni(1) – O(2)	1.885(2)	1.892(2)
Ni(2) – O(1)	1.882(3)	1.869(3)
Ni(2) – O(2)	1.934(2)	1.926(2)
Ni(1) – P	2.1769(10)	-
Ni(2) – Br	2.2866(6)	2.3299(6)
Ni(1)···Ni(2)	2.9208(6)	2.8713(6)
N(1) – C_{NHC} – N(2)	118.2(3)	118.2(3)
N(3) – C_{NHC} – N(4)	116.8(3)	116.5(3)
Ni(1) – O(1) – Ni(2)	101.24(12)	96.63(12)
Ni(1) – O(2) – Ni(2)	99.78(11)	97.53(11)
O(1) – Ni(1) – O(2)	79.08(10)	80.55(10)
O(1) – Ni(2) – O(2)	78.24(10)	80.18(10)

Table 4.8 Table of selected bond lengths (Å) and angles (º) for **25** and **13**. The atom numbers refer to complex **25**, with the metrics for the corresponding bond/angle for **13** shown in the same row.

The ^{1}H NMR spectrum of **25** displayed diamagnetic characteristics, consistent with a Ni(II)-Ni(II) species. As observed for **13** and **14**, a low frequency resonance assignable to μ-OH was apparent at -2.35 ppm (THF-d_8), which disappeared upon addition of D_2O. The $^{31}P\{^{1}H\}$ NMR spectrum revealed the presence of a bound PPh_3 ligand as well as the $[PF_6]^-$ counterion at 24.5 and -105.7 ppm (THF-d_8) respectively. No evidence for any double oxygenative C-H activation products analogous to **15** and **16** were observed during any experimental or analytical manipulations of **25**.

Scheme 4.8 depicts the reactivity of **24** observed following exposure to CO. Upon addition of 1 atm CO to a freeze-pump-thaw degassed THF solution of **24**, the pale yellow colour of the starting material instantaneously changed to green, followed by orange upon standing at room temperature for 1 h. After a further 48 h, the solution was yellow. Attempts to isolate or

identify each complex responsible for the specific coloured solutions proved partially successful, as detailed below.

Halting the reaction < 1 min after addition of CO by freezing the THF solution and removing CO by freeze-pump-thaw degassing gave a green residue, which produced light green/yellow crystals upon recrystallisaton from THF/hexane. If the green solution was immediately reduced to dryness *in vacuo* rather than simply degassed, the green colour was seen to change back to the initial yellow colour of **24**, suggestive of reversible CO coordination. Crystallographic analysis revealed the crystals to be the cationic, three coordinate Ni(I)-CO complex [Ni(6Mes)(PPh_3)(CO)]PF_6 **(26; Figure 4.20)**.

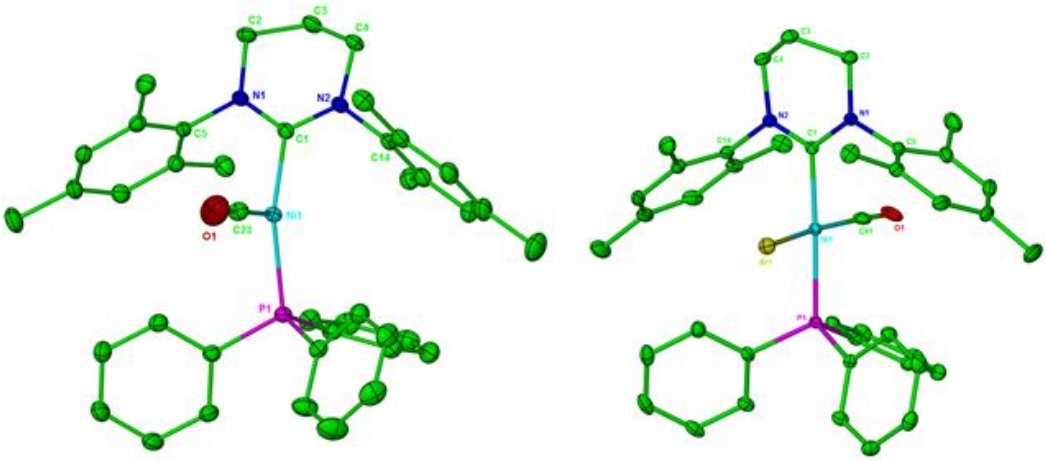

Figure 4.20 X-ray structures of the cation in **26** (left) and **27** (right). Thermal ellipsoids are set at 30 % probability and all hydrogen atoms have been omitted for clarity.

Complex **26** displayed a distorted T-shaped geometry (C_{NHC}-Ni-P: 151.93(9)°; C_{NHC}-Ni-C_{CO}: 106.24(13)° (see **Table 4.9** for metrics)). These values are close to those measured for the Ni(I)-THF starting material **24** (C_{NHC}-Ni-P: 158.59(6); C_{NHC}-Ni-O_{THF}: 102.65(8)°), showing that substitution of THF by CO leads to only a minimal structural change.

	26	**27**	***Ii*** [41]	***Iii*** [42]
Ni – C_{NHC}	1.943(3)	1.962(2)	-	-
Ni – P	2.2374(8)	2.2647(7)	-	-
Ni – C_{CO}	1.787(3)	1.782(3)	1.827(8)	1.770(3)
C_{CO} – O	1.132(4)	1.052(4)	1.155(8)	1.142(3)
Ni – Br	-	2.2979(4)	-	-
C_{NHC} – Ni – P	151.93(9)	175.86(8)	-	-
C_{NHC} – Ni – C_{CO}	106.24(13)	88.83(11)	-	-
Br – Ni – C_{CO}	-	170.90(11)	-	-
N – C_{NHC} – N	118.9(3)	120.1(2)	-	-

Table 4.9 Selected bond lengths (Å) and angles (°) for Ni(I)- (**26**, ***Ii*** and ***Iii***) and Ni(II)- **(27)** carbonyl complexes.

When the reaction of **24** with CO was left to form a yellow solution over 48 h, removal of the solvent and recrystallisation of the residue from THF/Et_2O produced very few pale yellow crystals of the Ni(II) complex [Ni(6Mes)(PPh_3)(CO)Br]PF_6 **(27; Figure 4.20)**. The source of the bromide is most likely the residual TlBr remaining from the synthesis of **24**. The isolation and time scale for formation of the CO substitution products suggests immediate formation of **26**, followed by gradual coordination of Br^- to generate **27** over time.

Table 4.9 also shows selected bond length and angles in **27**. Some comparison of metrics in **26** and **27** can be made, despite their differences in oxidation state and geometry. The Ni-C_{NHC} bond length in **27** (1.962(2) Å) is slightly longer than **26** (1.943(3) Å), mostly likely due to the greater *trans* effect of the now almost linear PPh_3 group arising from square planarity (C_{NHC}-Ni-P: **26**: 151.93(9)°; **27**: 175.86(8)°) and from enhanced steric interactions naturally arising with an increased coordination number. A similar effect is seen with the slightly lengthened Ni-P distance in **27** (**27**: 2.2647(7) Å; **26**: 2.2374(8) Å; **24**: 2.2196(5) Å). As expected for a higher oxidised metal centre, the C_{CO}-O distance in **27** (1.052(4) Å) is shorter than the 1.132(4) Å measured in **26**. The 6Mes N-C_{NHC}-N angle in **27** is significantly enlarged over any of the Ni-6Mes complexes described thus far in this thesis (**26**: 118.9(3)°; **27**: 120.1(2)°).

Preliminary efforts have been made at following the incorporation of CO by IR spectroscopy. A C_6D_6 solution of **24** was exposed to 1 atm CO and an IR spectrum taken immediately,

followed by every 5 min for a total of 40 min. At t = 1 min, small bands were visible at 2032 and 1668 cm^{-1}, the latter indicative of a bridging CO ligand. With time, further bands grew in at 1956, 1967, 1996 and 2069 cm^{-1}. The complex nature of the IR spectrum suggests the reaction with CO is not simple, with the apparent formation of a variety of different Ni-$(CO)_n$ species formed in solution. This was corroborated through preliminary low temperature (233 K) $^{13}C\{^1H\}$ NMR studies, which showed numerous high frequency Ni-^{13}CO signals upon addition of ^{13}CO to a THF solution of **24** in a J. Youngs NMR tube (see **Appendix 6** for IR and $^{13}C\{^1H\}$ PENDANT NMR spectra).

Ni(I)-CO complexes are extremely rare within the literature, with only a handful of them being monomeric[41-47] as opposed to dimers with bridging CO ligands. A Ni(I) carbonyl species bearing a PNP pincer ligand (PNP = $P(^tBu)_2CH_2Si(Me)_2NSi(Me)_2CH_2P(^tBu)_2$) was reported by Ingleson *et al.*[41] Reaction of anhydrous $NiCl_2$ with (PNP)MgCl in THF yielded Ni(PNP)Cl, which was reduced at 295 K by Mg powder to generate three coordinate Ni(PNP). Exposure of this to CO (1 atm) led to the isolation of Ni(PNP)(CO) ***(li*; Figure 4.21)**. IR spectroscopic analysis of ***li*** showed a signal at 1940 cm^{-1} indicative of moderate backbonding from the Ni(I) ion, while the EPR spectrum at 77 K displayed three ***g*** values consistent with Ni(I) and hyperfine coupling to the two equivalent ^{31}P atoms. X-ray crystallography revealed an intermediate coordination between tetrahedral and square planar (P-Ni-P: 149.59(4)°; N-Ni-C_{CO}: 148.50(15)°), a marked contrast from the planar geometry in analogous Co(PNP)(CO).[41]

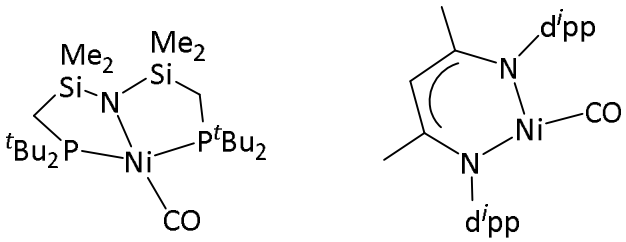

li ***lii***

Figure 4.21 Examples of monomeric Ni(I) carbonyl complexes, Ni(PNP)(CO) ***(li)*** and Ni(N^N^{Me})(CO) ***(lii)***.

In 2005 Holland and coworkers[42] reported the first three coordinate Ni(I)-CO complex, Ni(N^N^{Me})(CO) ***(lii*; Figure 4.21)**. Reduction of $[Ni(N^\wedge N^{Me})Cl]_2$ with 2 eq MeLi in Et_2O followed by exposure of 1 atm CO at 77 K generated ***lii*** in 61 % yield. Spectroscopic analyses were consistent with a d^9 electronic configuration. The ^1H NMR spectrum contained only broad signals and its EPR spectrum displayed a rhombic profile with ***g*** values of 2.19, 2.17 and 2.01. IR spectroscopy revealed a band at 2022 cm^{-1}, confirming the presence of one CO ligand.

The X-ray crystal structure displayed internal angles similar to those in **26**. A T-geometry was indicated by the N-Ni-C_{CO} angles of 104.6(1) and 158.9(1)°. A longer Ni-N bond distance *trans* to CO was observed (1.917(2) Å *vs.* 1.868(2) Å), presumably due to the strong *trans* effect of the carbonyl ligand. The C-O bond length (1.142(3) Å) was only slightly longer than that in free CO (1.128 Å),[48] consistent with the relatively weak backbonding implied by the carbonyl IR frequency. The C_{CO}-O distances in **26** and **27** (1.132(4) and 1.052(4) Å respectively) are both shorter than in ***Ii*** (1.155(8) Å) and ***Iii*** (1.142(3) Å), possibly as a result of the greater σ-donation of the RE NHC and thus Ni → CO backbonding.

The isolation of **25**, **26** and **27** highlights interesting reactivity of **24** and thus $[Ni(I)\text{-}L]^+$ fragments (L = bulky ligand such as RE NHC) for small molecule activation, as shown by the generation of extremely rare species such as the three coordinate Ni(I)-CO complex **26**. However, the presence of small quantities of residual bromide in **24** hampers clean reactivity by incorporation of bromide into these nickel complexes. The issue of removing all TlBr impurities would need to be fully addressed to gain a complete understanding of cationic Ni(I) reactivity.

4.3 Reaction of Ni(6Mes)(PPh_3)Br (1) with $NaBH_4$

To investigate the possibility of generating nickel hydride complexes, **1** was reacted with a variety of hydride sources, including $LiAlH_4$, $LiBEt_3H$, $NaBH_3(CN)$ and $NaBH_4$. Despite ^1H NMR studies and visible colour changes indicating reactions taking place, only a single organonickel complex from the reaction with $NaBH_4$ could be isolated reproducibly.

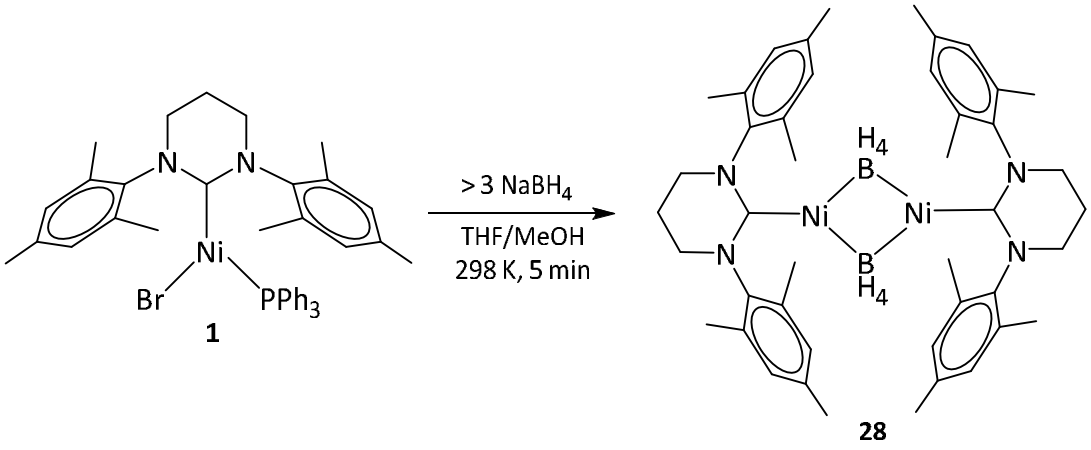

Scheme 4.9 Reaction of **1** with $NaBH_4$ to form the BH_4 bridged Ni(I) dimer **(28)**.

MeOH was added to a mixture of **1** and excess $NaBH_4$ (*ca.* 3 eq) suspended in THF and stirred for 5 min at room temperature. The bright yellow coloured solution of **1** immediately turned to an intense dark green/black colour. Recrystallisation from toluene/hexane yielded dark green crystals of the Ni(I) dimer $[Ni(6Mes)(\kappa^2\text{-}BH_4)]_2$ **(28; Scheme 4.9)**. The molecular structure of the compound is shown in **Figure 4.22**. Each nickel atom is bound to a 6Mes ligand and bridged by two BH_4 groups that bind κ^2 to each metal centre *via* three individual hydrogens. As expected the κ-BH_4 hydrogen atoms were only partially defined by X-ray crystallography and their positions restrained and refined subject to being located equidistant from the boron centres to which they are attached. Neutron diffraction was also undertaken, during which the crystal underwent a phase transition. As a consequence, the asymmetric unit became half a molecule of **28** and all asymmetry observed in the X-ray structure (*vide infra*) was lost in crystallographic disorder. No credible model could therefore be proposed, thus proving no more conclusive in determining the exact hydrogen locations.

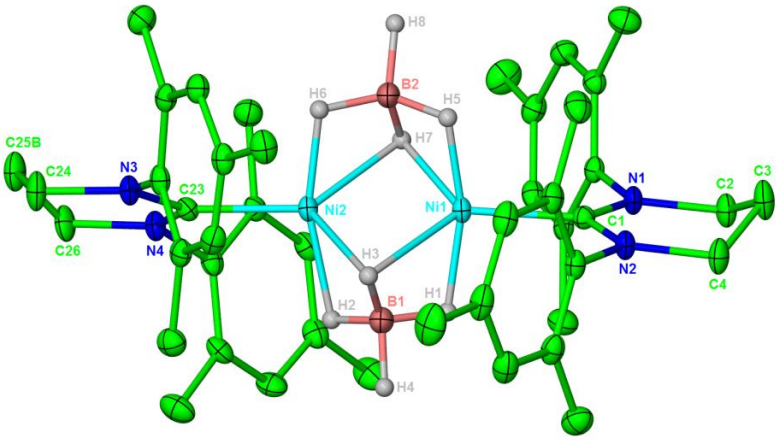

Figure 4.22 X-ray structure of **28**. Thermal ellipsoids are set at 30 % probability. All hydrogen atoms have been omitted for clarity, except for bridging BH_4 ligands. H(1) – H(8) were restrained subject to being located equidistant from the boron centres to which they are attached.

There is slight asymmetry in the bridging BH_4 ligands. B(1) is located 1.611 Å below the $(N)_2C_{NHC}$-Ni-Ni-$C_{NHC}(N)_2$ mean plane and B(2) 1.673 Å above, while B(2) deviates 0.59 Å from the central plane perpendicular to $(N)_2C_{NHC}$-Ni-Ni-$C_{NHC}(N)_2$ compared to 0.40 Å for B(1). Selected metrics associated with **28** are displayed in **Table 4.10**. The Ni···Ni distance (2.4137(5) Å) is *ca.* 0.45 Å shorter than in the hydroxyl/aryloxy bridged dimers **13** and **14** (2.8713(6) and 2.8871(8) Å respectively). Dinickel complexes, such as ***xxiii*** $(Ni_2(L)(\mu\text{-}Cl)_2$, L = *p*-terphenyl diphosphine) and its cationic analogue, $[Ni_2(L)(\mu\text{-}Cl)]^+$, **(Chapter 1, 1.1.4)** have

reported Ni···Ni distances of 2.3658(2) Å and 2.5248(3) Å respectively,[30] short enough for the nickels to be considered bonded (based on the van der Waals radius of nickel (1.63 Å)[49]). This suggests that in **28**, the nickel centres reside in close enough proximity for a direct bonding interaction to be considered.

	28		**28**
Ni(1) – C_{NHC}	1.914(3)	**Ni(2) – B(1)**	2.143(4)
Ni(2) – C_{NHC}	1.911(3)	**Ni(2) – B(2)**	2.172(4)
Ni···Ni	2.4137(5)	**N(1) – C_{NHC} – N(2)**	116.0(2)
Ni(1) – B(1)	2.161(4)	**N(3) – C_{NHC} – N(4)**	166.1(2)
Ni(1) – B(2)	2.144(4)		

Table 4.10 Selected bond lengths (Å) and angles (°) for dimer **28**.

The ^{1}H NMR spectrum of **28** was diamagnetic in nature, consistent with antiferromagnetic coupling between the two Ni(I) metals centres. In contrast to the solid-state, the ^{1}H spectrum suggested a symmetric geometry, displaying a single set of signals. The BH_4 ligands appeared as a broad doublet (singlet in the $^{1}H\{^{11}B\}$ spectrum) at -5.74 ppm in THF-d_8, which remained unchanged on cooling down to 198 K. A singlet corresponding to the eight aryl hydrogens (6.71 ppm), carbene backbone signals at 3.10 (NCH_2) and 2.02 ppm (NCH$_2$CH_2) and methyl protons resonances at 2.36 (*p*-CH_3) and 2.02 ppm (*o*-CH_3) were also observed. The $^{11}B\{^{1}H\}$ NMR spectrum at 298 K revealed a broad singlet at -32.0 ppm.

Despite the tetrahydroborate anion being widely known to coordinate to transition metals,[50-57] Ni(I)-BH_4 complexes are rare with the only two species known being monomeric, as shown in **Figure 4.23**.[52,58]

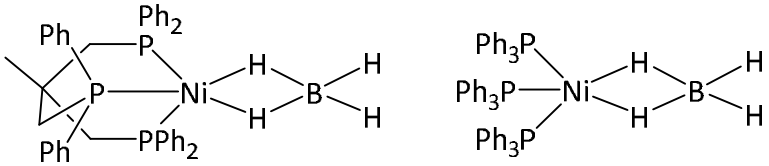

Figure 4.23 Monomeric Ni(I)-BH_4 complexes, Ni(triphos)(κ^2-BH_4) (left) and Ni(κ^2-BH_4)(PPh_3)$_3$ (right).

Complex **28** proved hard to isolate in good yields. Thus, only preliminary reaction studies have been conducted using samples of the borohydride dimer formed *in situ*. Addition of 1 atm O_2 to THF solutions of **28** led to a colour change from dark green to light green and ultimately

orange within 2 min, but attempts to isolate any nickel containing products gave instead just the RE NHC borane adduct 6Mes.BH_3 (see **Appendix 2** for crystal structure), suggesting that **28** may undergo complete degradation under oxidative conditions. The formation of 6Mes.BH_3 again highlights the ease with which RE NHCs can dissociate and form adducts, similar to the formation of [6MesH][$B(C_6F_5)_4$] in the syntheses of **21**, **22** and **23**. In the case of CO, addition of 1 atm ^{13}CO to a NMR sample of crude **28** led to multiple Ni-^{13}CO resonances in the $^{13}C\{^1H\}$ NMR spectrum recorded at 230 K. This was corroborated by the occurrence of several solution colour changes observed during the reaction (dark green to light yellow initially, followed by green, orange and ultimately light brown during a 2 h period). Despite failure to isolate any organonickel complexes, these initial reactivity studies suggest molecularity associated with complex **28** and thus provide potential routes to isolable nickel, perhaps Ni(I)-CO/O, species.

4.4 Chapter Summary

The three coordinate Ni(I)-RE NHC complex **1** undergoes a variety of reactions to generate further interesting low coordinate, low oxidation state nickel complexes. First and foremost was the formation of a rare two coordinate Ni(I) complex **(19)** upon addition of 6Mes to **1**. SQUID measurements on this highly linear complex were indicative of SMM properties; the first time such behaviour has been seen for mononuclear nickel. This notable characteristic arises as a direct result of the partially filled unexpected 2:1:2 metal based *d* orbital splitting pattern determined by DFT calculations. Reduction of **19** was achieved to obtain the analogous closed shell Ni(0) complex **20**.

Attempted halide abstraction from **1** with $[Et_3Si]^+$ or Tl^+ led to the formation of monovalent **21/22/23** and **24** respectively. In both cases, solvent molecules are ligated to the metal centre to increase saturation of the coordination sphere. In addition, **21**, **22** and **23** (of general formula [Ni(RE NHC)(η^2-arene)]$^+$) show additional stabilisation by π and *ipso* carbon interactions from surrounding aromatic moieties. They are the first examples of monomeric Ni(I)-arene compounds where an arene is neutrally bound to the nickel centre as an independent ligand in its own right. Despite this success, further analogues of [Ni(RE NHC)(η^2-arene)]$^+$ could not be formed. The lack of complexation across a variety of RE NHCs and arenes reveals the sensitivity of Ni(I) ions, where only subtle changes in either RE NHC geometry or the identity of the stabilising arene can prevent formation of Ni(I)-arene species. From these initial studies it seems that large and sterically encumbered N-mesityl substituents are required, presumably protecting the nickel metal centre to a much greater

extent than N-^{o}Tol, a trend previously observed in the formation of **19** (section **4.1.1**) and upon reaction of **1** and **2** with O_2 **(Chapter 2)**. The nature of the arene used is also important; monosubstituted toluene and trisubstituted mesitylene generated **21/22** and **23** respectively, whereas the use of the disubstituted 1,4-xylene with **1** + $[Et_3Si]^+$ led to sole formation of 6Mes pyrimidinium, suggesting the steric and electronic implications of arene functionalisation have to be considered. Complex **24** comprised a THF molecule coordinated to a Ni(I) metal centre, along with 6Mes and PPh_3. This underwent further small molecule reactivity with O_2 and CO to generate $Ni_2(\mu\text{-OR})_2$ **(25)** and low coordinate Ni(I)-CO **(26)** species respectively.

Abstraction of bromide from **1** in the presence of a potentially coordinating anion was possible *via* reaction of **1** with excess $NaBH_4$ to form the $[BH_4]^-$ bridged dinuclear Ni(I) species **28**, which displayed a rarely observed bridging mode of $[BH_4]^-$. Unfortunately, this could not be generated in great enough yields to successfully carry out any reactivity studies.

4.5 References

1. R. C. Poulten, I. Lopez, A. Llobet, M. F. Mahon and M. K. Whittlesey, *Inorg. Chem.*, 2014, **53**, 7160-7169.
2. R. C. Poulten, M. J. Page, A. G. Algarra, J. J. Le Roy, I. Lopez, E. Carter, A. Llobet, S. A. Macgregor, M. F. Mahon, D. M. Murphy, M. Murugesu and M. K. Whittlesey, *J. Am. Chem. Soc.*, 2013, **135**, 13640-13643.
3. S. Miyazaki, Y. Koga, T. Matsumoto and K. Matsubara, *Chem. Commun.*, 2010, **46**, 1932-1934.
4. DFT calculations were carried out by Prof. Stuart Macgregor and coworkers at Heriot-Watt University, Edinburgh, 2015.
5. K. Matsubara, S. Miyazaki, Y. Koga, Y. Nibu, T. Hashimura and T. Matsumoto, *Organometallics*, 2008, **27**, 6020-6024.
6. L. R. Titcomb, S. Caddick, F. G. N. Cloke, D. J. Wilson and D. McKerrecher, *Chem. Commun.*, 2001, 1388-1389.
7. P. P. Power, *Chem. Rev.*, 2012, **112**, 3482-3507.
8. J. C. Green, R. G. Scurr, P. L. Arnold and F. G. N. Cloke, *Chem. Commun.*, 1997, 1963-1964.
9. J. C. Green and B. J. Herbert, *Dalton Trans.*, 2005, 1214-1220.
10. O. Kahn, *Molecular Magnetism*, Wiley-VCH, New York, 1993.
11. D. Gatteschi, R. Sessoli and J. Villain, *Molecular Nanomagnets*, Oxford University Press, New York, 2006.
12. P. H. Rieger, *Electron Paramagnetic Resonance: Analysis and Interpretation*, RSC Publishing, Cambridge, U.K., 2007.
13. J. A. Weil, J. R. Bolton and J. E. Wertz, *Electron Paramagnetic Resonance: Elementary Theory and Practical Applications*, Wiley, New York, 1994.
14. C. R. Ganivet, B. Ballesteros, G. de la Torre, J. M. Clemente-Juan, E. Coronado and T. Torres, *Chem. Eur. J.*, 2013, **19**, 1457-1465.
15. R. A. Layfield, *Organometallics*, 2014, **33**, 1084-1099.
16. F. Neese and D. A. Pantazis, *Farad. Discuss.*, 2011, **148**, 229-238.
17. G. Rogez, J. N. Rebilly, A. L. Barra, L. Sorace, G. Blondin, N. Kirchner, M. Duran, J. van Slageren, S. Parsons, L. Ricard, A. Marvilliers and T. Mallah, *Angew. Chem., Int. Ed.*, 2005, **44**, 1876-1879.

18. R. Ruamps, R. Maurice, L. Batchelor, M. Boggio-Pasqua, R. Guillot, A. L. Barra, J. Liu, E. E. Bendeif, S. Pillet, S. Hill, T. Mallah and N. Guihery, *J. Am. Chem. Soc.*, 2013, **135**, 3017-3026.
19. R. Ruamps, L. J. Batchelor, R. Maurice, N. Gogoi, P. Jimenez-Lozano, N. Guihery, C. de Graaf, A. L. Barra, J. P. Sutter and T. Mallah, *Chem. Eur. J.*, 2013, **19**, 950-956.
20. J. Krzystek, J. H. Park, M. W. Meisel, M. A. Hitchman, H. Stratemeier, L. C. Brunel and J. Telser, *Inorg. Chem.*, 2002, **41**, 4478-4487.
21. M. Nava and C. A. Reed, *Organometallics*, 2011, **30**, 4798-4800.
22. J. B. Lambert, S. Z. Zhang and S. M. Ciro, *Organometallics*, 1994, **13**, 2430-2443.
23. S. P. Hoffmann, T. Kato, F. S. Tham and C. A. Reed, *Chem. Commun.*, 2006, 767-769.
24. J. S. Bajwa, X. L. Jiang, J. Slade, K. Prasad, O. Repic and T. J. Blacklock, *Tetrahedron Lett.*, 2002, **43**, 6709-6713.
25. C. J. E. Davies, M. J. Page, C. E. Ellul, M. F. Mahon and M. K. Whittlesey, *Chem. Commun.*, 2010, **46**, 5151-5153.
26. V. Cesar, N. Lugan and G. Lavigne, *J. Am. Chem. Soc.*, 2008, **130**, 11286.
27. N. Imlinger, K. Wurst and M. R. Buchmeiser, *J. Organomet. Chem.*, 2005, **690**, 4433-4440.
28. Y. Zhang, D. R. Wang, K. Wurst and M. R. Buchmeiser, *J. Organomet. Chem.*, 2005, **690**, 5728-5735.
29. I. Fernandez, N. Lugan and G. Lavigne, *Organometallics*, 2012, **31**, 1155-1160.
30. A. Velian, S. Lin, A. J. M. Miller, M. W. Day and T. Agapie, *J. Am. Chem. Soc.*, 2010, **132**, 6296.
31. M. Ito, T. Matsumoto and K. Tatsumi, *Inorg. Chem.*, 2009, **48**, 2215-2223.
32. S. Pfirrmann, S. Yao, B. Ziemer, R. Stoesser, M. Driess and C. Limberg, *Organometallics*, 2009, **28**, 6855-6860.
33. C. Jones, C. Schulten, L. Fohlmeister, A. Stasch, K. S. Murray, B. Moubaraki, S. Kohl, M. Z. Ertem, L. Gagliardi and C. J. Cramer, *Chem. Eur. J.*, 2011, **17**, 1294-1303.
34. A. Meltzer, C. Praesang, C. Milsmann and M. Driess, *Angew. Chem., Int. Ed.*, 2009, **48**, 3170-3173.
35. T. Nickel, R. Goddard, C. Kruger and K. R. Porschke, *Angew. Chem., Int. Ed. Engl.*, 1994, **33**, 879-882.
36. C. H. Lee, D. S. Laitar, P. Mueller and J. P. Sadighi, *J. Am. Chem. Soc.*, 2007, **129**, 13802.
37. Y. Hoshimoto, Y. Hayashi, H. Suzuki, M. Ohashi and S. Ogoshi, *Organometallics*, 2014, **33**, 1276-1282.

38. R. M. Kumar, M. Elango, R. Parthasarathi, D. Vijay and V. Subramanian, *J. Chem. Sci.*, 2012, **124**, 193-202.
39. R. Wolf and E. M. Schnoeckelborg, *Chem. Commun.*, 2010, **46**, 2832-2834.
40. C. A. Laskowski and G. L. Hillhouse, *J. Am. Chem. Soc.*, 2008, **130**, 13846-13847.
41. M. J. Ingleson, B. C. Fullmer, D. T. Buschhorn, H. Fan, M. Pink, J. C. Huffman and K. G. Caulton, *Inorg. Chem.*, 2008, **47**, 407-409.
42. N. A. Eckert, A. Dinescu, T. R. Cundari and P. L. Holland, *Inorg. Chem.*, 2005, **44**, 7702-7704.
43. C. F. Lovitt, G. Frenking and G. S. Girolami, *Organometallics*, 2012, **31**, 4122-4132.
44. G. Tavcar, S. S. Sen, R. Azhakar, A. Thorn and H. W. Roesky, *Inorg. Chem.*, 2010, **49**, 10199-10202.
45. L. Postigo and B. Royo, *Adv. Synth. Catal.*, 2012, **354**, 2613-2618.
46. P. Pietrzyk, K. Podolska and Z. Sojka, *J. Phys. Chem. A*, 2008, **112**, 12208-12219.
47. V. Yempally, L. Zhu, D. Isrow and B. Captain, *J. Cluster Sci.*, 2010, **21**, 417-426.
48. *National Institute of Standards and Technology - http:/webbook.nist.gov/chemistry/*.
49. A. Bondi, *J. Phys. Chem.*, 1964, **68**, 441.
50. T. J. Marks and J. R. Kolb, *Chem. Rev.*, 1977, **77**, 263-293.
51. D. P. Curran, A. Solovyev, M. M. Brahmi, L. Fensterbank, M. Malacria and E. Lacote, *Angew. Chem., Int. Ed.*, 2011, **50**, 10294-10317.
52. M. Kandiah, G. S. McGrady, A. Decken and P. Sirsch, *Inorg. Chem.*, 2005, **44**, 8650-8652.
53. M. Maekawa, C. G. Daniliuc, P. G. Jones, J. Hohenberger, J. Sutter, K. Meyer and M. D. Walter, *Eur. J. Inorg. Chem.*, 2013, 4097-4104.
54. W. H. Harman, T. P. Lin and J. C. Peters, *Angew. Chem., Int. Ed.*, 2014, **53**, 1081-1086.
55. I. Koehne, T. J. Schmeier, E. A. Bielinski, C. J. Pan, P. O. Lagaditis, W. H. Bernskoetter, M. K. Takase, C. Wuertele, N. Hazari and S. Schneider, *Inorg. Chem.*, 2014, **53**, 2133-2143.
56. Y. Journaux, V. Lozan, J. Klingele and B. Kersting, *Chem. Commun.*, 2006, 83-84.
57. W. H. Harman and J. C. Peters, *J. Am. Chem. Soc.*, 2012, **134**, 5080-5082.
58. D. G. Holah, A. N. Hughes, B. C. Hui and K. Wright, *Can. J. Chem.*, 1974, **52**, 2990-2999.
59. Y. F. Chen, C. Sui-Seng and D. Zargarian, *Angew. Chem., Int. Ed.*, 2005, **44**, 7721-7725.

CHAPTER 5

5 Catalytic Studies on Nickel(I) Complexes

5.1 Nickel Complexes as Catalysts

5.1.1 Nickel NHC Catalysts

As previously described, NHCs and their subclasses have proven to be excellent ligands for transition metals and now have a central role in nickel chemistry. A wide variety of Ni-NHC complexes have been synthesised, varying in oxidation state, stability, coordination number, degree and denticity of NHC binding and identity of additional spectator ligands. Several of these have been applied as homogeneous catalysts to a number of organic transformations, such as reductive coupling,[1] cycloadditions,[2] transfer hydrogenation[3] and C-H/C-C/C-F bond activations.[4] **Scheme 5.1** illustrates a generic nickel catalytic cycle which can, for example, be applied to cross-coupling reactions of aryl halides in Kumada or Suzuki reactions for C-C bond formation.

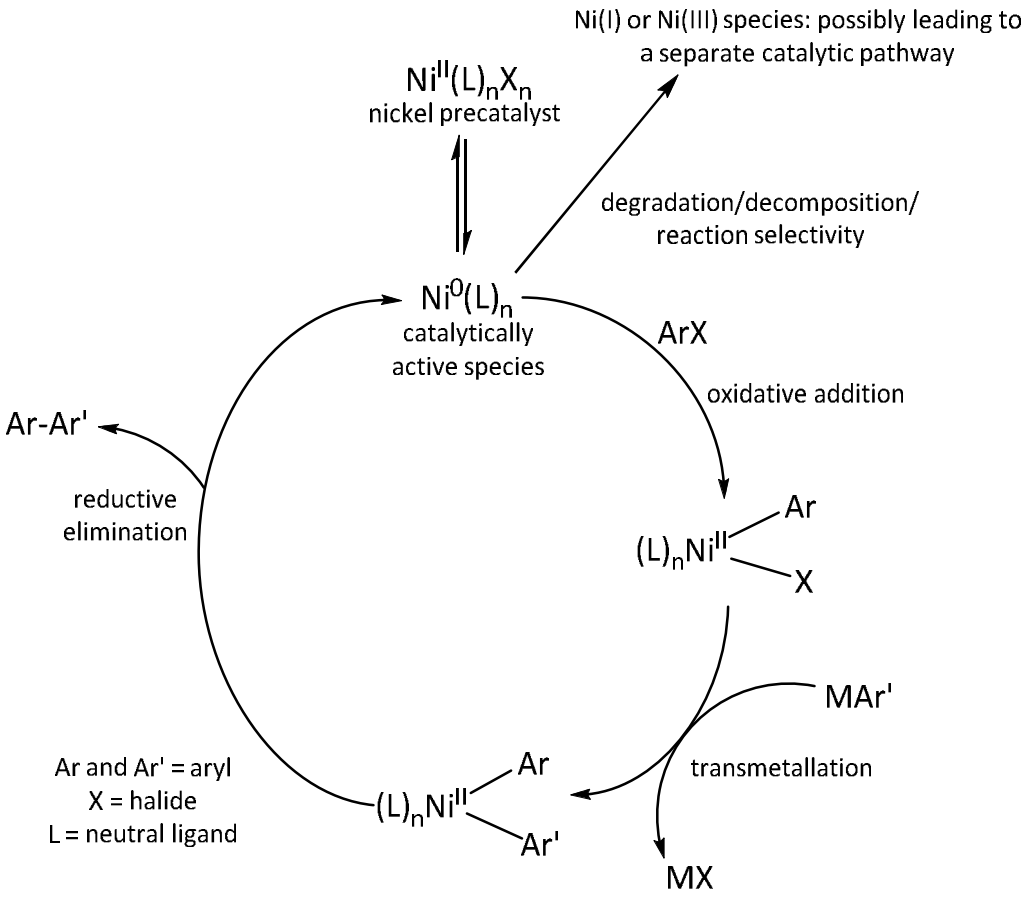

Scheme 5.1 Generalised nickel catalytic cycle for C-C coupling.

As expected for reactions which involve oxidative addition/reductive elimination processes, the oxidation state of the metal centre alters by two electrons during the sequence. In the simplest case for nickel, this involves a Ni(0)/Ni(II) couple. The Ni(II) precatalyst is often the only isolable species within the cycle, with the catalytically active Ni(0) species usually formed *in situ* and its identity frequently remaining unknown. Ni(II)-phosphine complexes, such as $Ni(PR_3)_2Br_2$, were initially used as precatalysts in Kumada coupling.[4] However, due to the improved activity of M-NHC catalysts and the success in using the fellow group 10 $Pd(NHC)_n$ complexes for this transformation,[5] Ni-NHC and mixed ligand Ni-NHC/PR_3 based systems have been investigated. In studies involving the use of $Ni(NHC)(PR_3)X$ (X = Br, Cl) for coupling reactions, the presence of an initial phosphine ligand or addition of free PPh_3 has been shown to improve catalytic activity compared to the corresponding Ni-*bis*(NHC) species.[6,7] One explanation of this could be that after completion of a catalytic cycle, the phosphine binds to the metal to reform a stabilised coordinatively saturated metal centre. The greater σ-donor properties of the NHC compared to the phosphine then facilitates the re-dissociation of this phosphine, forming the coordinatively unsaturated Ni(0) active species which allows the cycle to propagate once more.

In order for the catalytic cycle to proceed, any Ni(0) complex must be sufficiently stable to have a long enough lifetime to react rather than simply decompose. Five membered ring NHCs with sterically large N-substituents were the first bulky carbene ligands investigated as potential ligands to stabilise low coordinate Ni(0) species targeted for catalytic C-C bond formation.[4,8,9] In 2000, Hermann *et al.*[10] reported the first example of the cross-coupling of haloarenes to form substituted biaryl compounds using a $Ni^0(NHC)_2$ catalyst (NHC = IPr ***(xvi)***) **(Scheme 5.2)**. Complex ***xvi*** was formed *in situ* from a 1:1 mixture of $Ni^{II}(acac)_2$ and imidazolium salt, the synthesis of which is described in much greater detail in **Chapter 1, 1.3.2**.

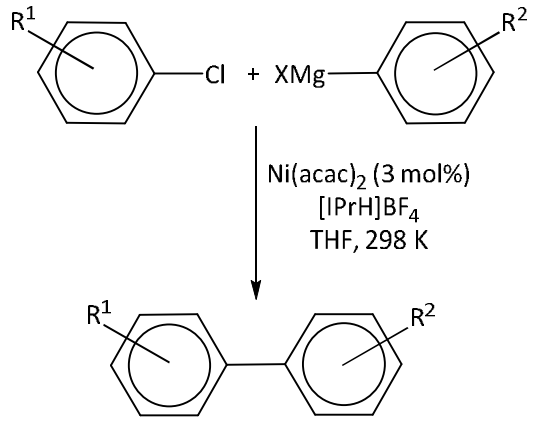

Scheme 5.2 Kumada cross-coupling of aryl halides by *in situ* generated $Ni^0(IPr)_2$ ***(xvi)***.

Despite the unexpected formation and isolation of a *bis*(NHC) nickel complex from 1:1 stoichiometry, further investigation into how ***xvi*** catalyses the reaction has only recently come to light.[11,12] A comprehensive overview of this is provided in **Chapter 1, 1.1.3**, but in summary, mono-oxidation of ArX takes place to give the T-shaped Ni(I) complex $Ni(IPr)_2X$ (***xvii*** when X = Cl). This work, as well as subsequent research into other nickel catalysed transformations,[3,13-22] suggests that reaction selectivity and/or degradation/decomposition of the assumed Ni(0) catalytically active species may alter the catalytic cycle from that in **Scheme 5.1** to an alternative Ni(I) initiated pathway.

An example of a two coordinate Ni(0) complex bearing CAAC (cyclic(alkyl)(amino)carbene) ligands was reported to be a moderate mediator for the catalytic homocoupling of various unactivated aryl halides.[23] Addition of 2 eq of free CAAC to $NiCl_2$ initially generated the Ni(II) complex $Ni(CAAC)_2Cl_2$, which upon reduction with LDA produced dark purple $Ni(CAAC)_2$ ***(liii*; Scheme 5.3)**. LDA, rather than more commonly employed reducing agents such as $KN(SiMe_3)_2$, is needed as dehalogenation of $Ni^{II}(CAAC)_2Cl_2$ occurs through an α-hydride transfer from LDA to Ni(II) (*via* elimination of LiCl) to form a *bis*(CAAC) Ni(II)-chlorohydride intermediate, which then reductively eliminates HCl en-route to ***liii***. The HCl is consumed by a second equivalent of LDA to generate HN^iPr_2 and LiCl, with the formation of HN^iPr_2 and $Me_2C{=}N^iPr$ confirmed by mass spectrometry.

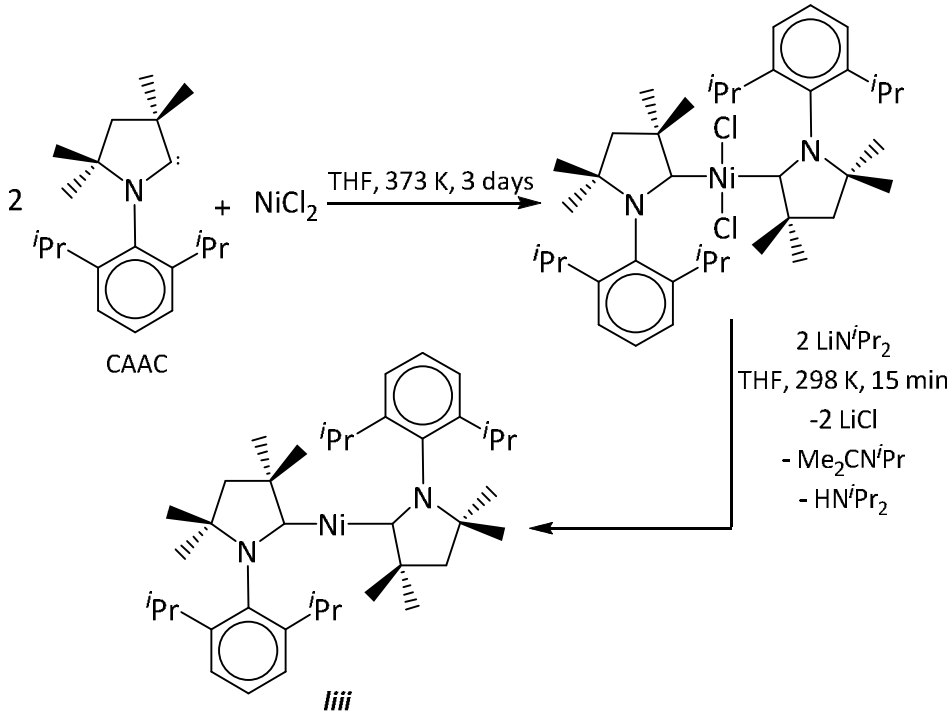

Scheme 5.3 Synthesis of the zero-valent $Ni(CAAC)_2$ ***liii*** *via* formation and subsequent reduction of a Ni(II)-CAAC species.

Complex ***liii*** was subsequently employed as a precursor in the catalytic formation of biaryls *via* the homocoupling of aryl halides in the presence of a reducing agent **(Scheme 5.4)**. After extensive optimisation, mild reaction conditions of 10 mol% catalyst for 4 – 6 hr at 323 K were employed, in which ***liii*** successfully produced the desired biaryl products in good yields, even upon using ArCl and ArF substrates **(Table 5.1)**.[23]

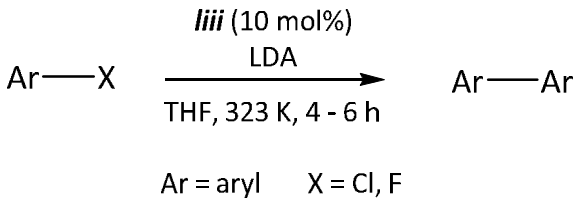

Scheme 5.4 Catalytic homocoupling of haloarenes mediated by ***liii***.

Entry	Aryl Halide	Product	Yield / %
1	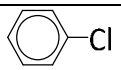	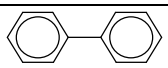	78
2	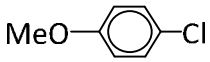	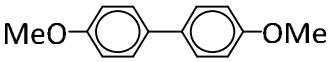	91
3	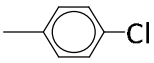	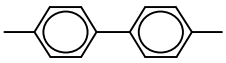	84
4	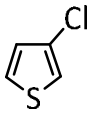	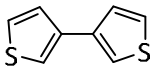	85
5	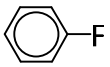	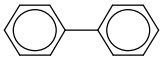	55
6	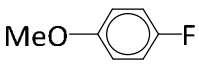	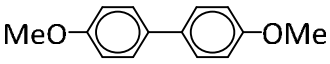	62

Table 5.1 Isolated yields (%) of homocoupled products from various aryl chlorides and fluorides catalytically mediated by ***liii***.

A possible mechanism for this catalytic process is shown in **Scheme 5.5** and builds upon that given in **Scheme 5.1**, cycling through a Ni(I)/Ni(III) couple accessed from zero-valent ***liii***. As commonly observed in coupling reactions, the first step (**A**) consists of activation of the Ar-X bond *via* oxidative addition across the nickel centre in ***liii***. The second step (**B**) then comprises a dehalogenation by LDA to give a three coordinate Ni(I) species ($Ni(CAAC)_2Ar$) that is experimentally supported by the previous synthesis and characterisation of $Ni(IMes)_2Cl$ **(*xxii*)**

and Ni(IMes)$_2$Ar[12] **(Chapter 1, 1.1.3)**. For Ar homocoupling to ensue, two aryl groups must be in close proximity to each other, therefore a second Ar-X oxidative addition is proposed (**C**) to give a five coordinate Ni(III) intermediate. Product formation (Ar-Ar) then takes place *via* reductive elimination (**D**), allowing the zero-valent Ni(CAAC)$_2$ to be ultimately regenerated upon reductive dehalogenation from the newly formed three coordinate Ni^{I}(CAAC)$_2$X species (**E**), thus completing the cycle.

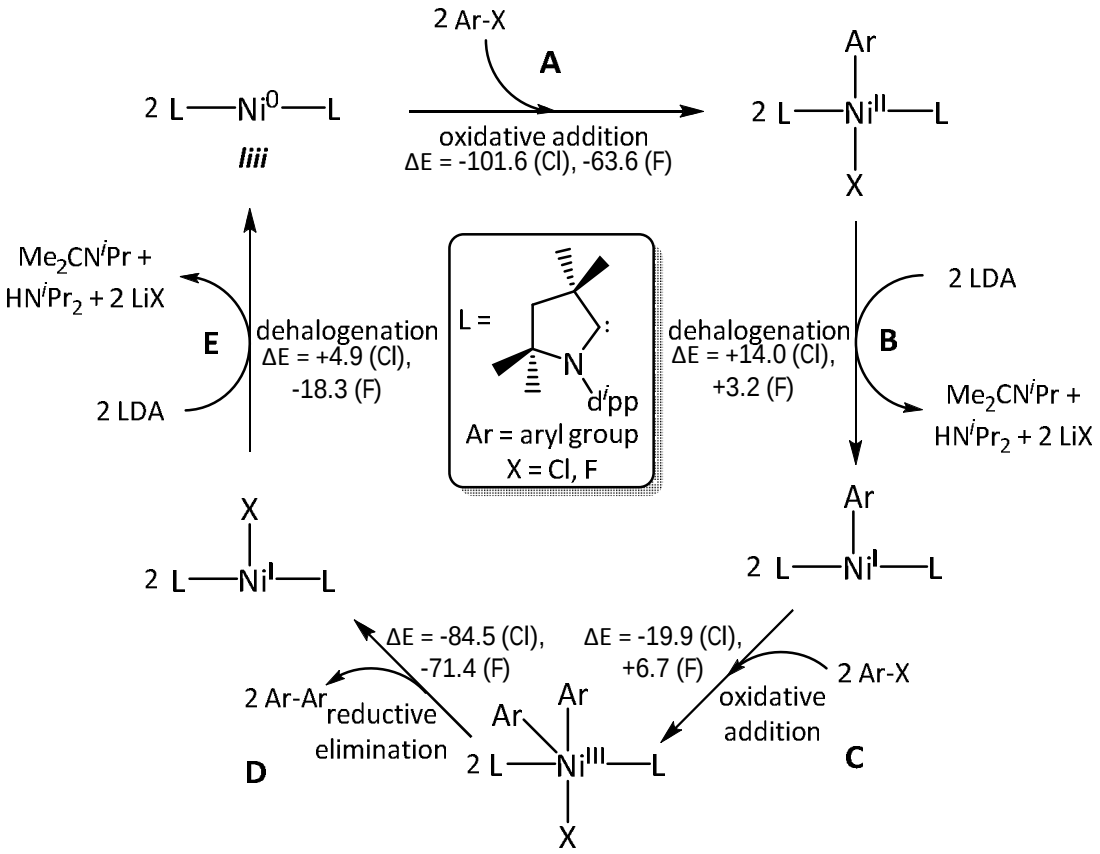

Scheme 5.5 Proposed mechanism for aryl homocoupling catalysed by Ni(CAAC)$_2$ ***(liii)*** accompanied by the calculated energy barriers for each step (kcal mol^{-1}).

DFT calculated energy barriers for these steps (using PhX as the model substrate) confirmed the likelihood of this mechanism, as well as ruling out other possible routes.[23] For example, a second oxidative addition process to form a six coordinate Ni(IV) species (Ni(CAAC)$_2$(Ar)$_2$X$_2$) could be possible instead of the first dehalogenation step (**B**). This would eliminate Ni(I) from playing a central role in the catalytic cycle. However, the barrier for hexacoordinate formation is calculated to be highly endothermic (ΔE = +50.5 kcal mol^{-1} (X = Cl), +44.7 kcal mol^{-1} (X = F)), compared to the marginal energy required for the formation of the three coordinate species Ni^{I}(CAAC)$_2$Ar (ΔE = +14.0 kcal mol^{-1} (Cl), +3.2 kcal mol^{-1} (F)). The strong Li-F bond formed during the dehalogenation with LDA accounts for the small barrier of only *ca.* +3 kcal mol^{-1}.

The overall catalytic reaction in **Scheme 5.5** is energetically favourable for both PhCl and PhF, with the overall highly exothermic nature of the reaction supporting the high yields obtained during the homocoupling and the high reactivity of the CAAC as a ligand.[23]

5.1.2 Nickel(I) Complexes as Catalysts

Due to their inherent lack of stability, evidence for Ni(I) species as either initiators or intermediates in catalytic processes is limited. However, some theoretical and experimental research has come to light in recent years.[3,13,15,23,24] One example involves the use of a *bis*(trop) (trop = tropylidenylamine) Ni(I) species ***(liv)*** in the dehydrogenation of amine boranes.[3] **Scheme 5.6** illustrates the synthesis of ***liv*** from reaction of Ni(II)-difluoroacetate and $NH(trop)_2$ in the presence of zinc powder, and its subsequent reduction to a zero-valent species ***(lv)*** upon reaction with Zn in the presence of PPh_3. In each case, the $Ni(NH(trop)_2)$ moiety adopts the same coordination (one Ni-N σ-bond and two Ni-diene interactions), with the ancillary ligand completing the overall geometry observed.

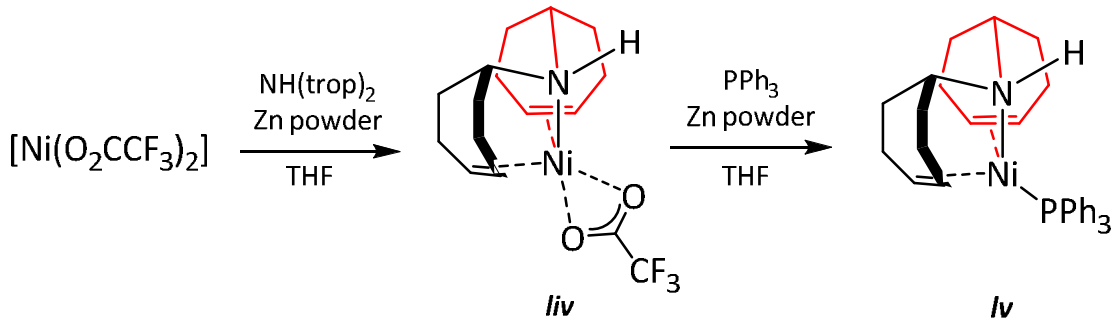

Scheme 5.6 Synthesis of $Ni^{I}(NH(trop)_2)(O_2CCF_3)$ ***(liv)*** and reduction to $Ni^{0}(NH(trop)_2)(PPh_3)$ ***(lv)***.

Due to the high activity observed with other nickel complexes (*i.e.* Ni(0)-NHC species) in the dehydrogenation of amine boranes,[25] ***liv*** and ***lv*** were investigated as precursors for the catalytic dehydrogenation of Me_2HNBH_3 **(Scheme 5.7)**. Under inert conditions and with $K[Me_2NBH_3]$ as a cocatalyst, 0.3 – 1.0 mol% ***liv*** or 1.0 mol% ***lv*** was reacted with a solution of Me_2HNBH_3 and the resulting dehydrogenated borane compound identified *via* ^{11}B NMR spectroscopy. Even at low catalytic loadings, ***liv*** displayed significantly greater activity than ***lv***, releasing equimolar equivalents of hydrogen gas in *ca.* 85 s (to give the borane dimer almost quantitatively and traces of $Me_2N{=}BH_2$ monomer). Complex ***lv*** generated the kinetically controlled linear borane species **(Scheme 5.7)**, liberating only 0.5 eq of H_2 in > 300 s. Addition of PPh_3 shut the whole reaction down. The rate of hydrogen evolution was much greater with

liv, demonstrating the fastest dehydrogenation rate of Me_2NHBH_3 catalysed by a non-noble metal complex at the time of the report.

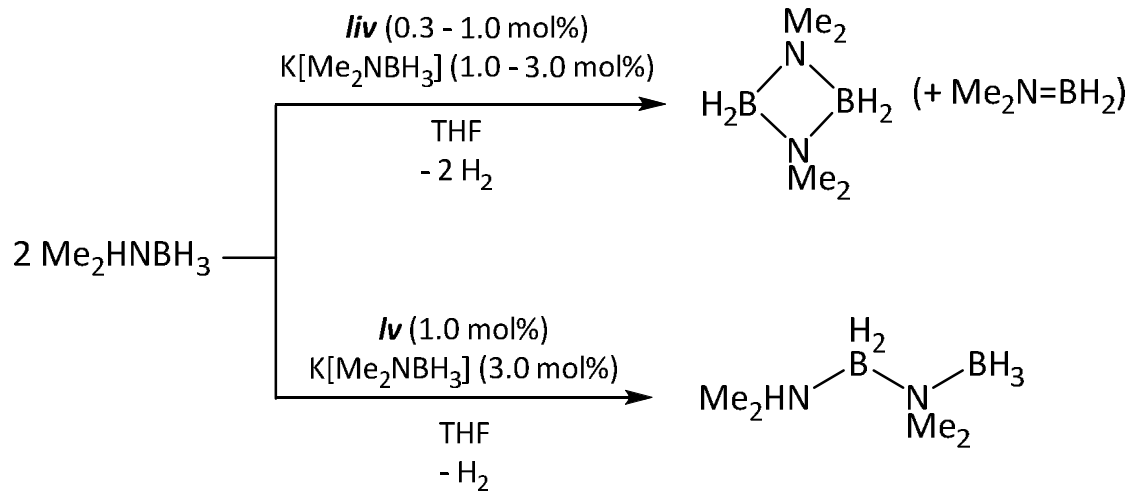

Scheme 5.7 Dehydrogenation of Me_2HNBH_3 catalysed by Ni(I) ***(liv)*** and Ni(0) ***(lv)*** with cocatalyst $K[Me_2NBH_3]$.

The catalytic mechanism for dehydrogenation with ***liv*** is thought to proceed *via* a radical pathway. However, some stoichiometric reactions of ***liv*** with the $K[Me_2NBH_3]$ cocatalyst in the presence of ***lv*** have hinted at formation of nickel hydride species $K[Ni(NH(trop)_2)(H)]$ and $K[(Ni(NH(trop)_2))_2(\mu\text{-}H)]$, which were also shown to catalyse comparatively fast hydrogen release from Me_2HNBH_3. Thus, ***lv*** cannot be completely excluded from any potential catalytic cycle.[3] Despite this, the excellent catalytic activity observed by monovalent ***liv*** alludes to the potential further applications of this and other functionalised Ni(I) complexes to a whole host of catalytic transformations.

5.1.2.1 Cross-coupling reactions

Cross-coupling reactions of an organic halide and organometallic reagent is a primary way to form C-C bonds and therefore one of the most fundamental and important reactions within organic synthesis. Previous research has shown that group 10 metal complexes[6,7,10,11,26-41] frequently display superior activity towards catalysing this versatile and diverse reaction, commonly *via* the catalytic cycle shown in **Scheme 5.1**. Zero- and divalent nickel complexes have therefore been extensively researched in C-C bond forming reactions.[6,7,10,32,37,38,42,43] In 1980, Kochi *et al.*[42,43] investigated the oxidative addition of aryl halides to $Ni(PEt)_4$ in great detail, ultimately concluding that this occurs in a facile manner for Ni(0) complexes, with a charge transfer process often being the rate limiting step. It was proposed **(Scheme 5.8)** that during oxidative addition, a one electron transfer from Ni(0) to the aryl halide occurs, affording

a Ni(I)-aryl-halide radical anion which subsequently converts to either the Ni(I)-halide (as in the formation of ***xvii*** **(Chapter 1, 1.1.3)**) or Ni(II)-aryl-halide (depicted in **Scheme 5.1**).

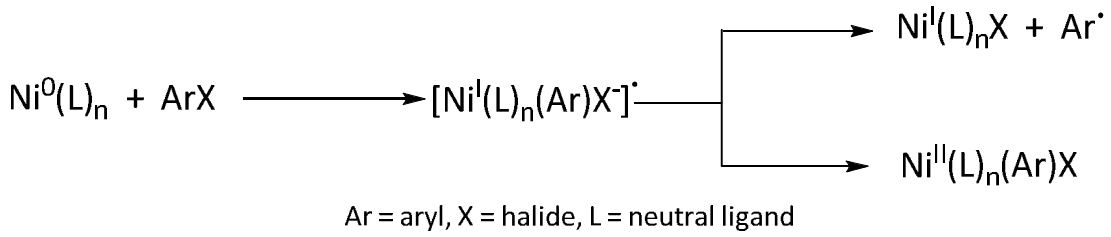

Scheme 5.8 Oxidation of $Ni^0(L)_n$ with aryl halides.

Ni(I)-alkyl mediated catalytic cross-coupling of alkyl electrophiles was reported by Vicic and coworkers[13] and alluded to the possibility of a radical mechanism for the process, similar to that proposed by Kochi. Formation of monovalent Ni(tpy)(CH_3) ***(lvi)*** was achieved *via* reaction of Ni(tmeda)(CH_3)$_2$ and terpyridine (tpy) **(Scheme 5.9)**, with cyclic voltammetry and magnetic susceptibility measurements confirming the presence of a single unpaired *d* electron (μ_{eff} = 1.64 μB using the Evans method). It was presumed that the formation of ***lvi*** arose through tpy displacing tmeda to form a five coordinate Ni(II)-dimethyl species, followed by Ni-C bond homolysis to simultaneously generate a methyl radical. 0.5 eq of ethane can then be produced from combination of two methyl radicals. The fact that the proposed dimethyl intermediate failed to reductively eliminate a full equivalent of ethane upon addition of tpy suggests that Ni(II)-dialkyl intermediates may play a part in radical catalytic cross-coupling of saturated alkyl electrophiles. To probe this, ***lvi*** was applied to a number of stoichiometric and catalytic reactions involving alkyl halide substrates.

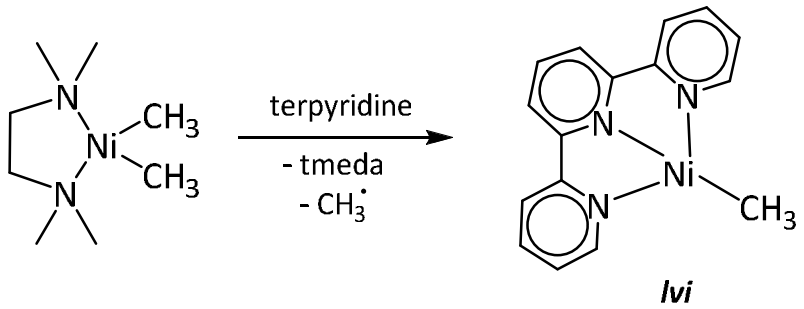

lvi

Scheme 5.9 Synthesis of the tpy stabilised Ni(I)-methyl complex ***lvi***.

NMR monitoring of the reaction of ***lvi*** with 1 eq of iodocyclohexane over 24 h at room temperature in C_6D_6 showed that transfer of the nickel bound methyl group took place to give methylcyclohexane in 79 % yield. Analysis of the volatiles indicated that this was the major product of the reaction, with no significant levels of alkenes resulting from β-hydride

elimination formed. This is a side reaction commonly observed in alkyl-alkyl cross-coupling processes. Elemental analysis of the organometallic component of the reaction was consistent with formation of Ni(tpy)I. No disproportionation products were identified during alkyl transfer, implying the inclusion of a Ni(I) species in the process.

Table 5.2 displays the results from employing ***Ivi*** in catalytic quantities (5 mol%) towards various alkyl halides in the presence of *n*-pentylzinc bromide **(Scheme 5.10)**. The results show that moderate yields of alkane can be achieved without vast levels of competing β-hydride elimination. Of most note is the superior efficiency of cross-coupling utilising alkyl iodides rather than bromides. Greater yields of a bulkier tertiary carbon (sp^3) containing cross-coupled product were achieved upon turning to secondary alkyl iodides such as iodocyclohexane (entry 4).

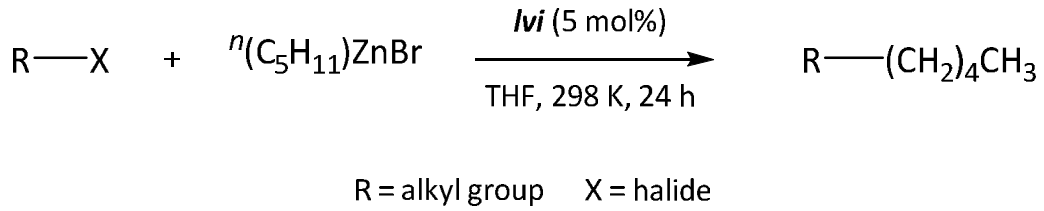

Scheme 5.10 Alkyl cross-coupling reactions catalysed by ***Ivi***.

Entry	Alkyl Halide	Product	Yield / %
1	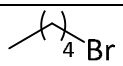	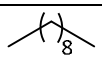	15
2	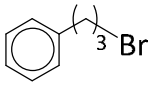	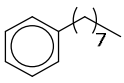	13
3	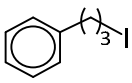	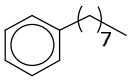	60
4	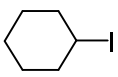	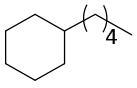	64

Table 5.2 Yield (%) of cross-coupled products from the reaction of alkyl halides with *n*-pentylzinc bromide catalysed by ***Ivi***.

$Ph(CH_2)_6Ph$ and dicyclohexyl were detected as minor products upon analysis of entries 3 and 4 respectively. Additionally, when ***Ivi*** was reacted with the radical clock iodomethylcyclopropane, substantial amounts of alkene products were identified by ^1H NMR spectroscopy. The detection of all these species, along with the fact that i) both the Ni(II)-alkyl-halide and -dialkyl complexes were unstable with respect to their Ni(I) decomposition products, ii) DFT calculations indicated the lone electron was delocalised around the tpy ligand system[39] **(Chapter 1, 1.1.3)** and iii) ***Ivi*** acts as a precursor for catalytic alkyl cross-coupling, it was proposed that a radical mechanism ensued under catalytic conditions **(Scheme 5.11)**. Chemical support for this was obtained from stoichiometric reactions carried out on ***Ivi***, which showed that it was thermodynamically capable of reducing alkyl iodides in THF. This is perhaps unsurprising given that its reduction potential is close to that of SmI_2, a renowned alkyl iodide reduction catalyst.[44] The isolation of Ni(tpy)I upon completion of stoichiometric cross-coupling confirms that continuation of the catalytic cycle can ensue. The presence of an alkylzinc halide reagent leads to transmetallation with Ni(tpy)I, affording a new monovalent Ni(tpy)R complex which can initiate further cross-coupling **(Scheme 5.11)**.[13]

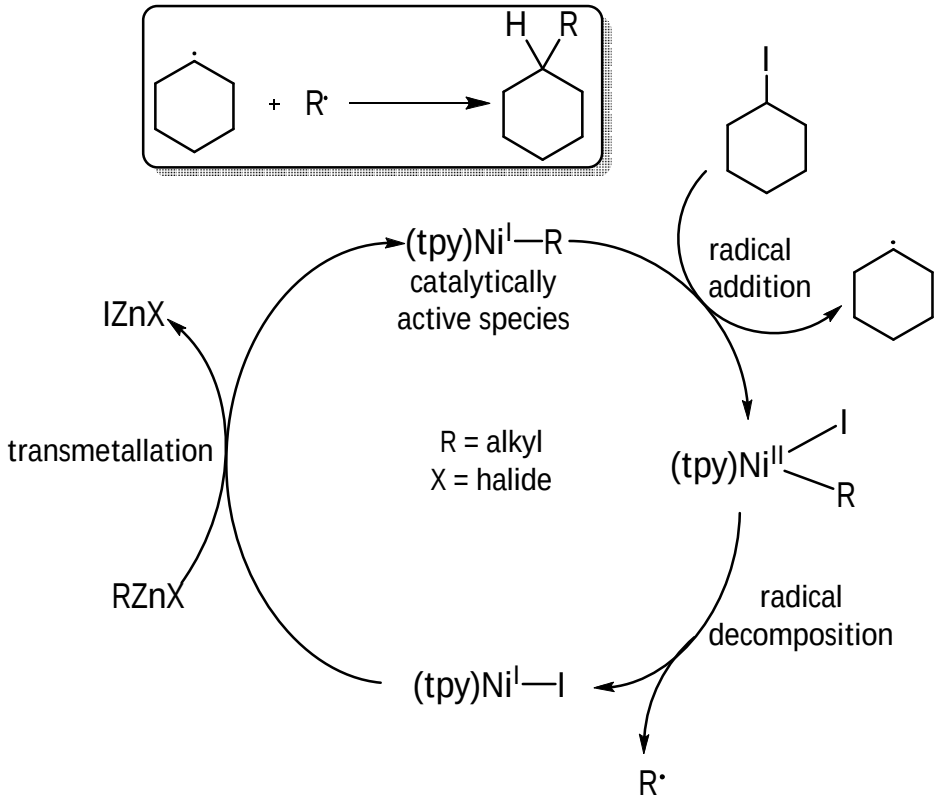

Scheme 5.11 Possible radical mechanism for the cross-coupling of alkyl electrophiles mediated by Ni^{I}(tpy)R, such as ***Ivi***.

With the number of reports into the involvement of Ni(I) species within catalytic cycles increasing, it raises the question of how prevalent Ni(III) systems are and whether they exist in catalytic processes alongside Ni(I) affording Ni(I)/Ni(III) catalytic couples.[14,20-22] Evidence for Ni(III) complexes in the form of $Ni(CAAC)_2(Ar)_2X$ have already been discussed in section **5.1.1**. Further support for their inclusion arises from a recent publication by Mirica and coworkers,[14] who reported the synthesis of Ni(III)-aryl-halide complexes stabilised by the tetradentate ligand $^{t\text{Bu}}$N4, as shown in **Scheme 5.12**. In the presence of $^{t\text{Bu}}$N4, *p*-F-C_6H_4X (X = Br, Cl) was reacted with $Ni(COD)_2$, resulting in oxidative addition to form the Ni(II) complexes $Ni(^{t\text{Bu}}N4)(C_6H_4F)X$. These underwent facile oxidation with 1 eq of ferrocenium to yield the Ni(III) derivatives $[Ni(^{t\text{Bu}}N4)(C_6H_4F)X]^+$ (***lvii*** (X = Br) and ***lviii*** (X = Cl); **Scheme 5.12**). As expected, these were paramagnetic, with the effective magnetic moments (μ_{eff} = 2.11 – 2.03 μB for X = Br and Cl at 253 K) and EPR spectra suggestive of a single unpaired electron present in distorted octahedral d^7 Ni(III) metal centres.

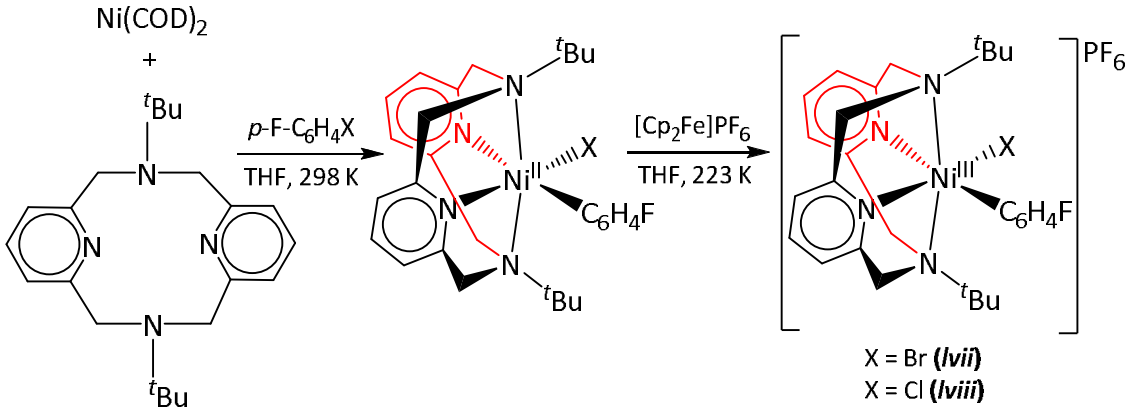

Scheme 5.12 Synthesis of a Ni(II) and Ni(III) complex stabilised by the $^{t\text{Bu}}$N4 ligand.

The room temperature instability of ***lvii*** and ***lviii*** suggested the likelihood of elimination type reactions. Stoichiometric studies revealed they were stable at 223 K, but underwent rapid reductive elimination of a C-halogen bond at 298 K, generating the corresponding *p*-fluorophenyl halide.[14] Thus, MeCN solutions of ***lvii*** (X = Br) gave 54 % *p*-F-C_6H_4Br upon warming the complex from 223 to 298 K **(Scheme 5.13A)**. Further support for the possibility of this Ni(III) species acting as an intermediate in catalytic reactions arose upon attempts to promote transmetallation. Addition of MeMgI to a THF solution of ***lvii*** at 223 K gave *p*-F-C_6H_4Me in 48 % yield upon warming to 298 K, presumably *via* reductive elimination from a newly generated Ni(III)-alkyl species **(*lix*; Scheme 5.13B)**. The formation of ***lix*** was confirmed by direct transmetallation of the Ni(II) complex $Ni(^{t\text{Bu}}N4)(C_6H_4F)Br$ with MeMgCl, followed by oxidation using ferrocenium.

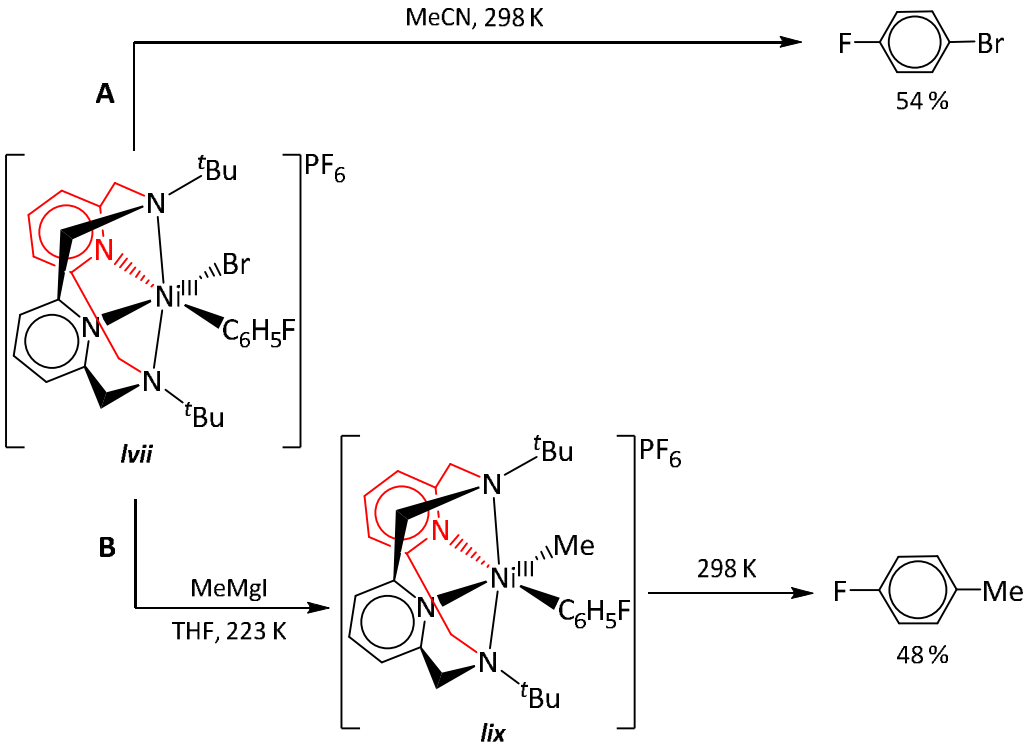

Scheme 5.13 Reductive elimination (**A**) and transmetallation (**B**) reactions with ***lvii***.

Complex ***lvii*** was also found to be active towards the complete cycle of Kumada and Negishi cross-couplings and not just the isolated events of transmetallation and reductive elimination. Thus, 5 mol% ***lvii*** gave an isolated yield of 70 % *p*-Me-biphenyl from coupling of *p*-iodotoluene and PhMgBr. In addition, formation of THF solvent adducts with the Ni(II) organometallic reagent were detected, alluding to a radical mechanism taking place.

In 2014, Tilley and coworkers[22] set about trying to rigorously define the involvement of Ni(III) species in operative catalytic cycles through use of the isolable *bis*(amido) Ni(III)-methyl complex Ni(N(SiMe$_3$)(d^{i}pp))$_2$(CH$_3$) **(*lx*; Scheme 5.14)**. Species ***lx*** was initially investigated as a catalyst towards cross-coupling, however stoichiometric reactions of ***lx*** with equimolar quantities of PhI or C$_{12}$H$_{25}$I did not lead to any reaction before ***lx*** decomposed to ethane and Ni^{II}(N(SiMe$_3$)(d^{i}pp))$_2$ **(*lxi*)** over 24 h. Previous literature by Hu and coworkers[45] had reported that Ni(II)-alkyl complexes activated alkyl halide coupling, hence reduction of complex ***lx*** with KC$_8$ was attempted and successfully generated K[Ni(N(SiMe$_3$)(d^{i}pp))$_2$(CH$_3$)] **(*lxii*; Scheme 5.14)** in 64 % yield at 243 K. Similarly to ***lx***, ***lxii*** was thermally unstable and decomposed in C$_6$D$_6$ over a period of 7 days to give the anionic Ni(I) complex K[Ni(N(SiMe$_3$)(d^{i}pp))$_2$] **(*lxiii*)** *via* elimination of ethane through reductive homolysis.

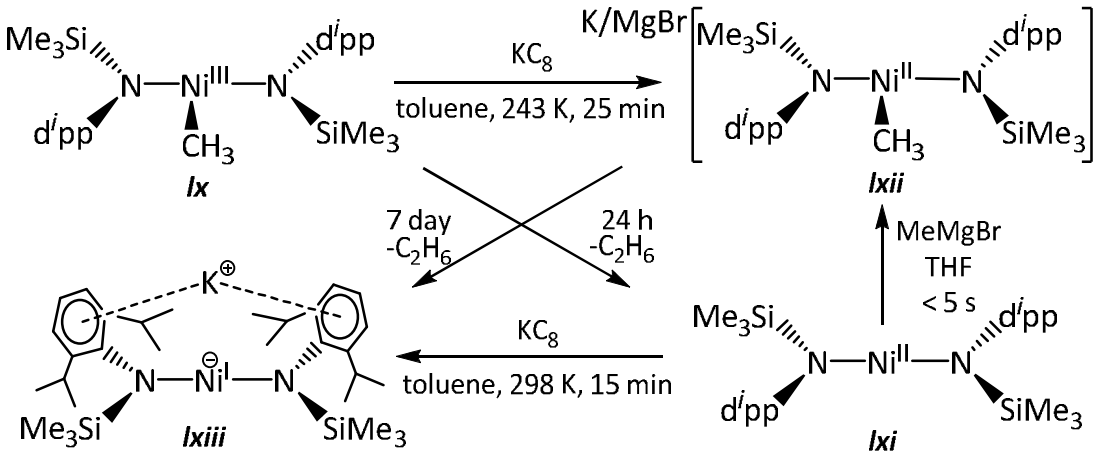

Scheme 5.14 Reactions involving Ni(III)- **(*lx*)**, Ni(II)- (***lxi*** and ***lxii***) and Ni(I)- **(*lxiii*)** *bis*(amido) complexes.

The accessibility of analogous Ni(I)-, Ni(II)- and Ni(III)-alkyl amide complexes and the possible inclusion of these as intermediates in catalytic cross-coupling reactions, led to the investigation of ***lxi*** as a catalyst for cross-coupling with alkyl or aryl halides with Grignard reagents. In the presence of 5 mol% ***lxi***, a range of electron-poor and electron-rich aryl chlorides, bromides and iodides were coupled with both aryl and alkyl Grignard reagents at room temperature in Et_2O. **Table 5.3** summarises the yields obtained with PhMgBr, which shows that on the whole, electron-poor substrates are preferred over electron-rich ones (*e.g.* entry 4 *vs.* 6) and that the more challenging aryl chloride substrates were coupled in good yields, along with aryl bromides and iodides. Pyridine containing substrates were also tolerated, despite concerns they may coordinate to ***lxi*** and hamper any catalysis (entries 4, 8 and 9). Attempts to couple alkyl halides (entries 10 and 11) were unsuccessful, resulting in only trace levels of cross-coupled products.

Analysis of post-catalytic reaction mixture from MeMgBr with PhI revealed the major organonickel product to be ***lxii*** as the $[MgBr]^+$ salt. A small amount of ***lxiii*** was detected, presumably from thermal decomposition of ***lxii***. The relatively large proportion of nickel complexes left after the termination of the catalysis indicates that these species may be directly involved in the catalytic cycle.

Entry	Alkyl Halide	Product	Time / h	Yield / % [a]
1		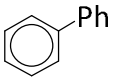	0.5	98
2	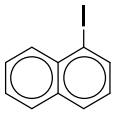	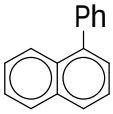	0.5	100
3	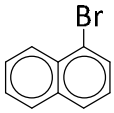	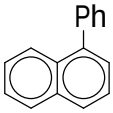	1.0	68
4	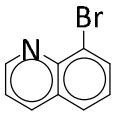	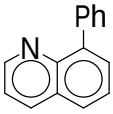	1.5	93
5	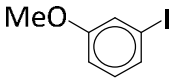	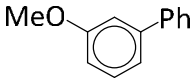	1.5	99
6	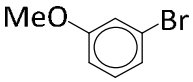	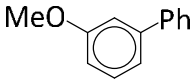	5.5	< 10
7	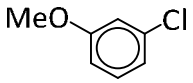	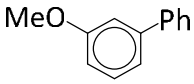	66.0	< 10
8	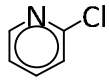	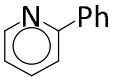	2.0	78
9	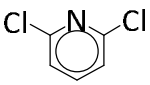	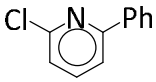	6.0	92
10		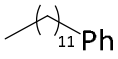	0.75	< 1
11	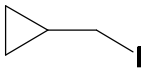	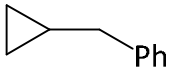	0.7	0

Table 5.3 Product yields (%) of cross-coupling aryl and alkyl halides to PhMgBr with 5 mol% ***lxi*** in Et_2O. [a] Yields determined by GC.

Stoichiometric reactions involving ***lx – lxiii*** were undertaken and supported the proposed catalytic mechanism shown in **Scheme 5.15**. The first step (**A**) involves addition of a Grignard reagent to neutral ***lxi*** to form the anionic Ni(II) complex **(*lxii'*)** analogous to ***lxii***. Addition of 1.1 eq of MeMgBr to ***lxi*** in THF at 243 K confirmed the likelihood of this step by generating diamagnetic ***lxii*** in nearly quantitative yields (> 98 %). This is believed to be the resting state of the catalytic cycle and proceeds well within the time frame for the catalysis. Anionic ***lxii'*** then reduces the organic halide to form the Ni(III)-alkyl or –aryl species **(*lx'*)** and an organic radical, as demonstrated in step **B**. To validate this process, equimolar quantities of ***lxii*** with

1-iodonaphthalene were reacted to form the cross-coupled product 1-methylnaphthalene, although this was over a long period of 45 min and in a low 13 % yield. The Ni(III)-methyl complex ***lx*** was also detected (confirming the occurrence of ***lx'*** in the proposed catalytic cycle), along with 1,1'-binaphthalene by-product and unreacted 1-iodonaphthalene in 64 % and 23 % yields respectively. Optimisation studies on this reaction revealed 2 eq of ***lxii*** were necessary to produce 1-methylnaphthalene (98 % yield within 5 min). Complex ***lxii*** was the only species capable of effectively trapping the organic radical fragment, with an equivalent of ***lx*** providing no enhanced yields of 1-methylnaphthalene (10 %). To confirm the formation of a radical, cross-coupling studies involving the radical clock iodomethylcyclopropane and 1.1 eq PhMgBr in the presence of 5 mol% ***lxi*** (**Table 5.3**, entry 11) were carried out and resulted in the formation of 4-phenyl-1-butene from rearrangement of the (cyclopropyl)methyl radical. No unrearranged products or any cross-coupled products in the absence of ***lxi*** were observed. This is indicative of a radical intermediate forming upon reduction of the alkyl halide, corroborating the proposed step **B**. However, the exact nature of the organic radical is undefined and assumed to not be 'free'.

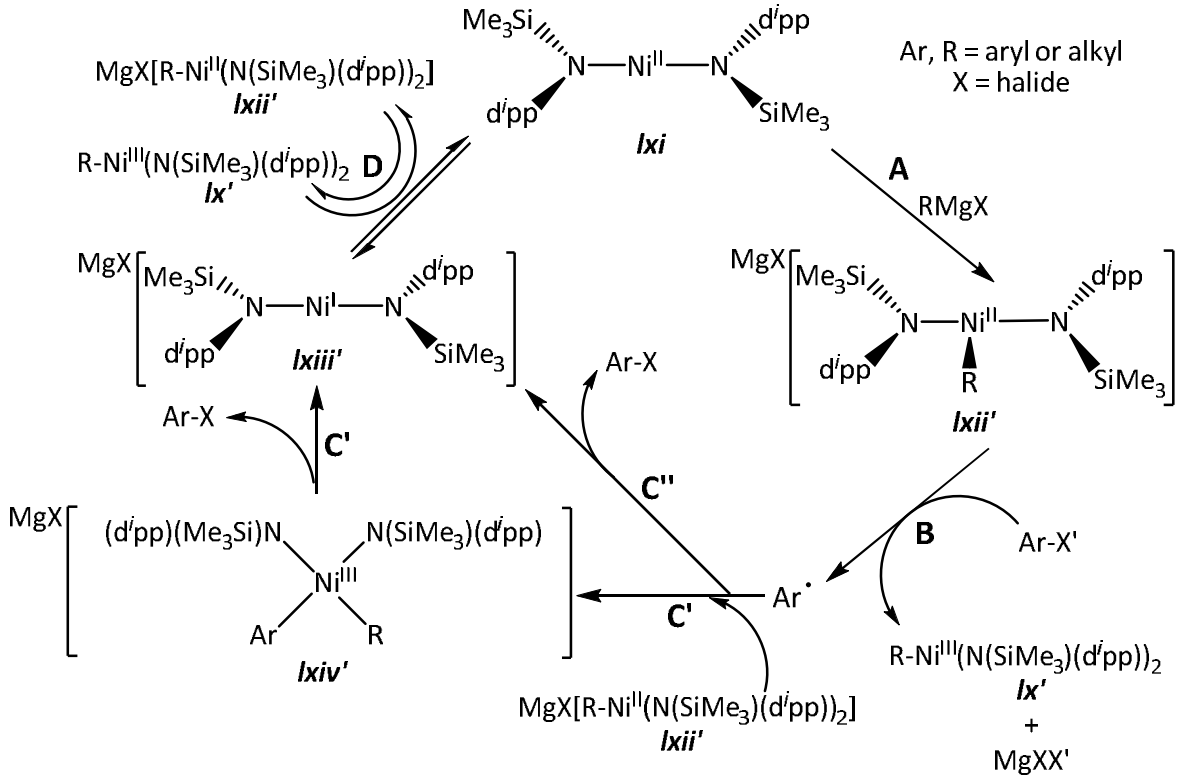

Scheme 5.15 Proposed mechanism for the catalytic coupling of Grignard reagents with aryl or alkyl halides by ***lxi***. Complex ***lxiv'*** is the only species not directly observed.

The reaction pathway of the organic radical with anionic Ni(II) **(*lxii'*)** is the most speculative part of the reaction mechanism. The step may proceed through attack of the radical species to the nickel centre in ***lxii'*** generating an unobserved Ni(III) anionic complex ***lxiv'*** (step **C'**). The coupled product is then formed from reductive elimination. Alternatively, the radical may directly attack the R ligand on ***lxii'*** to give ***lxiii'*** and the coupled ArX product (step **C''**). The pathway including ***lxiv'*** is favoured due to spectroscopic observation of similar intermediates[46] and known reductive elimination from Ni(III)-alkyl species described by Mirica[14] (*vide supra*) and other researchers.[47]

The final step in the catalytic process (step **D**) comprises the Ni(I) anion ***lxiii'*** reducing the Ni(III) ***lx'*** generated in step **B** to reform 1 eq of ***lxii'*** and ***lxi***, hence completing the cycle. This reduction was confirmed by reaction of equimolar amounts of ***lx*** and ***lxiii*** (as the $[N^nBu_4]^+$ salt) in THF which led to the isolation of $[N^nBu_4]$[***lxii***] in 29 % yield. The redox potentials of ***lx*** (-1.30 V *vs.* Fc/Fc^+) and ***lxi*** (-1.28 V *vs.* Fc/Fc^+) suggest this process is in equilibrium, confirmed from detection of all four species (***lx***, ***lxi***, ***lxii*** and ***lxiii***) during the stoichiometric reaction. The highly paramagnetic nature of ***lx***, ***lxi*** and ***lxiii*** and resulting extreme broadness of ^1H NMR signals prevented accurate measurement of the equilibrium constant.

This isolation and complete characterisation of Ni(I) and Ni(III) complexes observably involved in cross-coupling transformations, along with the stoichiometric and catalytic reactions carried out by Mirica and Tilley, heavily support their inclusion in redox catalytic mechanisms and hence the importance of paramagnetic species in other such processes.

5.1.2.2 Nickel(I) NHC complexes as Kumada cross-coupling catalysts

The findings of Kochi[42,43] and Vicic[13] along with i) other research postulating Ni(I) and Ni(III)[14,22,31,47] species as possible alternative intermediates in cross-coupling reactions and ii) the benefits of using NHCs as organometallic ligands, has significantly increased the interest in Ni(I)-NHC complexes as potential catalysts. $Ni^I(IPr)_2Cl$ **(*xvii*)** (1 mol%) was investigated as a precatalyst towards the Kumada coupling of *p*-bromobiphenyl and *p*-bromoanisole with PhMgCl in the presence of 5 eq of IPr, giving *p*-terphenyl and *p*-methoxybiphenyl in yields of 89 % and 93 % respectively.[11] Similar conversions were also found when $Ni(IPr)_2Cl_2$ **(*xviii*)** was employed, indicating that ***xvii*** may be an intermediate in the cycle catalytically mediated by ***xviii***. This was the first example of a Ni(I)-NHC species demonstrating catalytic activity for the cross-coupling of aryl halides.

In **Chapter 1, 1.1.3**, the synthesis of *bis*(NHC) Ni(I) complexes of formulation $Ni(IMes)_2X$ (X = Br ***(xxi)***, Cl ***(xxii)***) was detailed. Louie *et al.* subsequently compared ***xxi*** and ***xxii*** with the Ni(0) precursor $Ni(IMes)_2$ ***(xx)*** and square planar $Ni^{II}(IMes)_2X_2$ (X = Br ***(lxv)***, Cl) as precatalysts for Suzuki reactions.[12] Both electron-rich (*p*-MeO-C_6H_4Br) and electron-poor (*p*-CF_3-C_6H_4Br) substrates coupled with $PhB(OH)_2$ at 353 K using 10 mol% ***xx***, ***xxi***, ***xxii*** and ***lxv*** **(Scheme 5.16)** to give biaryl products in good and comparable yields (64 – 75 %) **(Table 5.4)** regardless of the oxidation state of the nickel, although the Ni(I) bromide complex ***(xxi)*** proved superior to the chloride analogue ***(xxii)***. In contrast to previous findings,[38,48,49] higher yields were obtained with *p*-MeO-C_6H_4F compared to the electron-poor *p*-CF_3-C_6H_4Br substrate.

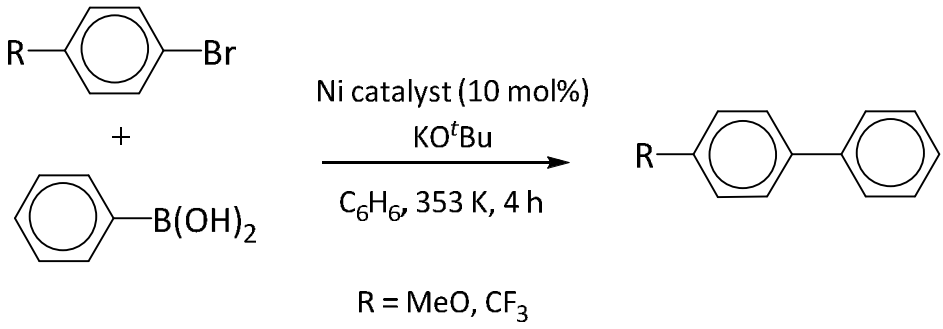

Scheme 5.16 Suzuki cross-coupling reactions catalysed by either Ni(0) ***(xx)***, Ni(I) (***xxi*** and ***xxii***) or Ni(II) ***(lxv)*** species.

All of the nickel complexes also displayed similar catalytic activity in Kumada coupling reactions, with biaryl cross-coupled products generated in reasonable yields of 73 – 79 % **(Table 5.4)**. Chlorobenzene was coupled to MesMgBr in THF with 3 mol% nickel at room temperature for 20 h. A brief study into the rate of reaction also suggested no marked difference between the nickel complexes. When repeated in C_6H_6, the yields obtained were lower, which appears to be due to the reduced solubility of the catalysts.

Suzuki Coupling With $PhB(OH)_2$			Kumada Coupling of PhCl and MesMgBr		
Catalyst	**Aryl Halide**	**Yield / %**	**Catalyst**	**Solvent**	**Yield / %**
xx	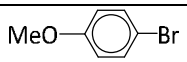	72	***xx***	THF	73
xxi	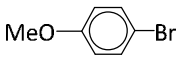	75	***xxi***	THF	73
xxii	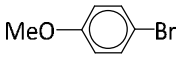	64	***xxii***	THF	77
lxv	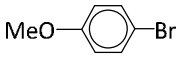	74	***lxv***	THF	79
xx	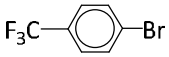	59	***xx***	C_6H_6	54
xxi	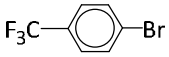	66	***xxi***	C_6H_6	64
lxv	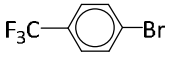	52	***lxv***	C_6H_6	25

Table 5.4 Isolated yields (%) for Suzuki cross-coupling (left) and Kumada cross-coupling (right) reactions catalysed by Ni(0) **(*xx*)**, Ni(I) (***xxi*** and ***xxii***) and Ni(II) **(*lxv*)** species.

These experimental data suggest that ***xxi*** and ***xxii*** can act as precursors for cross-coupling reactions. However, the mechanism shown in **Scheme 5.1** does not account for how a Ni(I) species could initiate this. Louie *et al.*[12] proposed a radical based mechanism (mechanism **A**) **(Scheme 5.17)** involving an initial cleavage of ArX to give a Ni(I) halide, akin to that described by Kochi.[42] Oxidative addition of another molecule of the aryl halide can then take place, affording a Ni(III) species. The catalytic cycle subsequently proceeds *via* interchanging Ni(I)/Ni(III) complexes through transmetallation and reductive elimination processes, ultimately forming the biaryl cross-coupled product and regenerating the catalytically active $Ni^{I}(NHC)_nX$ species.

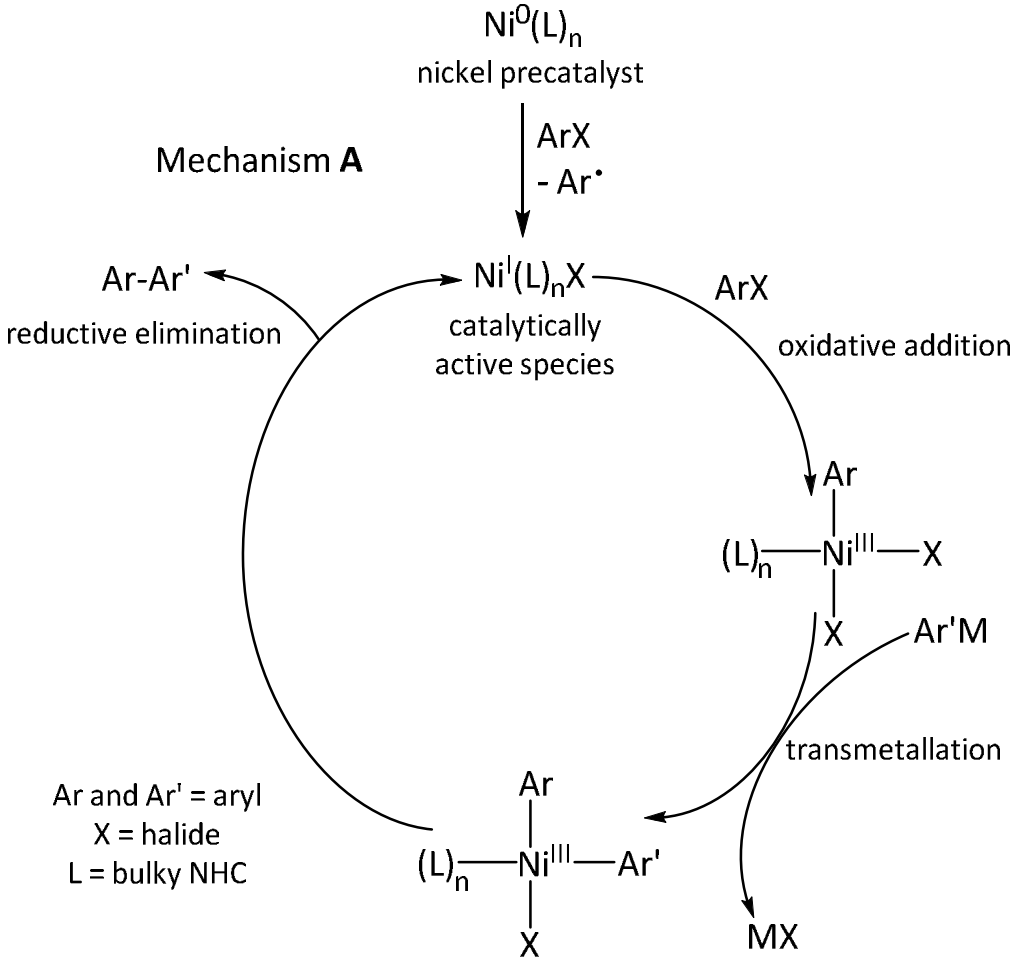

Scheme 5.17 Louie's proposed mechanism **A** for Ni(I) catalysed cross-coupling reactions involving Ni(0)-NHC precatalysts.

However, stoichiometric reactions of ***xxi*** indicated that this mechanism did not occur in practice, as treatment of ***xxi*** with either PhCl or PhBr gave no evidence of a Ni(III) oxidative addition product, even at prolonged reaction times. Moreover, *p*-MeO-C_6H_4Br and *p*-CF_3-C_6H_4Br led to the decomposition of ***xxi*** within 10 min at 353 K. Oxidative addition of any electronic class of aryl halide to ***xxi*** therefore appears to be unachievable.

To address these mechanistic shortcomings, Louie *et al.* postulated a modified mechanism (**B**) shown in **Scheme 5.18**. The transmetallation and oxidative addition steps have essentially swapped over from that in mechanism **A**. Initial formation of $Ni^I(NHC)_nX$ is followed by transmetallation to give a $Ni^I(NHC)_nAr$ complex. This undergoes oxidative addition of the aryl halide to form the same Ni(III) species as in mechanism **A**. Reductive elimination of the biaryl product completes the cycle. Reactions of ***xxi*** with both $PhB(OH)_2$ or MesMgBr were carried out, and although isolation of the resulting nickel species proved unsuccessful, analysis

suggested that $Ni^{I}(IMes)_2Ar$ species were generated, thus providing evidence for the plausibility of this mechanism.

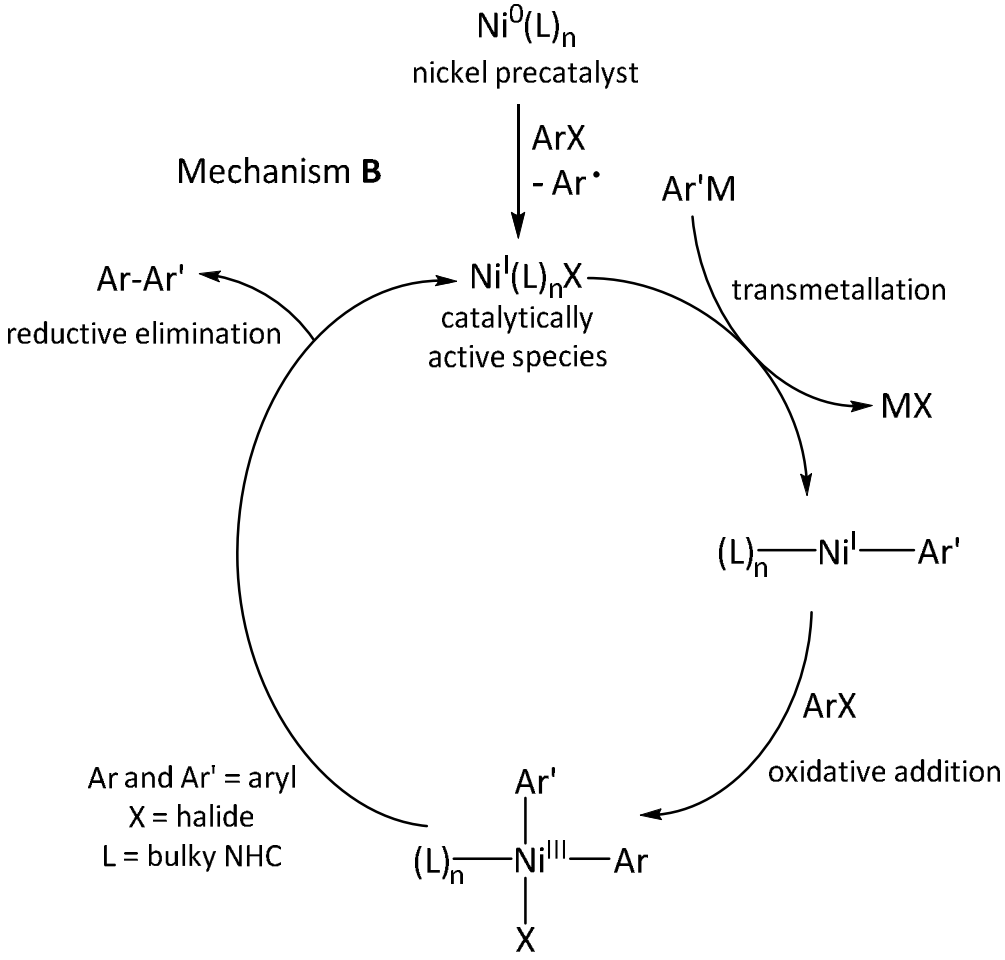

Scheme 5.18 Louie's proposed mechanism **B** for Ni(I) catalysed cross-coupling reactions.

5.1.3 Metal RE NHC Complexes as Catalysts

Despite the vast levels of literature into the reactivity and catalytic potential of transition metal NHC complexes, less research has been carried out into metal-RE NHC species.[27,50,51] Rhodium and iridium are established catalytically active metals for alkene hydrogenation and, along with phosphines,[52,53] 5- and 6-membered monodentate NHCs[54] have been investigated as possible ligands for these metals to improve catalytic activity. In 2013, the synthesis of a series of Rh(I) and Ir(I) complexes of the general formula M(RE NHC)(COD)Cl (NHC = 6Neo, 7Neo, 7^{i}Pr) was reported.[55] Yellow solids (69 – 91 % yield) of these complexes were isolated from addition of the *in situ* generated free RE NHC to the corresponding $[M(COD)Cl]_2$ dimers. The iridium based 6Neo version (Ir(6Neo)(COD)Cl) was employed in catalytic alkene hydrogenation studies. Using low catalyst loadings of 0.01 mol% and 5 bar H_2

in ethanol, non-hindered terminal alkenes (such as styrene, allyl benzene and 1-octene) were quantitatively hydrogenated to their saturated derivatives when left for 0.5 h at room temperature **(Scheme 5.19)**.

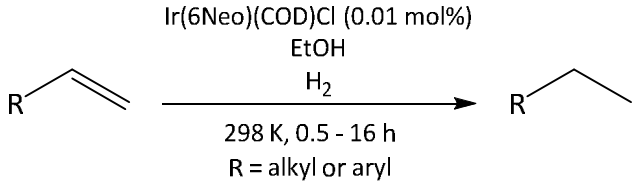

Scheme 5.19 Alkene hydrogenation with an Ir(I)-RE NHC precatalyst.

Entry	Substrate	Product	Time / h	Yield / % [a]
1	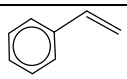	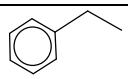	0.5	100
2	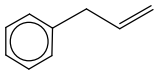	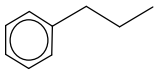	0.5	100
3	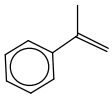	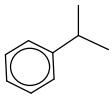	1.0	43
4	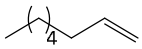	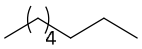	0.5	100
5	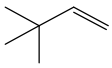	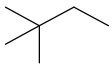	0.5	100
6	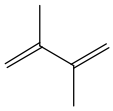	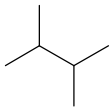	1.0	52
7			16	46
8			16	1
9	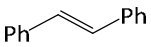	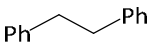	16	1

Table 5.5 Yield (%) for alkene hydrogenation reactions mediated by Ir(6Neo)(COD)Cl.
[a] Percentage yield based on consumption of substrate by GC-MS.

As apparent from **Table 5.5**, the catalytic activities significantly reduced as a function of the increased steric demands of the substrate, even with lengthened reaction times. For example, 43 % conversion of α-methylstyrene (entry 3) was measured after 1 h, while hydrogenation of *cis*-cyclooctene (entry 7) gave only 46 % cyclooctane even after 16 h. Entries 8 and 9 show extreme cases of steric influence, with only 1 % yields detected for both 1-methylcyclohexene and *trans*-stilbene. In spite of Ir(6Neo)(COD)Cl overall yielding excellent results for this

transformation, the activity was no better than systems based on 5-membered NHCs described by Crabtree and coworkers.[56] Rh(III)-*bis*(NHC) complexes of the general formula Rh(NHC)(OAc)I_2, where the NHC is an imidazolium derived bidentate carbene **(Figure 5.1)**, catalysed hydrogenation of all substrates studied to >99 % yield, including less hindered alkenes and α,β-unsaturated ketones (no alcohol formation was observed in the case of ketones).

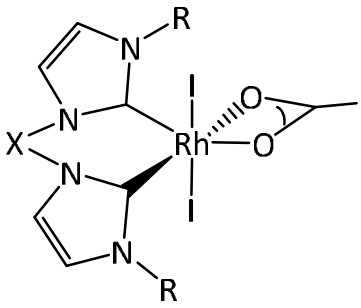

R = ^{n}Bu, ^{i}Pr X = CH_2, *o*-C_6H_4

Figure 5.1 Rh(III)-*bis*(NHC) species bearing an imidazolium derived bidentate carbene.

Although not demonstrated with Ir(6Neo)(COD)Cl, there are examples where substitution of a imidazolium based NHC with a RE NHC does lead to catalytic improvements. Herrmann *et al.*[57] investigated the use of 5-membered NHC complexes, such as Rh(IMes)(COD)Cl, but found them to be ineffective for alkene hydrogenation due to reduction and elimination of the COD ligand. Although this degradation formed a potentially catalytically active linear rhodium complex,[51] it was unstable and decomposed to form inactive nanoparticulate rhodium **(Scheme 5.20)**.

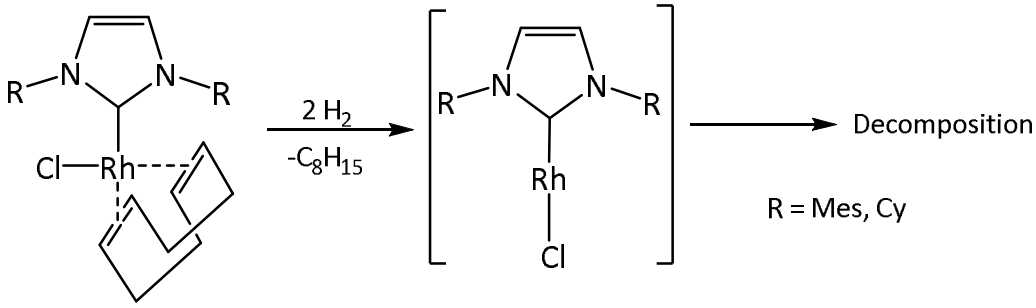

Scheme 5.20 Decomposition of Rh(NHC)(COD)Cl complexes.

6- and 7-membered RE NHCs were thus investigated as replacement ligands. In the hydrogenation of methyl-(Z)-N-acetamido cinnamate **(Scheme 5.21)**, Rh(RE NHC)(COD)Cl bearing 6Mes and 7Mes gave higher conversions to the alkane (6Mes: 32 %; 7Mes: 30 %) than

their 5-membered SIMes counterpart which was totally inactive **(Table 5.6)**. This suggests that the larger ringed NHCs retained the catalytic integrity of the rhodium species under the reaction conditions. The comparable activity of 6Mes and 7Mes seems to imply that there is a threshold N-C_{NHC}-N bond angle in species of this type **(Table 5.6)**.

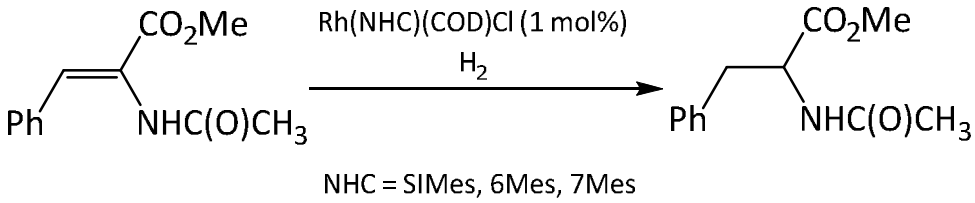

Scheme 5.21 Catalytic hydrogenation of methyl-(Z)-N-acetamido cinnamate with Rh(NHC)(COD)Cl.

NHC	Yield / %	N-C_{NHC}-N bond angle / ° [58]
SIMes	0	101.4
6Mes	32	114.6
7Mes	30	116.6

Table 5.6 Yield (%) for alkene hydrogenation of methyl-(Z)-N-acetamido cinnamate catalysed with Rh(NHC)(COD)Cl, accompanied with the N-C_{NHC}-N angles for the NHC ligands.

In 2006, Cavell and coworkers undertook a study into the effect of carbene backbone size on Pd(0) catalysed Mizoroki-Heck cross-coupling reactions.[27] A variety of NHC Pd(0)-(dvtms) (divinyltetramethyldisiloxane) complexes were prepared *via* reaction of the *in situ* generated RE NHCs with 1 eq Pd(dvtms) **(Scheme 5.22)**. The carbene ligands employed comprised N-Mes, -^{m}Xyl, -^{o}Anis and -^{o}Tol substituted 6- and 7-membered NHCs and the activity of the resulting complexes was compared to that of the Pd(IMes) derivative in the coupling of 4-bromoacetophenone and *n*-butyl acrylate **(Scheme 5.23)**.

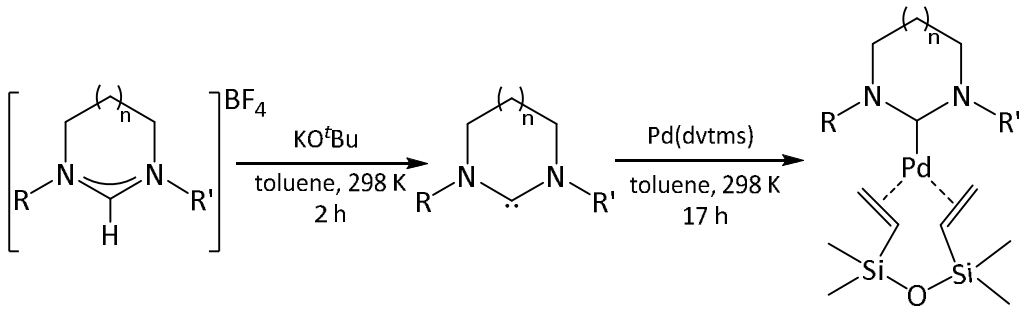

Scheme 5.22 Synthesis of zero-valent Pd(RE NHC)(dvtms) complexes.

The results obtained from this study are summarised in **Table 5.7** and suggest that the larger, 7-membered RE NHC palladium complexes (entries 5 – 7) demonstrate superior activity when compared to their smaller ring counterparts (entries 1 – 4 and 8). This is most strikingly observed with comparisons of the 5-, 6- and 7-membered mesityl substituted complexes **(Figure 5.2)**. Upon increasing ring size from five to six and ultimately seven, a rise in activity is clearly apparent, with a massive fivefold increase in turnover frequency (TOF) upon expansion from 6Mes to 7Mes (**Table 5.7** (entries 1 and 5)).

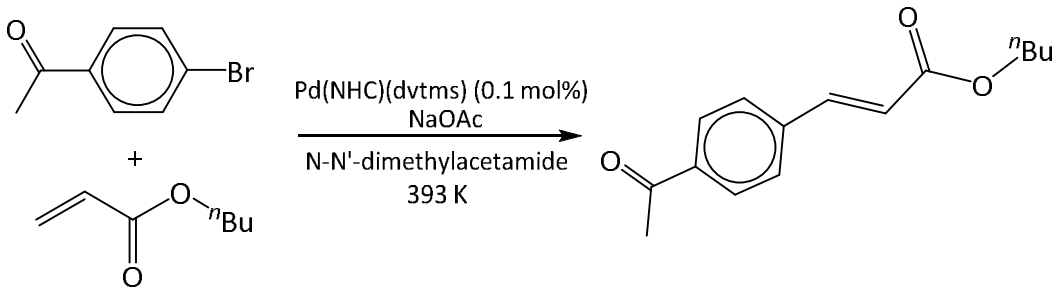

Scheme 5.23 Mizoroki-Heck cross-coupling of 4-bromoacetophenone and *n*-butyl acrylate catalytically mediated with Pd^0(NHC)(dvtms).

Entry	Pd(NHC)(dvtms) NHC	Yield / %	TOF*
1	6Mes	61	217
2	6^{m}Xyl	50	287
3	6^{o}Tol	59	520
4	6^{o}AnisMes	85	353
5	7Mes	100	1140
6	7^{m}Xyl	100	512
7	7^{o}Tol	64	443
8	IMes	14	8

Table 5.7 Yield (%) and TOFs for Mizoroki-Heck cross-coupling of 4-bromoacetophenone and *n*-butyl acrylate catalytically mediated with Pd^{0}(NHC)(dvtms) after 3 h. * TOF values calculated after 30 min.

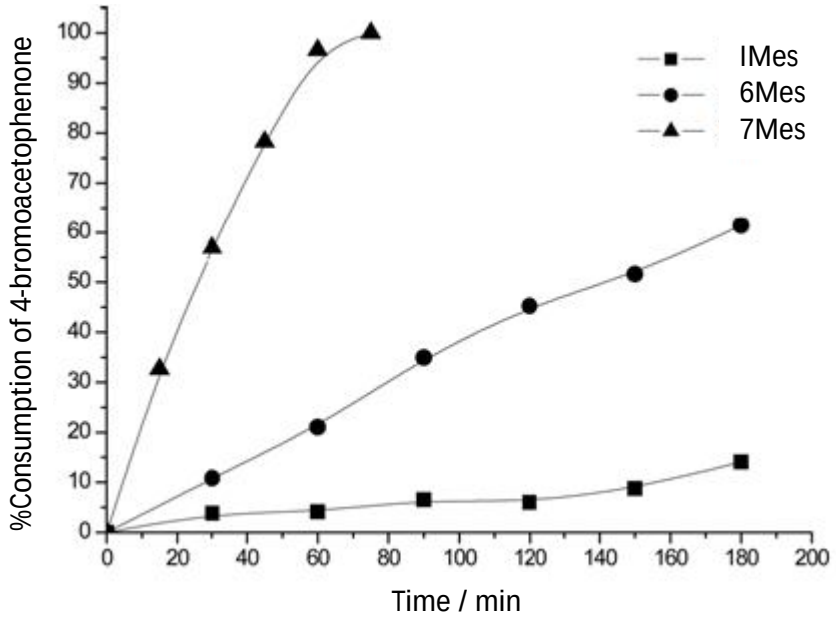

Figure 5.2 Graphical comparison of Mizoroki-Heck cross-coupling of 4-bromoacetophenone and *n*-butyl acrylate catalytically mediated by Pd^{0}(NHC)(dvtms) bearing different sized carbene rings (NHC = IMes, 6Mes and 7Mes).

As the only variable changing throughout these three complexes is the NHC ring size, the results suggest that the increased σ-donating properties and steric hindrance of the expanded NHCs afford transition metal catalysts with superior activity when applied to this type of cross-coupling reactions. The influence of the steric hindrance of the R groups was also analysed. Within the 6-membered RE NHC ligands, the impact of different R groups was relatively small. However, for the 7-membered analogues the effect was far more pronounced. After 3 hr, the more sterically bulky 7Mes and 7^{m}Xyl complexes gave 100 % conversions, while only 64 % conversion was observed for the smaller 7^{o}Tol. This variation adds weight to the idea of steric bulk playing a key role in catalytic performance.

5.2 Catalytic Activity of Ni(6Mes)(PPh$_3$)Br (1)

The suggestion that RE NHCs can facilitate the formation of low coordinate Ni(I) species has been demonstrated by the formation of the neutral Ni(RE NHC)(PPh$_3$)Br series **(1 – 10)** along with their derivatives, such as neutral **13 – 16**, **20** and **28** and cationic **19**, **21 – 26**. Given the limited number of studies on transition metal RE NHC complexes in catalysis, investigations into the potential catalytic applications of Ni(6Mes)(PPh$_3$)Br **(1)** were explored and compared to other Ni-RE NHC complexes to gain insight into the effect of i) carbene ring size and N-substituent bulk, ii) charge and iii) oxidation state.

5.2.1 Kumada Cross-Coupling

5.2.1.1 Effect of RE NHC steric bulk

The 6-membered **(1)**, 7-membered **(7)** and 8-membered (**8** and **9**) Ni-RE NHC species were investigated as precatalysts for Kumada cross-coupling reactions to assess the impact of varying NHC ring size and N-substituents **(Scheme 5.24)**.

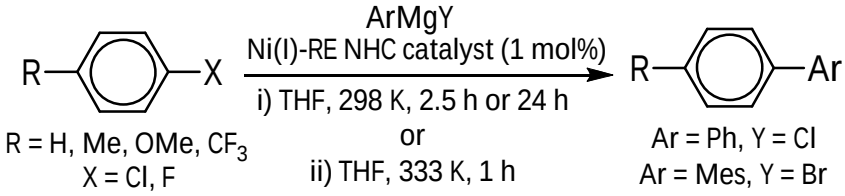

Scheme 5.24 Ni(RE NHC)(PPh$_3$)Br (**1**, **7 – 9**) catalysed Kumada cross-coupling.

Challenging substrates in the form of electron-rich aryl chlorides and aryl fluorides were employed in order to i) establish whether Ni(I) species displayed above average activity and ii) highlight any discrimination in the relative efficiencies of the four Ni(I)-RE NHC complexes. Both PhMgCl and MesMgBr were tested to probe the influence of the Grignard reagent. The average isolated yields of the biphenyl products from two separate runs for a range of ArX (X = Cl, F) are given in **Table 5.8** (data for **1** and **7** are shown).

				Yield / %	
Entry	**Aryl Halide**	**Grignard Reagent**	**Product**	**1**	**7**
1[a]	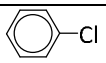	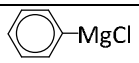	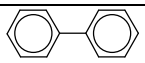	77 (-)	64 (-)
2[a]	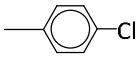	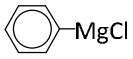	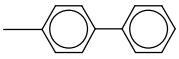	83 (79)	51 (45)
3[b]	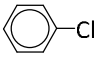	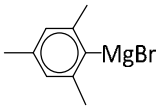	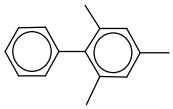	51 (83)	41 (7)
4[b]		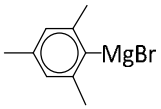	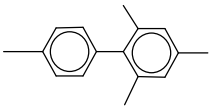	36 (9)	29 (26)
5[c]	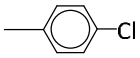	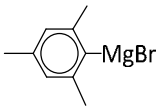	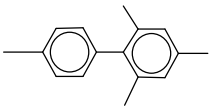	37 (-)	- (-)
6[a]		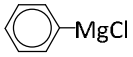	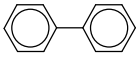	72 (-)	14 (-)
7[a]	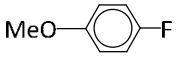	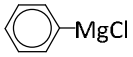	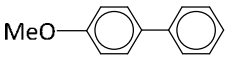	26 (18)	8 (4)
8[a]	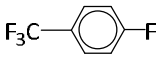	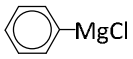	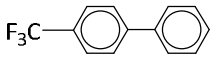	28 (20)	18 (23)
9[b]		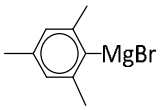	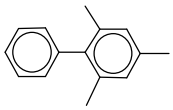	8 (12)	16 (2)
10[a]	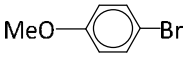	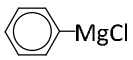		90 (-)	- (-)

Table 5.8 Average isolated yields (%) of two runs from Kumada cross-coupling of aryl halides catalysed by **1** and **7** (1 mol%) at 298 K in THF. The corresponding results recorded at 333 K are shown in parentheses. [a] 2.5 h at 298 K or 1 h at 333 K. [b] 24 h at 298 K or 1 h at 333 K. [c] 2.5 h at 298 K + PPh_3 (5 eq). – denotes no reaction attempted.

Successful cross-coupling was observed in all cases, often occurring in comparable yields to previously reported Ni(0)[10] and Ni(II)[32] catalysts. Good activity was found for reaction of aryl chlorides (entries 1 – 5) with **1** proving to be the more active precursor. In the case of PhMgCl

and PhCl (entry 1), an isolated yield of 77 % biphenyl was obtained with **1**, however a contribution to the yield of this product could result from homocoupling of the Grignard reagent and/or aryl chloride. Thus, a range of *para* substituted substrates were investigated, containing both deactivating, electron-donating groups (*p*-MeO-) and activating, electron-withdrawing groups (*p*-CF_3-). As previously reported in the literature,[38,48,49] electron-withdrawing groups located in the *para* position give higher product yields, while the converse is true for electron-donating groups. The use of a bulkier MesMgBr provided an alternative means to prevent homocoupling, along with easier identification of the desired cross-coupled products.

As expected, cross-coupling of ArCl (entries 1 – 5) was more efficient than for an ArF (entries 6 – 9). Reasonable yields with ArF substrates were obtained, with **1** showing the highest level of activity. In comparison to similar Kumada cross-coupling of aryl fluorides with $Ni^0(NHC)_n$ complexes reported by Herrmann *et al.*,[59] the activities of **1** and **7** are significantly inferior. For example, $Ni(IPr)_2$ gave 95 and 52 % product yields from *p*-CF_3-C_6H_4F and *p*-MeO-C_6H_4F respectively with PhMgBr, compared to just 28 and 26 % achieved using **1** with PhMgCl as the Grignard reagent.

The reactions with *p*-MeO- and *p*-CF_3- substituted substrates (entries 7 and 8 respectively) produced a mixture of products as shown in **Figure 5.3**: the expected cross-coupled products, along with biphenyl and terphenyl from side reactions. The isolated yields of desired cross-coupled product obtained for these substrates followed the trends reported in the literature, with the presence of a *p*-CF_3- group enhancing the overall yield. Cross-coupling reactions with *p*-MeO- substrates are notoriously hard to achieve,[60-63] often leading to very little or no conversion. Despite Herrmann *et al.*[10] reporting conversions of > 67 % with $Ni^0(L)_n$ (L = Mes, IPr, P^tBu_3) catalysts using *p*-MeO-C_6H_4Cl, a 26 % isolated yield for the fluoride substrate with **1** can be considered respectable **(Table 5.8)**.

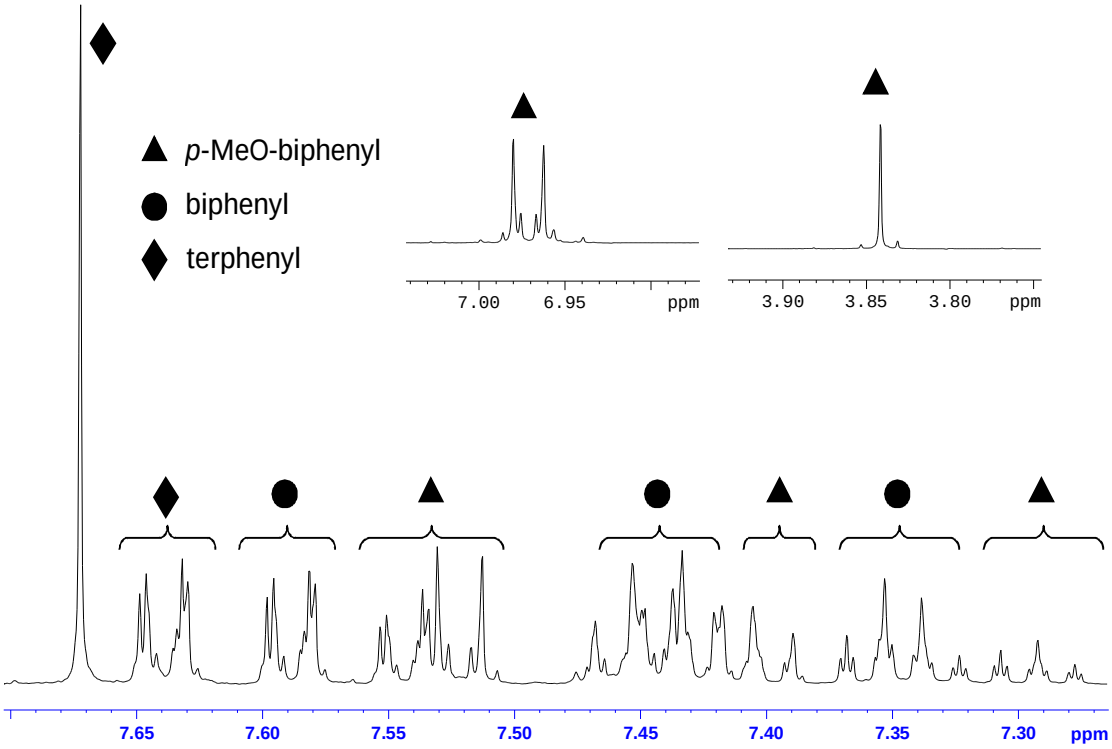

Figure 5.3 ^{1}H NMR spectrum of the product mixture from cross-coupling of *p*-MeO-C_6H_4F and PhMgCl catalysed by **1** ($CDCl_3$, 500 MHz, 298 K).

For all reactions, increasing the temperature from 298 K to 333 K failed to significantly increase conversions (data for 333 K are shown in parentheses in **Table 5.8**). In most cases, comparable yields were obtained (*i.e.* for **1**, 83 and 79 % at 298 and 333 K respectively for *p*-Me-C_6H_4Cl with PhMgCl), although the decrease with elevated temperature seen in some cases may point to catalyst degradation. Even at longer reactions times of 24 h, MesMgBr was less reactive than PhMgCl, suggesting the increased bulk, unsurprisingly, makes it a less effective cross-coupling partner (entries 3 – 5 and 9). The isolated yields obtained from **1** with MesMgBr and aryl chlorides (36 – 51 %) were a lot lower than those reported by Louie and coworkers[12] for the Kumada coupling of chlorobenzene and MesMgBr with $Ni^0(IMes)_2$ (***xx***, 73 %), $Ni^I(IMes)_2Br$ (***xxi***, 73 %) and $Ni^I(IMes)_2Cl$ (***xxii***, 77 %) **(Table 5.4)**.

Further studies are required to explain the greater activity of **1** compared to the 7^{o}Tol analogue **7**, although simple sterics appear to be a factor given that this trend does progress further upon expansion to the 8-membered Ni(I)-RE NHC complexes (**8** (mixed Br/Cl): 3 %, **9** (mixed Br/Cl): 39 % and **9** (Br): 44% conversion for the coupling of *p*-Me-C_6H_4Cl and PhMgCl). Thus, there is a clear effect of NHC ring size on activity, with activity decreasing in the order of 6- > 7- > 8-membered NHC. The sterics of the *o*-tolyl N-substituent on **7** may also have an influence with the lesser bulk destabilising any catalytically active nickel species, thus reducing

the overall activity. Future work should target the 6^{o}Tol derivative (**2**) to provide more insight into the influence of N-substituents.

When compared to the activity of the 5-membered Ni(I) complex Ni(IPr)$_2$Cl ***(xvii)*** in Kumada coupling (section **5.1.2.2**), **1** and **7** display superior performance. Here, low 1 mol% loadings of **1** and **7** have been shown to catalyse the cross-coupling of aryl chlorides and fluorides in respectable yields of *ca.* 70 %, using mild reaction conditions of 2.5 h at room temperature. Although conversions of *ca.* 90 % were achieved with ***xvii*** at an identical catalytic loading and temperature, this was with the less challenging aryl bromide substrates, as well as for longer reaction times (18 h) and in the presence of an additional 5 mol% IPr.[11] To provide a direct comparison, coupling of *p*-MeO-C$_6$H$_4$Br and PhMgCl with **1** at 298 K (**Table 5.8**, entry 10) was carried out, giving a 90 % conversion in 2.5 h.

Interestingly, in comparison to *bis*(phosphine), *bis*(NHC) and mono(NHC)/mono(phosphine) Ni(II)[6] and Pd(II)[64] complexes, Matsubara *et al.*[6] and Herrmann and coworkers[64] found that the mixed NHC/phosphine ligand systems Ni(I^{i}Pr)(PPh$_3$)Cl and Pd(NHC)(PR$_3$)I$_2$ (NHC = IMe, I^{i}Pr; R = ^{t}Bu, Ph, ^{o}Tol, Cy) showed enhanced activity compared to the *bis*(NHC) species Ni(I^{i}Pr)$_2$Cl$_2$ and [Pd(NHC)(I)(μ-I)]$_2$ in both Kumada and Suzuki coupling respectively, further highlighting the potential catalytic benefits of complexes such as **1**. Entry 5 shows the isolated yield obtained from coupling *p*-Me-C$_6$H$_4$Cl and MesMgBr in the presence of 5 eq free PPh$_3$, however a 37 % isolated yield with **1** is no better than the 36 % attained in the absence of additional phosphine (entry 4).

Catalytic Suzuki cross-coupling of *p*-MeO-C$_6$H$_4$Br and PhB(OH)$_2$ was attempted with **1** at both 298 and 343 K. No conversion to the cross-coupled *p*-MeO-biphenyl product was observed in either experiment, despite previous literature showing promising results with NHC bearing Ni(II) complexes, including ***xvii*** and the corresponding IMes analogues ***xxi*** and ***xxii***.[12,65]

5.2.1.1.1 Preliminary mechanistic studies

In order to fully determine what nickel oxidation states are involved in the catalytic reaction with **1** and **7**, mechanistic studies are necessary to evaluate how the Ni(I) complexes initiate C-C coupling. A preliminary EPR study was carried out in which X-band EPR (140 K) measurements were taken of a mixture of **1**, *p*-Me-C$_6$H$_4$Cl and PhMgCl (frozen in liquid N$_2$ immediately after addition of Grignard reagent to halt the reaction) and the spectrum compared to that of the Ni(I) starting precursor **(1)**. As can be seen in **Figure 5.4**, the spectrum

obtained for the catalytic reaction mixture (a) is very different to that of **1** (b) and indeed any other isolated Ni(I) spin species described in this thesis. As for **21** and **24**, the $\boldsymbol{g}_3 - \boldsymbol{g}_2$ value for the species shown in **Figure 5.4a** is greater than $\boldsymbol{g}_2 - \boldsymbol{g}_1$ **(Table 5.9)**, suggestive of a $3d_{x2-y2}$ ground state. This is in complete contrast to **1**, which displays $\boldsymbol{g}_3 - \boldsymbol{g}_2 < \boldsymbol{g}_2 - \boldsymbol{g}_1$ **(Table 2.4)** and a ground state consisting of mostly $3d_{z2}$ character. The acquired spectrum (a) did not change over a period of 30 min at 140 K.

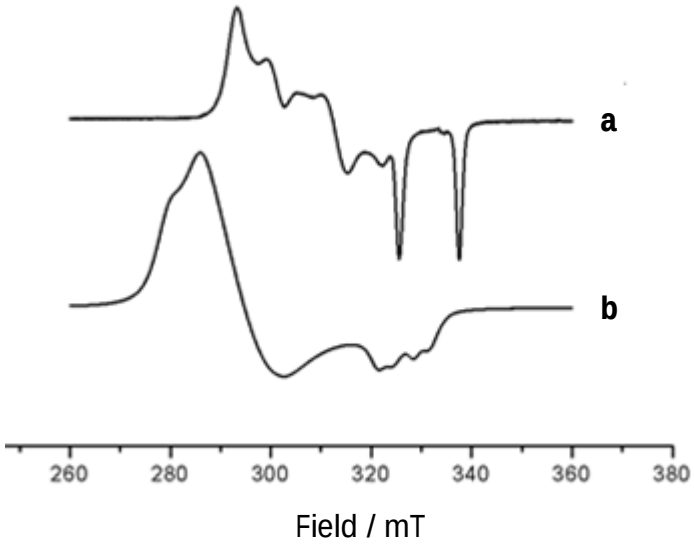

Figure 5.4 X-band EPR (140 K) spectra of Ni(6Mes)(PPh_3)Br **(1)** + *p*-Me-C_6H_4Cl + PhMgCl in THF (a) and **1** in THF (b).

Complex	$\boldsymbol{g_1}$	$\boldsymbol{g_2}$	$\boldsymbol{g_3}$	$\boldsymbol{g_3 - g_2}$	$\boldsymbol{g_2 - g_1}$	$\boldsymbol{A_1}$ / MHz	$\boldsymbol{A_2}$ / MHz	$\boldsymbol{A_3}$ / MHz
1 + *p*-Me-C_6F_4Cl + PhMgCl	2.020	2.113	2.262	0.149	0.093	339	207	190

Table 5.9 Spin Hamiltonian parameters for the Kumada cross-coupling reaction of *p*-Me-C_6H_4Cl and PhMgCl in THF with **1** as the catalytic precursor. $\boldsymbol{g}$ values ±0.005.

It is believed that the rhombic nature of the spectrum in **Figure 5.4a** is consistent with a Ni(I) ion. A Ni(III) ion with a spin system of $S > ½$, such as a high spin $S = {}^3/_2$ system, is ruled out as no domination of the zero-field parameter is observed in the spectrum. A species containing i) a Ni(III) ion with $S = ½$ or ii) a Ni(II) complex involving an electronic configuration with unpaired electrons were postulated, however analysis of the spin Hamiltonian parameters displayed in **Table 5.9** are more consistent with a Ni(I) d^9 species being responsible for the observed spectrum. This infers that a Ni(I) species does play a role within the catalytic cycle for

Kumada cross-coupling initiated by complex **1**. Due to the change of relationship between the ***g*** values and hence the nature of the ground state, it is believed this species has a geometry different from trigonal planar **1**. However, the degree of distortion to T-shaped (if still three coordinate) is less than that observed for **21** and **24**.

The participation of Ni(I) complexes in C-C bond formation was first postulated by Kochi[31,42,43] over three decades ago, however there is still very limited evidence for direct involvement of a d^9 species.[13,39] Despite these simple EPR studies providing preliminary evidence that a Ni(I) complex is involved in the catalytic cycle for these Kumada couplings, many mechanistic questions still remain unanswered. Further stoichiometric reactions and detailed EPR analysis are needed to determine the exact identity of this new Ni(I) species, whether **1** is directly involved in the cycle (or simply converts to another complex which is catalytically active under the reactions conditions employed) and the nature of any other species involved (*i.e.* is there a cycle between Ni(I) and Ni(III) oxidation states or a radical mechanism?).

5.2.1.2 Effect of charge

To establish any correlation between catalytic performance for Kumada coupling and overall charge of the complex, the activity of the cationic, three coordinate Ni(I) complex $[Ni(6Mes)(PPh_3)(THF)]PF_6$ **(24)** was compared to that of neutral **1**. Using the same reaction conditions employed with **1**, a range of ArX (X = Br, Cl, F) substrates were coupled with PhMgCl. Isolated yields of the biaryl derivatives obtained from **24** are shown in **Table 5.10**, together with the values for **1** in parentheses.

Entry	Aryl Halide	Grignard Reagent	Product	Yield / %
1	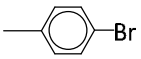	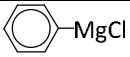	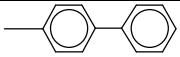	35 (-)
2	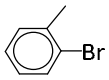	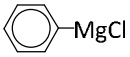	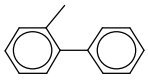	25 (-)
3	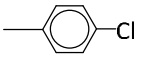	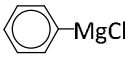	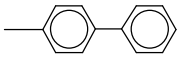	52 (83)
4	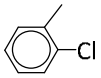	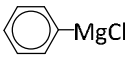	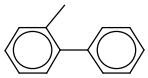	32 (-)
5	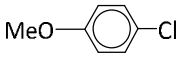	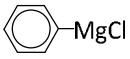	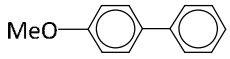	28 (-)
6	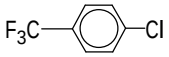	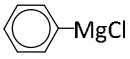	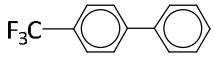	58(-)
7		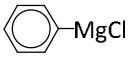	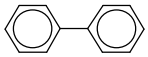	16 (72)
8	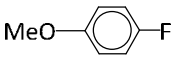	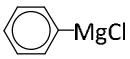	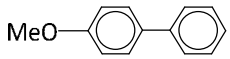	- (26)
9	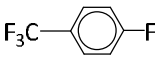	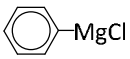	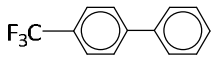	21 (28)

Table 5.10 Average isolated yields (%) of two runs from Kumada cross-coupling of aryl halides with PhMgCl catalysed by **24** (1 mol%) for 2.5 h at 298 K in THF. The corresponding results with **1** are shown in parentheses. – denotes no reaction attempted.

Consideration of the results shows that i) the isolated yields obtained using cationic **24** were lower than those with **1** (entries 3, 7 and 9), ii) as for **1**, **24** was more active towards ArX containing electron-withdrawing (*p*-CF_3-) rather than electron-donating (*p*-MeO-) groups (entries 5 and 6) and iii) *ortho* substituted ArX substrates were less reactive than *para* substituted derivatives (entries 2/4 and 1/3 respectively). The latter is what might be expected for *ortho* substituted substrates and matches observations of Herrmann *et al*.,[59] who reported a 38 % yield from $Ni^0(IPr)_2$ catalysed Kumada coupling between *o*-Me-C_6H_4F and PhMgBr (**24**: 25 and 32 % for *o*-Me-C_6H_4Br and *o*-Me-C_6H_4Cl respectively with PhMgCl). Small quantities of biphenyl were detected in the ^1H NMR spectrum upon use of *o*-Me-C_6H_4Br (13 % biphenyl) and *o*-Me-C_6H_4Cl (9 % biphenyl) with **24**, most likely arising from homocoupling.

Due to the charged nature of **24** compared to **1**, the coupling of *p*-Me-C_6H_4X (X = Br, Cl) with PhMgCl was also run in C_6H_5F as the solvent, but no real change in efficiency was observed (X = Br: 40 %; X = Cl: 47 %).

5.2.1.3 Effect of oxidation state

To gain a better idea of exactly how the catalytic performance of the Ni(I) complexes compare to Ni(II) species, Ni(6Mes)(PPh_3)Br_2 **(29)**, Ni(6^{o}Tol)(PPh_3)Br_2 **(17)** and Ni(7^{o}Tol)(PPh_3)Br_2 **(18)** were tested as catalyst precursors. All three complexes were synthesised by reacting the corresponding *in situ* generated RE NHCs with Ni(PPh_3)$_2Br_2$ and isolated as purple air stable solids, albeit in low yields of 52, 15 and 12 % respectively (see **Appendices** for experimental data **(Appendix 7)** and crystal structure **(Appendix 2)** of **29**). **Table 5.11** gives the isolated yields of cross-coupled products between a variety of aryl halide substrates and PhMgCl, along with the corresponding conversions for **1** and **7** for comparison.

			Yield / %				
Entry	**Aryl Halide**	**Product**	**29**	**17**	**18**	**1**	**7**
1	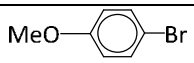	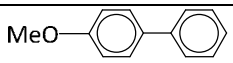	60	44	24	-	-
2	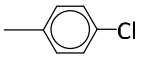	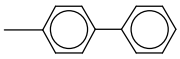	65	38	34	83	51
3	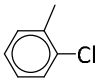	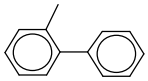	9	17	21	-	-
4	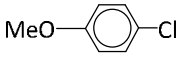		61	38	31	-	-
5	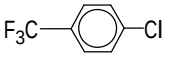	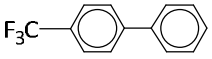	37	21	13	-	-
6	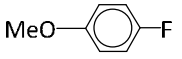	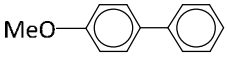	-	-	9	26	8
7	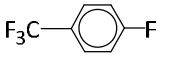	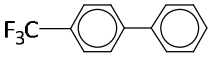	-	-	14	28	18

Table 5.11 Average isolated yields (%) of two runs from Kumada cross-coupling of aryl halides with PhMgCl catalysed by the Ni(II) complexes **29**, **17** and **18** (1 mol%) for 2.5 h at 298 K in THF. The corresponding results for **1** and **7** are also shown as a comparison. – denotes no reaction attempted.

Overall, the Ni(II) catalysts do not seem to exhibit any enhanced catalytic effectiveness relative to Ni(I), with 6Mes bearing complex **29** giving the highest product yield of the three Ni(II) species (entries 1, 2, 4 and 5). This observation is similar to that of Louie and coworkers[12] who found very comparable yields for Suzuki and Kumada coupling initiated by Ni(0) ***xx***, Ni(I) ***xxi*** and ***xxii*** and Ni(II) ***lxv*** (see section **5.1.2.2**). Compared to the values obtained by Louie (52 – 77 %), complexes **29**, **17** and **18** exhibit slightly lower yields. However, harsher conditions were employed for ***xx***, ***xxi***, ***xxii*** and ***lxv*** (3 mol% catalyst, 20 h at 298 K) suggesting greater activity with the RE NHC nickel systems.

Further comparisons of entries 1, 2, 4 and 5 in **Table 5.11** indicate that as also seen for the Ni(I) species **1** and **7**, there is a general trend of decreasing activity upon i) decreasing the steric requirements of the N-substituent, *i.e.* N-Mes > N-^{o}Tol and ii) increasing NHC ring size (6- > 7-membered). Thus, the overall catalytic activity trend for this set of Ni(I)-RE NHC complexes is 6Mes > 6^{o}Tol > 7^{o}Tol > 8-membered.

It is unclear as to whether the Ni(I) systems provide a significantly more efficient route to Kumada cross-coupling over the Ni(II) complexes, as the results shown in entries 6 and 7 for **7** are similar to the corresponding 7^{o}Tol Ni(II) complex **18**. However overall, the results obtained for **1** are slightly better than those observed for all the other complexes investigated.

5.3 Chapter Summary

Ni(I) complexes bearing 6-, 7- and 8-membered RE NHCs have proved active towards Kumada cross-coupling reactions, with the 6Mes complex **1** in particular displaying efficient behaviour for the reactions of both aryl chlorides and, to a lesser extent, aryl fluorides. Complex **1** showed enhanced activity compared to the larger ringed complexes (6 > 7 > 8), and for complexes with less bulky N-substituents (N-Mes > N-^{o}Tol). No enhancement of activity was observed for the three coordinate cationic complex **24** or with the Ni(II) species **29**, **17** and **18**. Preliminary investigations of the reaction mechanism by EPR spectroscopy suggest that **1** is rapidly converted to a long lived Ni(I) species, which exhibits ***g*** tensor values consistent with a T-shaped geometry.

5.4 References

1. A. Velian, S. Lin, A. J. M. Miller, M. W. Day and T. Agapie, *J. Am. Chem. Soc.*, 2010, **132**, 6296.
2. T. N. Tekavec, G. Zuo, K. Simon and J. Louie, *J. Org. Chem.*, 2006, **71**, 5834-5836.
3. M. Vogt, B. de Bruin, H. Berke, M. Trincado and H. Gruetzmacher, *Chem. Sci.*, 2011, **2**, 723-727.
4. S. Diez-Gonzalez, N. Marion and S. P. Nolan, *Chem. Rev.*, 2009, **109**, 3612-3676.
5. O. Navarro, R. A. Kelly and S. P. Nolan, *J. Am. Chem. Soc.*, 2003, **125**, 16194-16195.
6. K. Matsubara, K. Ueno and Y. Shibata, *Organometallics*, 2006, **25**, 3422-3427.
7. Z. H. Liu, Y. C. Xu, L. Z. Xie, M. Sun, Q. Shen and Y. Zhang, *Dalton Trans.*, 2011, **40**, 4697-4706.
8. T. Hatakeyama, S. Hashimoto, K. Ishizuka and M. Nakamura, *J. Am. Chem. Soc.*, 2009, **131**, 11949-11963.
9. C. B. Kim, H. Jo, B. K. Ahn, C. K. Kim and K. Park, *J. Org. Chem.*, 2009, **74**, 9566-9569.
10. V. P. W. Bohm, T. Weskamp, C. W. K. Gstottmayr and W. A. Herrmann, *Angew. Chem., Int. Ed.*, 2000, **39**, 1602.
11. S. Miyazaki, Y. Koga, T. Matsumoto and K. Matsubara, *Chem. Commun.*, 2010, **46**, 1932-1934.
12. K. Zhing, M. Conda-Sheridan, S. R. Cooke and J. Louie, *Organometallics*, 2011, **30**, 2546-2552.
13. T. J. Anderson, G. D. Jones and D. A. Vicic, *J. Am. Chem. Soc.*, 2004, **126**, 8100-8101.
14. B. Zheng, F. Tang, J. Luo, J. W. Schultz, N. P. Rath and L. M. Mirica, *J. Am. Chem. Soc.*, 2014, **136**, 6499-6504.
15. J. Cornella, E. Gomez-Bengoa and R. Martin, *J. Am. Chem. Soc.*, 2013, **135**, 1997-2009.
16. B. Horn, C. Limberg, C. Herwig and B. Braun, *Chem. Commun.*, 2013, **49**, 10923-10925.
17. S. O. N. Lill and P. E. M. Siegbahn, *Biochemistry*, 2009, **48**, 1056-1066.
18. X. Lin and D. L. Phillips, *J. Org. Chem.*, 2008, **73**, 3680-3688.
19. C. Markert, M. Neuburger, K. Kulicke, M. Meuwly and A. Pfaltz, *Angew. Chem., Int. Ed.*, 2007, **46**, 5892-5895.
20. A. N. Vedernikov, *ChemCatChem*, 2014, **6**, 2490-2492.
21. M. I. Lipschutz, X. Yang, R. Chatterjee and T. D. Tilley, *J. Am. Chem. Soc.*, 2013, **135**, 15298-15301.
22. M. I. Lipschutz and T. D. Tilley, *Angew. Chem., Int. Ed.*, 2014, **53**, 7290-7294.

23. K. C. Mondal, P. P. Samuel, Y. Li, H. W. Roesky, S. Roy, L. Ackermann, N. S. Sidhu, G. M. Sheldrick, E. Carl, S. Demeshko, S. De, P. Parameswaran, L. Ungur, L. F. Chibotaru and D. M. Andrada, *Eur. J. Inorg. Chem.*, 2014, **2014**, 818-823.
24. M. Henrion, V. Ritleng and M. J. Chetcuti, *ASC Catal.*, 2015, **5**, 1283-1302.
25. V. Pons, R. T. Baker, N. K. Szymczak, D. J. Heldebrant, J. C. Linehan, M. H. Matus, D. J. Grant and D. A. Dixon, *Chem. Commun.*, 2008, 6597-6599.
26. S. K. Schneider, W. A. Herrmann and E. Herdtweck, *J. Mol. Catal. A: Chem.*, 2006, **245**, 248-254.
27. J. J. Dunsford and K. J. Cavell, *Dalton Trans.*, 2011, **40**, 9131-9135.
28. A. Weichert, M. Bauer and P. Wirsig, *Synlett*, 1996, 473.
29. C. Kayan, N. Biricik, M. Aydemir and R. Scopelliti, *Inorg. Chim. Acta.*, 2012, **385**, 164-169.
30. B. Milde, R. Packheiser, S. Hildebrandt, D. Schaarschmidt, T. Rueffer and H. Lang, *Organometallics*, 2012, **31**, 3661-3671.
31. X. Hu, *Chem. Sci.*, 2011, **2**, 1867-1886.
32. Z. Xi, B. Liu and W. Chen, *J. Org. Chem.*, 2008, **73**, 3954-3957.
33. S. K. Schneider, C. F. Rentzsch, A. Krueger, H. G. Raubenheimer and W. A. Herrmann, *J. Mol. Catal. A: Chem.*, 2007, **265**, 50-58.
34. V. B. Phapale and D. J. Cardenas, *Chem. Soc. Rev.*, 2009, **38**, 1598-1607.
35. S. Lin and T. Agapie, *Synlett*, 2011, 1-5.
36. N. Yoshikai, H. Mashima and E. Nakamura, *J. Am. Chem. Soc.*, 2005, **127**, 17978-17979.
37. A. M. Oertel, V. Ritleng and M. J. Chetcuti, *Organometallics*, 2012, **31**, 2829-2840.
38. I. Colon and D. R. Kelsey, *J. Org. Chem.*, 1986, **51**, 2627-2637.
39. G. D. Jones, J. L. Martin, C. McFarland, O. R. Allen, R. E. Hall, A. D. Haley, R. J. Brandon, T. Konovalova, P. J. Desrochers, P. Pulay and D. A. Vicic, *J. Am. Chem. Soc.*, 2006, **128**, 13175-13183.
40. K. C. Nicolaou, P. G. Bulger and D. Sarlah, *Angew. Chem., Int. Ed.*, 2005, **44**, 4442-4489.
41. N. Miyaura and A. Suzuki, *Chem. Rev.*, 1995, **95**, 2457-2483.
42. J. K. Kochi, *Pure Appl. Chem.*, 1980, **52**, 571-605.
43. T. T. Tsou and J. K. Kochi, *J. Am. Chem. Soc.*, 1979, **101**, 7547-7560.
44. E. Prasad and R. A. Flowers, *J. Am. Chem. Soc.*, 2002, **124**, 6895-6899.
45. J. Breitenfeld, J. Ruiz, M. D. Wodrich and X. Hu, *J. Am. Chem. Soc.*, 2013, **135**, 12004-12012.

46. C. P. Zhang, H. Wang, A. Klein, C. Biewer, K. Stimat, Y. Yarnaguchi, L. Xu, V. Gomez-Benitez and D. A. Vicic, *J. Am. Chem. Soc.*, 2013, **135**, 8141-8144.
47. T. T. Tsou and J. K. Kochi, *J. Am. Chem. Soc.*, 1978, **100**, 1634-1635.
48. R. R. Milburn and V. Snieckus, *Angew. Chem., Int. Ed.*, 2004, **43**, 888-891.
49. S. Saito, S. Ohtani and N. Miyaura, *J. Org. Chem.*, 1997, **62**, 8024-8030.
50. C. J. E. Davies, M. J. Page, C. E. Ellul, M. F. Mahon and M. K. Whittlesey, *Chem. Commun.*, 2010, **46**, 5151-5153.
51. A. Binobaid, M. Iglesias, D. J. Beetstra, B. Kariuki, A. Dervisi, I. A. Fallis and K. J. Cavell, *Dalton Trans.*, 2009, 7099-7112.
52. J. A. Osborn, F. H. Jardine, J. F. Young and Wilkinso.G, *J. Chem. Soc. A*, 1966, 1711.
53. D. A. Evans, G. C. Fu and A. H. Hoveyda, *J. Am. Chem. Soc.*, 1992, **114**, 6671-6679.
54. C. Desmarets, S. Kuhl, R. Schneider and Y. Fort, *Organometallics*, 2002, **21**, 1554-1559.
55. J. J. Dunsford, D. S. Tromp, K. J. Cavell, C. J. Elsevier and B. M. Kariuki, *Dalton Trans.*, 2013, **42**, 7318-7329.
56. M. Albrecht, R. H. Crabtree, J. Mata and E. Peris, *Chem. Commun.*, 2002, 32-33.
57. W. A. Herrmann, G. D. Frey, E. Herdtweck and M. Steinbeck, *Adv. Synth. Catal.*, 2007, **349**, 1677-1691.
58. M. Iglesias, D. J. Beetstra, J. C. Knight, L. L. Ooi, A. Stasch, S. Coles, L. Male, M. B. Hursthouse, K. J. Cavell, A. Dervisi and I. A. Fallis, *Organometallics*, 2008, **27**, 3279-3289.
59. V. P. W. Bohm, C. W. K. Gstottmayr, T. Weskamp and W. A. Herrmann, *Angew. Chem., Int. Ed.*, 2001, **40**, 3387.
60. R. Wilhelm and D. A. Widdowson, *J. Chem. Soc. Perk. Trans. 1*, 2000, 3808-3813.
61. K. Gouda, E. Hagiwara, Y. Hatanaka and T. Hiyama, *J. Org. Chem.*, 1996, **61**, 7232-7233.
62. A. F. Littke and G. C. Fu, *Angew. Chem., Int. Ed.*, 1998, **37**, 3387-3388.
63. D. W. Old, J. P. Wolfe and S. L. Buchwald, *J. Am. Chem. Soc.*, 1998, **120**, 9722-9723.
64. W. A. Herrmann, V. P. W. Bohm, C. W. K. Gstottmayr, M. Grosche, C. P. Reisinger and T. Weskamp, *J. Organomet. Chem.*, 2001, **617**, 616-628.
65. Z. Xi, X. Zhang, W. Chen, S. Fu and D. Wang, *Organometallics*, 2007, **26**, 6636-6642.

CHAPTER 6

6 Future Work

1. The successful formation of fully characterised three coordinate Ni(I) N-aryl bearing RE NHC complexes **(1 – 10)** directed attempts to form N-alkyl analogues **(Chapter 2, 2.3.1)**. However, employment of 6^{t}Bu led to the structural characterisation of a very different, C-H activated nickel product, Ni(6^{t}Bu)'Br **(11)**, along with a nickelate species. Reproducibility of this reaction was unachievable, thus paramount in the immediate future will be re-examination of this stoichiometric reaction to reproducibly afford **11**. Although not a Ni(I) species, the structure of **11** is unusual and the compound could be a precursor to other unusual lower coordinate Ni(II) products upon abstraction of bromide **(Scheme 6.1)**.[1]

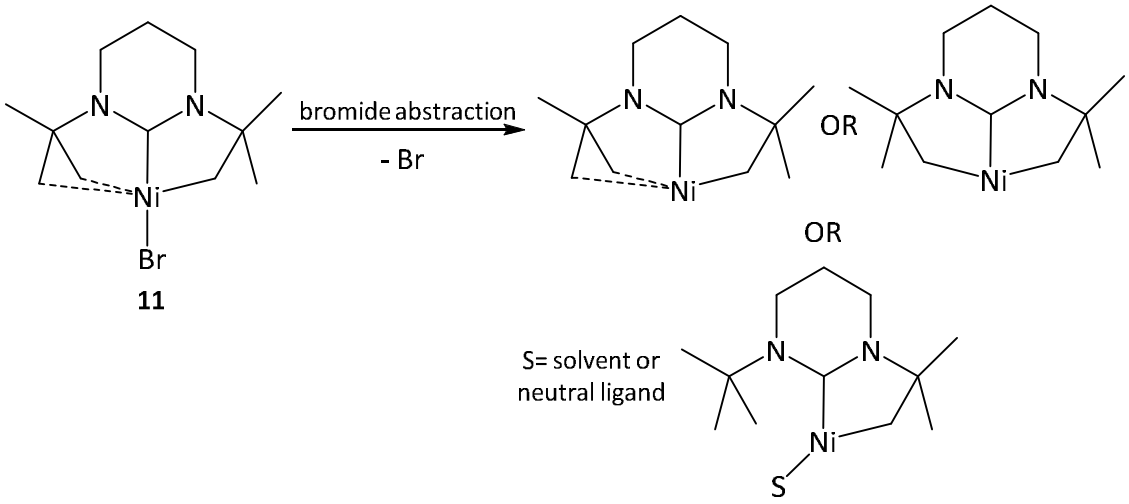

Scheme 6.1 Potential products from bromide extraction reactions on **11**.

2. The high sensitivity and reactivity of Ni(RE NHC)(PPh_3)Br has been established in studies of their stoichiometric chemistry with O_2, RE NHCs, electrophiles and hydride sources. Attempts to determine the oxygen intermediates involved during the activation of O_2 with **1** or **6** to give **13/15** and **14/16** respectively with low temperature UV-vis analysis were unsuccessful **(Chapter 3, 3.2)** and only emphasised the extremely fast timescale and facile nature of the reaction.[2,3] The use of stopped-flow techniques on analogues of **1** which are more difficult to oxidise (*i.e.* Ni(RE NHC)(L)Br, RE NHC = electronic deficient 6MesDAC; L = phosphine ligand with an electron withdrawing aryl group) might be a possible approach to gain further mechanistic insight into the reaction.

3. The interesting SMM properties of the two coordinate cation $[Ni(6Mes_2]^+$ **(19)** generated upon reaction of **1** with additional 6Mes **(Chapter 4, 4.1.1)** presents the question of whether this magnetic behaviour is inherent to this specific compound, or whether it is observed across a series of $[Ni(RE\ NHC)_2]^+$ analogues. For example, in conjunction with EPR and DFT calculations, SQUID magnetic determinations on the related asymmetric $[Ni(6Mes)(7Mes)]^+$ would allow simple inferences to be made on the effect of an extra 'CH_2' group in the carbene backbone on the *d* orbital splitting pattern and magnetic properties of two coordinate Ni(I) species.

4. Many of the reactivity products discussed in this thesis have been isolated in low yields or with significant levels of impurities which cannot be completely removed (*i.e.* **21 – 23** and **27**), which has therefore hampered full characterisation and any further reactivity studies. Extensive reaction optimisation of these is therefore required. Efforts to completely retard the formation of $[6MesH]^{\cdots}arene[B(C_6F_5)_4]$ in the synthesis of Ni(I)-arene species **(21 – 23; Chapter 4, 4.2.1)** from reaction of **1/6** with $[Et_3Si]^+$, would hopefully allow access to clean and pure **21 – 23** and thus opportunities to fully understand the electronic nature of these unusual complexes *via* EPR, electrochemistry and magnetic susceptibility measurements. Ogoshi and coworkers[4] recently reported the synthesis of $Ni^0(IPr)(\eta^6\text{-}C_6H_5R)$ (R = H, CH_3) from reaction of IPr with $Ni(COD)_2$ in the presence of the corresponding arene and high pressures of H_2. One potential route to clean **21 – 23** is to therefore synthesise zero-valent Ni(6/7Mes)(η-arene) complexes using this methodology and then oxidise them to the corresponding Ni(I) species. If successful, the lability of the coordinated arene can then be established in simple ligand substitution reactions and hence the accessibility of the Ni(I) centre towards oxidation/reduction. Preliminary investigations into the reactivity of the BH_4 bridged dimer **28** with O_2 and CO **(Chapter 4, 4.3)** have indicated some molecular activation. Upon optimisation of its synthesis, the reactivity of **28** could then be fully examined, including its potential as a reducing agent towards unsaturated C=O/C=C bonds. The reaction of **28** with Lewis bases should also be attempted, with the aim of removing BH_3 from the bridging ligands to form Ni(I)-hydride species **(Scheme 6.2)**. In relation to this, the reactivity of other hydride sources with **1** can then be investigated, in particular, those that are less likely to bridge, *i.e.* $LiAlH_4$ and $NaBH_3(CN)$.

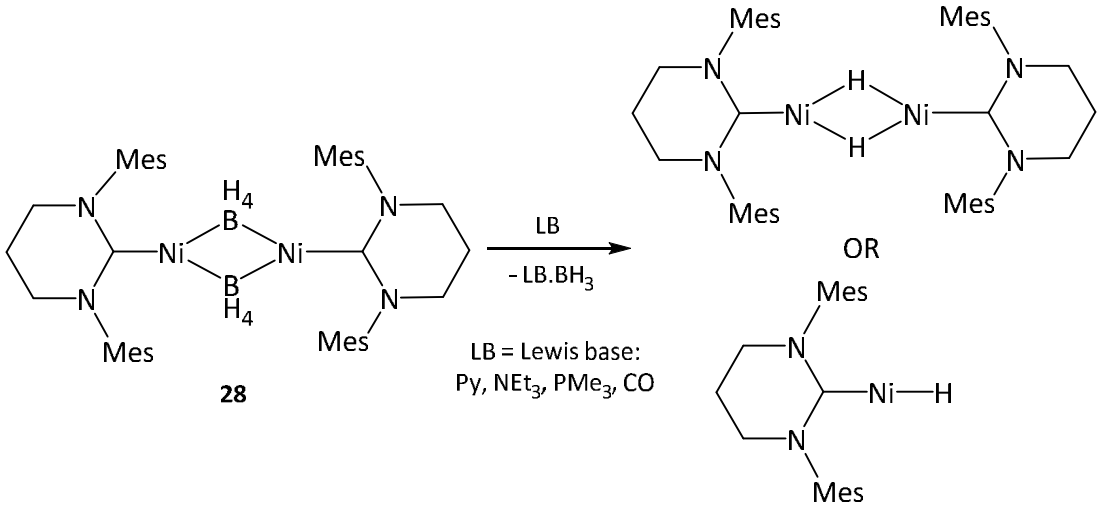

Scheme 6.2 Proposed reaction of **28** with a Lewis base to form Ni(I)-hydride species.

5. Reaction of **1** with $TlPF_6$ generated the solvent coordinated cation $[Ni(6Mes)(PPh_3)(THF)]^+$ **(24; Chapter 4, 4.2.2)**. A very preliminary study of the reactivity of this with small molecules revealed facile reactions with both O_2 and CO, albeit with inclusion of bromide from residual TlBr. $^{13}C\{^1H\}$ NMR studies of the ^{13}CO reaction indicated a complicated reaction profile and the formation of many $Ni\text{-}(CO)_n$ complexes/intermediates. One possibility to resolve this would be to employ ReactIR to provide a clearer indication of the structures of these species in real time.

6. The work described in **Chapter 5** probed the efficiency of $Ni(RE\ NHC)(PPh_3)Br$ in catalytic processes, with the 6Mes derivative **(1)** proving an active precursor for the Kumada coupling of aryl chlorides and aryl fluorides, outperforming the larger ring 7^oTol **(7)** and 8-membered species (**8** and **9**), cationic **23** and Ni(II) derivatives $Ni(RE\ NHC)(PPh_3)Br_2$ (**17**, **18** and **28**). Preliminary EPR studies were employed to probe the catalytic cycle and these have revealed the formation of an initial Ni(I) species which remains to be properly characterised. Additional EPR, along with ENDOR measurements, are warranted to probe the structure and then subsequent reactivity of what is most likely a Ni(I)-aryl complex.

6.1 References

1. G. Berthon-Gelloz, B. de Bruin, B. Tinant and I. E. Marko, *Angew. Chem., Int. Ed.*, 2009, **48**, 3161-3164.
2. B. R. Dible, M. S. Sigman and A. M. Arif, *Inorg. Chem.*, 2005, **44**, 3774-3776.
3. B. S. Mandimutsira, J. L. Yamarik, T. C. Brunold, W. W. Gu, S. P. Cramer and C. G. Riordan, *J. Am. Chem. Soc.*, 2001, **123**, 9194-9195.
4. Y. Hoshimoto, Y. Hayashi, H. Suzuki, M. Ohashi and S. Ogoshi, *Organometallics*, 2014, **33**, 1276-1282.

CHAPTER 7

7 Experimental

7.1 General Procedures

All air-sensitive manipulations and analysis were carried out under argon using standard Schlenk line, high vacuum and glove box techniques with dried and degassed solvents, unless otherwise stated. Glassware (ampoules and NMR tubes fitted with a J. Youngs resealable PTFE valve and Schlenk flasks) was oven dried at 413 K overnight or flame dried *in vacuo*. Solvents were dried and degassed *via* purification through columns on an MBraun solvent purification system (dichloromethane, diethylether, hexane, pentane, toluene) or from i) purple solutions of sodium dispersion with benzophenone (benzene, THF), ii) Mg/I_2 (ethanol, methanol), iii) calcium hydride followed by distillation (fluorobenzene, mesitylene) and iv) P_2O_5 (*in vacuo*) and sublimed (naphthalene). All solvents and liquid reagents were stored over molecular sieves following three freeze-pump-thaw cycles. Deuterated solvents (Sigma Aldrich and Euriso-top) were vacuum transferred from potassium (benzene-d_6, toluene-d_8, THF-d_8) or calcium hydride (dichloromethane-d_2). Chloroform-d_1, H_2 (BOC, 99.9 %), CO (BOC, 99.9 %), ^{13}CO (Cambridge Isotope Laboratories, 99 %), O_2 (BOC, 99.9 %), $Ni(PPh_3)_2Br_2$ (Sigma Aldrich, 99 %), $Ni(COD)_2$ (Sigma Aldrich) and $[Ph_3C][B(C_6F_5)_4]$ (Strem Chemicals, 97 %) were all used as received. 6MesDAC,[1] $[6^{i}PrH]BF_4$,[2] $[6^{t}BuH]BF_4$[3] and all 8-membered Ni(RE NHC)(PPh_3)X (X = Br, Cl) **(8 – 10)**[4] were prepared according to the literature and kindly donated by Mr. Lee Collins (University of Bath), Dr. Michael Page (University of Bath), Miss Nicola Bramananthan (University of Bath) and Mr. Wei Lu (Cardiff University) respectively.

7.2 Physical and Analytical Techniques

All solution NMR spectra were recorded on Bruker Avance 300, 400 and 500 MHz NMR spectrometers at 298 K, unless otherwise stated, and referenced to the residual protio and ^{13}C solvent signals as follows (^{1}H; $^{13}C\{^{1}H\}$): benzene-d_6 (δ 7.15; δ 128.0), chloroform-d_1 (δ 7.26; δ 77.4), dichloromethane-d_2 (δ 5.32; δ 54.5), THF-d_8 (δ 3.58; δ 25.4) or toluene-d_8 (δ 2.04; δ 20.4). $^{31}P\{^{1}H\}$ NMR chemical shifts were referenced externally to 85 % H_3PO_4 (δ 0.0), $^{11}B\{^{1}H\}$ to 15 % $BF_3.OEt_2$ (δ 0.0) and ^{19}F to neat $CFCl_3$ (δ 0.0). 2D experiments (^{1}H COSY, ^{1}H-$^{31}C\{^{1}H\}$ HMQC, HSQC, HMBC, $^{31}P\{^{1}H\}$-$^{31}P\{^{1}H\}$ EXSY) were performed using standard Bruker pulse sequences. Evans solution magnetic susceptibility measurements were recorded in C_6H_6, THF or CH_2Cl_2 on a 500 MHz NMR spectrometer at 298 K.

IR spectra were recorded as either a nujol mull, KBr disc or in solution on a Nicolet Nexus FTIR spectrometer.

Mass spectrometry was undertaken by Dr. Anneke Luben at the University of Bath, England using a micrOTOF electrospray time-of-flight (ESI-TOF) mass spectrometer (Bruker Daltonik GmbH) coupled to a syringe driver (Hamilton). Samples, of concentration 60 μg/mL in acetonitrile, were infused at a rate of 3 μL/min and fragments detected in positive mode. The data was externally calibrated using sodium formate clusters at a concentration of 5 mM, which acted as a calibrant over the mass range 50 – 2500 *m/z*.

CW X-band EPR spectra were recorded by Professor Damien Murphy and Dr. Emma Carter at Cardiff University, Wales on a Bruker EMX spectrometer equipped with a high sensitivity cavity (ER 4119HS), operating at 100 kHz field modulation and a microwave power of 10 mW. CW Q-band EPR/ENDOR spectra were recorded at 10 K on a Bruker ESP 300E series spectrometer equipped with an ESP360 DICE ENDOR unit, operating at 12.5 kHz field modulation in a Q-band ENDOR cavity (Bruker ER 5106 QT-E). The ENDOR spectra were obtained using 8 dB RF power from an ENI A-300 RF amplifier, with 50 or 200 kHz RF modulation depth and 1 mW microwave power. Accurate ***g*** values were obtained using an NMR Gaussmeter (Bruker ER 035 M) calibrated using the perylene radical cation in concentrated H_2SO_4 (***g*** = 2.002569). Pulsed X-band ENDOR experiments were performed on a Bruker E580 Elexsys spectrometer (operating at 9.76 GHz) equipped with a liquid helium cryostat from Oxford Inc. The magnetic field was measured with a Bruker ER035M NMR Gaussmeter. All EPR samples were prepared in a concentration of 1 mg/μL in dry THF and sealed in a glove box.

DFT calculations were carried out at Heriot-Watt University by Professor Stuart Macgregor and Dr. Andrés Algarra and run with Gaussian 09 (Revision A.0.2)[5] and employed the B3LYP hybrid functional.[6-8] SDD pseudopotentials and associated basis sets were used for Ni,[9] P and Br[10] (with *d* orbital polarisation on P and Br[11]) and 6-31g** basis sets in all other atoms.[12,13] Geometries were based on the heavy atoms positions determined by X-ray crystallography with H atom positions being optimised using the above level of theory.

X-ray crystal structures were recorded on a Nonius KappaCCD diffractometer or an Oxford Diffraction Gemini diffractometer, with structural solutions and refinements performed using SHELXS-97[14] and SHELXL-97[14] respectively.

SQUID measurements were collected at the University of Ottawa, Canada by Jennifer Le Roy and Professor Muralee Murugesu on a Quantum Design SQUID magnetometer (MPMS-XL7) operating between 1.8 and 300 K for dc applied fields ranging from -7 to 7 T.

CV experiments were carried out at The Institute of Chemical Research (ICIQ), Spain by Mr. Isidoro López in an MBraun glove box (O_2 < 0.1 ppm, H_2O = 0.3 ppm) using a IJ-Cambria CHI-660 potentiostat with anhydrous inhibitor free THF (containing 0.1 M [^{n}Bu$_4$N]PF$_6$) as solvent. Glassy carbon disks were used as the working electrode, platinum wire as a counter electrode and Ag/$AgNO_3$ solution as a quasi-reference electrode. The CVs were run at 150 mV s^{-1} scan rate, with the potentials referenced to ferrocene (added at the end of each experiment) and subsequently converted to NHE.

UV-visible spectroscopy was also performed at ICIQ by Mr. Isidoro López on a CARY 50 (Varian) UV-visible spectrophotometer using an all-quartz immersion probe with 1 cm optical path length from Hellma. The temperature was kept constant at 190 K by means of a liquid N_2/acetone bath and monitored by a low temperature thermometer. Kinetic data were processed by use of the program SPECFIT/32 Global Analysis System, which uses the method of Singular Value Decomposition (SVD).

Cryoscopic measurements were carried out by Professor Dominic Wright at the University of Cambridge, England using nitrobenzene.

Elemental analyses were performed by the Elemental Analysis Service, London Metropolitan University, London.

7.3 Preparation of RE NHC Precursors

All the 6- and 7-membered RE NHC precursors (pyrimidinium and diazepinium salts respectively) were synthesised *via* a formamidine route adapted from literature published by Cavell and coworkers.[15-18] All syntheses were carried out open to air.

7.3.1 Preparation of 1,3-bis(2,4,6-trimethylphenyl)-3,4,5,6-tetrahydropyrimidin-1-ium tetrafluoroborate ([6MesH]BF_4)

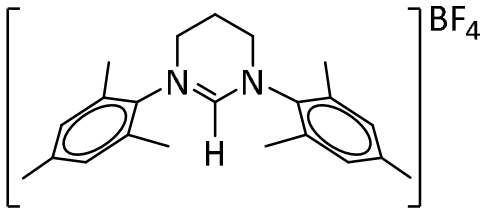

7.3.1.1 Preparation of N,N'-bis(2,4,6-trimethylphenyl)formamidine

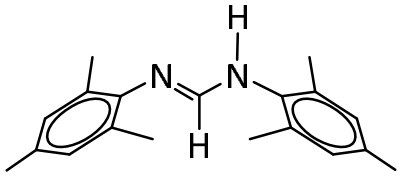

2,4,6-Trimethylaniline (20.0 mL, 0.130 mol) and triethyl orthoformate (9.9 mL, 0.065 mol) were charged in distillation apparatus and heated at 413 K for 2 h. After all the ethanol generated was distilled off, the resulting orange precipitate was cooled and washed with Et_2O (2 x 50 mL), leaving a white precipitate of desired product which was dried *in vacuo*. Yield: 14.2 g (65 %). ^{1}H NMR ($CDCl_3$, 500 MHz): δ 7.20 (s, 1H, NC*H*N), 7.18 (s, 1H, N*H*), 6.91 (s, 4H, *m*-CH_{aryl}), 2.27 (s, 6H, *p*-CH_3), 2.20 (s, 12H, *o*-CH_3).

7.3.1.2 Preparation of 1,3-bis(2,4,6-trimethylphenyl)-3,4,5,6-tetrahydropyrimidin-1-ium tetrafluoroborate ([6MesH]BF_4)

N,N'-*bis*(2,4,6-trimethylphenyl)formamidine (14.2 g, 0.051 mol), 1,3-dibromopropane (5.1 mL, 0.051 mol) and K_2CO_3 (6.8 g, 0.051 mol) were dissolved in MeCN (100 mL) and refluxed overnight. The solvent was removed *via* a rotary evaporator and the resulting white powder extracted into CH_2Cl_2 (30 mL) and filtered to removed excess K_2CO_3. Et_2O (50 mL) was added to crash out a white precipitate of [6MesH]Br. Yield: 16.2 g (80 %). All of this pyrimidinium bromide salt (16.2 g, 0.040 mol) was fully dissolved in MeCN (150 mL) and a solution of $NaBF_4$ (4.9 g, 0.045 mol) in H_2O (70 mL) was added and left stirring for 1 h. After removing the solvents *in vacuo*, the white residue was extracted into CH_2Cl_2 (100 mL) and washed with H_2O (3 x 80 mL). The CH_2Cl_2 solution was dried with $MgSO_4$ and Et_2O (150 mL) added to yield a white precipitate of [6MesH]BF_4. Yield: 10.6 g (64 %). ^{1}H NMR ($CDCl_3$, 300 MHz): δ 7.48 (s, 1H, NC*H*N), 6.93 (s, 4H, *m*-CH_{aryl}), 3.88 (t, $^3J_{HH}$ = 5.6 Hz, 4H, NCH_2), 2.54 (quin, $^3J_{HH}$ = 5.6 Hz, 2H, NCH$_2$CH_2), 2.28 (s, 12H, *o*-CH_3), 2.25 (s, 6H, *p*-CH_3).

7.3.2 Preparation of 1,3-bis(2-methylphenyl)-3,4,5,6-tetrahydropyrimidin-1-ium tetrafluoroborate ([6^{o}TolH]BF$_4$)

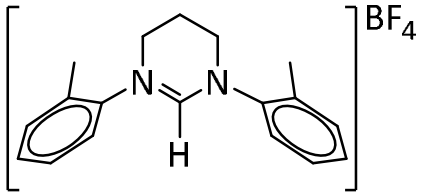

7.3.2.1 Preparation of N,N'-bis(2-methylphenyl)formamidine

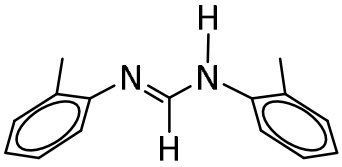

Method as for N,N'-*bis*(2,4,6-trimethylphenyl)formamidine (section **7.3.1.1**), but using 2-methylaniline (17.5 mL, 0.164 mol) and triethyl orthoformate (13.5 mL, 0.081 mol) to form a white solid of desired product. Yield: 11.5 g (63 %). ^{1}H NMR ($CDCl_3$, 300 MHz): δ 8.06 (s, 1H, NC*H*N), 7.18 – 7.02 (m, 9H, C*H*$_{aryl}$ and N*H*), 2.32 (s, 6H, C*H*$_3$).

7.3.2.2 Preparation of 1,3-bis(2-methylphenyl)-3,4,5,6-tetrahydropyrimidin-1-ium tetrafluoroborate ([6^{o}TolH]BF$_4$)

Method as for [6MesH]BF_4 (section **7.3.1.2**), but using N,N'-*bis*(2-methylphenyl)formamidine (2.2 g, 0.010 mol), 1,3-dibromopropane (1.0 mL, 0.010 mol) and K_2CO_3 (0.65 g, 0.005 mol) in MeCN (50 mL) to generate a white precipitate of [6^{o}TolH]Br. Yield: 1.56 g (46 %). Identical anion exchange reaction conditions applied for [6MesH]BF_4 were then employed, using [6^{o}TolH]Br (1.37 g, 0.004 mol) in MeCN (50 mL) and $NaBF_4$ (0.52 g, 0.045 mol) in H_2O (30 mL) to generate [6^{o}TolH]BF_4 as a white solid. Yield: 0.57 g (54 %). ^{1}H NMR ($CDCl_3$, 300 MHz): δ 7.75 (d, $^3J_{HH}$ = 8.0 Hz, 2H, *o*-C*H*$_{aryl}$), 7.62 (s, 1H, NC*H*N), 7.31 - 7.17 (m, 6H, *m*,*p*-C*H*$_{aryl}$), 4.02 (t, $^3J_{HH}$ = 5.4 Hz, 4H, NC*H*$_2$), 2.54 (quin, $^3J_{HH}$ = 5.4 Hz, 2H, NCH_2CH_2), 2.34 (s, 6H, C*H*$_3$).

7.3.3 Preparation of 1,3-bis(2-methoxyphenyl)-3,4,5,6-tetrahydropyrimidin-1-ium tetrafluoroborate ([6°AnisH]BF$_4$)

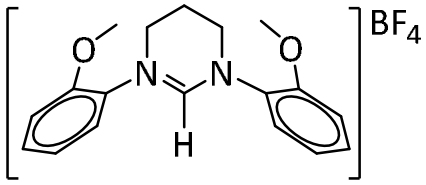

7.3.3.1 Preparation of N,N'-bis(2-methoxyphenyl)formamidine

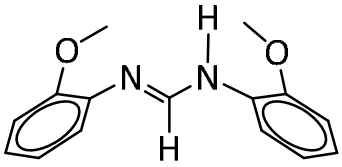

Method as for N,N'-*bis*(2,4,6-trimethylphenyl)formamidine (section **7.3.1.1**), but using 2-methoxyaniline (10.5 mL, 0.093 mol) and triethyl orthoformate (7.8 mL, 0.045 mol) to form a white precipitate of desired product. Yield: 10.6 g (44 %). ^{1}H NMR ($CDCl_3$, 500 MHz): δ 8.23 (s, 1H, NC*H*N), 7.14 (br s, 1H, N*H*), 7.09 – 6.90 (m, 8H, C*H*$_{aryl}$), 3.89 (s, 6H, OC*H*$_3$).

7.3.3.2 Preparation of 1,3-bis(2-methoxyphenyl)-3,4,5,6-tetrahydropyrimidin-1-ium tetrafluoroborate ([6°AnisH]BF$_4$)

Method as for [6MesH]BF_4 (section **7.3.1.2**), but using N,N'-*bis*(2-methoxyphenyl)formamidine (1.46 g, 0.006 mol), 1,3-dibromopropane (1.2 mL, 0.012 mol) and K_2CO_3 (0.50 g, 0.003 mol) in MeCN (140 mL) to generate a waxy white precipitate, which when recrystallised from CH_2Cl_2/Et_2O, yielded a white precipitate of [6°AnisH]Br. Yield: 1.30 g (61 %). Identical anion exchange reaction conditions applied for [6MesH]BF_4 were then employed, using [6°AnisH]Br (1.30 g, 0.003 mol) in MeCN (20 mL) and $NaBF_4$ (0.53 g, 0.005 mol) in H_2O (5 mL) to generate a white precipitate of [6°AnisH]BF_4. Yield: 0.98 g (74 %). ^{1}H NMR ($CDCl_3$, 300 MHz): δ 7.68 – 7.65 (m, 3H, C*H*$_{aryl}$ and NC*H*N), 7.40 – 7.34 (m, 2H, C*H*$_{aryl}$), 7.07 – 7.01 (m, 2H, C*H*$_{aryl}$), 6.99 – 6.96 (m, 2H, C*H*$_{aryl}$), 3.94 (t, $^3J_{HH}$ = 5.8 Hz, 4H, NC*H*$_2$), 3.90 (s, 6H, OC*H*$_3$), 2.44 (quin, $^3J_{HH}$ = 5.7 Hz, 2H, NCH_2CH_2).

7.3.4 Preparation of 1-(2-methoxyphenyl)-3-(2,4,6-trimethylphenyl)-3,4,5,6-tetrahydropyrimidin-1-ium tetrafluoroborate ([6°AnisMesH]BF$_4$)

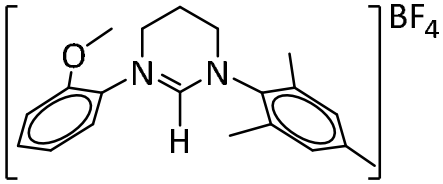

7.3.4.1 Preparation of ethyl-N-(2-methoxyphenyl)formamidate

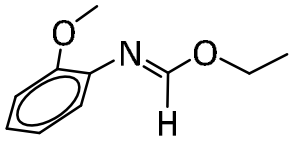

2-methoxyaniline (22.5 mL, 0.200 mol) and triethyl orthoformate (33.2 mL, 0.200 mol) were charged in distillation apparatus and heated at 393 K for 2 h. When all the ethanol generated had distilled off, the remaining triethyl orthoformate was distilled at 207 K under vacuum. The desired ethyl-N-(2-methoxyphenyl)formamidate product was then distilled off at 346 K (achieved by heating to 373 K) as a clear, colourless oil. Yield: 16.0 g (45 %). ^{1}H NMR ($CDCl_3$, 500 MHz): δ 6.59 (m, 1H, C*H*$_{aryl}$), 6.43 – 6.39 (m, 4H, C*H*$_{aryl}$ and NC*H*O), 3.89 (q, $^3J_{HH}$ = 7.3 Hz, 2H, OC*H*$_2$), 3.32 (s, 3H, OC*H*$_3$), 0.90 (t, $^3J_{HH}$ = 7.3 Hz, 3H, OCH_2CH_3).

7.3.4.2 Preparation of N-(2-methoxyphenyl)-N'-(2,4,6-trimethylphenyl)formamidine

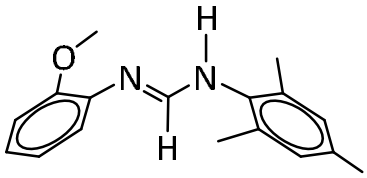

Ethyl-N-(2-methoxyphenyl)formamidate (5.38 g, 0.030 mol) and 2,4,6-trimethylaniline (4.05 g, 0.030 mol) were combined and refluxed at 323 K for 3 h. Upon cooling, the red solution solidified to give a peach coloured solid, which was recrystallised from toluene/Et_2O, washed with MeOH (50 mL) and dried *in vacuo* to afford a peach coloured precipitate of the desired product. Yield: 3.84 g (48 %). Two isomers detected. Isomer 1: ^{1}H NMR ($CDCl_3$, 400 MHz): δ 7.87 (s, 1H, NC*H*N), 7.44 (v br s, 1H, N*H*), 7.16 – 6.81 (m, 6H, C*H*$_{aryl}$), 3.91 (s, 3H, OC*H*$_3$), 2.28 (s, 3H, *p*-C*H*$_3$), 2.19 (s, 6H, *o*-C*H*$_3$). Isomer 2: ^{1}H NMR ($CDCl_3$, 400 MHz): δ 7.87 (s, 1H, NC*H*N), 7.44 (v br s, 1H, N*H*), 7.16 – 6.81 (m, 6H, C*H*$_{aryl}$), 3.73 (s, 3H, OC*H*$_3$), 2.28 (s, 3H, *p*-C*H*$_3$), 2.13 (two s, 6H, *o*-C*H*$_3$).

7.3.4.3 Preparation of 1-(2-methoxyphenyl)-3-(2,4,6-trimethylphenyl)-3,4,5,6-tetrahydropyrimidin-1-ium tetrafluoroborate ([6^{o}AnisMesH]BF$_4$)

Method as for [6MesH]BF_4 (section **7.3.1.2**), but using N-(2-methoxyphenyl)-N'-(2,4,6-trimethylphenyl)formamidine (1.13 g, 0.004 mol), 1,3-dibromopropane (0.9 mL, 0.008 mol) and K_2CO_3 (0.37 g, 0.003 mol) in MeCN (80 mL) and refluxed for 48 h to give a white precipitate of [6^{o}AnisMesH]Br. Yield: 1.33 g (81 %). Identical anion exchange reaction conditions applied for [6MesH]BF_4 were then employed, using [6^{o}AnisMesH]Br (1.33 g, 0.003 mol) in MeCN (70 mL) and $NaBF_4$ (0.40 g, 0.004 mol) in H_2O (20 mL) to generate a white precipitate of [6^{o}AnisMesH]BF_4. Yield: 1.10 g (82 %). ^{1}H NMR ($CDCl_3$, 500 MHz): δ 7.65 (d, $^3J_{HH}$ = 7.7 Hz, 1H, *m*-C*H*$_{Anis}$), 7.59 (s, 1H, NC*H*N), 7.39 (t, $^3J_{HH}$ = 8.0 Hz, 1H, *p*-C*H*$_{Anis}$), 7.08 (t, $^3J_{HH}$ = 7.6 Hz, 1H, *m*-C*H*$_{Anis}$), 7.00 (d, $^3J_{HH}$ = 8.3 Hz, 1H, *o*-C*H*$_{Anis}$), 6.96 (s, 2H, *m*-C*H*$_{Mes}$), 4.04 (t, $^3J_{HH}$ = 5.0 Hz, 2H, NC*H*$_2$), 3.89 (s, 3H, OC*H*$_3$), 3.84 (t, $^3J_{HH}$ = 5.1 Hz, 2H, NC*H*$_2$), 2.54 (quin, $^3J_{HH}$ = 5.0 Hz, 2H, NCH$_2$C*H*$_2$), 2.34 (s, 6H, *o*-C*H*$_3$), 2.29 (s, 3H, *p*-C*H*$_3$).

7.3.5 Preparation of 1,3-bis(2,4,6-trimethylphenyl)-4,5,6,7-tetrahydro-3H-[1,3]-diazepin-1-ium tetrafluoroborate ([7MesH]BF$_4$)

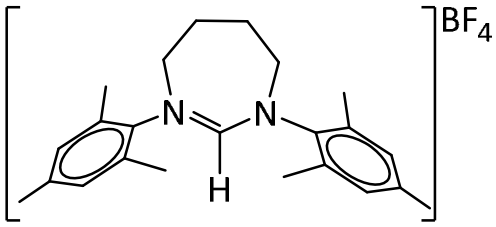

N,N'-*bis*(2,4,6-trimethylphenyl)formamidine (section **7.3.1.1**) (4.02 g, 0.014 mol), 1,4-diiodobutane (2.0 mL, 0.015 mol) and K_2CO_3 (1.98 g, 0.014 mol) were dissolved in MeCN (50 mL) and refluxed overnight. The solvent was removed *via* rotary evaporation and the resulting white powder extracted into CH_2Cl_2 (30 mL) and filtered to removed excess K_2CO_3. Et_2O (50 mL) was added to crash out a white precipitate of [7MesH]Br. Yield: 5.02 g (84 %). All of this diazepinium bromide salt (5.02 g, 0.012 mol) was fully dissolved in MeCN (80 mL) and a solution of $NaBF_4$ (1.53 g, 0.014 mol) in H_2O (30 mL) was added and left stirring for 1 h. After removal of the solvents *in vacuo*, the resulting white residue was extracted into CH_2Cl_2 (50 mL) and washed with H_2O (3 x 100 mL). The CH_2Cl_2 solution was dried with $MgSO_4$ and Et_2O (100 mL) added to yield a white precipitate of [7MesH]BF_4. Yield: 3.39 g (66 %). ^{1}H NMR ($CDCl_3$, 400 MHz): δ 7.20 (s, 1H, NC*H*N), 6.95 (s, 4H, *m*-C*H*$_{aryl}$), 4.38 (t, $^3J_{HH}$ = 5.6, 4H, NC*H*$_2$), 2.53 (br m, 4H, NCH$_2$C*H*$_2$), 2.39 (s, 12H, *o*-C*H*$_3$), 2.28 (s, 6H, *p*-C*H*$_3$)

7.3.6 Preparation of 1,3-bis(2-methylpheny)l-4,5,6,7-tetrahydro-3H-[1,3]-diazepin-1-ium tetrafluoroborate ([7^{o}TolH]BF$_4$)

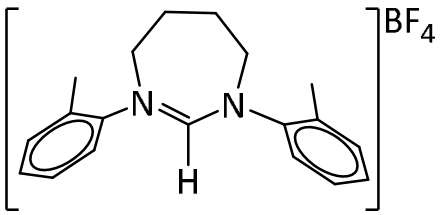

Same method as for [7MesH]BF_4 (section **7.3.5**) but with N,N'-*bis*(2-methylphenyl)formamidine (section **7.3.2.1**) (11.4 g, 0.051 mol), 1,4-diiodobutane (6.8 mL, 0.052 mol) and K_2CO_3 (7.06 g, 0.051 mol) in MeCN (200 mL) and refluxed for 48 h to give a white precipitate of [7^{o}TolH]BF_4. Yield: 15.9 g (85 %). Identical anion exchange reaction conditions applied for [7MesH]BF_4 were then employed, using [7^{o}TolH]BF_4 (15.9 g, 0.043 mol) in MeCN (50 mL) and $NaBF_4$ (4.29 g, 0.039 mol) in H_2O (35 mL) to generate a white crystalline precipitate of [7^{o}TolH]BF_4. Yield: 5.21 g (36 %). ^{1}H NMR ($CDCl_3$, 400 MHz): δ 7.71 (br s, 2H, *o*-CH_{aryl}), 7.36 (s, 1H, NC*H*N), 7.28 – 7.22 (m, 6H, *m*,*p*-CH_{aryl}), 4.34 (br s, 4H, NCH_2), 2.40 (br s, 4H, NCH_2CH_2), 2.36 (s, 6H, CH_3).

7.4 Synthesis of Low Coordinate Nickel(I) Species (Ni(RE NHC)(PPh_3)Br)

7.4.1 In Situ Generation of RE NHCs

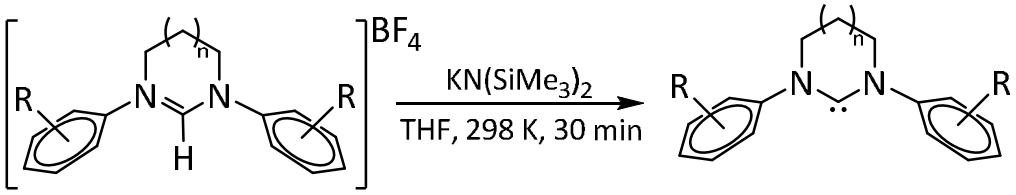

Unless otherwise described, in all the syntheses that required formation of the free RE NHC, it was generated *in situ* from reaction of equimolar amounts of the corresponding [pyrimidinium]BF_4 or [diazepinium]BF_4 salt and $KN(SiMe_3)_2$ in THF. After stirring at room temperature for 30 min the carbene solution was transferred *via* cannula to the nickel starting precursor(s).

7.4.2 Synthesis of Ni(6Mes)(PPh_3)Br (1)[19]

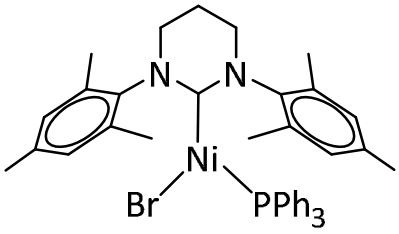

A solution of 6Mes (prepared *in situ* by stirring the pyrimidinium tetrafluoroborate salt [6MesH]BF_4 (684 mg, 1.68 mmol) with $KN(SiMe_3)_2$ (334 mg, 1.68 mmol) in THF (30 mL) for 30 min) was added to a mixture of $Ni(COD)_2$ (231 mg, 0.84 mmol) and $Ni(PPh_3)_2Br_2$ (624 mg, 0.84 mmol). The mixture was stirred at room temperature for 1 h to afford a dark yellow solution and fine beige precipitate. This suspension was filtered and hexane (30 mL) added to the filtrate to generate a yellow precipitate. The solid was isolated by filtration, washed with hexane (10 mL) and dried *in vacuo*. Analytically pure **1** was obtained by recrystallisation from THF/hexane. Yield: 920 mg (76 %). ^{1}H NMR (C_6D_6, 500 MHz): δ 30.04 (v br s, 2H), 16.05 (v br s, 1H), 10.79 (s, 7H), 9.68 (br s), 8.70 (v br s), 7.73 (br s) (10H for overlapping resonances 9.68 - 7.73), 3.96 (s, 7H), 1.90 (br s, 3H), 0.73 (v br m, 10H), -1.16 (br s, 1H), -16.67 (v br s, 2H). Anal. calcd. (found) for $C_{40}H_{43}N_2PNiBr$ (%): C 66.60 (66.45), H 6.01 (6.16), N 3.88 (3.95). Solution magnetic moment (Evans method): 2.1 μB.

7.4.3 Synthesis of Ni(6^{o}Tol)(PPh_3)Br (2)[20]

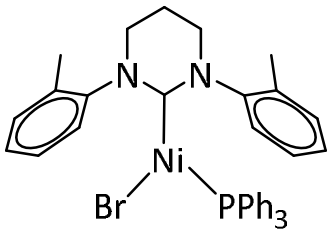

Method as for **1** (section **7.4.2**), but with [6^{o}Tol]BF_4 (153 mg, 0.58 mmol), $KN(SiMe_3)_2$ (116 mg, 0.58 mmol), $Ni(COD)_2$ (80 mg, 0.29 mmol) and $Ni(PPh_3)_2Br_2$ (215mg, 0.29 mmol) in THF (15 mL) and left stirring for 2 h to ultimately afford a yellow precipitate of **2**. Analytically pure product was achieved upon recrystallisation from C_6H_6/hexane. Yield: 220 mg (57 %). ^{1}H NMR (C_6D_6, 500 MHz): δ 31.25 (v br s), 17.66 (v br m), 11.00 (v br m), 9.28 (s), 8.74 (br m), 7.80 (br m), 7.56 (br s), 4.69 (v br s), 3.58 (s), 1.45 – 0.21 (multiple overlapping br m), -11.31 (v br s), -19.68 (v br s). Anal. calcd. (found) for $C_{36}H_{35}N_2PNiBr$ (%): C 65.00 (64.81), H 5.30 (5.21), N 4.21 (4.35).

7.4.4 Synthesis of Ni(6^{o}Anis)(PPh$_3$)Br (3)[4]

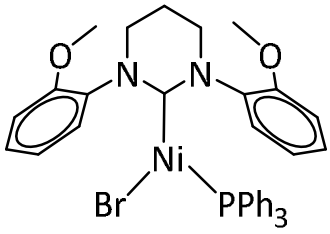

In situ generated 6^{o}Anis ([6^{o}AnisH]BF$_4$ (272 mg, 0.71 mmol) and KN(SiMe$_3$)$_2$ (141 mg, 0.71 mmol)) was transferred to a mixture of Ni(COD)$_2$ (97 mg, 0.35 mmol) and Ni(PPh$_3$)$_2$Br$_2$ (263 mg, 0.35 mmol). After stirring for 2 h at room temperature, the yellow reaction solution was filtered and hexane (50 mL) added to the filtrate to form a mottled black/yellow precipitate. This was isolated, extracted into C$_6$H$_6$ (20 mL), filtered again to remove a fine black solid, and then reprecipitated with hexane (60 mL). Another cycle of this procedure afforded **3** as a homogeneous, pale yellow precipitate, which was filtered and dried *in vacuo*. Yield: 157 mg (64 %). ^{1}H NMR (C$_6$D$_6$, 500 MHz): δ 30.56 (v br s), 17.35 (v br s), 11.04 (s), 8.48 (br s), 5.42 – 3.45 (br m), 1.26 (br s), 0.91 (br s), 0.43 (br m), -16.37 (v br s). Anal. calcd. (found) for C$_{36}$H$_{35}$N$_2$O$_2$PNiBr (%): C 62.01 (61.94), H 5.06 (5.15), N 4.02 (3.93). Solution magnetic moment (Evans method): 2.6 μB.

7.4.5 Synthesis of Ni(6^{o}AnisMes)(PPh$_3$)Br (4)[4]

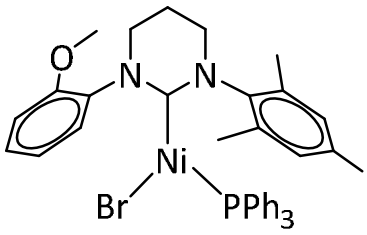

As for **1** (section **7.4.2**), but with [6^{o}AnisMesH]BF$_4$ (156 mg, 0.39 mmol), KN(SiMe$_3$)$_2$ (78 mg, 0.39 mmol), Ni(COD)$_2$ (54 mg, 0.20 mmol) and Ni(PPh$_3$)$_2$Br$_2$ (146 mg, 0.20 mmol) and for 2 h at room temperature. Yield: 119 mg (43 %). ^{1}H NMR (C$_6$D$_6$, 500 MHz): δ 36.90 (v br s), 28.85 (v br s), 15.54 (br s), 12.58 (br s), 11.10 (s), 8.60 (br m), 7.67 (br s), 4.99 (br s), 3.14 (br m), 1.29 (br s), 0.27 (s), -0.83 (br s), -13.04 (v br s), -21.82 (v br s). Anal. calcd. (found) for C$_{38}$H$_{39}$N$_2$OPNiBr (%): C 64.35 (64.41), H 5.54 (5.41), N 3.95 (4.01). Solution magnetic moment (Evans method): 2.0 μB.

7.4.6 Synthesis of Ni(6MesDAC)(PPh$_3$)Br (5)[20]

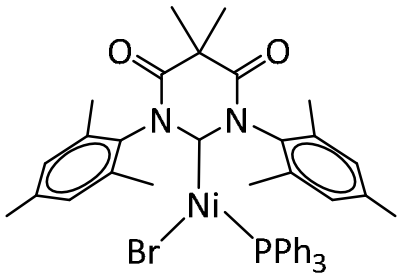

A THF (20 mL) solution of free 6MesDAC (386 mg, 1.02 mmol) was added to a mixture of $Ni(COD)_2$ (139 mg, 0.50 mmol) and $Ni(PPh_3)_2Br_2$ (381 mg, 0.51 mmol). The mixture was stirred at room temperature for 2.5 h to afford a dark orange solution. After filtration, the filtrate was concentrated and hexane (20 mL) added to precipitate a dark purple solid, which was filtered, washed with hexane (10 mL) and dried *in vacuo*. Yield: 490 mg (62 %). Dark purple X-ray quality crystals of **5** were obtained by recrystallisation from C_6H_6/hexane. ^{1}H NMR (C_6D_6, 500 MHz): δ 10.34 (br s), 9.01 (v br s), 8.35 (br s), 7.64 (br s), 7.01 – 6.70 (br m of overlapping resonances), 4.42 (br s), 3.69 (br s), 3.56 (br s), 3.25 (br s), 2.91 (v br s), 2.44 (br s), 2.33 (br s), 2.09 (br s), 1.89 (br s), 1.61 (br s), 1.41 (br s), 1.22 (br s), 1.11 (br s), 0.46 (br m), -0.02 (v br s), -0.82 (v br s). Anal. calcd. (found) for $C_{42}H_{43}N_2O_2PNiBr$ (%): C 64.89 (64.61), H 5.58 (5.39), N 3.60 (3.41). Solution magnetic moment (Evans method): 1.2 μB.

7.4.7 Synthesis of Ni(7Mes)(PPh$_3$)Br (6)

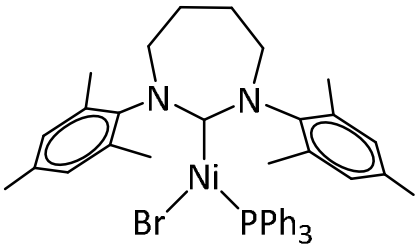

Syntheses for the 7-membered RE NHC Ni(I) analogues of Ni(RE NHC)(PPh_3)Br were identical to the corresponding 6-membered complexes **(1 – 5)**. Free 7Mes was generated *in situ* ([7MesH]BF_4 (206 mg, 0.49 mmol) and $KN(SiMe_3)_2$ (97 mg, 0.48 mmol) in THF (15 mL)) and cannula transferred to a mixture of $Ni(PPh_3)_2Br_2$ (180 mg, 0.24 mmol) and $Ni(COD)_2$ (66 mg, 0.24 mmol). After stirring at room temperature for 30 min a suspension of a dark yellow precipitate in a yellow solution was observed. This was filtered and hexane (20 mL) added to the filtrate to yield a yellow precipitate of **6**. Recrystallisation from THF/hexane provided clean **6**. Yield: 187 mg (52 %). ^{1}H NMR (C_6D_6, 500 MHz): δ 12.29 (v br s), 11.47 (v br s),

10.61 – 10.48 (overlapping br s), 9.95 – 9.71 (overlapping br s), 8.09 (v br s), 4.58 – 4.46 (overlapping br s), 3.59 (br m), 2.65 (s), 2.52 (br s), 1.61 (v br m), 0.97 (br m), -1.33 (v br s). Anal. calcd. (found) for $C_{41}H_{45}N_2PNiBr$ (%): C 66.96 (67.22), H 6.17 (6.26), N 3.81 (3.41). Solution magnetic moment (Evans method): 1.8 μB.

7.4.8 Synthesis of Ni(7^{o}Tol)(PPh$_3$)Br (7)[4]

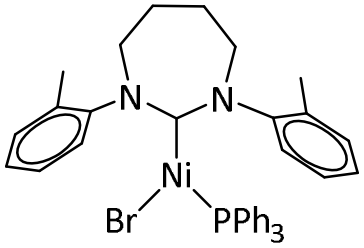

Same as **6** (section **7.4.7**), but with [7^{o}TolH]BF_4 (206 mg, 0.56 mmol), $KN(SiMe_3)_2$ (112 mg, 0.56 mmol), $Ni(COD)_2$ (77 mg, 0.28 mmol) and $Ni(PPh_3)_2Br_2$ (209 mg, 0.28 mmol). Filtration of the resulting yellow solution from a beige precipitate yielded a yellow precipitate of **7** upon addition of hexane (60 mL). This was isolated, washed with hexane (10 mL) and recrystallised from C_6H_6/hexane. Yield: 165 mg (43 %). ^{1}H NMR (C_6D_6, 500 MHz): δ 11.01 (v br s), 9.41 (s), 7.90 (br m), 4.49 (v br s), 3.28 (s), 1.92 – 0.29 (v br overlapping s and m). Anal. calcd. (found) for $C_{37}H_{37}N_2PNiBr$ (%): C 65.42 (65.38), H 5.49 (5.39), N 4.12 (4.02). Solution magnetic moment (Evans method): 1.7 μB.

7.4.9 Attempted Nickel(I) Synthesis with N-Alkyl RE NHCs

7.4.9.1 Synthesis of Ni(6^{i}Pr)$_2$Br$_2$ ***(12)***

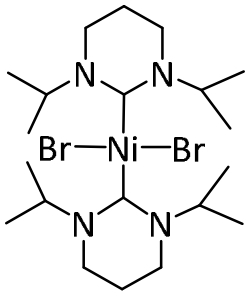

[6^{i}PrH]BF$_4$ (174 mg, 0.681 mmol) and KN(SiMe$_3$)$_2$ (136 mg, 0.682 mmol) in THF (25 mL) was charged to a mixture of Ni(COD)$_2$ (106 mg, 0.385 mmol) and Ni(PPh$_3$)$_2$Br$_2$ (264 mg, 0.355 mmol) and left to stir at 298 K for 2 h. The resulting dark orange brown solution was filtered and hexane (50 mL) added to the filtrate to precipitate a dark orange residue which was washed with hexane (2 x 10 mL). Dark red crystals appeared upon recrystallisation from THF/hexane. Yield: 24 mg (13 %). ^{1}H NMR (CD_2Cl_2, 500 MHz): δ 7.89 (m, $^{3}J_{HH}$ = 6.8 Hz, 4H, C*H*$_{iPr}$), 2.89 (t, $^{3}J_{HH}$ = 5.8 Hz, 8H, NC*H*$_2$), 1.66 (m, $^{3}J_{HH}$ = 5.8 Hz, 4H, CH$_2$C*H*$_2$), 1.42 (d, $^{3}J_{HH}$ = 6.8 Hz, 24H, C*H*$_3$). Anal. calcd. (found) for $C_{20}H_{40}N_4NiBr_2$ (%): C: 43.06 (43.12), H: 7.70 (7.60), N: 9.94 (10.06).

7.5 Reactivity of Ni(RE NHC)(PPh_3)Br with O_2

7.5.1 Synthesis of Ni(6Mes)Br(μ-OH)(μ-O-6Mes)'NiBr (13) and [NiBr(μ-O-6Mes)']$_2$ (15)[20]

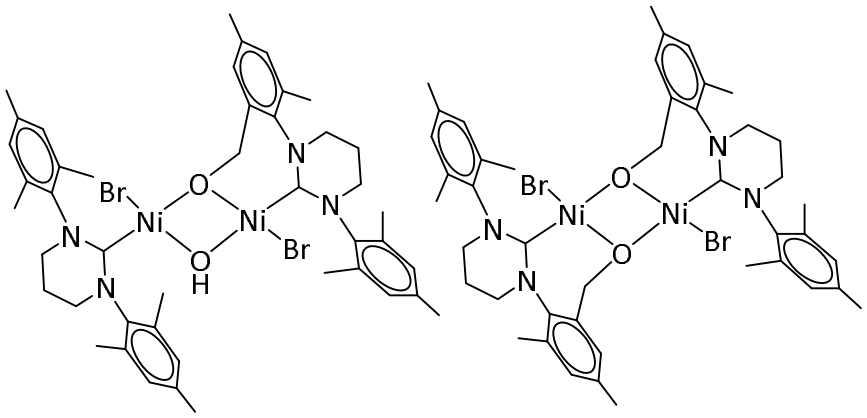

A THF (15 mL) solution of **1** (140 mg, 0.194 mmol) was freeze-pump-thaw degassed three times and the yellow solution exposed to of O_2 (1 atm), leading to the instantaneous formation of a purple coloured solution. After stirring for 5 min, the solvent was removed under vacuum and the residue washed with hexane (10 mL). Dissolution in C_6H_5F (10 mL) and addition of hexane (20 mL) with vigorous stirring overnight yielded **13** as a purple microcrystalline solid. Yield: 47.5 mg (52 %). Crystals appropriate for X-ray crystallography were grown from THF/hexane. Anal. calcd. (found) for $C_{44}H_{56}N_4O_2Br_2Ni_2$ (%): C 55.62 (55.39), H 5.94 (5.94), N 5.90 (5.85). IR (nujol, cm^{-1}): 3401 (ν_{OH}). Solution characterisation, consisting of ^{1}H NMR and mass spectrometry, on this microcrystalline solid indicated **15** was also present. ^{1}H NMR (CD_2Cl_2, 500 MHz): δ 8.31 (br s), 7.83 (br s), 7.30 (br s), 7.46 – 7.37 (br m), 7.04 – 6.97 (br m), 4.13 (br s), 3.20 – 2.21 (br m of overlapping resonances), 1.88 (br s), 1.67 (br s), 1.29 (br s) 0.90 (br s), 0.12 (br s), -6.19 (br s, O*H*$_{(13)}$). Total integration of all ^{1}H signals to O*H*$_{(13)}$ is 103:1. No $[MH]^+$ for **13** or **15** was observed in the ESI-MS, however, the expected isotope pattern for the presence of both compounds was detected at $[M_{(13)} - HBr + H]^+$. ESI-MS calcd. (found) for $[C_{44}H_{56}N_4O_2BrNi_2]^+$ (*m/z*): 867.2106 (867.2231).

7.5.2 Synthesis of Ni(7Mes)Br(μ-OH)(μ-O-7Mes)'NiBr (14) and [NiBr(μ-O-7Mes)']$_2$ (16)[20]

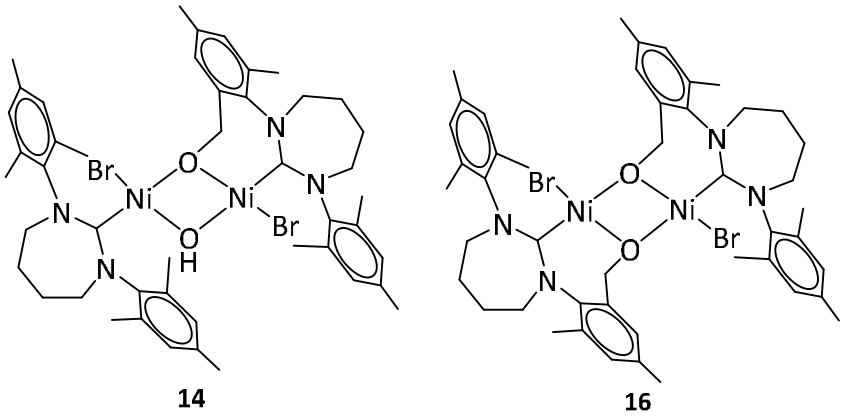

Method as for **13** and **15** (section **7.5.1**), but with **6** (162 mg, 0.22 mmol). Yield of microcrystalline solid: 56.5 mg (52 %). X-ray quality crystals of **14** were grown from this isolated solid out of CH_2Cl_2/hexane. Anal. calcd. (found) for $C_{46}H_{60}N_4O_2Br_2Ni_2$ (%): C 55.62 (56.29), H 5.94 (5.97), N 5.90 (5.87). IR (nujol, cm^{-1}): 3436 (ν_{OH}). ^{1}H NMR and mass spectrometry analysis again alluded to a mixture of **14** and **16** in solution. ^{1}H NMR (CD_2Cl_2, 400 MHz): δ 7.74 – 7.42 (br m of overlapping resonances), 6.69 (v br m), 4.99 (br s), 4.35 (br s), 4.09 (br s), 3.74 (br m), 2.86 – 1.81 (br m of overlapping resonances), 1.40 (br s), 0.07 (br s), -8.84 (br s, O*H*$_{(14)}$). Total integration of all hydrogens:O*H*$_{(14)}$ is 229:1. No $[MH]^+$ for **14** or **16** was observed in the ESI-MS, however, the expected isotope pattern for the presence of both compounds was detected at $[M_{(16)} - HBr + H]^+$. ESI-MS calcd. (found) for $[C_{46}H_{58}N_4O_2BrNi_2]^+$ (*m/z*): 897.7615 (897.2520).

7.5.3 Reaction of Ni(6MesDAC)(PPh_3)Br (5) with O_2[20]

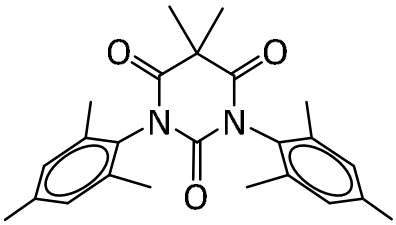

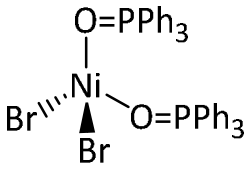

A THF (10 mL) solution of **5** (97 mg, 0.13 mmol) was freeze-pump-thaw degassed (three cycles) and the solution opened to O_2 (1 atm). A colour change from dark orange-red to nearly colourless ensued in < 1 min. After stirring for 5 min, the solution was reduced to dryness and the residue washed with hexane (10 mL) to afford a creamy-green material. Recrystallisation from CH_2Cl_2/hexane generated 70 mg of a mixture, comprising of the already reported $Ni(O{=}PPh_3)_2Br_2$[21] and (6MesDAC)=O.[22] Both could be simultaneously crystallised from CH_2Cl_2/Et_2O, yielding colourless crystals of (6MesDAC)=O, while green for $Ni(O{=}PPh_3)_2Br_2$. ^{1}H NMR (CD_2Cl_2, 400 MHz): δ 7.82 (br s), 7.03 (br s), 6.72* (s, 4H), 2.07* (s, 12H), 2.05* (s, 6H), 1.61* (s, 6H). The resonances marked * match with those reported for (6MesDAC)=O.[22]

7.5.4 Synthesis of Ni(6^{o}Tol)(PPh_3)Br_2 (17)[20]

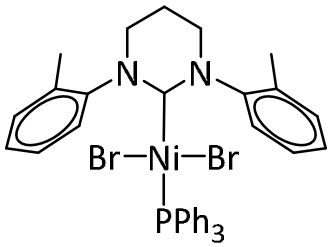

Exposure of a freeze-pump-thaw degassed (three cycles) THF solution (10 mL) of **2** (41 mg, 0.062 mmol) to O_2 (1 atm) led to an instantaneous colour change from yellow to red-pink. Removal of the solvent *in vacuo* gave a purple/red residue, which was washed with hexane (10 mL), dissolved in C_6H_5F (10 mL) and layered with hexane (20 mL) to give **17** as a purple microcrystalline solid. Yield: 9 mg (20 %). Alternatively, a toluene solution (20 mL) of 6^{o}Tol (prepared *in situ* by reaction of the pyrimidinium salt [6^{o}TolH]BF_4 (345 mg, 1.30 mmol) and $KN(SiMe_3)_2$ (257 mg, 1.29 mmol)) was added to a toluene solution (10 mL) of $Ni(PPh_3)_2Br_2$ (959 mg, 1.29 mmol). The mixture was stirred at room temperature for 1 h to give a dark purple solution. After cannula filtration, the volatiles were removed under vacuum and the residue washed with hexane (15 mL). The resulting purple-green residue was recrystallised repeatedly from toluene/hexane to remove all traces of [6^{o}TolH][$Ni(PPh_3)Br_3$] (section **7.5.4.1**)

and leave solely **17**. Yield 141 mg (15%). ^{1}H NMR ($CDCl_3$, 500 MHz): δ 8.66 (br s), 8.58 (br s), 7.79 (br m), 7.69 (br m), 7.59 – 7.54 (v br m of overlapping signals), 7.35 (br s), 3.69 – 3.56 (br m of overlapping signals), 2.53 (br s), 2.50 (br s), 2.30 (v br s), 1.74 (v br s), 1.35 (v br s), 0.98 (br s), 0.62 – 0.54 (br m of overlapping resonances), 0.17 (br s). ^{31}P{^{1}H} NMR (CD_2Cl_2, 162 MHz): δ 17.3 (s, *P*PH_3), 16.6 (s, *P*PH_3). ^{13}C{^{1}H} NMR (CD_2Cl_2, 126 MHz): δ 194.1 (d, $^{2}J_{CP}$ = 122 Hz, NCN), 193.7 (d, $^{2}J_{CP}$ = 123 Hz, NCN), 146.3 (s, N-*C*$_{ipso}$), 145.9 (s, N-*C*$_{ipso}$), 137.7 (s), 136.9 (s), 135.2 (br m), 132.9 (s), 132.6 (s), 131.9 (s), 131.7 (s) 129.7 (s), 128.6 (s), 128.4 (s), 127.8 (s), 127.7 (s), 127.0 (s), 126.7 (s), 49.4 (s, NCH_2), 49.0 (s, NCH_2), 21.3 (s, NCH_2CH_2), 20.2 (s, *o*-CH_3), 19.8 (s, *o*-CH_3). Anal. calcd. (found) for $C_{36}H_{35}N_2PNiBr_2$ (%): C 58.03 (57.85), H 4.73 (4.83), N 3.76 (3.69). Solution magnetic moment (Evans method): 0.6 μB.

7.5.4.1 Characterisation of [6^{o}TolH][Ni(PPh$_3$)Br$_3$]^{20}

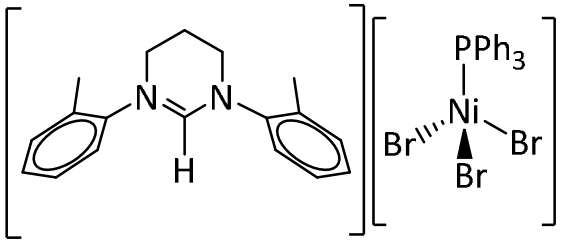

A toluene solution (20 mL) of 6^{o}Tol (prepared *in situ* by reaction of [6^{o}TolH]BF_4 (345 mg, 1.30 mmol) with $KN(SiMe_3)_2$ (257 mg, 1.29 mmol) was added to a toluene solution (10 mL) of $Ni(PPh_3)_2Br_2$ (959 mg, 1.29 mmol). The mixture was stirred at room temperature for 1 h. After cannula filtration, the volatiles were removed under vacuum and the residue washed with hexane (15 mL). The resulting purple-green residue was extracted with toluene (10 mL), reduced to dryness and recrystallised from toluene/hexane to afford the Ni(II) complex **17**. The filtrate was removed, reduced to dryness and recrystallised from CH_2Cl_2/hexane to give X-ray quality crystals of [6^{o}TolH][Ni(PPh$_3$)Br$_3$]. Yield 15 mg (2 %). ^{1}H NMR (CD_2Cl_2, 500 MHz): δ 19.55 (br s), 12.57 (v br s), 10.48 (br s), 9.38 (v br s), 8.20 (s), 8.06 (s), 7.96 (s), 7.57 (br m), 4.10 (br s), 2.94 (v br s), 0.48 (br m), 0.10 (s), -4.85 (br s). Anal. calcd. (found) for $C_{36}H_{36}N_2PNiBr_3$ (%): C 52.34 (52.17), H 4.39 (4.49), N 3.39 (3.56).

7.5.5 Synthesis of Ni(7^{o}Tol)(PPh$_3$)Br$_2$ (18)[20]

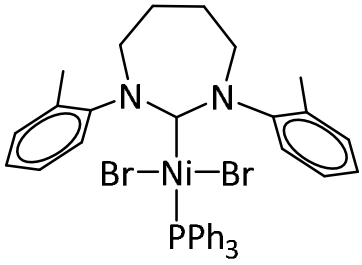

Same method as for **17** (section **7.5.4**), by reaction of **7** (47 mg, 0.069 mmol) with O_2 (1 atm) to give 10 mg (38 %) of **18**. The alternative route to **17** could also be applied to **18**, starting with addition of a toluene solution (20 mL) of 7^{o}Tol (prepared *in situ* by reaction of [7^{o}TolH]BF_4 (200 mg, 0.55 mmol) with $KN(SiMe_3)_2$ (110 mg, 0.55 mmol)) to a toluene solution (5 mL) of $Ni(PPh_3)_2Br_2$ (406 mg, 0.55 mmol). Yield: 47 mg (12 %). ^{1}H NMR (C_6D_6, 400 MHz): δ 9.15 (br d, *J* = 7.5 Hz), 9.05 (br d, *J* = 8.0 Hz), 8.93 (br d, *J* = 7.0 Hz), 8.84 (br d, *J* = 7.5 Hz), 7.49 (br m), 7.39 (br m), 7.32 – 7.28 (br m), 7.00 (br s), 3.57 (br t, *J* = 11.7 Hz), 3.37 (br m), 3.17 (br m), 2.89 (br s), 2.85 (br s), 2.49 (br s), 2.39 (br s), 2.09 (br s), 2.03 (br m), 1.29 (v br m), 0.99 (br d, *J* = 8.0 Hz), 0.28 (br s). ^{31}P{^{1}H} NMR (C_6D_6, 162 MHz): δ 21.4 (s, *P*PH_3), 21.3 (s, *P*PH_3), 20.3 (s, *P*PH_3), 17.5 (s, *P*PH_3), 16.7 (s, *P*PH_3). ^{13}C{^{1}H} NMR (C_6D_6, 100 MHz): δ 206.7 (d, $^2J_{CP}$ = 123 Hz, NCN), 148.7 (s), 147.4 (s), 147.1 (s), 137.4 (s), 137.2 (s), 135.6 (s), 135.5 (s), 133.0 (s), 131.6 (s), 129.2 (s) 127.6 (d, J_{CP} = 9 Hz), 126.7 (s), 56.0 (s, *C*H_2), 55.9 (s, *C*H_2), 55.7 (s, *C*H_2), 55.6 (s, *C*H_2), 25.5 (s, *C*H_2), 23.7 (s, *C*H_2), 21.4 (s, *o*-*C*H_3), 20.8 (s, *o*-*C*H_3), 20.6 (s, *o*-*C*H_3), 20.1 (s, *o*-*C*H_3). Anal. calcd. (found) for $C_{37}H_{37}N_2PNiBr_2$ (%): C 58.69 (58.54), H 4.93 (5.05), N 3.69 (3.60). Solution magnetic moment (Evans method): 0.6 μ_B.

7.6 Reactivity of Ni(6Mes)(PPh_3)Br (1)

7.6.1 Synthesis of [Ni(6Mes)$_2$]Br (19)[23]

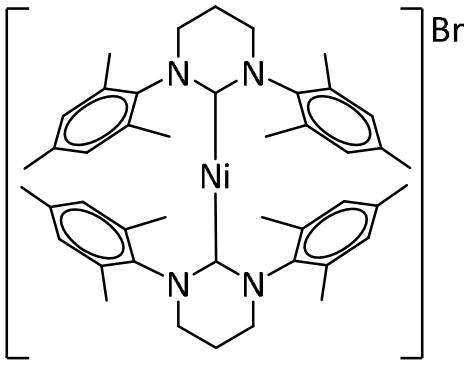

A solution of the free 6Mes carbene was prepared *in situ* by addition of $KN(SiMe_3)_2$ (102 mg, 0.51 mmol) to a solution of the pyrimidinium salt [6MesH]BF_4 (208 mg, 0.51 mmol) in THF (10 mL). After 30 min, the solution was added to a sample of **1** (242 mg, 0.34 mmol) and stirred overnight at room temperature to give a brown precipitate suspended in a beige solution. The precipitate was isolated by cannula filtration and washed with hexane (10 mL). The resulting residue was extracted into CH_2Cl_2 (15 mL) and hexane (15 mL) added to give a cream precipitate of **19**. Analytically pure material was isolated by slow recrystallisation from CH_2Cl_2/hexane. Yield: 160 mg (62 %). ^{1}H NMR (CD_2Cl_2, 500 MHz): δ 52.5 (br s, 4H, NCH_2CH_2), 50.0 (br s, 8H, NCH_2), -10.5 (s, 12H, *p*-CH_3), -12.7 (v br s, 24H, *o*-CH_3), -20.7 (br s, 8H, CH_{aryl}). Anal. calcd. (found) for $C_{44}H_{56}N_4NiBr$ (%): C 67.79 (67.86), H 7.24 (7.24), N 7.19 (6.98). ESI-MS calcd. (found) for $[C_{44}H_{56}N_4Ni]^+$ (*m/z*): 698.3853 (698.3985). Solution magnetic moment (Evans method): 3.3 μ_B. Solid magnetic moment (Gouy method): 2.7 μB. Cryoscopy (nitrobenzene): 0.53 molecular weight fraction.

7.6.2 Synthesis of Ni(6Mes)$_2$ (20)[23]

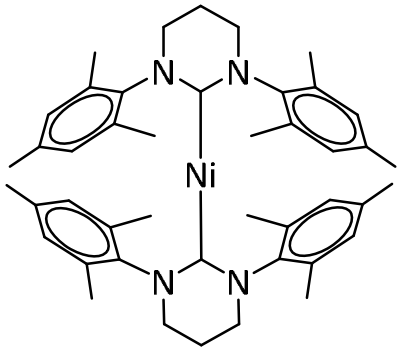

A THF (5 mL) solution of **19** (53 mg, 0.052 mmol) and excess KC_8 (30 mg, 0.22 mmol) was stirred at room temperature overnight to give a very dark purple solution. This was reduced to dryness and the residue extracted into hexane (2 x 10 mL). After filtering through celite in a glove box, the volatiles were removed *in vacuo* to give a very air-sensitive purple residue of **20**. Yield: 23 mg (63 %). The compound could be recrystallised from a concentrated solution in hexane at 243 K. ^{1}H NMR (THF-d_8, 400 MHz, 183 K): δ 6.75 (s, 8H, CH_{aryl}), 2.46 (br s, 8H, NCH_2), 2.28 (s, 12H, *p*-CH_3), 1.86 (s, 24H, *o*-CH_3), 1.80 (br s, 4H, NCH$_2$CH_2). ^{13}C{^{1}H} NMR (THF-d_8, 100 MHz, 183 K): δ 207.8 (s, NCN), 144.4 (s, N-C_{ipso}), 136.0 (s, *o*-C_{Mes}), 134.8 (s, *p*-C_{Mes}), 129.3 (s, *m*-CH_{aryl}), 43.8 (s, NCH$_2$), 22.5 (s, NCH$_2$CH$_2$), 21.8 (s, *p*-CH_3), 19.4 (s, *o*-CH_3). Anal. calcd. (found) for $C_{44}H_{56}N_4Ni$ (%): C 75.54 (75.46), H 8.07 (8.13), N 8.01 (7.92).

7.6.3 Synthesis of [Ni(6Mes)(7Mes)]Br

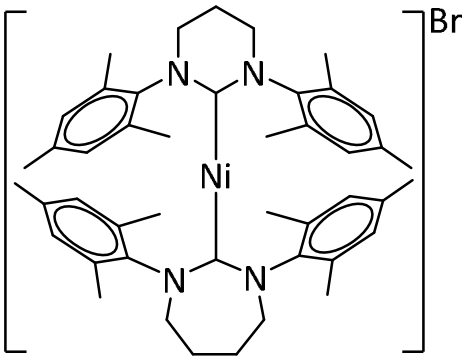

Method as for **19** (section **7.6.1**), but with addition of free 7Mes carbene (prepared *in situ* from [7MesH]BF$_4$ (161 mg, 0.38 mmol) and KN(SiMe$_3$)$_2$ (76 mg, 0.38 mmol) in THF (10 mL)) to **1** (160 mg, 0.22 mmol) to generate a cream precipitate of [Ni(6Mes)(7Mes)]Br. Yield: 130 mg (74 %). ^{1}H NMR (CD_2Cl_2, 500 MHz): δ 51.36 (br s, 4H, NC$H_{2(6Mes)}$ or NC$H_{2(7Mes)}$ or NCH$_2$C$H_{2(7Mes)}$), 48.84 (br s, 2H, NCH$_2$C$H_{2(6Mes)}$), 47.09 (br s, 4H, NC$H_{2(6Mes)}$ or NC$H_{2(7Mes)}$ or NCH$_2$C$H_{2(7Mes)}$), 41.14

(br s, 4H, NC*H*$_{2(6Mes)}$ or NC*H*$_{2(7Mes)}$ or NCH$_2$C*H*$_{2(7Mes)}$), -8.82 (s, 6H, *p*-C*H*$_{3(6\text{- or }7Mes)}$), -9.28 (s, 6H, *p*-C*H*$_{3(6\text{- or }7Mes)}$), -11.35 (v br s, 12H, *o*-C*H*$_{3(6\text{- or }7Mes)}$), -12.06 (v br s, 12H, *o*-C*H*$_{3(6\text{- or }7Mes)}$), -17.43 (br s, 4H, C*H*$_{aryl(6\text{- or }7Mes)}$), -20.41 (br s, 4H, C*H*$_{aryl(6\text{- or }7Mes)}$). Anal. calcd. (found) for $C_{45}H_{58}N_4NiBr$ (%): C 68.11 (68.21), H 7.37 (7.29), N 7.06 (6.97). ESI-MS calcd. (found) for $[C_{45}H_{58}N_4Ni]^+$ (*m/z*): 712.4009 (712.3966). Solution magnetic moment (Evans method): 0.6 μB.

7.6.4 Synthesis of Ni(6Mes)(7Mes)

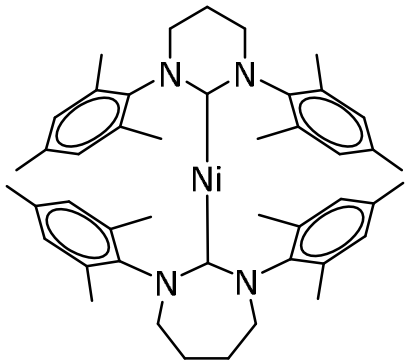

As for **20** (section **7.6.2**), but with [Ni(6Mes)(7Mes)]Br (73 mg, 0.092 mmol) and KC_8 (35 mg, 0.26 mmol) in THF (5 mL) to generate a purple residue of product Ni(6Mes)(7Mes). Yield: 43 mg (86 %). The compound could be recrystallised from a concentrated solution in hexane chilled at 243 K. ^{1}H NMR (THF-d_8, 500 MHz): δ 6.70 (br s, 8H, C*H*$_{aryl}$), 2.98 (br s, 4H, NC*H*$_{2(6\text{- or }7Mes)}$ or NCH$_2$C*H*$_{2(7Mes)}$), 2.54 (br s, 4H, NC*H*$_{2(6\text{- or }7Mes)}$ or NCH$_2$C*H*$_{2(7Mes)}$), 2.26 (s, 6H, *p*-C*H*$_{3(6\text{- or }7Mes)}$), 2.24 (s, 6H, *p*-C*H*$_{3(6\text{- or }7Mes)}$), 1.96 (s, 12H, *o*-C*H*$_{3(6\text{- or }7Mes)}$), 1.90 (s, 12H, *o*-C*H*$_{3(6\text{- or }7Mes)}$), 1.83 (br s, 2H, NCH$_2$C*H*$_{2(6Mes)}$), 1.64 (br s, 4H, NC*H*$_{2(6\text{- or }7Mes)}$ or NCH$_2$C*H*$_{2(7Mes)}$). ^{13}C{^{1}H} NMR (THF-d_8, 125 MHz): δ 217.2 (NCN), 213.3 (NCN), 147.3 (NC$_{ipso}$), 144.4 (NC$_{ipso}$), 136.0 (*o*-C$_{Mes}$), 135.7 (*o*-C$_{Mes}$), 135.2 (*p*-C$_{Mes}$), 134.1 (*p*-C$_{Mes}$), 129.8 (*m*-CH), 129.4 (*m*-CH), 52.7 (CH$_2$), 44.5 (CH$_2$), 27.2 (CH$_2$), 22.5 (CH$_2$), 21.6 (*p*-CH$_3$), 21.5 (*p*-CH$_3$), 19.9 (*o*-CH$_3$), 19.0 (*o*-CH$_3$). Anal. calcd. (found) for $C_{45}H_{58}N_4Ni$ (%): C 75.73 (75.79), H 8.19 (8.06), N 7.85 (7.76).

7.6.5 Formation of [Ni(6Mes)(η^2-$C_6H_5CH_3$)][$B(C_6F_5)_4$] (21)

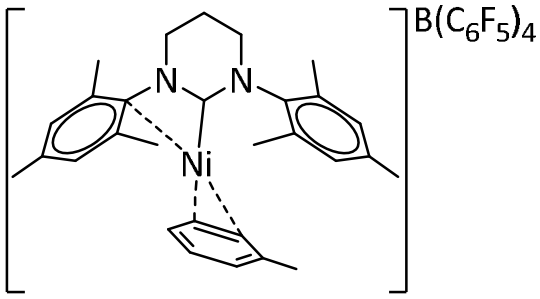

With the whole reaction being carried out in a glove box, bright yellow [Ph_3C][$B(C_6F_5)_4$] (75 mg, 0.081 mmol) was suspended in excess Et_3SiH (2 mL) and stirred for 48 h, leaving a white solid of the reactive cation [Et_3Si]$^+$.* Excess silane was filtered off, the precipitate washed with hexane (5 x 1.5 mL) and left to dry overnight. A yellow C_6H_5F (2mL) solution of **1** (59 mg, 0.082 mmol) was directly added to the cation, instantaneously turning a deep red. Layering this with toluene produced pale green crystals, which were recrystallised from THF/toluene to give 46 mg of compound. X-ray crystallographic characterisation established the crystals to be a mixture of **21** and [6MesH]$^{\cdots}$($C_6H_5CH_3$)[$B(C_6F_5)_4$] in a ratio of 65:35. ^{1}H NMR (THF-d_8, 500 MHz): δ 8.48 (s, 1H, $C_{NHC}H$ from [6MesH]$^{\cdots}$($C_6H_5CH_3$)[$B(C_6F_5)_4$]), 7.18 (m, 2H, CH_{Mes}), 7.13 (m, 2H, CH_{Mes}), 7.08 (br s, 5H, CH_{tol}), 3.88 (t, $^3J_{HH}$ = 4.8 Hz, 4H, NCH_2), 2.58 (quin, $^3J_{HH}$ = 4.8 Hz, 2H, NCH_2CH_2), 2.33 (br s, 12H, *o*-C$H_{3(Mes)}$), 2.30 – 2.28 (br m, 9H, *p*-C$H_{3(Mes)}$ and C$H_{3(tol)}$). ^{11}B{^{1}H} NMR (THF-d_8, 160 MHz): δ -18.4 (s, [Ni(6Mes)(η^2-$C_6H_5CH_3$)][$B(C_6F_5)_4$]$^-$), -16.6 (s, [6MesH]$^{\cdots}$($C_6H_5CH_3$)[$B(C_6F_5)_4$]). Solely [6MesH][$B(C_6F_5)_4$] could be formed *via* the exact same reaction, but instead layering with cyclohexane. ^{1}H NMR (THF-d_8, 500 MHz): δ 8.48 (s, 1H, $C_{NHC}H$), 7.08 (br s, 4H CH_{Mes}), 3.87 (t, $^3J_{HH}$ = 5.2 Hz, 4H, NCH_2), 2.57 (quin, $^3J_{HH}$ = 5.2 Hz, 4H, NCH_2CH_2), 2.33 (br s, 12H, *o*-C$H_{3(Mes)}$), 2.29 (s, 6H, *p*-C$H_{3(Mes)}$). ^{11}B{^{1}H} NMR (THF-d_8, 160 MHz): δ -16.6 (s, [$B(C_6F_5)_4$]$^-$).

*It is now recognised that [Et_3Si]$^+$ might not be the molecular formula and may instead exist as [Et_3Si–H–$SiEt_3$]$^+$ **(Chapter 4, 4.2.1)**.[24]

7.6.6 Formation of [Ni(7Mes)(η^2-$C_6H_5CH_3$)][$B(C_6F_5)_4$] (22)

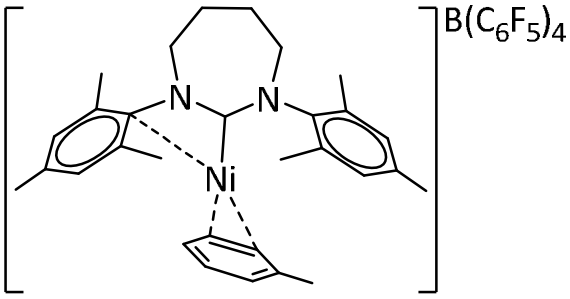

Method as for **21** (section **7.6.5**), but with **6** (72 mg, 0.098 mmol) in C_6H_5F (2 mL) reacting with $[Et_3Si]^{+\dagger}$ formed from $[Ph_3C][B(C_6F_5)_4]$ (90 mg, 0.098 mmol) in Et_3SiH (2 mL). The same colour changes were observed and upon layering with toluene, 24 mg of crystals were obtained (after recrystallisation from THF/toluene) and identified to be **22** and [7MesH]$^{+}$$(C_6H_5CH_3)[B(C_6F_5)_4]$ (65:35 respectively). ^{1}H NMR (THF-d_8, 500 MHz): δ 8.13 (s, 1H, $C_{NHC}H$ from [7MesH]$^{+}$$(C_6H_5CH_3)[B(C_6F_5)_4]$), 7.18 – 7.05 (m, 9H CH_{Mes} and CH_{tol}), 4.19 (br s, 4H, NCH_2 or NCH_2CH_2), 2.45 (br s, 4H, NCH_2 or NCH_2CH_2), 2.36 – 2.27 (m, 21H, $CH_{3(Mes)}$ and $CH_{3(tol)}$). ^{11}B{^{1}H} NMR (THF-d_8, 160 MHz): δ -18.4 (s, [Ni(7Mes)(η^2-$C_6H_5CH_3$)][$B(C_6F_5)_4$]$^-$), -16.6 (s, [7MesH]$^{+}$$(C_6H_5CH_3)[B(C_6F_5)_4]$).

7.6.7 Formation of [Ni(6Mes)(η^2-$C_6H_3(CH_3)_3$)][$B(C_6F_5)_4$] (23)

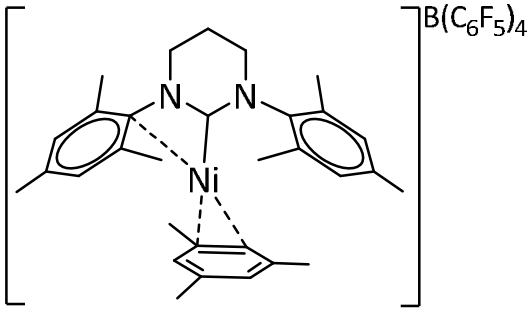

Method as for **21** (section **7.6.5**), but with **1** (73 mg, 0.10 mmol) in C_6H_5F (2 mL) being directly added to $[Et_3Si]^{+*}$ formed from $[Ph_3C][B(C_6F_5)_4]$ (92 mg, 0.10 mmol) in Et_3SiH (2 mL), initiating the instantaneous colour change from yellow to dark red. Layering this C_6H_5F solution with mesitylene yielded 41 mg of **23** and [6MesH]$^{+}$$(C_6H_3(CH_3)_3)[B(C_6F_5)_4]$ (after recrystallisation from THF/mesitylene) in a ratio of 80:20 respectively. ^{1}H NMR (THF-d_8, 500 MHz): δ 8.46 (s, 1H, $C_{NHC}H$ from [6MesH]$^{+}$$(C_6H_3(CH_3)_3)[B(C_6F_5)_4]$), 7.06 (s, 4H, $CH_{(6Mes)}$), 6.72 (s, 3H, CH_{Mes}),

† It is now recognised that $[Et_3Si]^+$ might not be the molecular formula and may instead exist as $[Et_3Si–H–SiEt_3]^+$ **(Chapter 4, 4.2.1)**.[24]

3.87 (br s, 4H, NCH_2), 2.57 (br s, 2H, NCH_2CH_2), 2.32 (s, 12H, *o*-$CH_{3(6Mes)}$), 2.27 (s, 6H, *p*-$CH_{3(6Mes)}$), 2.20 (s, 9H, $CH_{3(Mes)}$). $^{11}B\{^1H\}$ NMR (THF-d_8, 160 MHz): δ -18.4 (s, [Ni(6Mes)(η^2-$C_6H_3(CH_3)_3$)][$B(C_6F_5)_4$]$^-$), -16.6 (s, [6MesH]$^{\cdots}$($C_6H_3(CH_3)_3$)[$B(C_6F_5)_4$]).

7.6.8 Synthesis of [Ni(6Mes)(PPh$_3$)(THF)]PF$_6$ (24)

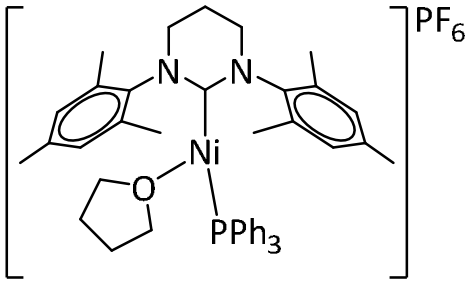

A solution of **1** (222 mg, 0.31 mmol) and excess $TlPF_6$ (124 mg, 0.36 mmol) in THF (10 mL) was stirred at room temperature for 30 min. Insoluble material was filtered off and hexane (30 mL) added to the filtrate to give a very pale yellow precipitate. Recrystallisation from THF/hexane afforded product **24**. Yield: 228 mg (86 %). ^1H NMR (THF-d_8, 500 MHz): δ 16.94 (v br s), 9.92 (br s), 6.06 (br s), 5.29 (br s), 3.10 (br s), 0.12 (v br s). $^{31}P\{^1H\}$ NMR (THF-d_8, 202 MHz): δ -114.8 (sept, $^1J_{PF}$ = 704 Hz, PF_6). ^{19}F NMR (THF-d_8, 470 MHz): δ -75.06 (d, $^1J_{FP}$ = 708 Hz, PF_6). Anal. calcd. (found) for $C_{44}H_{51}N_2OP_2F_6Ni$ (%): C 61.56 (61.39), H 5.99 (5.85), N 3.26 (3.18). ESI-MS calcd. (found) for [M - C_4H_8O – PF_6]$^+$ ([$C_{40}H_{43}N_2PNi$]$^+$) (*m/z*): 640.2512 (640.2494). Solution magnetic moment (Evans method): 2.2 μB.

7.6.8.1 Reactivity of [Ni(6Mes)(PPh$_3$)(THF)]PF$_6$ ***(24)***

7.6.8.1.1 Synthesis of [Ni(6Mes)Br(μ-OH)(μ-O-6Mes)'Ni(PPh$_3$)]PF$_6$ ***(25)***

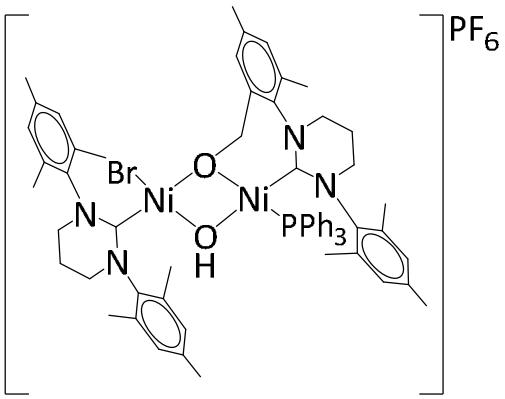

Upon addition of O_2 (1 atm) to a freeze-pump-thawed (three cycles) THF (10 mL) solution of **24** (50 mg, 0.058 mmol), an instantaneous colour change from light yellow to purple occurs. Removing the volatiles *in vacuo* and washing with hexane (10 mL), followed by recrystallisation of the resulting purple residue with THF/hexane, led to a purple precipitate of **25**. Yield: 27 mg (84 %). Analytically pure crystalline material was achieved *via* a layering system of THF/hexane. ^{1}H NMR (THF-d_8, 500 MHz): δ 7.64 – 7.43 (br m, 8H, C*H*$_{Mes}$), 7.03 (s, 15H, C*H*$_{PPh3}$), 3.89 (s, 8H, NC*H*$_2$), 2.52 (br s, 2H, OC*H*$_2$), 2.32 (s, 21H, *o*-C*H*$_3$), 2.27 (s, 12H, *p*-C*H*$_3$), 2.19 (m, 4H, NCH$_2$C*H*$_2$), -2.35 (br s, O*H*). ^{31}P{^{1}H} NMR (THF-d_8, 202 MHz): δ 24.5 (br s, *P*Ph$_3$), -105.7 (m, $^1J_{PF}$ = 720 Hz, *P*F$_6$). Anal. calcd. (found) for $C_{62}H_{71}N_4O_2P_2F_6Ni_2Br$ (%): C 65.75 (65.35), H 6.32 (6.50), N 4.95 (5.12).

7.6.8.1.2 Synthesis of [Ni(6Mes)(PPh_3)(CO)]PF_6 ***(26)*** *and [Ni(6Mes)(PPh_3)(CO)Br]PF_6* ***(27)***

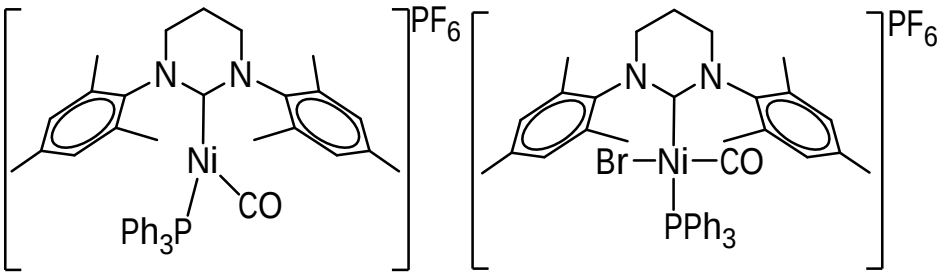

26 **27**

Light yellow THF solutions of **24** were freeze-pump-thaw degassed (three cycles) and exposed to CO (1 atm). They immediately turned green, which when left standing became orange after 1h, gradually changing to a yellow colour over 48 h. Halting a reaction mixture (consisting of **24** (43 mg, 0.050 mmol) in THF (5 mL)) immediately after addition of CO by freezing the THF solution and freeze-pump-thaw degassing three times to remove all CO led to a green solution. When dried *in vacuo* and washed with hexane (10 mL), light green/yellow X-ray quality crystals of **26** could be formed from recrystallisation with THF/hexane. Yield: 15 mg (37 %). ^{1}H NMR (THF-d_8, 500 MHz): δ 16.92* (br s), 10.96, (v br s), 9.92* (br s), 8.35 (s), 7.67 (br m), 7.30 (s), 7.04 (s), 6.41* (v br s), 5.30 (br s), 4.93 (v br s), 3.89 (s), 2.33 (s), 2.28 (s), 0.10(s), -10.78* (br s), -13.09* (v br s). ^{31}P{^{1}H} NMR (THF-d_8, 202 MHz): δ 33.4 (s, *P*Ph_3), -144.9 (m, $^{1}J_{PF}$ = 710 Hz, *P*F_6). When a reaction mixture (consisting of **24** (47 mg, 0.055 mmol) in THF (5 mL)) was instead left to go to completion over 48 h the yellow solution was reduced to dryness and washed with hexane (10 mL) to leave a dark yellow residue. Slow dissolution of Et_2O into a THF solution of this residue yielded yellow crystals of **27**. Yield: 4 mg (8 %). The ^{1}H NMR (THF-d_8, 500 MHz) was identical to **26**, apart from the absence of the signals marked with an *. ^{31}P{^{1}H} NMR (THF-d_8, 202 MHz): δ 31.6 (s, *P*Ph_3), -145.0 (m, $^{1}J_{PF}$ = 711 Hz, *P*F_6), 31.56 (s).

7.6.9 Synthesis of [Ni(6Mes)(κ²-BH₄)]₂ (28)

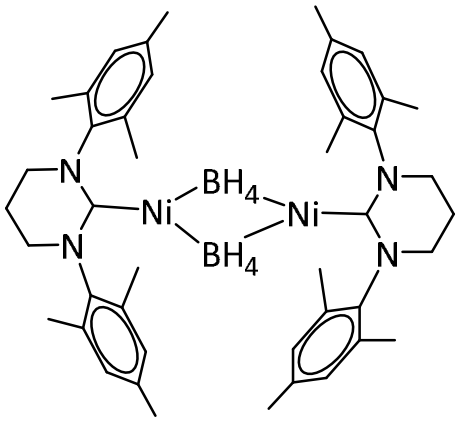

A mixture of **1** (204 mg, 0.28 mmol) and excess $NaBH_4$ (30 mg, 0.79 mmol) was suspended in THF (5 mL). Upon addition of MeOH (2 mL), a dark green colour change was observed and the solution stirred for 5 min before being reduced to dryness *in vacuo*. The residue was extracted into toluene (5 mL), filtered and reduced to dryness, with the resulting residue being washed with hexane (5 mL) to give a dark green powder of product **28**. Yield: 9 mg (8 %). Analytically pure compound could be obtained by recrystallisation from toluene/hexane. ^{1}H NMR (THF-d_8, 400 MHz): δ 6.71 (s, 8H, CH_{aryl}), 3.10 (t, $^{3}J_{HH}$ = 5.7 Hz, 8H, NCH_2), 2.36 (s, 12H, *p*-CH_3), 2.02 (br s, 28H, *o*-CH_3 and NCH$_2$CH_2), -5.74 (br d, $^{1}J_{HB}$ = 72.3 Hz, 8H, BH_4). ^{13}C{^{1}H} NMR (THF-d_8, 100 MHz): δ 213.0 (NCN), 144.6 (NC$_{ipso}$), 136.2 (*o*-C$_{Mes}$), 136.1 (*p*-C$_{Mes}$), 129.7 (*m*-CH$_{aryl}$), 45.2 (NCH$_2$), 22.7 (NCH$_2$CH$_2$), 21.7 (*p*-CH$_3$), 18.6 (*o*-CH$_3$). ^{11}B{^{1}H} NMR (THF-d_8, 160 MHz): δ -32.0 (br s, BH_4). Anal. calcd. (found) for $C_{44}H_{64}N_4B_2Ni$ (%): C 67.06 (66.97), H 8.19 (8.28), N 7.11 (6.98).

7.7 Nickel Mediated Catalytic Reactions

7.7.1 Kumada Cross-Coupling C-C Formation

In each case, the nickel catalyst **(1, 7, 17, 18, 24 or 29)** (4 – 8 mg, 1 mol%) was dissolved in THF (0.5 mL) and stirred for 10 min. The aryl halide substrate (1 eq) was added to the solution, followed by excess Grignard reagent (PhMgCl (2M in THF): 0.5 mL or MesMgBr (1M in THF): 1 mL, 1.00 mmol). The reaction mixture was stirred for either i) 2.5 h if using PhMgCl at 298 K, ii) 24 h if using MesMgBr at 298 K or iii) 1 h if using PhMgCl or MesMgBr at 333 K. MeOH (1.0 mL) was added to quench the reaction and the organic products then extracted into CH_2Cl_2 and dried over $MgSO_4$. After drying on a rotary evaporator, the resulting residue was purified using column purification through a silica plug using a 2:8 CH_2Cl_2:hexane eluent. Evaporation of the eluent yielded the product as either a white precipitate or colourless oil, depending on the substrate used. ^{1}H NMR spectroscopic analysis confirmed the presence of the desired coupled product.[25-27]

7.8 References

1. T. W. Hudnall, J. P. Moerdyk and C. W. Bielawski, *Chem. Commun.*, 2010, **46**, 4288-4290.
2. W. A. Herrmann, S. K. Schneider, K. Ofele, M. Sakamoto and E. Herdtweck, *J. Organomet. Chem.*, 2004, **689**, 2441-2449.
3. A. Aidouni, S. Bendahou, A. Demonceau and L. Delaude, *J. Comb. Chem.*, 2008, **10**, 886-892.
4. M. J. Page, W. Y. Lu, R. C. Poulten, E. Carter, A. G. Algarra, B. M. Kariuki, S. A. Macgregor, M. F. Mahon, K. J. Cavell, D. M. Murphy and M. K. Whittlesey, *Chem. Eur. J.*, 2013, **19**, 2158-2167.
5. M. J. Frisch, ed. R. A. Gaussian 09, Gaussian Inc., Wallingford CT, 2009.
6. C. T. Lee, W. T. Yang and R. G. Parr, *Phys. Rev. B*, 1988, **37**, 785-789.
7. B. Miehlich, A. Savin, H. Stoll and H. Preuss, *Chem. Phys. Lett.*, 1989, **157**, 200-206.
8. A. D. Becke, *J. Chem. Phys.*, 1993, **98**, 5648-5652.
9. M. Dolg, U. Wedig, H. Stoll and H. Preuss, *J. Chem. Phys.*, 1987, **86**, 866-872.
10. G. Igelmann, H. Stoll and H. Preuss, *Molecular Physics*, 1988, **65**, 1321-1328.
11. A. Hollwarth, M. Bohme, S. Dapprich, A. W. Ehlers, A. Gobbi, V. Jonas, K. F. Kohler, R. Stegmann, A. Veldkamp and G. Frenking, *Chem. Phys. Lett.*, 1993, **208**, 237-240.
12. W. J. Hehre, R. Ditchfie and J. A. Pople, *J. Chem. Phys.*, 1972, **56**, 2257.
13. P. C. Harihara and J. A. Pople, *Theor. Chem. Acta.*, 1973, **28**, 213-222.
14. G. M. Sheldrick, *Acta. Crystallogr.*, 1990, 467-473.
15. A. Binobaid, M. Iglesias, D. J. Beetstra, B. Kariuki, A. Dervisi, I. A. Fallis and K. J. Cavell, *Dalton Trans.*, 2009, 7099-7112.
16. M. Iglesias, D. J. Beetstra, J. C. Knight, L. L. Ooi, A. Stasch, S. Coles, L. Male, M. B. Hursthouse, K. J. Cavell, A. Dervisi and I. A. Fallis, *Organometallics*, 2008, **27**, 3279-3289.
17. M. Iglesias, D. J. Beetstra, A. Stasch, P. N. Horton, M. B. Hursthouse, S. J. Coles, K. J. Cavell, A. Dervisi and I. A. Fallis, *Organometallics*, 2007, **26**, 4800-4809.
18. M. Iglesias, D. J. Beetstra, B. Kariuki, K. J. Cavell, A. Dervisi and I. A. Fallis, *Eur. J. Inorg. Chem.*, 2009, 1913-1919.
19. C. J. E. Davies, M. J. Page, C. E. Ellul, M. F. Mahon and M. K. Whittlesey, *Chem. Commun.*, 2010, **46**, 5151-5153.
20. R. C. Poulten, I. Lopez, A. Llobet, M. F. Mahon and M. K. Whittlesey, *Inorg. Chem.*, 2014, **53**, 7160-7169.

21. W. E. Daniels, *Inorg. Chem.*, 1964, **3**, 1800.
22. K. M. Wiggins, J. P. Moerdyk and C. W. Bielawski, *Chem. Sci.*, 2012, **3**, 2986-2992.
23. R. C. Poulten, M. J. Page, A. G. Algarra, J. J. Le Roy, I. Lopez, E. Carter, A. Llobet, S. A. Macgregor, M. F. Mahon, D. M. Murphy, M. Murugesu and M. K. Whittlesey, *J. Am. Chem. Soc.*, 2013, **135**, 13640-13643.
24. M. Nava and C. A. Reed, *Organometallics*, 2011, **30**, 4798-4800.
25. J. H. Li, W. J. Liu and Y. X. Xie, *J. Org. Chem.*, 2005, **70**, 5409-5412.
26. L. Li, J. Wang, T. Wu and R. Wang, *Chem. Eur. J.*, 2012, **18**, 7842-7851.
27. Z. Y. Wang, G. Q. Chen and L. X. Shao, *J. Org. Chem.*, 2012, **77**, 6608-6614.

APPENDICES

APPENDIX 1 - CRYSTALLOGRAPHIC DATA

Appendix 1 – Crystallographic Data

	Ni(6Mes)(PPh_3)Br (1)	Ni(6^{o}Tol)(PPh_3)Br (2)	Ni(6^{o}Anis)(PPh_3)Br (3)
Identification Code	k09mkw40	h12mkw20	k10mkw14
Empirical Formula	C40 H43 Br N2 Ni P	C42 H41 Br N2 Ni P	C40 H43 Br N2 Ni O3 P
Formula Weight	721.35	743.36	769.35
Temperature	150(2) K	150(2) K	150(2) K
Wavelength	0.71073 Å	0.71073 Å	0.71073 Å
Crystal System	Monoclinic	Triclinic	Monoclinic
Space Group	P21/n	P-1	P21/a
Unit Cell Dimensions	a = 10.8540(1) Å, α = 90^o b = 17.1720(2) Å, β = 102.454(1)^o c = 18.9610(2) Å, γ = 90^o	a = 9.7450(2) Å, α = 83.531(1)^o b = 9.9650(2) Å, β = 87.454(1)^o c = 19.6340(5) Å, γ = 75.760(2)^o	a = 14.8320(1) Å, α = 90^o b = 14.4560(1) Å, β = 108.778(1)^o c = 17.9880(1) Å, γ = 90^o
Volume	3450.89(6) Å^3	1836.01(7) Å^3	3651.54(4) Å^3
Z	4	2	4
Density (calculated)	1.388 Mg m^{-3}	1.345 Mg m^{-3}	1.399 Mg m^{-3}
Absorption Coefficient	1.797 mm^{-1}	1.691 mm^{-1}	1.709 mm^{-1}
F(000)	1500	770	1596
Crystal Size	0.20 x 0.20 x 0.18 mm	0.40 x 0.30 x 0.25 mm	0.50 x 0.40 x 0.35 mm
Theta Range for Data Collection	3.51 to 30.01^o	3.84 to 27.51 ^{o}.	3.55 to 30.05 ^{o}.
Index Ranges	-15<=h<=15; -24<=k<=24; -26<=l<=26	-12<=h<=12; -12<=k<=12; -25<=l<=25	-20<=h<=20; -19<=k<=20; -25<=l<=25
Reflections Collected	68858	29542	61423
Independent Reflections	10058 [R(int) = 0.0831]	8322 [R(int) = 0.0348]	10648 [R(int) = 0.0524]
Reflections Observed (> 2σ)	6772	6649	8125
Data Completeness	0.998	0.986	0.997
Absorption Correction	Semi-empirical from equivalents	Semi-empirical from equivalents	Semi-empirical from equivalents
Max. and Min. Transmission	0.561 and 0.494	0.663 and 0.635	0.558 and 0.459
Refinement Method	Full-matrix least-squares on F^2	Full-matrix least-squares on F^2	Full-matrix least-squares on F^2
Data/Restraints/Parameters	10058/0/414	8322/42/472	10648/30/451
Goodness-of-Fit on F2	1.005	1.026	1.022
Final R Indices [I > 2σ(I)]	R1 = 0.0404 wR2 = 0.0761	R1 = 0.0551 *w*R2 = 0.1562	R1 = 0.0372 wR2 = 0.0823
R Indices (all data)	R1 = 0.0828 wR2 = 0.0889	R1 = 0.0714 *w*R2 = 0.1696	R1 = 0.0580 wR2 = 0.0918
Largest Diff. Peak and Hole	0.542 and -0.499 eÅ^{-3}	1.573 and -1.103 eÅ^{-3}	0.381 and -0.527 eÅ^{-3}

	Ni(6^{o}AnisMes)(PPh_3)Br (4)	Ni(6MesDAC)(PPh_3)Br (5)	Ni(7Mes)(PPh_3)Br (6)
Identification Code	k10mkw15	k13mkw15	k13mkw6
Empirical Formula	C42 H47 Br N2 Ni O2 P	C42 H43 Br N2 Ni O2 P	C41 H45 Br N2 Ni P
Formula Weight	781.41	777.37	735.38
Temperature	150(2) K	150(2) K	150(2) K
Wavelength	0.71073 Å	0.71073 Å	0.71073 Å
Crystal System	Monoclinic	Monoclinic	Monoclinic
Space Group	P21/n	P21/n	P21/n
Unit Cell Dimensions	a = 10.6640(1) Å, α = 90^o	a = 11.3530(1) Å, α = 90^o	a = 11.0370(2) Å, α = 90^o
	b = 10.3170(1) Å, β = 92.201(1)^o	b = 17.9990(2) Å, β = 100.635(1)^o	b = 17.5000(2) Å, β = 101.226(1)^o
	c = 34.9420(5) Å, γ = 90^o	c = 18.3910(2) Å, γ = 90^o	c = 19.0460(2) Å, γ = 90^o
Volume	3841.50(8) Å^3	3693.51(7) Å^3	3608.30(9) Å^3
Z	4	4	4
Density (calculated)	1.351 Mg m^{-3}	1.398 Mg m^{-3}	1.354 Mg m^{-3}
Absorption Coefficient	1.624 mm^{-1}	1.689 mm^{-1}	1.720 mm^{-1}
F(000)	1628	1612	1532
Crystal Size	0.35 x 0.25 x 0.25 mm	0.40 x 0.20 x 0.10 mm	0.60 x 0.50 x 0.40 mm
Theta Range for Data Collection	3.52 to 27.45 ^{o}.	3.79 to 27.49^o	3.63 to 27.48 ^{o}.
Index Ranges	-13<=h<=13; -13<=k<=13; -45<=l<=45	-14<=h<=14; -23<=k<=23; -23<=l<=23	-14<=h<=14; -22<=k<=22; -24<=l<=24
Reflections Collected	44143	72526	44224
Independent Reflections	8538 [R(int) = 0.0635]	8447 [R(int) = 0.0516]	8225 [R(int) = 0.0467]
Reflections Observed (> 2σ)	6132	7242	6715
Data Completeness	0.972	0.994	0.993
Absorption Correction	Semi-empirical from equivalents	Semi-empirical from equivalents	Semi-empirical from equivalents
Max. and Min. Transmission	0.679 and 0.565	0.764 and 0.645	0.507 and 0.442
Refinement Method	Full-matrix least-squares on F^2	Full-matrix least-squares on F^2	Full-matrix least-squares on F^2
Data/Restraints/Parameters	8538/60/491	8447/0/450	8225/0/421
Goodness-of-Fit on F2	1.021	1.047	1.027
Final R Indices [I > 2σ(I)]	R1 = 0.0404 wR2 = 0.0807	R1 = 0.0309 *wR*2 = 0.0771	R1 = 0.0334 *wR*2 = 0.0741
R Indices (all data)	R1 = 0.0716 wR2 = 0.0910	R1 = 0.0404 *wR*2 = 0.0829	R1 = 0.0476 *wR*2 = 0.0808
Largest Diff. Peak and Hole	0.287 and -0.379 eÅ^{-3}	0.474 and -0.622 eÅ^{-3}	0.599 and -0.438 eÅ^{-3}

	Ni(7^{o}Tol)(PPh$_3$)Br (7)	Ni(8Mes)(PPh$_3$)Br/Cl (8)	Ni(8^{o}Tol)(PPh$_3$)Br/Cl (9)
Identification Code	h10mkw16	kjc1138	kjc1131b
Empirical Formula	C37 H37 Br N2 Ni P	C42 H47 Br0.70 Cl0.30 N2 Ni P	C38 H39 Br0.70 Cl0.30 N2 Ni P
Formula Weight	679.28	736.07	679.96
Temperature	153(2) K	150(2) K	150(2) K
Wavelength	0.71073 Å	0.71073 Å	0.71073 Å
Crystal System	Monoclinic	Monoclinic	Triclinic
Space Group	P21/n	P21/n	P-1
Unit Cell Dimensions	a = 10.7900(2) Å, α = 90^o	a = 11.1633(7) Å, α = 90^o	a = 10.2478(5) Å, α = 89.879(3)^o
	b = 17.1150(4) Å, β = 99.688(1)^o	b = 17.5068(11) Å, β = 100.254(4)^o	b = 10.3288(5) Å, β = 84.943(3)^o
	c = 18.1020(3) Å, γ = 90^o	c = 19.1295(13) Å, γ = 90^o	c = 16.1139(9) Å, γ = 75.256(3)^o
Volume	3295.24(11) Å^3	3678.8(4) Å^3	1642.67(15) Å^3
Z	4	4	2
Density (calculated)	1.369 Mg m^{-3}	1.329 Mg m^{-3}	1.375 Mg m^{-3}
Absorption Coefficient	1.878 mm^{-1}	1.385 mm^{-1}	1.544 mm^{-1}
F(000)	1404	1542	707
Crystal Size	0.40 x 0.25 x 0.25 mm	0.50 x 0.50 x 0.45 mm	0.30 x 0.20 x 0.06 mm
Theta Range for Data Collection	3.82 to 30.24^o	3.63 to 23.27^o	3.57 to 27.68^o
Index Ranges	-15<=h<=15; -24<=k<=24; -25<=l<=25	-12<=h<=12; -19<=k<=17; -21<=l<=21	-13<=h<=13; -13<=k<=13; -20<=l<=20
Reflections Collected	62480	8642	10764
Independent Reflections	9652 [R(int) = 0.0551]	5197 [R(int) = 0.0363]	10771 [R(int) = 0.0000]
Reflections Observed (> 2σ)	6746	3994	7709
Data Completeness	0.982	0.980	0.972
Absorption Correction	Semi-empirical from equivalents	Semi-empirical from equivalents	Semi-empirical from equivalents
Max. and Min. Transmission	0.639 and 0.474	0.58 and 0.53	0.92 and 0.64
Refinement Method	Full-matrix least-squares on F^2	Full-matrix least-squares on F^2	Full-matrix least-squares on F^2
Data/Restraints/Parameters	9652/0/382	5197/2/435	10771/2/396
Goodness-of-Fit on F2	1.024	1.110	1.020
Final R Indices [I > 2σ(I)]	R1 = 0.0494 wR2 = 0.1295	R1 = 0.0621 *wR*2 = 0.1112	R1 = 0.0706 *wR*2 = 0.1686
R Indices (all data)	R1 = 0.0805 wR2 = 0.1474	R1 = 0.0899 *wR*2 = 0.1214	R1 = 0.1069 *wR*2 = 0.1935
Largest Diff. Peak and Hole	1.157 and -0.565 eÅ^{-3}	0.564 and -0.390 eÅ^{-3}	0.765 and -0.459 eÅ^{-3}

	Ni(O-8^{o}Tol)(PPh$_3$)Br/Cl (10)	Ni(6^{t}Bu)'Br (11)	Ni(6^{i}Pr)$_2$Br$_2$ (12)
Identification Code	kjc1133	k12mkw12	k11mkw10
Empirical Formula	C37 H37 Br0.70 Cl0.30 N2 Ni O P	C12 H23 Br N2 Ni	C26 H46 Br2 N4 Ni
Formula Weight	681.94	333.94	633.20
Temperature	150(2) K	150(2) K	150(2) K
Wavelength	0.71073 Å	0.71073 Å	0.71073 Å
Crystal System	Triclinic	Monoclinic	Triclinic
Space Group	P-1	C2/c	P-1
Unit Cell Dimensions	a = 10.2776(7) Å, α = 96.382(4)^o b = 10.3430(6) Å, β = 90.831(4)^o c = 15.7043(8) Å, γ = 103.338(3)^o	a = 13.8400(2) Å, α = 90^o b = 12.5040(2) Å, β = 100.436(1)^o c = 16.4340(2) Å, γ = 90^o	a = 8.3650(1) Å, α = 88.957(1)^o b = 10.5290(2) Å, β = 80.192(1)^o c = 17.4610(3) Å, γ = 74.958(1)^o
Volume	1612.90(17) Å^3	2796.95(7) Å^3	1462.93(4) Å^3
Z	2	8	2
Density (calculated)	1.404 Mg m^{-3}	1.586 Mg m^{-3}	1.437 Mg m^{-3}
Absorption Coefficient	1.575 mm^{-1}	4.222 mm^{-1}	3.415 mm^{-1}
F(000)	707	1376	656
Crystal Size	0.15 x 0.15 x 0.10 mm	0.30 x 0.20 x 0.15 mm	0.30 x 0.25 x 0.25 mm
Theta Range for Data Collection	3.52 to 24.42 ^{o}.	4.12 to 27.48^o	3.98 to 27.49^o
Index Ranges	-11<=h<=9; -10<=k<=12; -18<=l<=18	-17<=h<=17; -16<=k<=16; -20<=l<=21	-10<=h<=10; -13<=k<=13; -22<=l<=22
Reflections Collected	8219	24324	25512
Independent Reflections	5262 [R(int) = 0.0561]	3191 [R(int) = 0.0429]	6660 [R(int) = 0.0402]
Reflections Observed (> 2σ)	3497	2998	5596
Data Completeness	0.992	0.997	0.992
Absorption Correction	Semi-empirical from equivalents	Semi-empirical from equivalents	Semi-empirical from equivalents
Max. and Min. Transmission	0.86 and 0.80	1.246 and 0.880	0.718 and 0.607
Refinement Method	Full-matrix least-squares on F^2	Full-matrix least-squares on F^2	Full-matrix least-squares on F^2
Data/Restraints/Parameters	5262/2/394	3191/5/169	6660/0/306
Goodness-of-Fit on F2	1.073	1.098	1.055
Final R Indices [I > 2σ(I)]	R1 = 0.0731 *wR*2 = 0.1687	R1 = 0.0222 *wR*2 = 0.0551	R1 = 0.0330 wR2 = 0.0855
R Indices (all data)	R1 = 0.1217 *wR*2 = 0.1933	R1 = 0.0244 *wR*2 = 0.0564	R1 = 0.0414 wR2 = 0.0920
Largest Diff. Peak and Hole	0.880 and -0.488 eÅ^{-3}	0.346 and -0.578 eÅ^{-3}	0.726 and -1.032 eÅ^{-3}

	Ni(6Mes)Br(μ-OH)(μ-O-6Mes)'NiBr (13)	Ni(7Mes)Br(μ-OH)(μ-O-7Mes)'NiBr (14)	[NiBr/Cl(μ-O-6Mes)']$_2$ (15)
Identification Code	k12mkw6	k13mkw10	k13mkw24
Empirical Formula	C44 H56 Br2 N4 Ni2 O2	C46 H60 Br2 N4 Ni2 O2	C44 H54 Br0.40 Cl1.60 N4 Ni2 O2
Formula Weight	950.17	978.22	877.02
Temperature	150(2) K	150(2) K	150(2) K
Wavelength	0.71073 Å	0.71073 Å	0.71073 Å
Crystal System	Monoclinic	Triclinic	Triclinic
Space Group	P21/n	P-1	P-1
Unit Cell Dimensions	a = 14.0430(2) Å, α = 90°	a = 12.6730(2) Å, α = 101.027(1)°	a = 12.8530(2) Å, α = 107.486(1)°
	b = 15.6560(2) Å, β = 90.194(1)°	b = 12.8470(3) Å, β = 110.711(1)°	b = 13.4070(2) Å, β = 99.498(1)°
	c = 19.5740(3) Å, γ = 90°	c = 16.0810(3) Å, γ = 104.940(1)°	c = 14.8420(3) Å, γ = 114.349(1)°
Volume	4303.46(11) Å^3	2247.65(8) Å^3	2095.99(6) Å^3
Z	4	2	2
Density (calculated)	1.467 Mg m^{-3}	1.445 Mg m^{-3}	1.390 Mg m^{-3}
Absorption Coefficient	2.772 mm^{-1}	2.656 mm^{-1}	1.423 mm^{-1}
F(000)	1960	1012	918
Crystal Size	0.15 x 0.12 x 0.10 mm	0.20 x 0.10 x 0.05 mm	0.30 x 0.20 x 0.05 mm
Theta Range for Data Collection	4.31 to 27.47°	3.57 to 27.42°	3.66 to 27.57°
Index Ranges	-18<=h<=18; -20<=k<=20; -25<=l<=25	-16<=h<=16; -16<=k<=16; -19<=l<=20	-16<=h<=16; -17<=k<=17; -19<=l<=19
Reflections Collected	75160	44832	34804
Independent Reflections	9813 [R(int) = 0.0883]	10169 [R(int) = 0.0605]	9558 [R(int) = 0.0488]
Reflections Observed (> 2σ)	7272	7434	7592
Data Completeness	0.994	0.993	0.985
Absorption Correction	Semi-empirical from equivalents	Semi-empirical from equivalents	Semi-empirical from equivalents
Max. and Min. Transmission	1.079 and 0.909	0.883 and 0.800	0.870 and 0.785
Refinement Method	Full-matrix least-squares on F^2	Full-matrix least-squares on F^2	Full-matrix least-squares on F^2
Data/Restraints/Parameters	9813/1/502	10169/1/520	9558/0/504
Goodness-of-Fit on F2	1.100	1.070	1.035
Final R Indices [I > 2σ(I)]	R1 = 0.0431 wR2 = 0.0848	R1 = 0.0508 *wR*2 = 0.1226	R1 = 0.0370 *wR*2 = 0.0858
R Indices (all data)	R1 = 0.0725 wR2 = 0.0971	R1 = 0.0809 *wR*2 = 0.1369	R1 = 0.0542 *wR*2 = 0.0935
Largest Diff. Peak and Hole	0.461 and -0.628 eÅ^{-3}	1.821 and -0.924 eÅ^{-3}	0.428 and -0.639 eÅ^{-3}

	Ni(6^{o}Tol)(PPh_3)Br_2 (17)	Ni(7^{o}Tol)(PPh_3)Br_2 (18)	[Ni(6Mes)$_2$]Br (19)
Identification Code	h12mkw15	k12mkw11	k10mkw10
Empirical Formula	C36 H35 Br2 N2 Ni P	C74 H74 Br4 N4 Ni2 P2	C46 H60 Br Cl4 N4 Ni
Formula Weight	745.16	1518.37	949.40
Temperature	150(2) K	150(2) K	150(2) K
Wavelength	0.71073 Å	0.71073 Å	0.71073 Å
Crystal System	Monoclinic	Orthorhombic	Monoclinic
Space Group	P21/n	Pcab	P21
Unit Cell Dimensions	a = 14.8730(4) Å, α = 90^o	a = 18.4520(1) Å, α = 90^o	a = 10.3210(1) Å, α = 90^o
	b = 13.5120(4) Å, β = 109.392(2)^o	b = 20.0770(2) Å, β = 90^o	b = 21.8360(3) Å, β = 94.612(1)^o
	c = 17.3700(5) Å, γ = 90^o	c = 36.8620(3) Å, γ = 90^o	c = 10.4070(2) Å, γ = 90^o
Volume	3292.71(16) Å^3	13655.93(19) Å^3	2337.82(6) Å^3
Z	4	8	2
Density (calculated)	1.503 Mg m^{-3}	1.477 Mg m^{-3}	1.349 Mg m^{-3}
Absorption Coefficient	3.092 mm^{-1}	2.984 mm^{-1}	1.534 mm^{-1}
F(000)	1512	6176	990
Crystal Size	0.30 x 0.20 x 0.20 mm	0.30 x 0.25 x 0.08 mm	0.20 x 0.20 x 0.15 mm
Theta Range for Data Collection	3.53 to 27.48^o	3.54 to 27.40^o	3.73 to 27.46^o
Index Ranges	-19<=h<=19; -17<=k<=17; -22<=l<=22	-23<=h<=23; -26<=k<=26; -47<=l<=47	-13<=h<=13; -28<=k<=28; -13<=l<=13
Reflections Collected	55969	152549	46015
Independent Reflections	7522 [R(int) = 0.0760]	15331 [R(int) = 0.1087]	10667 [R(int) = 0.0492]
Reflections Observed (> 2σ)	5219	10420	8383
Data Completeness	0.996	0.987	0.997
Absorption Correction	Semi-empirical from equivalents	Semi-empirical from equivalents	Semi-empirical from equivalents
Max. and Min. Transmission	0.554 and 0.354	1.270 and 0.785	0.502 and 0.455
Refinement Method	Full-matrix least-squares on F^2	Full-matrix least-squares on F^2	Full-matrix least-squares on F^2
Data/Restraints/Parameters	7522/43/416	15331/90/813	10667/13/530
Goodness-of-Fit on F2	1.178	1.039	1.018
Final R Indices [I > 2σ(I)]	R1 = 0.0578 *wR*2 = 0.1399	R1 = 0.0570 *wR*2 = 0.1346	R1 = 0.0365 wR2 = 0.0842
R Indices (all data)	R1 = 0.0941 *wR*2 = 0.1542	R1 = 0.0971 *wR*2 = 0.1548	R1 = 0.0567 wR2 = 0.0935
Largest Diff. Peak and Hole	0.975 and -0.626 eÅ^{-3}	1.320 and -1.316 eÅ^{-3}	0.002(7)

	Ni(6Mes)$_2$ (20)	**[Ni(6Mes)(η^2-$C_6H_5CH_3$][B(C_6F_5)$_4$] (21)**	**[6MesH]$^{\cdots}$($C_6H_5CH_3$)[B(C_6F_5)$_4$]**
Identification Code	k10mkw13	k13mkw33	k13mkw34
Empirical Formula	C44 H56 N4 Ni	C53 H36.75 B F20 N2 Ni0.25	C52 H34 B F21 N2
Formula Weight	699.64	1107.08	1096.62
Temperature	150(2) K	150(2) K	150(2) K
Wavelength	0.71073 Å	0.71073 Å	0.71073 Å
Crystal System	Monoclinic	Monoclinic	Monoclinic
Space Group	P21/c	C2/c	C2/c
Unit Cell Dimensions	a = 10.3690(2) Å, α = 90^o	a = 31.5610(3) Å, α = 90^o	a = 31.3660(3) Å, α = 90^o
	b = 21.2180(5) Å, β = 93.369(1)^o	b = 10.3090(1) Å, β = 92.760(1)^o	b = 10.3230(1) Å, β = 91.563(1)^o
	c = 17.6090(5) Å, γ = 90^o	c = 28.8690(4) Å, γ = 90^o	c = 29.0530(3) Å, γ = 90^o
Volume	3867.45(16) Å^3	9381.99(18) Å^3	9403.61(16) Å^3
Z	4	8	8
Density (calculated)	1.202 Mg m^{-3}	1.568 Mg m^{-3}	1.549 Mg m^{-3}
Absorption Coefficient	0.537 mm^{-1}	0.243 mm^{-1}	0.149 mm^{-1}
F(000)	1504	4486	4432
Crystal Size	0.18 x 0.12 x 0.06 mm	0.30 x 0.20 x 0.20 mm	0.35 x 0.10 x 0.10 mm
Theta Range for Data Collection	3.71 to 25.03^o	3.53 to 27.58^o	3.51 to 27.49 ^{o}.
Index Ranges	-11<=h<=11; -25<=k<=25; -18<=l<=20	-40<=h<=40; -13<=k<=13; -37<=l<=37	-40<=h<=40; -12<=k<=13; -37<=l<=37
Reflections Collected	17846	44048	59630
Independent Reflections	6348 [R(int) = 0.0518]	10585 [R(int) = 0.0539]	10742 [R(int) = 0.0364]
Reflections Observed (> 2σ)	5096	8005	7948
Data Completeness	0.928	0.974	0.994
Absorption Correction	Semi-empirical from equivalents	Semi-empirical from equivalents	Semi-empirical from equivalents
Max. and Min. Transmission	0.970 and 0.868	0.893 and 0.750	0.652 and 0.617
Refinement Method	Full-matrix least-squares on F^2	Full-matrix least-squares on F^2	Full-matrix least-squares on F^2
Data/Restraints/Parameters	6348/0/454	10585/1/705	10742/115/759
Goodness-of-Fit on F2	1.041	1.080	1.034
Final R Indices [I > 2σ(I)]	R1 = 0.0436 wR2 = 0.0967	R1 = 0.0449 *wR*2 = 0.1052	R1 = 0.0418 *wR*2 = 0.1007
R Indices (all data)	R1 = 0.0620 wR2 = 0.1053	R1 = 0.0674 *wR*2 = 0.1145	R1 = 0.0653 *wR*2 = 0.1132
Largest Diff. Peak and Hole	0.432 and -0.365 eÅ^{-3}	0.325 and -0.300 eÅ^{-3}	0.761 and -0.315 eÅ^{-3}

	[Ni(7Mes)(η^2-$C_6H_5CH_3$][$B(C_6F_5)_4$] (22)	[Ni(6Mes)(η^2-$C_6H_3(CH_3)_3$][$B(C_6F_5)_4$] (23)	[Ni(6Mes)(PPh_3)(THF)]PF_6 (24)
Identification Code	k13mkw41	s14mkw3	p10mkw7
Empirical Formula	C54 H38.60 B F20 N2 Ni0.40	C110 H80.20 B2 F40 N4 Ni1.80	C44 H51 F6 N2 Ni O P2
Formula Weight	1129.76	2345.28	858.52
Temperature	150(2) K	150(2) K	150(2) K
Wavelength	0.71073 Å	0.71073 Å	0.71073 Å
Crystal System	Monoclinic	Triclinic	Monoclinic
Space Group	C2/c	P-1	P21/c
Unit Cell Dimensions	a = 31.8660(2) Å, α = 90°	a = 10.4000(4) Å, α = 92.241(3)°	a = 16.0749(1) Å, α = 90°
	b = 10.1820(1) Å, β = 94.34°	b = 16.7387(6) Å, β = 90.291(3)°	b = 14.8045(1) Å, β = 111.435(1)°
	c = 29.3070(3) Å, γ = 90°	c = 29.4479(9) Å, γ = 107.737(4)°	c = 19.0391(1) Å, γ = 90°
Volume	9481.62(15) $Å^3$	4878.2(3) $Å^3$	4217.55(4) $Å^3$
Z	8	2	4
Density (calculated)	1.583 Mg m^{-3}	1.597 Mg m^{-3}	1.352 Mg m^{-3}
Absorption Coefficient	0.299 mm^{-1}	1.607 mm^{-1}	0.598 mm^{-1}
F(000)	4582	2377	1796
Crystal Size	0.20 x 0.10 x 0.10 mm	0.22 x 0.10 x 0.04 mm	0.36 x 0.31 x 0.19 mm
Theta Range for Data Collection	3.53 to 27.46°	4.51 to 72.10.	2.85 to 30.46°
Index Ranges	-41<=h<=41; -13<=k<=13; -37<=l<=38	-12<=h<=8; -20<=k<=19; -36<=l<=35	-22<=h<=22; -20<=k<=20; -26<=l<=25
Reflections Collected	65419	31281	101615
Independent Reflections	10802 [R(int) = 0.0588]	18573 [R(int) = 0.0393]	11811 [R(int) = 0.0292]
Reflections Observed (> 2σ)	8041	13518	8875
Data Completeness	0.996	0.967	0.922
Absorption Correction	Semi-empirical from equivalents	Semi-empirical from equivalents	Semi-empirical from equivalents
Max. and Min. Transmission	0.950 and 0.844	1.00000 and 0.74458	1.00000 and 0.96100
Refinement Method	Full-matrix least-squares on F^2	Full-matrix least-squares on F^2	Full-matrix least-squares on F^2
Data/Restraints/Parameters	10802/0/710	18573/244/1390	11811/0/511
Goodness-of-Fit on F2	1.156	1.046	1.028
Final R Indices [I > 2σ(I)]	R1 = 0.0521 *wR*2 = 0.1061	R1 = 0.0949 *wR*2 = 0.2577	R1 = 0.0302 wR2 = 0.0815
R Indices (all data)	R1 = 0.0777 *wR*2 = 0.1140	R1 = 0.1198 *wR*2 = 0.2831	R1 = 0.0454 wR2 = 0.0844
Largest Diff. Peak and Hole	0.324 and -0.268 e$Å^{-3}$	1.145 and -0.979 e$Å^{-3}$	0.602 and -0.401 e$Å^{-3}$

	[Ni(6Mes)Br(μ-OH)(μ-O-6Mes)'Ni(PPh_3)]PF_6 (25)	[Ni(6Mes)(PPh_3)(CO)]PF_6 (26)	[Ni(6Mes)(PPh_3)(CO)Br]PF_6 (27)
Identification Code	k14mkw7	k14mkw21	k14mkw20
Empirical Formula	C125 H144 Br2 Cl2 F12 N8 Ni4 O4 P4	C45 H51 F6 N2 Ni O2 P2	C41 H43 Br F6 N2 Ni O P2
Formula Weight	2639.92	886.53	894.33
Temperature	150(2) K	150(2) K	150(2) K
Wavelength	0.71073 Å	0.71073 Å	0.71073 Å
Crystal System	Triclinic	Monoclinic	Monoclinic
Space Group	P-1	P21/c	P21/c
Unit Cell Dimensions	a = 12.9970(1) Å, α = 107.784(1)°	a = 14.3080(3) Å, α = 90°	a = 12.1210(1) Å, α = 90°
	b = 18.3240(2) Å, β = 99.343(1)°	b = 16.4910(3) Å, β = 95.145(1)°	b = 13.6450(2) Å, β = 102.287(1)°
	c = 27.4000(3) Å, γ = 92.054(1)°	c = 18.8500(4) Å, γ = 90°	c = 24.6950(4) Å, γ = 90°
Volume	6105.85(11) $Å^3$	4429.8(1) $Å^3$	3990.78(9) $Å^3$
Z	2	4	4
Density (calculated)	1.436 Mg m^{-3}	1.329 Mg m^{-3}	1.489 Mg m^{-3}
Absorption Coefficient	1.432 mm^{-1}	0.574 mm^{-1}	1.631 mm^{-1}
F(000)	2732	1852	1832
Crystal Size	0.20 x 0.20 x 0.10 mm	0.20 x 0.10 x 0.10 mm	0.20 x 0.20 x 0.10 mm
Theta Range for Data Collection	3.62 to 27.49°	3.65 to 24.70°	3.63 to 27.43 °.
Index Ranges	-16<=h<=16; -23<=k<=23; -35<=l<=35	-16<=h<=16; -19<=k<=19; -22<=l<=22	-15<=h<=15; -17<=k<=17; -31<=l<=31
Reflections Collected	82841	41528	48488
Independent Reflections	27573 [R(int) = 0.0525]	7457 [R(int) = 0.0463]	9020 [R(int) = 0.0434]
Reflections Observed (> 2σ)	19801	6217	7430
Data Completeness	0.984	0.989	0.990
Absorption Correction	Semi-empirical from equivalents	Semi-empirical from equivalents	Semi-empirical from equivalents
Max. and Min. Transmission	0.933 and 0.789	0.866 and 0.811	0.8539 and 0.7363
Refinement Method	Full-matrix least-squares on F^2	Full-matrix least-squares on F^2	Full-matrix least-squares on F^2
Data/Restraints/Parameters	27573/74/1552	7457/104/565	9020/0/494
Goodness-of-Fit on F2	1.062	1.055	1.034
Final R Indices [I > 2σ(I)]	R1 = 0.0562 *wR*2 = 0.1336	*R*1 = 0.0428 *wR*2 = 0.1065	R1 = 0.0417 *wR*2 = 0.1043
R Indices (all data)	R1 = 0.0889 *wR*2 = 0.1517	*R*1 = 0.0548 *wR*2 = 0.1149	R1 = 0.0553 *wR*2 = 0.1114
Largest Diff. Peak and Hole	1.452 and -1.794 e$Å^{-3}$	0.452 and -0.449 e$Å^{-3}$	0.617 and -0.550 e$Å^{-3}$

	[Ni(6Mes)(κ^2-BH_4)]$_2$ (28)
Identification Code	h11mkw02
Empirical Formula	C22 H32 B N2 Ni
Formula Weight	394.02
Temperature	150(2) K
Wavelength	0.71073 Å
Crystal System	Monoclinic
Space Group	P21/c
Unit Cell Dimensions	a = 14.3100(3) Å, α = 90°
	b = 20.2410(4) Å, β = 91.322(1)°
	c = 14.9750(3) Å, γ = 90°
Volume	4336.33(15) Å^3
Z	8
Density (calculated)	1.207 Mg m^{-3}
Absorption Coefficient	0.902 mm^{-1}
F(000)	1688
Crystal Size	0.25 x 0.25 x 0.25 mm
Theta Range for Data Collection	3.62 to 27.50°
Index Ranges	-18<=h<=18; -26<=k<=22; -15<=l<=19
Reflections Collected	25192
Independent Reflections	9835 [R(int) = 0.0519]
Reflections Observed (> 2σ)	6506
Data Completeness	0.987
Absorption Correction	None
Max. and Min. Transmission	Full-matrix least-squares on F^2
Refinement Method	9835/12/524
Data/Restraints/Parameters	1.044
Goodness-of-Fit on F2	R1 = 0.0453 wR2 = 0.0942
Final R Indices [I > 2σ(I)]	R1 = 0.0892 wR2 = 0.1101
R Indices (all data)	0.488 and -0.351 eÅ^{-3}
Largest Diff. Peak and Hole	h11mkw02

APPENDIX 2 - CRYSTAL STUCTURES

Appendix 2 – Crystal Structures

Crystal Structure of [6^{t}BuH][Ni(PPh$_3$)Br$_2$]

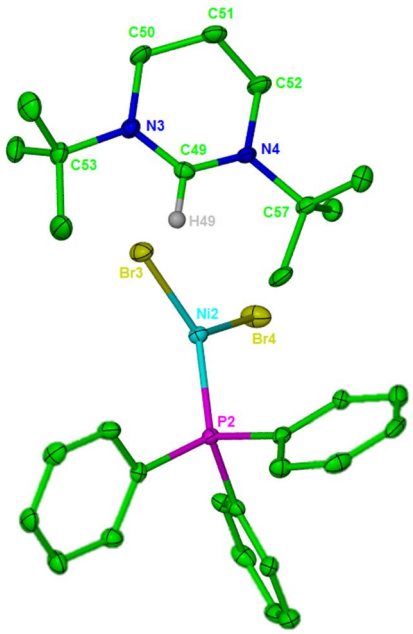

Thermal ellipsoids are set at 30 % probability. All hydrogen atoms have been omitted for clarity.

Bond lengths (Å) and angles (°) for [6^{t}BuH][Ni(PPh$_3$)Br$_2$]	
C_{NHC} – H	0.98(2)
Ni – Br(3)	2.3449(6)
Ni – Br(4)	2.3430(7)
Ni – P	2.1686(12)
N – C_{NHC} – N	126.1(4)

	[6^{t}BuH][Ni(PPh$_3$)Br$_2$]
Identification Code	k12mkw13
Empirical Formula	C60 H80 Br4 N4 Ni2 P2
Formula Weight	1356.28
Temperature	150(2) K
Wavelength	0.71073 Å
Crystal System	Monoclinic
Space Group	P21/c
Unit Cell Dimensions	a = 10.4190(1) Å, α = 90^o b = 15.1039(2) Å, β = 95.857(1)^o c = 39.3547(5) Å, γ = 90^o
Volume	6160.82(13) Å^3
Z	4
Density (calculated)	1.462 Mg m^{-3}
Absorption Coefficient	3.297 mm^{-1}
F(000)	2776
Crystal Size	0.20 x 0.10 x 0.08 mm
Theta Range for Data Collection	3.52 to 27.48^o
Index Ranges	-13<=h<=13; -19<=k<=19; -51<=l<=51
Reflections Collected	60527
Independent Reflections	13722 [R(int) = 0.0931]
Reflections Observed (> 2σ)	7662
Data Completeness	0.970
Absorption Correction	Semi-empirical from equivalents
Max. and Min. Transmission	0.863 and 0.782
Refinement Method	Full-matrix least-squares on F^2
Data/Restraints/Parameters	13722/2/669
Goodness-of-Fit on F2	1.011
Final R Indices [I > 2σ(I)]	R1 = 0.0521 *wR*2 = 0.0876
R Indices (all data)	R1 = 0.1308 *wR*2 = 0.1078
Largest Diff. Peak and Hole	1.268 and -0.906 eÅ^{-3}

Crystal Structure of $Ni(O=PPh_3)_2Br_2$

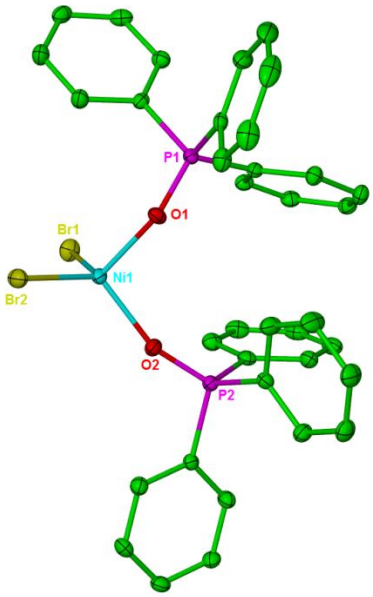

Thermal ellipsoids are set at 30 % probability. All hydrogen atoms have been omitted for clarity.

Bond lengths (Å) and angles (°) for $Ni(O=PPh_3)_2Br_2$	
Ni – Br(1)	2.3622(4)
Ni – Br(2)	2.3734(4)
Ni – O(1)	1.9447(18)
Ni – O(2)	1.9561(19)
O(1) – P(1)	1.5103(19)
O(2) – P(2)	1.504(2)
Br(1) – Ni – Br(2)	116.512(16)
Br(1) – Ni – O(1)	111.75(6)
Br(1) – Ni – O(2)	106.16(6)
Br(2) – Ni – O(1)	101.65(6)
Br(2) – Ni – O(2)	118.82(6)
O(1) – Ni – O(2)	100.72(8)
Ni – O(1) – P(1)	143.96(12)
Ni – O(2) – P(2)	159.27(13)

	$Ni(O=PPh_3)_2Br_2$
Identification Code	k13mkw19
Empirical Formula	C36 H30 Br2 Ni O2 P2
Formula Weight	775.07
Temperature	150(2) K
Wavelength	0.71073 Å
Crystal System	Triclinic
Space Group	P1
Unit Cell Dimensions	a = 9.9800(2) Å, α = 65.486(1)° b = 10.0030(2) Å, β = 63.506(1)° c = 10.4560(2) Å, γ = 89.169(1)°
Volume	831.13(3) $Å^3$
Z	1
Density (calculated)	1.549 Mg m^{-3}
Absorption Coefficient	3.115 mm^{-1}
F(000)	390
Crystal Size	0.20 x 0.10 x 0.10 mm
Theta Range for Data Collection	3.59 to 27.49°
Index Ranges	-12<=h<=12; -12<=k<=12; -13<=l<=13
Reflections Collected	15860
Independent Reflections	7065 [R(int) = 0.0321]
Reflections Observed (> 2σ)	6648
Data Completeness	0.994
Absorption Correction	Semi-empirical from equivalents
Max. and Min. Transmission	0.159 and 0.118
Refinement Method	Full-matrix least-squares on F^2
Data/Restraints/Parameters	7065/3/389
Goodness-of-Fit on F2	1.063
Final R Indices [I > 2σ(I)]	R1 = 0.0278 *wR*2 = 0.0622
R Indices (all data)	R1 = 0.0315 *wR*2 = 0.0645
Largest Diff. Peak and Hole	0.005(4)

Crystal Structure of [6°TolH][Ni(PPh$_3$)Br$_3$]

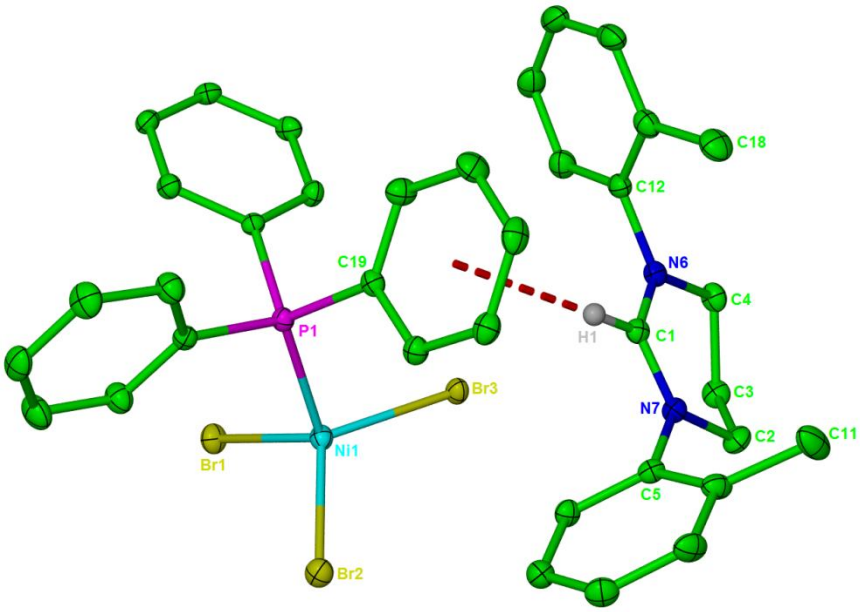

Thermal ellipsoids are set at 30 % probability. All hydrogen atoms have been omitted for clarity, except for H(1).

Bond lengths (Å) and angles (°) for [6°TolH][Ni(PPh$_3$)Br$_3$]	
Ni – Br(1)	2.3780(6)
Ni – Br(2)	2.3772(6)
Ni – Br(3)	2.3728(5)
Ni – P	2.3133(10)
C_{NHC} – H(1)	0.950(3)
H(1) – $Ph_{centroid}$	2.863(4)
Br(1) – Ni – Br(2)	110.73(2)
Br(1) – Ni – Br(3)	113.71(2)
Br(2) – Ni – Br(3)	116.67(2)
Br(1) – Ni – P	104.39(3)
Br(2) – Ni – P	108.90(3)
Br(3) – Ni – P	101.14(3)
N(6) – C_{NHC} – N(7)	124.9(3)

	[6°TolH][Ni(PPh$_3$)Br$_3$]
Identification Code	h12mkw16
Empirical Formula	C36 H36 Br3 N2 Ni P
Formula Weight	816.08
Temperature	150(2) K
Wavelength	0.71073 Å
Crystal System	Triclinic
Space Group	P-1
Unit Cell Dimensions	a = 9.8110(4) Å, α = 103.817(2)° b = 11.6620(5) Å, β = 96.655(2)° c = 17.5830(4) Å, γ = 114.004(1)°
Volume	1732.38(11) Å^3
Z	2
Density (calculated)	1.584 Mg m^{-3}
Absorption Coefficient	4.093 mm^{-1}
F(000)	828
Crystal Size	0.30 x 0.20 x 0.10 mm
Theta Range for Data Collection	3.74 to 27.47°
Index Ranges	-12<=h<=12; -15<=k<=15; -22<=l<=22
Reflections Collected	25776
Independent Reflections	7854 [R(int) = 0.0645]
Reflections Observed (> 2σ)	5512
Data Completeness	0.990
Absorption Correction	Semi-empirical from equivalents
Max. and Min. Transmission	0.726 and 0.509
Refinement Method	Full-matrix least-squares on F^2
Data/Restraints/Parameters	7854/0/392
Goodness-of-Fit on F2	1.009
Final R Indices [I > 2σ(I)]	R1 = 0.0417 *wR*2 = 0.0903
R Indices (all data)	R1 = 0.0759 *wR*2 = 0.1034
Largest Diff. Peak and Hole	0.713 and -0.705 eÅ^{-3}

Crystal Structure of [Ni(6Mes)(7Mes)]BPh$_4$

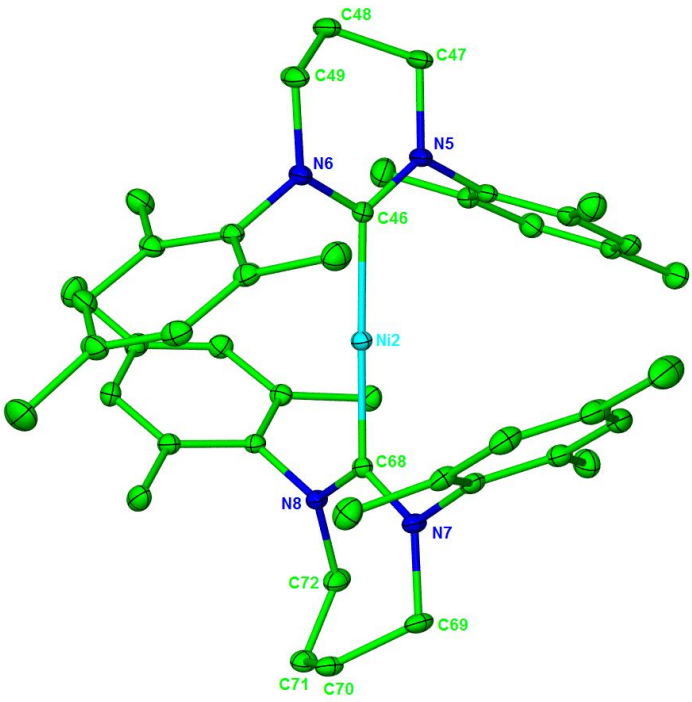

Thermal ellipsoids are set at 30 % probability. All hydrogen atoms and the $[BPh_4]^-$ anion have been omitted for clarity.

Bond lengths (Å) and angles (°) for [Ni(6Mes)(7Mes)]BPh$_4$	
Ni – C(46)	1.9424(18)
Ni – C(68)	1.9353(18)
C(46) – Ni – C(68)	178.85(8)
N(5) – C(46) – N(6)	117.16(16)
N(7) – C(68) – N(8)	118.74(16)

	[Ni(6Mes)(7Mes)]BPh_4
Identification Code	h11mkw03
Empirical Formula	C140.80 H159.20 B2 N8 Ni2
Formula Weight	2102.60
Temperature	123(2) K
Wavelength	0.71073 Å
Crystal System	Triclinic
Space Group	P-1
Unit Cell Dimensions	a = 15.1160(2) Å, α = 101.407(1)° b = 17.9800(2) Å, β = 98.606(1)° c = 22.4870(3) Å, γ = 94.000(1)°
Volume	5892.26(13) $Å^3$
Z	2
Density (calculated)	1.185 Mg m^{-3}
Absorption Coefficient	0.374 mm^{-1}
F(000)	2252
Crystal Size	0.35 x 0.35 x 0.15 mm
Theta Range for Data Collection	3.75 to 27.48°
Index Ranges	-19<=h<=19; -23<=k<=22; -29<=l<=29
Reflections Collected	97484
Independent Reflections	26792 [R(int) = 0.0491]
Reflections Observed (> 2σ)	20080
Data Completeness	0.990
Absorption Correction	Semi-empirical from equivalents
Max. and Min. Transmission	0.947 and 0.829
Refinement Method	Full-matrix least-squares on F^2
Data/Restraints/Parameters	26792/46/1466
Goodness-of-Fit on F2	1.013
Final R Indices [I > 2σ(I)]	R1 = 0.0449 wR2 = 0.1114
R Indices (all data)	R1 = 0.0691 wR2 = 0.1263
Largest Diff. Peak and Hole	1.304 and -0.398 $eÅ^{-3}$

Crystal Structure of Ni(6Mes)(7Mes)

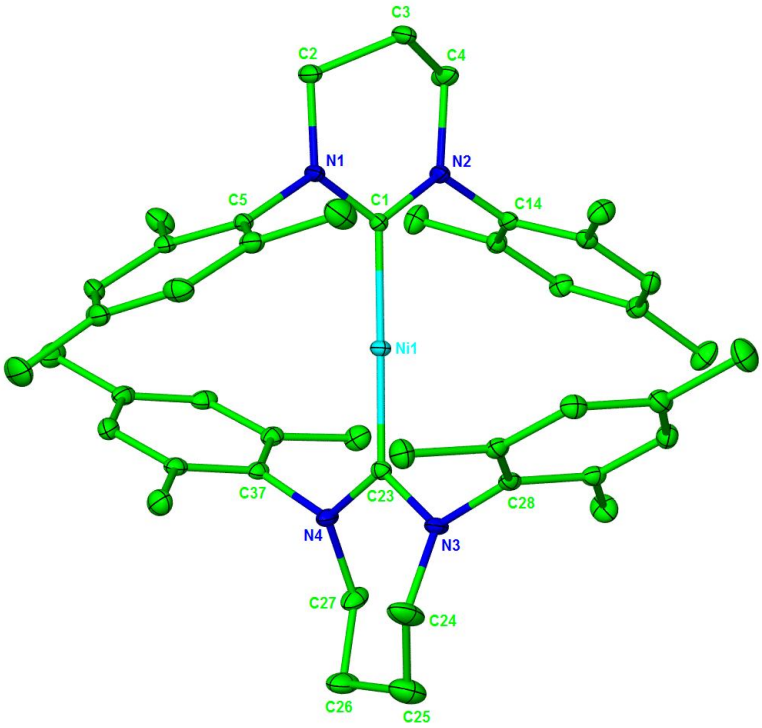

Thermal ellipsoids are set at 30 % probability. All hydrogen atoms have been omitted for clarity.

Bond lengths (Å) and angles (°) for Ni(6Mes)(7Mes)	
Ni – C(1)	1.89(5)
Ni – C(23)	1.83(5)
C(1) – Ni – C(23)	179(2)
N(1) – C(1) – N(2)	115(5)
N(3) – C(23) – N(4)	112(5)

	Ni(6Mes)(7Mes)
Identification Code	p11prr39
Empirical Formula	C48.50 H62 N4 Ni
Formula Weight	759.73
Temperature	150(2) K
Wavelength	0.7107 Å
Crystal System	Triclinic
Space Group	P-1
Unit Cell Dimensions	a = 10.0294(4) Å, α = 84.482(3)°
	b = 12.0665(4) Å, β = 79.837(3)°
	c = 18.6658(5) Å, γ = 69.948(3)°
Volume	2087.15(12) Å^3
Z	2
Density (calculated)	1.209 Mg m^{-3}
Absorption Coefficient	0.503 mm^{-1}
F(000)	818
Crystal Size	0.30 x 0.30 x 0.12 mm
Theta Range for Data Collection	2.91 to 27.48°
Index Ranges	-13<=h<=13; -15<=k<=15; -24<=l<=24
Reflections Collected	19929
Independent Reflections	9568 [R(int) = 0.0378]
Reflections Observed (> 2σ)	7064
Data Completeness	0.999
Absorption Correction	Semi-empirical from equivalents
Max. and Min. Transmission	1.00000 and 0.80309
Refinement Method	Full-matrix least-squares on F^2
Data/Restraints/Parameters	9568/51/508
Goodness-of-Fit on F2	1.024
Final R Indices [I > 2σ(I)]	R1 = 0.0537 wR2 = 0.1268
R Indices (all data)	R1 = 0.0817 wR2 = 0.1394
Largest Diff. Peak and Hole	0.983 and -0.749 eÅ^{-3}

Crystal Structure of 6Mes.BH_3

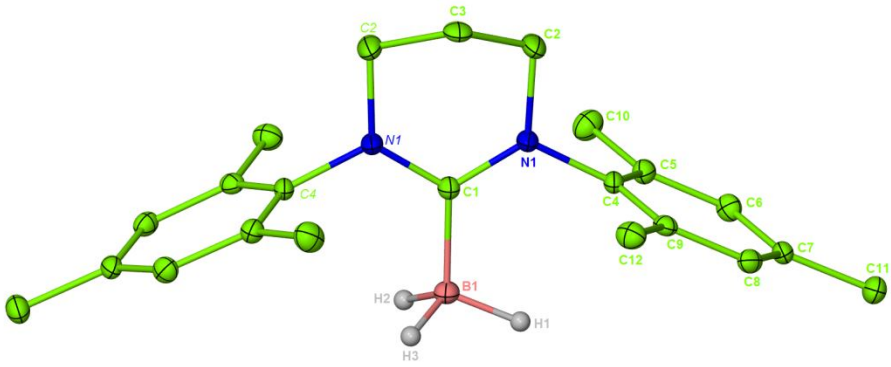

Thermal ellipsoids are set at 30 % probability. All hydrogen atoms have been omitted for clarity, except for H(1) – H(3).

Bond lengths (Å) and angles (°) for 6Mes.BH_3	
B – C_{NHC}	1.612(6)
N – C_{NHC} – N	117.1(4)

	6Mes.BH_3
Identification Code	k12mkw2
Empirical Formula	C22 H31 B N2
Formula Weight	334.30
Temperature	150(2) K
Wavelength	0.71073 Å
Crystal System	Orthorhombic
Space Group	Pcan
Unit Cell Dimensions	a = 7.8010(3) Å, α = 90 b = 15.6440(9) Å, β = 90 c = 16.1190(12) Å, γ = 90
Volume	1967.1(2) $Å^3$
Z	4
Density (calculated)	1.129 Mg m^{-3}
Absorption Coefficient	0.065 mm^{-1}
F(000)	728
Crystal Size	0.40 x 0.15 x 0.02 mm
Theta Range for Data Collection	3.86 to 25.01°
Index Ranges	-8<=h<=8; -18<=k<=18; -19<=l<=19
Reflections Collected	19227
Independent Reflections	1689 [R(int) = 0.1758]
Reflections Observed (> 2σ)	1073
Data Completeness	0.969
Absorption Correction	Semi-empirical from equivalents
Max. and Min. Transmission	0.996 and 0.895
Refinement Method	Full-matrix least-squares on F^2
Data/Restraints/Parameters	1689/9/141
Goodness-of-Fit on F2	1.072
Final R Indices [I > 2σ(I)]	R1 = 0.0649 wR2 = 0.1359
R Indices (all data)	R1 = 0.1165 wR2 = 0.1636
Largest Diff. Peak and Hole	0.217 and -0.262 e$Å^{-3}$

Crystal Structure of Ni(6Mes)(PPh_3)Br_2 (29)

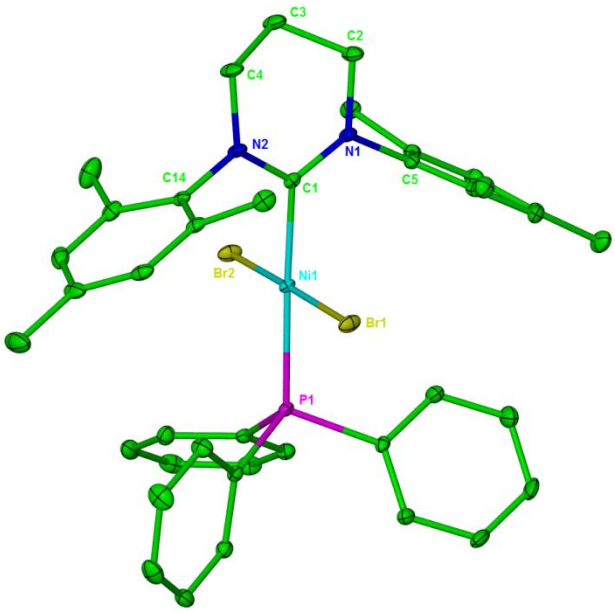

Thermal ellipsoids are set at 30 % probability. All hydrogen atoms have been omitted for clarity.

Bond lengths (Å) and angles (°) for **29**	
Ni – C_{NHC}	1.9402(14)
Ni – Br(1)	2.3026(2)
Ni – Br(2)	2.2997(2)
Ni – P	2.2586(4)
N(1) – C_{NHC} – N(2)	117.31(13)
C_{NHC} – Ni – P	177.24(4)
C_{NHC} – Ni – Br(1)	91.87(4)
C_{NHC} – Ni – Br(2)	90.73(4)
Br(1) – Ni – Br(2)	176.428(11)

	Ni(6Mes)(PPh_3)Br_2 (29)
Identification Code	p09mkw11
Empirical Formula	C40 H43 Br2 N2 Ni P
Formula Weight	801.26
Temperature	150(2) K
Wavelength	0.71073 Å
Crystal System	Monoclinic
Space Group	C2/c
Unit Cell Dimensions	a = 38.9620(14) Å, α = 90°
	b = 9.5046(2) Å, β = 98.538(3)°
	c = 19.6660(4) Å, γ = 90°
Volume	7202.0(3) $Å^3$
Z	8
Density (calculated)	1.478 Mg m^{-3}
Absorption Coefficient	2.833 mm^{-1}
F(000)	3280
Crystal Size	0.27 x 0.20 x 0.20 mm
Theta Range for Data Collection	2.95 to 30.49°
Index Ranges	-50<=h<=55; -11<=k<=13; -26<=l<=27
Reflections Collected	30743
Independent Reflections	9726 [R(int) = 0.0223]
Reflections Observed (> 2σ)	6750
Data Completeness	0.886
Absorption Correction	Semi-empirical from equivalents
Max. and Min. Transmission	1.00000 and 0.94452
Refinement Method	Full-matrix least-squares on F^2
Data/Restraints/Parameters	9726/0/421
Goodness-of-Fit on F2	0.900
Final R Indices [I > 2σ(I)]	R1 = 0.0230 wR2 = 0.0511
R Indices (all data)	R1 = 0.0403 wR2 = 0.0524
Largest Diff. Peak and Hole	0.419 and -0.587 $eÅ^{-3}$

APPENDIX 3 -

EPR SPECTROSCOPY

Appendix 3 – EPR Spectroscopy

EPR and ENDOR Spectra of Ni(RE NHC)(PPh$_3$)Br (1, 7 – 10)

Q-band EPR

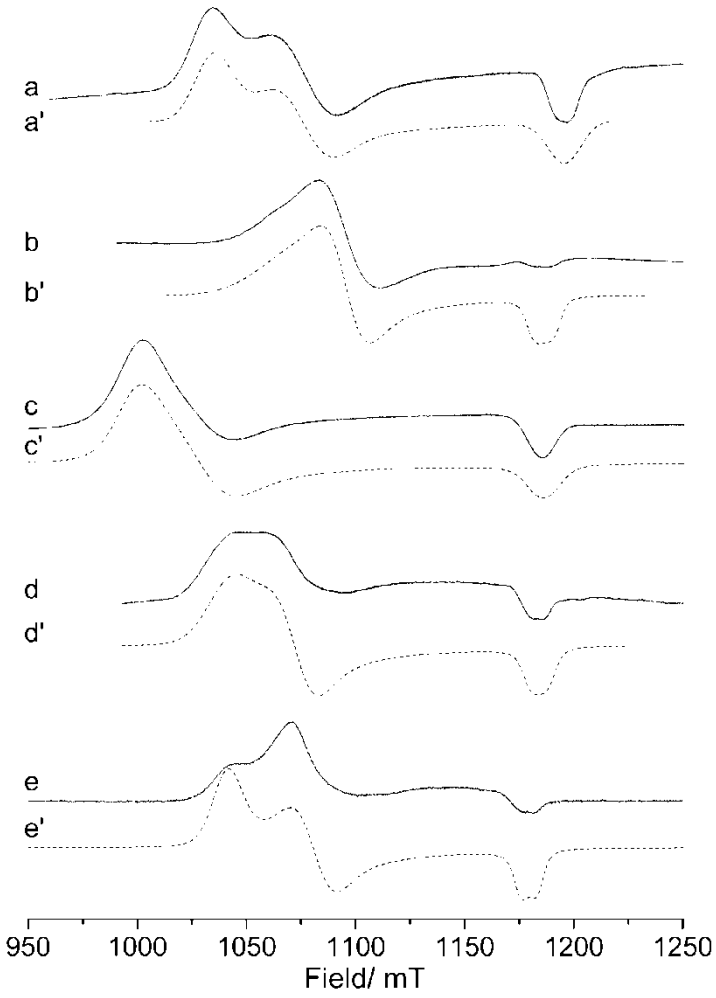

Q-band EPR (10 K) spectra of Ni(RE NHC)(PPh$_3$)X (a – e) and the corresponding simulations (a′ - e′). a: RE NHC = 6Mes, X = Br **(1)**; b: RE NHC = 7^{o}Tol, X = Br **(7)**; c: RE NHC = 8Mes, X = mixed Br/Cl **(8)**; d: RE NHC = 8^{o}Tol, X = mixed Br/Cl **(9)**; e: RE NHC = O-8^{o}Tol, X = mixed Br/Cl **(10)**.

^{1}H ENDOR

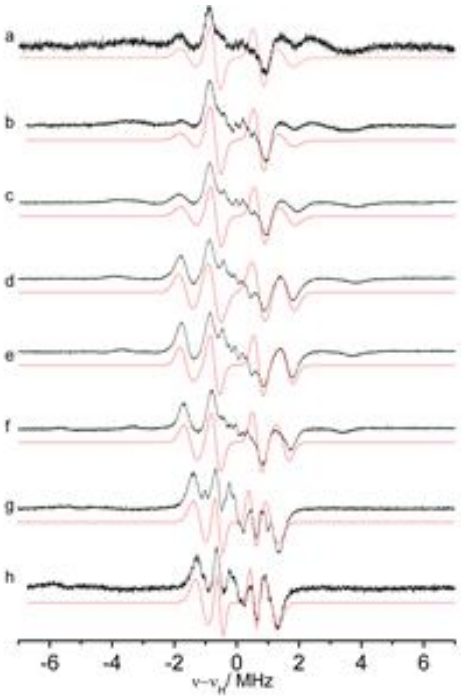

CW ^{1}H ENDOR (10 K) spectra of Ni(6Mes)(PPh_3)Br **(1)** recorded at the field positions (a) 10233, (b) 10336, (c) 10508, (d) 10748, (e) 10902, (f) 11125, (g) 11863 and (h) 11965 Gauss. Corresponding simulations are shown at each position with dotted lines.

APPENDIX 4 - MASS SPECTROMETRY

Appendix 4 – Mass Spectrometry Data for Ni(7Mes)Br(μ-OH)(μ-O-7Mes)'NiBr (14) and [Ni(7Mes)'Br]$_2$ (16)

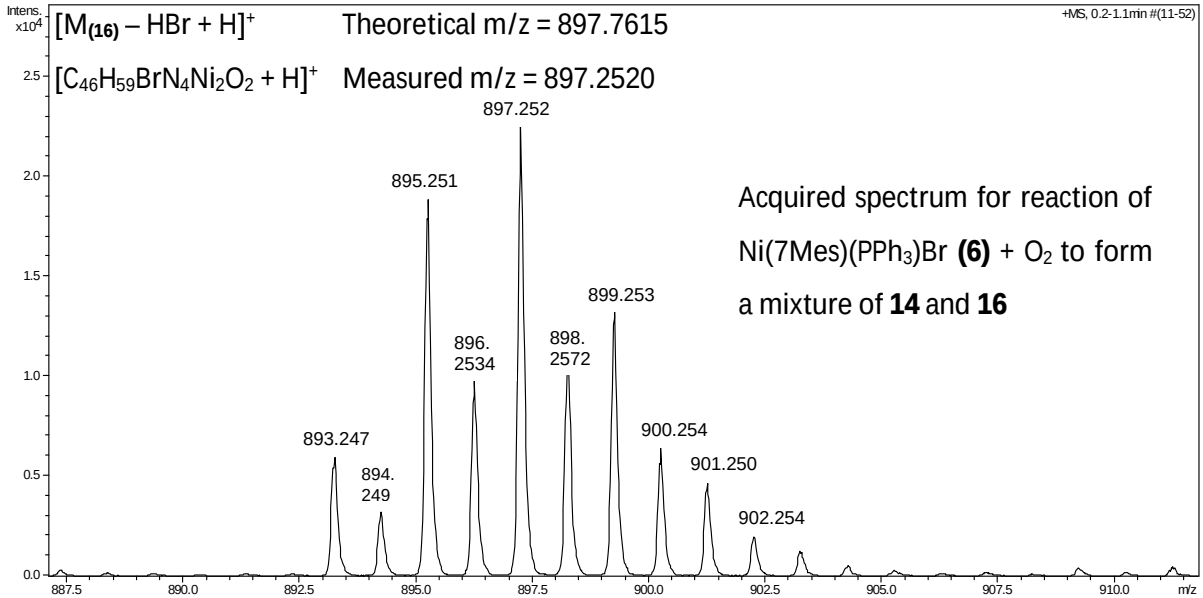

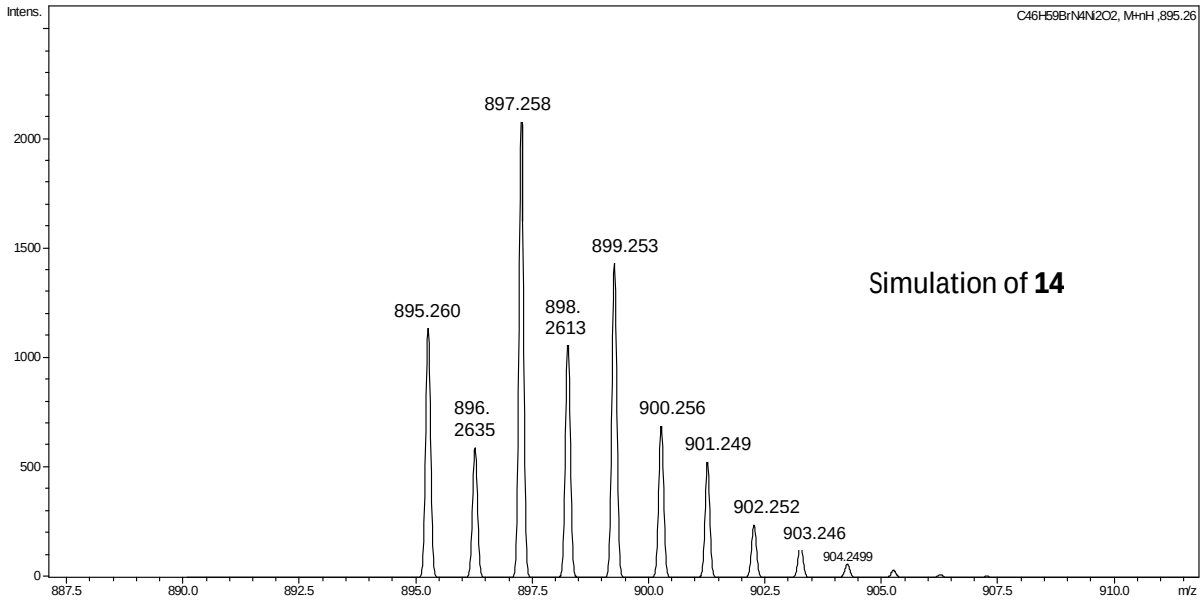

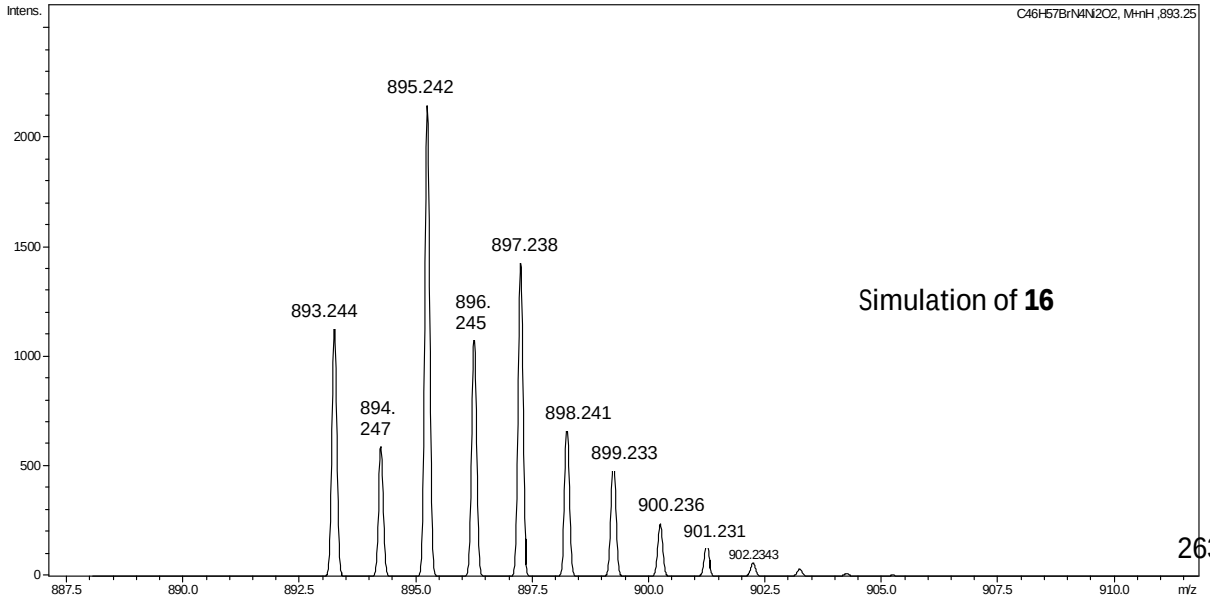

APPENDIX 5 - CRYOSCOPY MEASUREMENTS

Appendix 5 – Cryoscopy

Cryoscopy Measurements on [Ni(6Mes)$_2$]Br (19)

Molecular weight (MW) of [Ni(6Mes)$_2$]Br **(19)** = 779.56 g mol^{-1}.

As the complex is an ion pair, a result of half this value is expected (389.78 g mol^{-1}) by cryoscopy if it exists as a monomer in solution.

Solvent used: nitrobenzene.

Cryoscopic constant (K_b) of nitrobenzene: 8.1 ^{o}C g mol^{-1}

Arbitrary freezing point of nitrobenzene:

	Arbitrary freezing point / ^{o}C
1	0.930
2	0.933
3	0.932

Average = 0.932 ± 0.002 ^{o}C

Arbitrary freezing point of a 1.72 x 10^{-3} mol dm^{-3} nitrobenzene solution of **19** (0.0336 g in 25 mL).

	Arbitrary freezing point / ^{o}C
1	0.955
2	0.953
3	0.955

Average = 0.954 ± 0.001 ^{o}C

ΔT = 0.954 – 0.932 = 0.022 ^{o}C

MW = (1000 x K_b x mass(compound)) / (ΔT x mass(solvent))

MW = (1000 x 8.1 x 0.0336) / (0.022 x 30)

MW = 412.36 g mol^{-1}

As a fraction of total MW = 0.53

Final result = 0.53 ± 0.08

A value close to 0.5 MW fraction suggests that **19** exists as a monomer in solution. The value is slightly higher than 0.5, which can be attributed to a small level of association between the bromide anion and nickel cation.

APPENDIX 6 – REACTIVTY OF 24 WITH CO

Appendix 6 – Reaction of [Ni(6Mes)(PPh_3)(THF)]PF_6 (24) with CO

The IR and $^{13}C\{^1H\}$ PENDANT spectra for the reaction of [Ni(6Mes)(PPh_3)(THF)]PF_6 **(24)** with CO are shown below.

IR Spectra

A C_6D_6 solution of **24** was exposed to CO (1 atm) and an IR spectrum recorded immediately, followed by every 5 min for a total of 40 min. When the bands appear they remain until end of reaction. IR (C_6D_6, cm^{-1}): 2032, 1668 (1 min, ν_{CO}), 1956, 1967 (5 min, ν_{CO}), 1996 (10 min, ν_{CO}), 2069 (15 min, ν_{CO}).

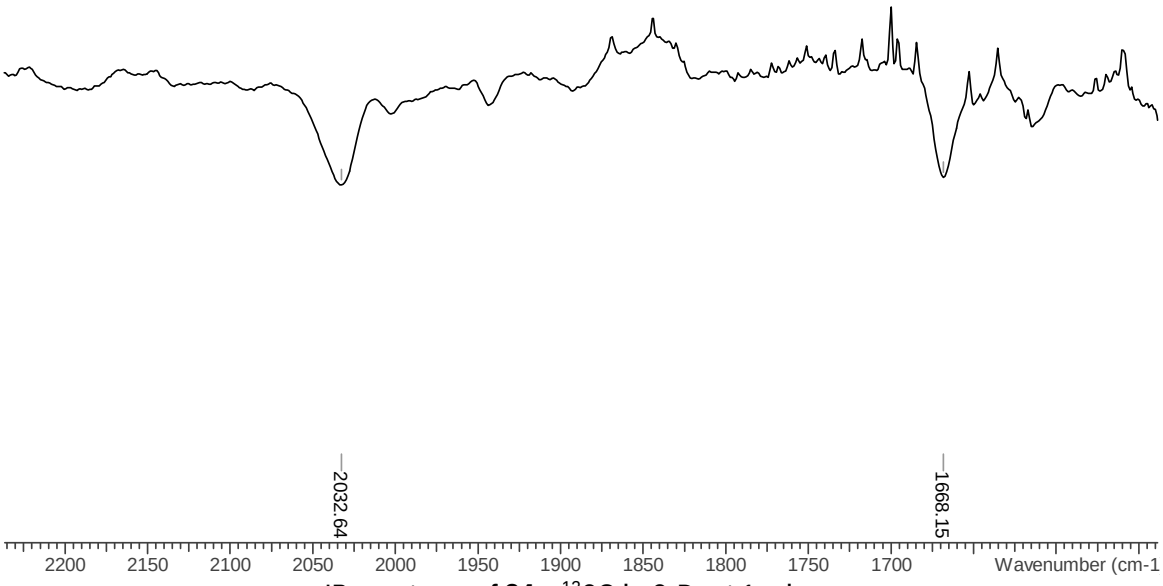

IR spectrum of **24** + ^{13}CO in C_6D_6 at 1 min.

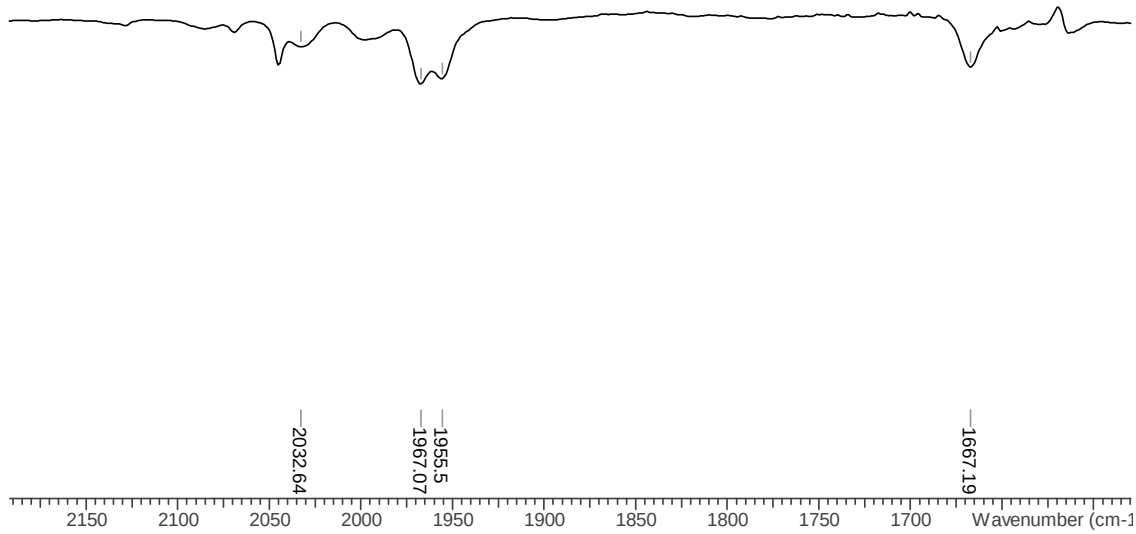

IR spectrum of **24** + ^{13}CO in C_6D_6 at 5 min.

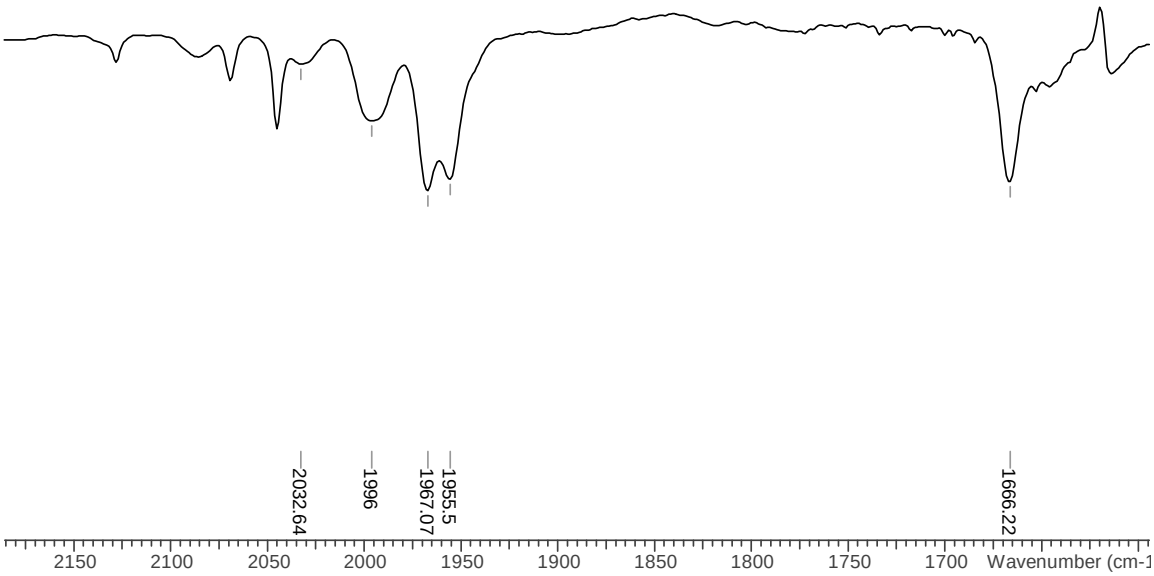

IR spectrum of **24** + ^{13}CO in C_6D_6 at 10 min.

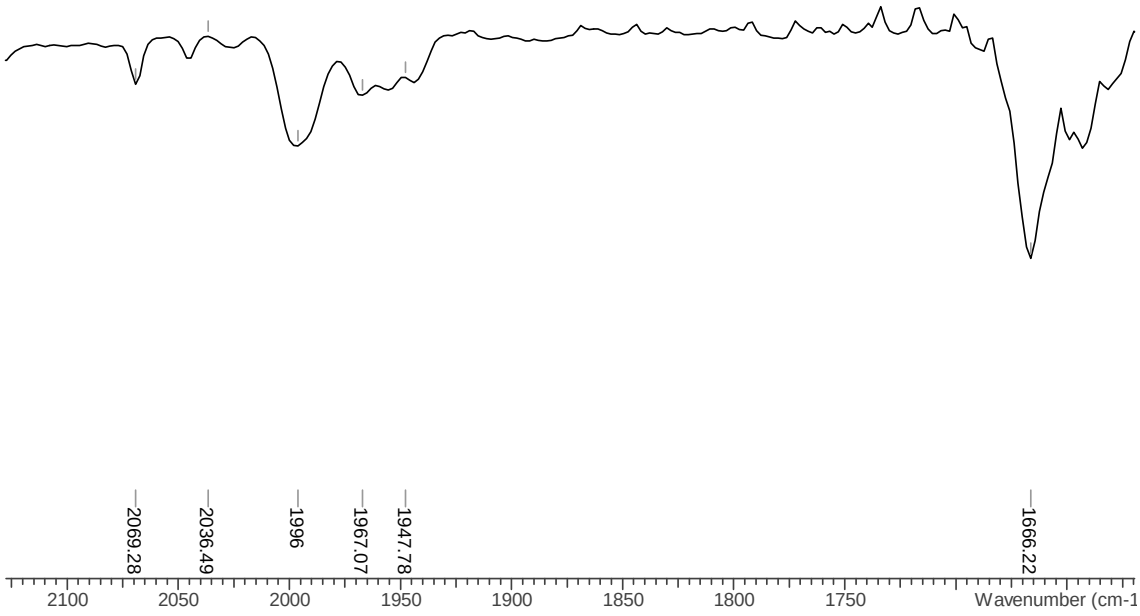

IR spectrum of **24** + ^{13}CO in C_6D_6 at 15 min.

NMR Spectra

A THF-d_8 solution of **24** was exposed to ^{13}CO (1 atm) and immediately frozen in liquid nitrogen. Spectrum **a**: $^{13}C\{^1H\}$ PENDANT (THF-d_8, 100 MHz, 233 K): δ 198.3 (*C*O), 194.5 (*C*O), 192.9 (*C*O). Spectrum **b**: warmed to 298 K: $^{13}C\{^1H\}$ PENDANT (THF-d_8, 100 MHz, 298 K): δ 198.1 (*C*O), 197.3 (*C*O), 193.9 (*C*O), 192.3 (*C*O). Spectrum **c**: left for 72 h at 298 K: $^{13}C\{^1H\}$ PENDANT (THF-d_8, 100 MHz, 298 K): δ 197.6 (*C*O), 196.5 (*C*O), 184.4 (*C*O), 180.9 (*C*O), 180.6 (*C*O).

a

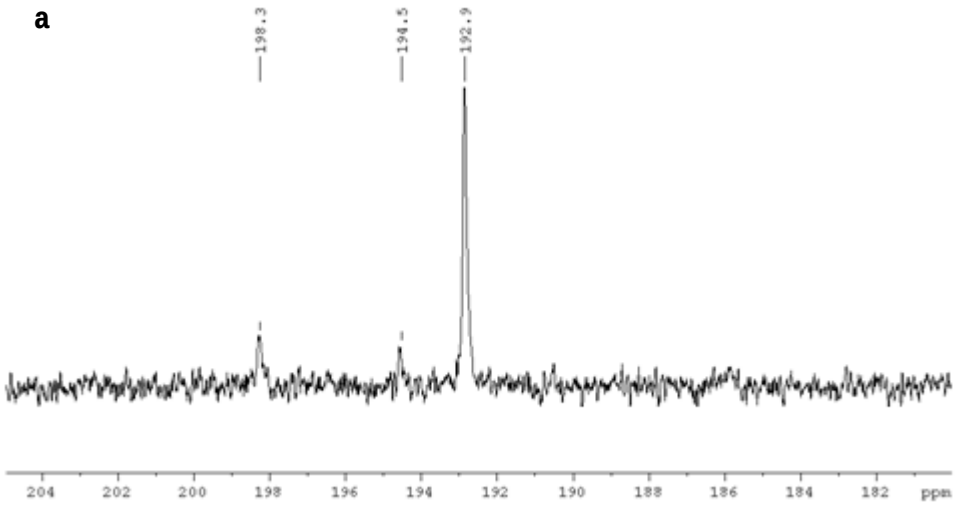

$^{13}C\{^{1}H\}$ PENDANT spectrum of **24** + ^{13}CO in THF-d_8 and immediately frozen (THF-d_8, 100 MHz, 233 K).

b

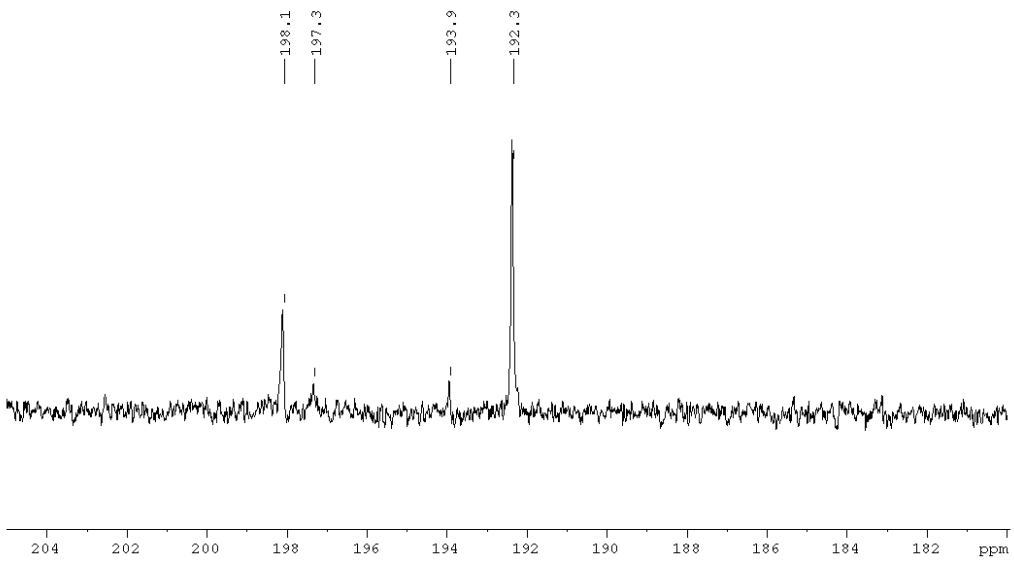

$^{13}C\{^{1}H\}$ PENDANT spectrum of **24** + ^{13}CO in THF-d_8 and immediately frozen, then warmed to 298 K (THF-d_8, 100 MHz, 298 K).

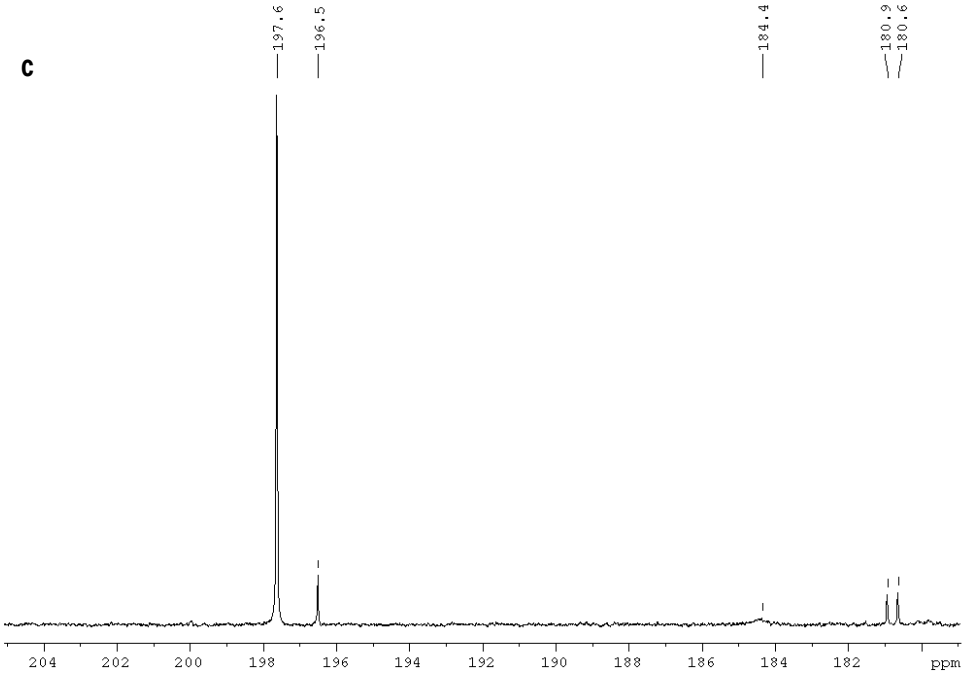

$^{13}C\{^{1}H\}$ PENDANT spectrum of **24** + ^{13}CO in THF-d_8 and immediately frozen, then warmed to 298 K and left for 72 h at 298 K (THF-d_8, 100 MHz, 298 K).

APPENDIX 7 - EXPERIMENTAL

Appendix 7 – Experimental

Synthesis of Ni(6^{t}Bu)Br (11) and [6^{t}BuH][Ni(PPh$_3$)Br$_2$]

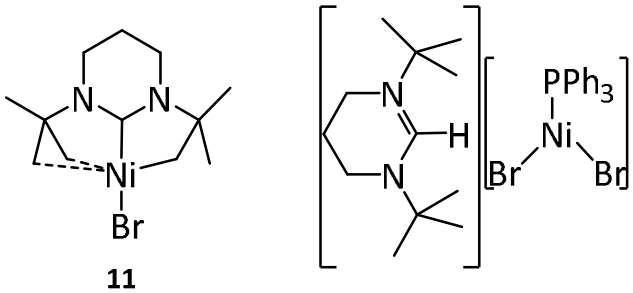

11

A THF (20 mL) solution of *in situ* generated 6^{t}Bu ([6^{t}BuH]BF_4 (79 mg, 0.278 mmol) and $KN(SiMe_3)_2$ (56 mg, 0.281 mmol)) was charged to a mixture of $Ni(COD)_2$ (41 mg, 0.149 mmol) and $Ni(PPh_3)_2Br_2$ (107 mg, 0.143 mmol) and stirred for 1.5 h at 298 K. The resultant orange solution was filtered and hexane (20 mL) added to precipitate out a yellow solid. This solid was washed with hexane (2 x 10 mL) and recrystallised from THF/hexane. Orange **(11)** and yellow ([6^{t}BuH][Ni(PPh$_3$)Br$_2$]) crystals were formed. Yield (of product mixture (**11** + [6^{t}BuH][Ni(PPh$_3$)Br$_2$])): 20 mg (35 %). ^{1}H NMR of product mixture (C_6D_6, 500 MHz): δ 21.36 (br s), 9.33 (v br s), 4.87 (v br s), 3.81 (br s), 3.66 (br m), 3.00 (br), 2.93 (br m), 2.31 (v br s), -2.76 (br s), -2.83 (br s). Consistent reproducibility of this reaction was not achieved.

Synthesis of Ni(6Mes)(PPh$_3$)Br$_2$ (29)

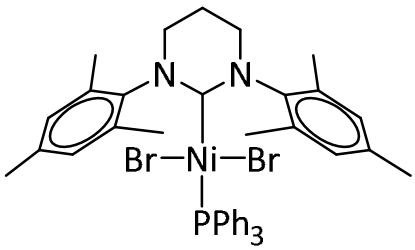

6Mes (formed *in situ* from [6MesH]BF_4 (256 mg, 0.627 mmol) and $KN(SiMe_3)_2$ (125 mg, 0.627 mmol) in toluene (10 mL)) was added to $Ni(PPh_3)_2Br_2$ (466 mg, 0.627 mmol) and stirred at room temperature for 1 h to give a dark purple solution. After filtration to remove KBF_4, the solution was reduced to dryness and washed with hexane (15 mL) to give a brown/purple residue. Recrystallisation of this residue from toluene/hexane yielded a purple precipitate of **29**. Yield: 263 mg (52 %). ^{1}H NMR ($CDCl_3$, 500 MHz): δ 7.36 (br m, 19H, C*H*$_{aryl}$), 3.46 (br s, 4H, NC*H*$_2$), 2.48 (v br s, 18H, *p*-C*H*$_3$ and *o*-CH_3), 1.29 (br s, 2H, NCH_2CH_2).

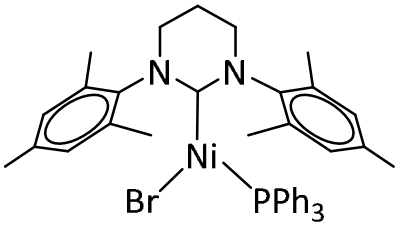

1

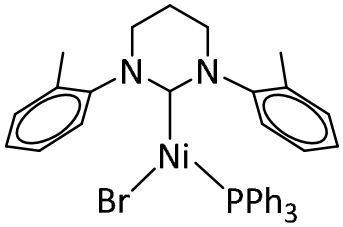

2

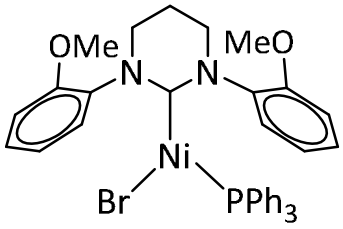

3

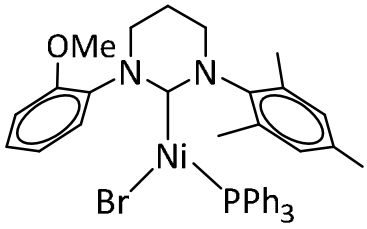

4

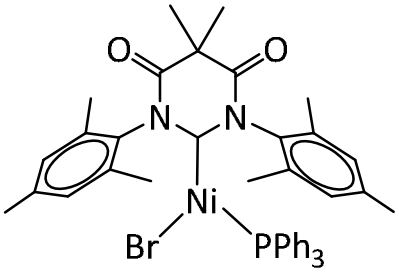

5

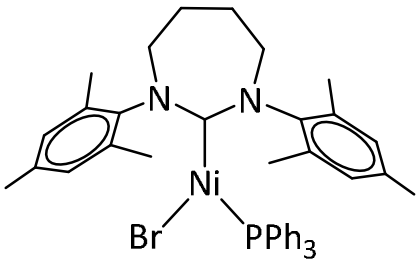

6

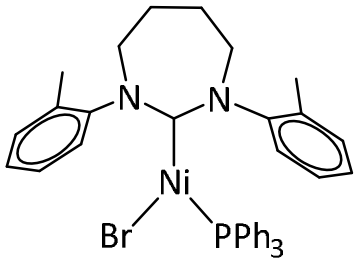

7

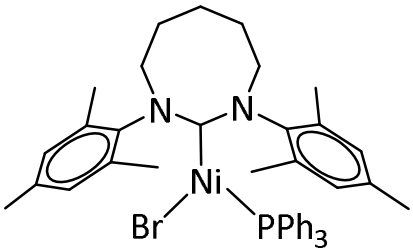

8

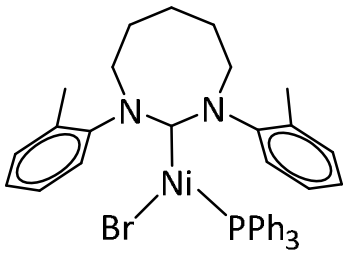

9

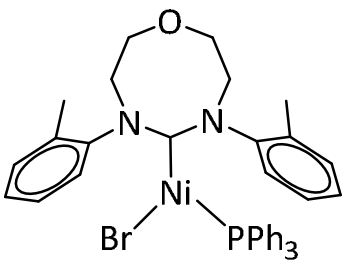

10

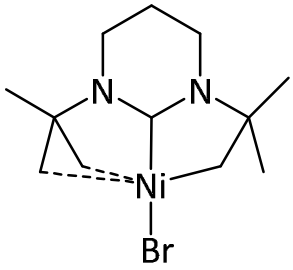

11

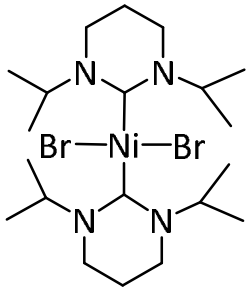

12

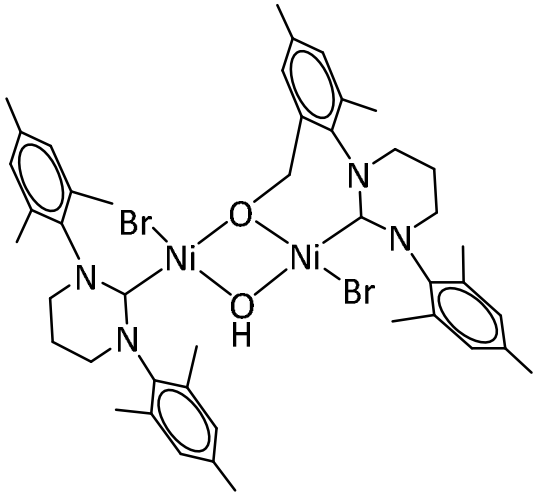

13

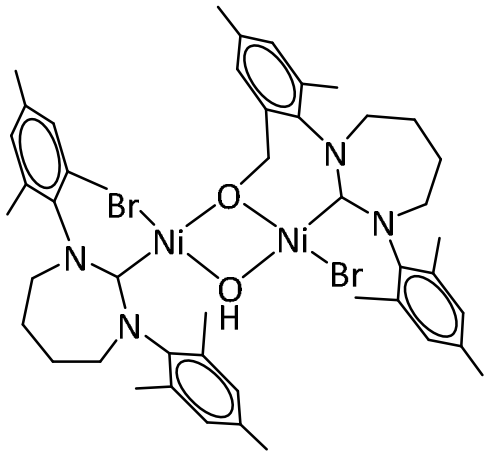

14

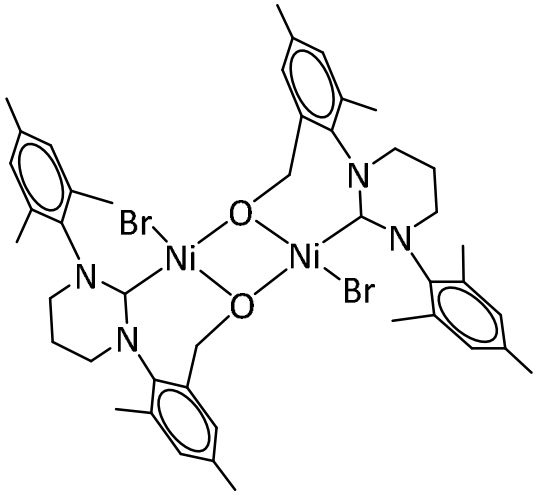

15

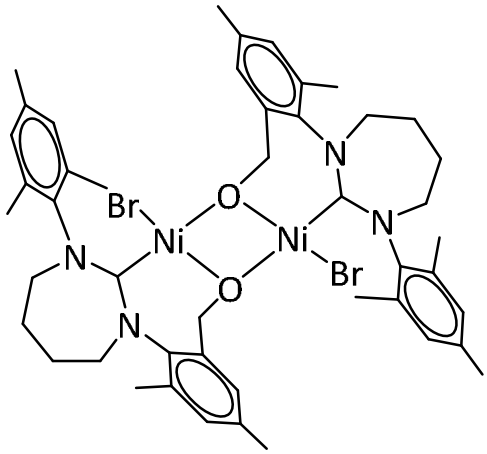

16

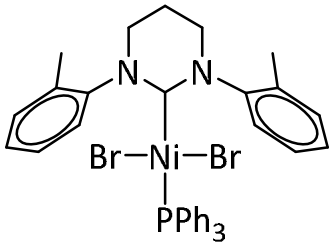

17

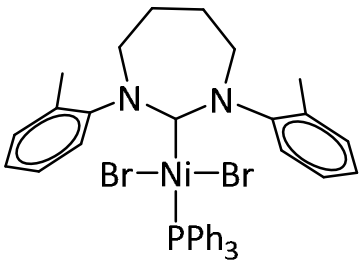

18

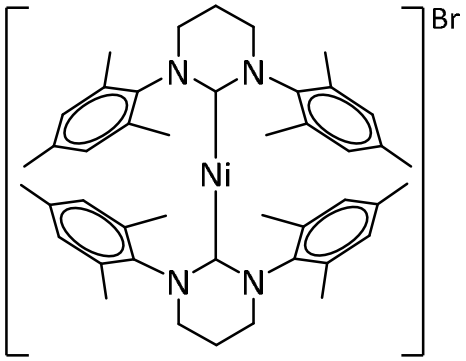

19

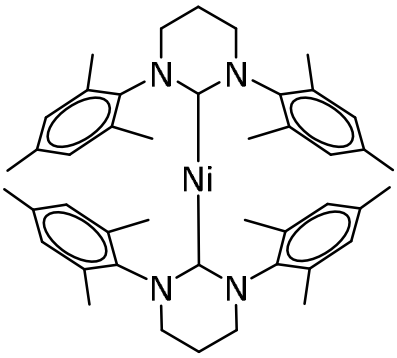

20

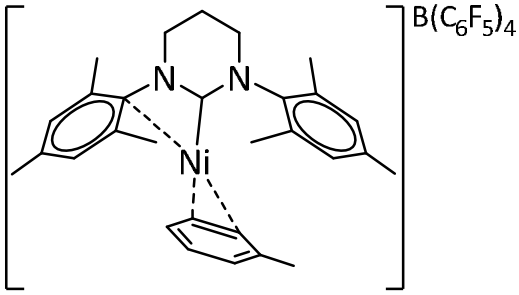

21

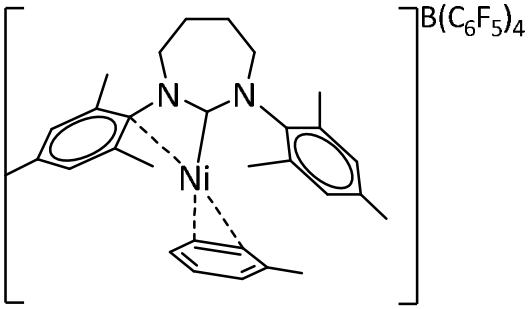

22

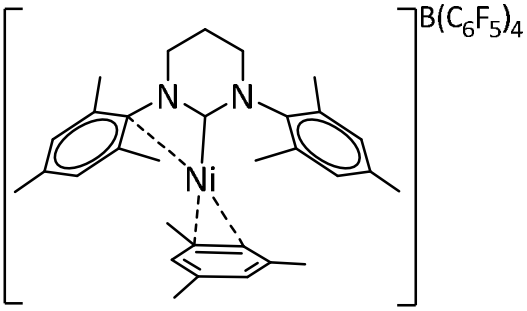

23

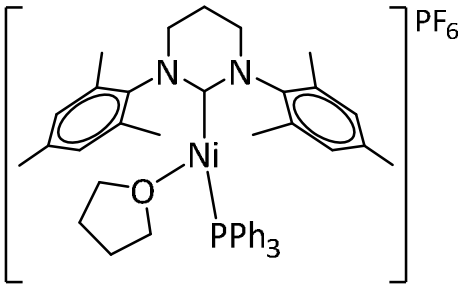

24

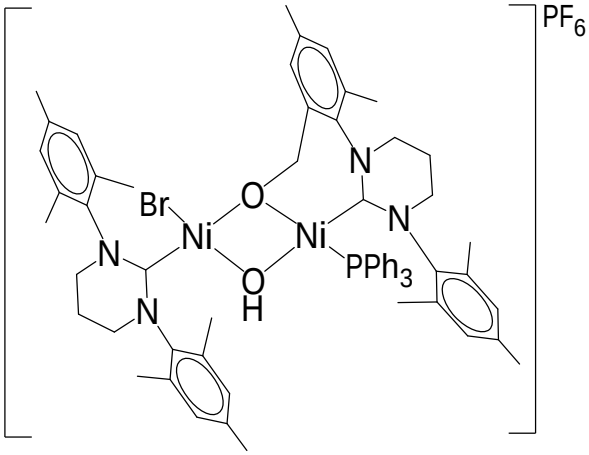

25

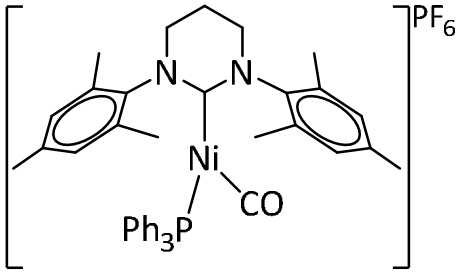

26

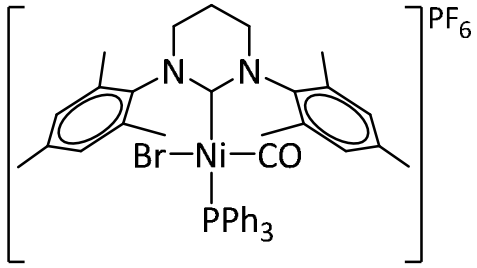

27

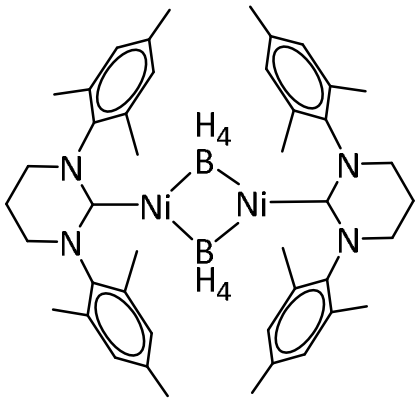

28

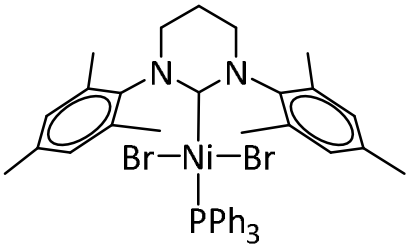

29